

PDF hosted at the Radboud Repository of the Radboud University Nijmegen

The following full text is a publisher's version.

For additional information about this publication click this link.

<http://hdl.handle.net/2066/196863>

Please be advised that this information was generated on 2019-06-02 and may be subject to change.

**Down the kidney tubes:
insights into renal proximal tubule drug handling
to improve *in vitro* nephrotoxicity screening**

Tom Nieskens

The research presented in this thesis was performed at the Department of Pharmacology and Toxicology, Radboud Institute for Molecular Life Sciences, Radboudumc, the Netherlands. Financial support was provided by the National Centre for the Replacement, Refinement and Reduction of Animals in Research.

Publication of this thesis was financially supported by the Radboud Institute for Molecular Life Sciences and the Radboud University Nijmegen, the Netherlands.

Copyright © Tom Nieskens 2018

All rights are reserved. No part of this book may be reproduced by any means, without written permission of the author.

ISBN: 978-94-92801-56-2

Cover design, layout and printing: proefschrift-aio.nl

About the cover: Fluorescent image of tight junction protein 1 (ZO-1, *TJP1*) expressed by MDCK cells cultured in the Organoplate™

**Down the kidney tubes:
insights into renal proximal tubule drug handling
to improve *in vitro* nephrotoxicity screening**

Proefschrift

ter verkrijging van de graad van doctor
aan de Radboud Universiteit Nijmegen
op gezag van de rector magnificus prof. dr. J.H.J.M. van Krieken,
volgens besluit van het college van decanen
in het openbaar te verdedigen op
woensdag 28 november 2018
om 10.30 uur precies

door

Tom Theodorus Gerarda Nieskens

geboren op 21 juni 1990
te Roermond

Promotoren

Prof. dr. R. Masereeuw (Universiteit Utrecht)

Prof. dr. F.G.M. Russel

Copromotor

Dr. ing. M.J.G. Wilmer

Manuscriptcommissie

Prof. dr. L.B. Hilbrands (voorzitter)

Prof. dr. P. Jennings (Vrije Universiteit Amsterdam)

Dr. ing. B. Smeets

Contents

Chapter 1	Introduction and Outline	7
Part I	2D Renal Proximal Tubule <i>In Vitro</i> Models to Evaluate Drug-Induced Kidney Injury	25
Chapter 2	A Human Renal Proximal Tubule Cell Line with Stable Organic Anion Transporter Expression Predictive for Antiviral Drug-Induced Toxicity	27
Chapter 3	Expression of Organic Anion Transporter 1 or 3 In Human Kidney Proximal Tubule Cells Reduces Cisplatin Sensitivity	53
Chapter 4	Antisense Oligonucleotide Therapy Causes Transient Low Molecular Weight Proteinuria via Competitive Inhibition of Receptor-Mediated Endocytosis in Proximal Tubules	77
Part II	Towards 3D Proximal Tubule <i>In Vitro</i> Models for Drug-Induced Toxicity Screening	95
Chapter 5	Kidney-on-a-Chip Technology for Renal Proximal Tubule Tissue Reconstruction	97
Chapter 6	Screening of Drug-Transporter Interactions in a 3D Microfluidic Renal Proximal Tubule on a Chip	123
Chapter 7	General Discussion	157
Chapter 8	Summary	177
Chapter 9	Samenvatting	183
Chapter 10	Dankwoord	190
	Curriculum vitae	200
	List of publications	202
	PhD portfolio	204



Introduction and Outline

Introduction

The main physiological role of the kidney is to maintain homeostasis of extracellular fluid. To this end, the kidney produces hormones, regulates blood pressure by fluid retention, maintains a physiological pH, retains essential nutrients and eliminates endogenous waste compounds, potentially harmful metabolites and exogenous drugs and toxins^[1,2]. As a consequence, the kidney is also a target for drug-induced injury. The potential of novel chemical entities to induce renal adverse effects is therefore determined in preclinical studies, as part of drug development. Nevertheless, acute kidney injury (AKI) is observed during clinical studies, leading to withdrawal of these compounds at a late stage of development. Improving *in vitro* preclinical evaluation of the nephrotoxic potential of candidate drugs is, therefore, required. The use of human-derived renal cell models that demonstrate proximal tubule characteristics in drug screenings, can be a valid strategy to enhance the success rate of compounds and reduce nephrotoxicity-related drug attrition in late-stage pharmaceutical development.

The clinical impact of drug-induced AKI

AKI is a major health issue with an increasing global incidence. An estimated 2% of hospitalized patients in the USA develop AKI, while the incidence rises to 5%-6% with a reported mortality rate of 15.2% in critically ill patients who require renal replacement therapy, as evaluated by a multinational study. Approximately 20% of hospital- and community acquired cases of AKI are induced by pharmaceutical compounds^[3-5]. AKI is characterized by a sudden decline in kidney function and urine production^[6]. Clinical diagnosis of AKI heavily depends on creatinine levels in serum to estimate the glomerular filtration rate (GFR). However, serum creatinine is a disputable marker for kidney function as it only changes when approximately 50% of GFR has been lost. In addition, it is dependent on other factors such as nutrition and muscle mass, making it unsuitable for early detection of renal damage^[7]. Treatment of AKI is mainly supportive and aims to maintain fluid and electrolyte balance, using hemodialysis when required by severity of the illness^[7]. While less severe AKI is reversible, 30% of patients acquire structural and functional renal aberrations with an increased risk of developing chronic kidney disease (CKD), underlining the importance of preventing renal injury^[3].

AKI is most frequently caused by acute tubular necrosis, following ischemia or exposure to nephrotoxicants. Commonly used potentially nephrotoxic drugs include aminoglycoside and β -lactam antibiotics, nonsteroidal anti-inflammatory drugs,

angiotensin receptor blockers and chemotherapeutics. The susceptibility of the kidneys to drug-induced injury is high, since they receive 20% to 25% of cardiac output volume, causing a high delivery rate of potentially harmful substances by the blood^[8]. Nephrotoxicity is further enhanced by the extensive concentrating ability of the renal tubules, increasing the exposure of (filtered) compounds in the tubule lumen. In addition, drug metabolism in the kidney by CYP450 and UDP-glucuronosyltransferase enzymes may result in production of toxic metabolites. Finally, extensive trafficking of compounds leading to a potential competition for apical secretory transporters, enhances drug accumulation and drug-induced toxicity, predominantly in the renal tubules. These transport processes are energy-dependent and particularly the proximal tubule is equipped with a high abundance of mitochondria to produce the required ATP by oxidative phosphorylation (OXPHOS). Hence, damage to the OXPHOS pathway increases drug-sensitivity of the renal tubules further^[9].

The role of proximal tubules in renal clearance of therapeutic drugs

Every healthy human kidney contains approximately 1 million filtration units, the nephrons (Figure 1.1A, B). The nephron is a complex 3D structure, encapsulated by extracellular matrix (ECM) and has an extensive vascular network. The glomerulus and renal tubules represent the functional units of the nephron, which facilitate filtration and both active and passive secretion and reabsorption of compounds, respectively. The section just downstream of the glomerulus, the proximal tubule, is lined with a tight monolayer of epithelial cells, which play a crucial role in renal excretion of drugs from plasma into urine (Figure 1.1C). The apical membrane, or brush border, of proximal tubule epithelial cells (PTEC) faces the tubular lumen, while the basolateral membrane is directed towards the interstitium and blood capillaries. The proximal tubule reabsorbs nutrients from the glomerular filtrate, which include water, glucose, amino acids and low-molecular weight proteins, and actively secretes protein-bound waste metabolites, endogenous and exogenous toxins, including therapeutic drugs^[1]. To this end, PTEC express dedicated membrane-spanning proteins termed drug transporters^[2,10]. Protein-bound waste metabolites and xenobiotics are actively taken up from the basolateral side by solute carrier (SLC) transporters, and transported into the tubule lumen by both SLC and ATP-binding cassette (ABC) transporters. SLC transporters are symporters, that derive the energy required to move a compound against an electrochemical gradient by coupling it to the movement of a second compound along its concentration gradient, or uniporters, that only facilitate transport along a concentration gradient; while ABC transporters hydrolyze ATP

to drive the cellular extrusion of compounds. Mediators of drug influx include the basolaterally expressed organic cation transporter 2 (OCT2/*SLC22A2*), organic anion transporter 1 (OAT1/*SLC22A6*) and 3 (OAT3/*SLC22A8*). Drugs are secreted into the proximal tubule lumen by apically located P-glycoprotein (Pgp/*ABCB1*), multidrug resistance protein 2 (MRP2/*ABCC2*) and 4 (MRP4/*ABCC4*), breast cancer resistance protein (BCRP/*ABCG2*), multidrug and toxin extrusion protein 1 (MATE1/*SLC47A1*) and 2-k (MATE2-k/*SLC47A2*). Organic cations are typically imported by OCT2, driven by the inward-directed negative membrane potential, followed by export mainly via MATE1 and MATE2-k, in exchange of H⁺ from the weakly acidic glomerular filtrate^[11, 12]. Classic examples of drugs cleared by the organic cation pathway include the chemotherapeutic cisplatin^[13], the antidiabetic metformin^[14, 15] and the histamine receptor antagonist cimetidine^[15, 16]. Organic anions are generally imported by OAT1 and OAT3 in exchange of dicarboxylates, mainly α -ketoglutarate, before being secreted by MRP2, MRP4 or BCRP^[17]. Typical examples of drugs cleared by the organic anion pathway include the chemotherapeutic methotrexate^[18, 19]; the antiviral agents adefovir and tenofovir^[20, 21]; the cholesterol-lowering drugs pitavastatin and rosuvastatin^[22-25]; and probenecid for treatment of hyperuricemia and gout^[26].

Regulatory pathways for drug transporters in the human renal proximal tubule have recently received increased attention, but knowledge is mostly limited to animal data. Examples include the glucocorticoid hormones, which induce Mrp2-mediated transport in killifish proximal tubules; and endothelin-1 which regulates Pgp- and MRP2-mediated transport in killifish and MDCK cells, in response to aminoglycoside antibiotics^[27]. In addition, the nephroprotective Nrf2 pathway induced protein expression of Mrp2 and Mrp4 in rat PTEC, following exposure to cisplatin^[28]. More recently, Nrf2 activation was demonstrated to reduce expression of OCT2 and increase expression of MATE1, in rat-derived kidney slices and human-derived PTEC, respectively, leading in both cases to reduced cisplatin-induced nephrotoxicity^[29, 30]. In a human-derived proximal tubule model, ciPTEC, the epidermal growth factor receptor (EGFR) recombinant antibody, cetuximab, downregulates OAT1 and BCRP while upregulating Pgp and MRP4 through the PI3K-AKT and MAPKK-ERK pathways^[31]. In addition, microenvironmental cues affect drug transporter expression, as recently evidenced for flow-mediated regulation of MATE2-k via the Nrf2 pathway^[32]. A thorough understanding of the regulatory pathways of drug transporters in the human proximal tubule is important to find new therapeutic avenues to modulate renal drug clearance and limit toxicity.

In addition to membrane transporters, receptor-mediated endocytosis is important in reabsorbing nutrients, peptides and proteins from the glomerular filtrate and drug exposure. PTEC express multi-ligand receptors megalin (*LRP2*) and cubilin (*CUBN*) at

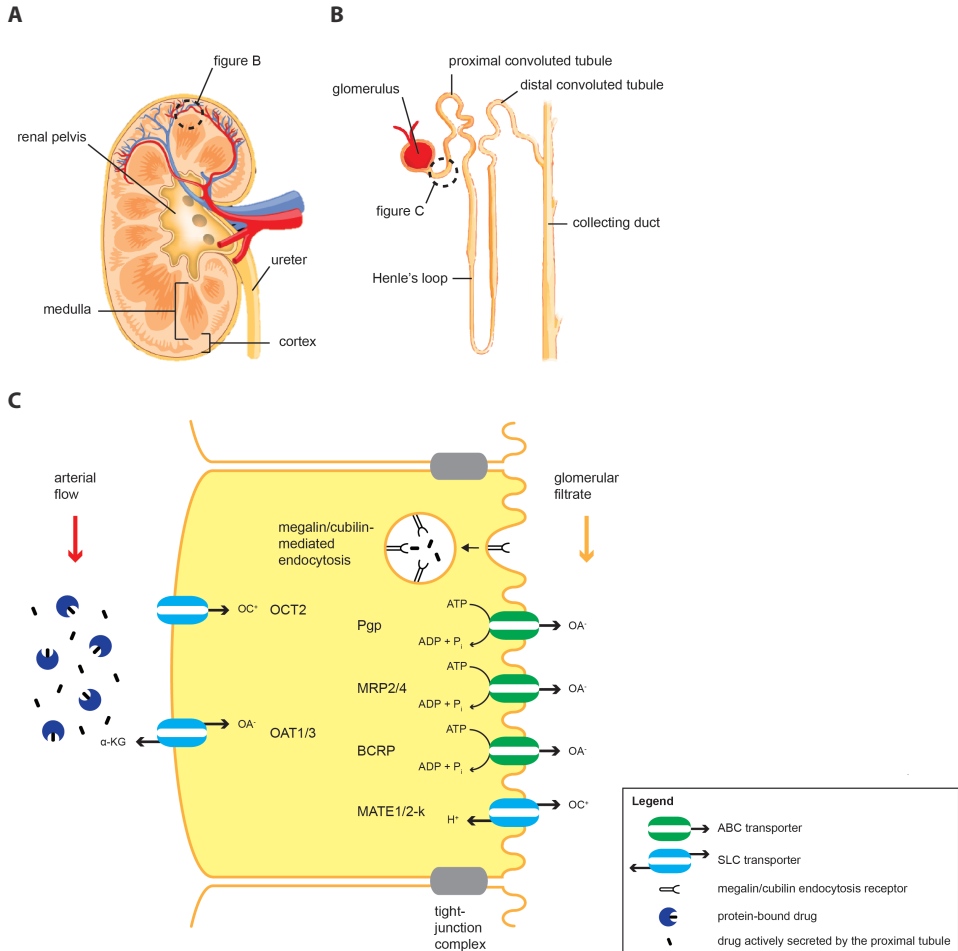


Figure 1.1 Renal anatomy and xenobiotic handling. (A) Sagittal section of the kidney, demonstrating the medulla and the cortex. (B) The renal tubule system; the glomerulus and the proximal tubule are located in the cortex, while the remainder of the tubule is primarily located in the medulla. (C) Schematic overview of the proximal tubule cell, demonstrating trans-membrane transport proteins involved in xenobiotic handling. SLC transporters (light blue) located at the basolateral membrane mediate active influx of protein-bound drugs into the proximal tubule cell, shifting the equilibrium towards the freely available drug fraction, using transport of compounds (α -ketoglutarate) down their concentration gradient (OAT) or the membrane potential (OCT) as driving force. SLC transporters and ABC transporters (green) located on the apical membrane mediate active efflux of drugs into the tubule lumen, using transport of compounds (H^+) down their concentration gradient or the hydrolysis of ATP into ADP as driving force, respectively. Low-molecular weight proteins are freely filtered by the glomerulus and subsequently reabsorbed into proximal tubule cell by multi-ligand receptor (megalins/cubilin)-mediated endocytosis. Abbreviations: ABC, ATP-binding cassette; α -KG, α -ketoglutarate; BCRP, breast cancer resistance protein; OA⁻, organic anion; OAT, organic anion transporter; OC⁺, organic cation; OCT, organic cation transporter; Pgp, P-glycoprotein; MATE, multidrug and toxin extrusion transporter; MRP, multiresistance protein; SLC, solute carrier. Adapted from^[83].

the apical membrane, which bind low-molecular weight proteins from the glomerular filtrate, such as α 1- and β 2-microglobulin, followed by reabsorption via endocytosis and eventually lysosomal degradation. Drugs and toxins demonstrated to be internalized by receptor-mediated endocytosis include the aminoglycoside antibiotic gentamicin, the phytochemical aristolochic acid and heavy metal cadmium^[33,34].

Transport proteins, similar to drug-metabolizing enzymes, are well-described targets for drug-drug interactions (DDIs) that may affect the pharmacokinetic profile of a drug. DDIs in the kidney usually result in decreased renal clearance of the victim drug involved, hence increasing its plasma concentration and systemic exposure, or increasing the concentration in renal tubular cells. Widely studied renal interactions involve probenecid or cimetidine, interacting on OAT transporters; or on OCT and MATE transporters, respectively. A historical clinical application is the co-administration of penicillin and probenecid, reducing renal clearance and dosing requirements of penicillin^[35]. Similarly, co-administration of the antiviral drug cidofovir and probenecid leads to reduced accumulation of cidofovir in the tubular cells and protects against drug-induced nephrotoxicity^[36]. However, DDIs often lead to adverse effects, both systemic and renal. When cimetidine and metformin are co-administered, the resulting interaction on MATE efflux transporters leads to increased concentrations of metformin, in the kidney and blood circulation, causing an increased risk for developing systemic toxicity^[37]. Similar observations have been made for cisplatin-induced nephrotoxicity in mice, which was enhanced by co-administration of the MATE-inhibitor pyrimethamine, suggesting a DDI on MATE1, causing increased proximal tubule accumulation of cisplatin^[38]. As DDIs may influence plasma concentrations, renal clearance rates and adverse effects on the kidney, the regulatory agencies (EMA and FDA) require for the renal transporters Pgp, BCRP, OAT1/3, OCT2 and MATE1/2-k to evaluate potential DDIs during drug development^[39,40].

The current status of nephrotoxicity screening in drug development

Over the past century, drug research has undisputedly contributed to the progress in medicine. Drug development has evolved from the isolation of morphine in 1815 as a purely empirical endeavor, and the coincidental discovery of penicillin in 1929, to a mature science capable of systematically developing the first tyrosine-kinase inhibitor imatinib at the end of the 20th century, for which a complete understanding of the pathology-related molecular mechanism was required^[41]. Therapeutic drugs are highly valued molecules and have become the cornerstone of modern

healthcare. While the medical benefits are clear, the costs of successfully developing a therapeutic molecule have been rising for several years and are estimated to range from approximately 600 million to several billion US-dollars^[42-44]. The number of new drug approvals, on the other hand, has only recently started to rise again after two decades of declining trends^[45], likely explained by an enhanced standard care and increased complexity of diseases for which drugs are being developed. Even for compounds that have entered first-in-man clinical trials, the rate of successful registration is only 11%. Lack of efficacy and lack of safety are the main causes for clinical drug attrition, accounting for a substantial 30% each^[46]. Cardiovascular and liver toxicity are the most common targets for drug-induced toxicity with 17-27% and 14%, respectively; while overall nephrotoxicity accounts for less than 10%^[47, 48]. Adverse effects on the kidney, however, arise more often during the clinical phases of drug development, where it accounts for 9% of drug attrition^[49]. This suggests that currently used preclinical models, both *in vitro* and *in vivo*, lack predictive value for clinically observed renal adverse effects. While *in vivo* animal models, mainly rodents, provide a physiological background, including drug disposition and metabolism, they demonstrate inherent interspecies differences and ethical opposition. Therefore, increasing attention has been generated for conducting research according to the 3Rs, involving Refinement, Reduction and Replacement of animal models in research. *In vitro* models, on the other hand, often lack human- and tissue-relevant expression of transporters and metabolic enzymes, which are crucial for drug-induced toxicity evaluation. To overcome these issues and accurately predict nephrotoxicity in the early phases of drug development, inexpensive and robust *in vitro* cell culture models are being developed that reflect the differentiation status of human renal PTEC, which are compatible with high-throughput drug screening^[50].

In vitro models used for drug-induced nephrotoxicity screening are mostly based on regular 2D culture systems. In the past, non-human derived cell lines were used extensively as models to predict nephrotoxicity, including Madin-Darby canine kidney (MDCKII) and proximal-like Lilly Laboratories Cell Porcine Kidney (LLC-PK1) cells. These models are stable cell lines and form tight epithelial monolayers, but their predictive value is low, mainly due to interspecies differences and the lack of functional differentiation^[51]. Frequently used human-derived models include human embryonic kidney 293 (HEK293) and human kidney-2 (HK-2) cell lines. While HEK293 cells are useful for overexpression of transport proteins, and are therefore suitable to study DDIs on the single transporter level and the contribution of a single transporter to drug-induced toxicity, this cell line expresses neuronal markers, rendering it irrelevant for studying integrated renal toxicity^[51-53]. HK-2 cells on the other hand, demonstrate limited functional differentiation of PTEC, including gene expression

of efflux transporters Pgp and MRP4, but lack expression of influx transporters^[53, 54]. These cells are therefore of limited value. Primary PTEC, which are freshly isolated from human tissue, resemble the physiological state of proximal tubule epithelial cells best. After 10 days in culture, they form tight junctions and demonstrate similar gene expression of OAT1, Pgp and BCRP compared to native human kidney cortex, while OAT3 and OCT2 are reduced^[55]. Active transport of para-aminohippuric acid (PAH), triethalonamide (TEA) and verapamil, demonstrating functionality of OAT, OCT and Pgp transporters, respectively, was found in primary PTEC, but only at 5 days in culture after the cells were passed once^[56]. Although this indicates that these models are valuable, they are dependent on supply of human renal cortex tissue, have limited proliferative capacity, suffer from dedifferentiation upon culturing and demonstrate high inter-donor variability^[53]. For toxicity screening in pharmaceutical industry, models with a more reproducible phenotype and continuous supply of material are required. Stable cell lines, including conditionally immortalized proximal tubule epithelial cells (ciPTEC) and renal proximal tubule epithelial cells (RPTEC/TERT1), do not suffer from these issues. ciPTEC were immortalized by expression of human telomerase reverse transcriptase (hTERT), in combination with temperature-sensitive expression of the SV40 large T antigen^[57]. These immortalized cells maintain endogenous expression and function of drug transporters, including OCT2, Pgp, MRP2/4, BCRP and receptor-mediated endocytosis^[57, 58]. In addition, matured monolayers of ciPTEC form tight junctions, as demonstrated by zonula occludens-1 (ZO-1) localization, they express primary cilia and demonstrate functional expression of phase-II enzymes UDP-glucuronosyltransferases (UGTs), which mediate conjugation of glucuronic acid to xenobiotics to enhance their urinary excretion^[59, 60]. Moreover, a hollow fiber-based 3D culture of ciPTEC demonstrated transepithelial transport of albumin-bound uremic toxins indoxyl sulphate and kynurenic acid, indicating that this *in vitro* proximal tubule model is an established and useful tool to study renal clearance and therefore drug-induced toxicity^[61]. Similar to ciPTEC, the RPTEC/TERT1 cell line was immortalized by expression of human telomerase reverse transcriptase (hTERT)^[62]. This cell line demonstrates proximal tubule characteristics, including ZO-1, endogenous gene expression of drug transporters, including OCT2, OAT1, OAT3, MATE1 and MATE2-k, and maintain transport function of Pgp, OCT2 and receptor-mediated endocytosis^[62, 63]. So far, functionality of OAT1 and OAT3 has not been demonstrated in RPTEC/TERT1. Finally, human embryonic stem cells (hESC) and induced pluripotent stem cells (iPSCs) are promising future opportunities to generate relevant *in vitro* models for drug-induced toxicity screening, as differentiation can be directed towards proximal tubule cells by exposure to medium supplemented with bone morphogenic protein 2 and 7^[64, 65]. Characterization of hESC-derived PTEC revealed gene expression of relevant drug transporters, although only Pgp expression was increased compared to

undifferentiated hESC cells^[65]. Proximal tubule cells derived from iPSCs demonstrated increased expression of hallmark genes aquaporin 1 (AQP1), γ -glutamyltransferase 1 (GGT1), and drug transporters OAT1/3 and OCT2, compared to undifferentiated iPSC. However, a high cisplatin concentration was needed to evaluate its toxic effect^[64]. Therefore, the differentiation status of these human-derived cells needs to be investigated and tailored further towards the proximal tubule epithelial phenotype, before they provide a suitable model for studying drug-induced toxicity.

In vitro drug-induced toxicity screening using monolayer cultures has the advantage of being simple and low in cost, is compatible with high-throughput systems, and has generated much of our current mechanistic understanding of nephrotoxicity. A representative example of drug screening includes the evaluation of a panel of 14 different well-known nephrotoxicants on the biochemical markers lactate production, ATP production, glutathione levels and cell viability, using regular *in vitro* cultures of the human-derived proximal tubule cell line RPTEC/TERT1. The same model was also applied for mechanistic investigation of cisplatin-induced toxicity at pharmacologically relevant concentrations^[66, 67]. To increase the physiological relevance and sensitivity of renal drug-induced toxicity testing, 3D culture models have gained increasing interest. Distinct approaches to develop 3D culture models have been published, including organoid cultures, *in vitro* bioengineered kidneys and microfluidic kidney-on-a-chip devices, each displaying unique advantages and disadvantages^[68, 69]. Supportive evidence for the hypothesis that 3D renal culture models improve sensitivity of drug-induced toxicity testing was generated using 3D organoid cultures of hTERT-immortalized human renal cortical epithelial (NKI-2) cells, embedded in extracellular matrix of matrigel and collagen I^[70]. Using lactate dehydrogenase (LDH) leakage and kidney injury molecule 1 (KIM-1) expression as markers for toxicity induced by cisplatin, an increased sensitivity was found in 3D cultures, compared to monolayers of the same cells^[70]. Advanced 3D models that resemble the morphology of the nephron best, are the rudiments of *in vitro* bioengineered kidney. Single cell suspensions of isolated epithelial ureteric bud cells, representing renal progenitor cells, develop autonomously into rudimentary kidneys organized around a single collecting duct that demonstrate morphologically distinct structures, such as loops of Henle. Activity of OAT, OCT and MRP drug transporters was demonstrated using fluorescent model substrates and inhibitors, indicating the potential of this 3D renal model to study transport and mechanistic evaluation of drug-induced toxicity^[71]. Kidney organoids derived from iPSCs are of special interest in this regard, as these can be acquired from human skin and adipose tissue while reducing the need for animal-derived material at the same time. Using induction of canonical Wnt signaling in iPSC aggregates, self-organizing nephrons developed

in vitro, surrounded by renal interstitium and endothelial cells. Nephron segments including proximal tubules were shown, which are sensitive to cisplatin-induced toxicity^[72]. Using similar techniques, human iPSCs-derived proximal tubule cells were shown to grow into 2D and 3D nephron-like structures, mimicking the *in vivo* developmental nephrogenesis process in a culture dish. In response to cisplatin and gentamicin, these organoids increased the expression of KIM-1^[73].

An important renal characteristic that is missing from the 3D models described so far is fluid flow. As the kidneys filter blood, glomerular filtrate enters the tubule lumen exposing proximal tubule cells to an estimated pulsatile fluid shear stress of 1 dyne·cm⁻²^[74]. Each proximal tubule cell presents a single sensory organelle protruding from the apical membrane, the primary cilium, which transduces fluid shear stress into intracellular signaling and contributes to the differentiation of tubule epithelial tissue^[75]. Supportive evidence that fluid shear stress improves drug-induced responses of PTEC, was generated using MDCK cells cultured on a fibronectin-coated chip surface^[76]. Compared to MDCK cells cultured statically, fluid shear stress increased gene expression of MRP4 (*ABCC4*) and -5 (*ABCC5*) and, moreover, reduced integrin-related gene expression in response to treatment with the antineoplastic drug ifosfamide^[76, 77]. In addition, receptor-mediated endocytosis of albumin was increased when opossum kidney (OK) cells and LLC-PK1 cells were exposed to a fluid shear stress of 0.1 dyne·cm⁻²^[78]. Despite the limited relevance of animal-derived cell lines for drug-induced toxicity screening, these models successfully demonstrated the influence of flow-mediated signal transduction on renal tubule transport function.

The most promising approach for 3D renal culture models in drug development that enables exposure to fluid shear stress, is the kidney-on-a-chip. These microfluidic-based devices allow for 3D cultures of PTEC in a perfused microchannel, with the aim to recapitulate the microphysiological niche of the kidney tubule and to achieve more *in vivo*-like cellular responses compared to regular 2D tissue culture^[69, 79]. Important characteristics include a tubule architecture, incorporation of extracellular matrix, multiple compartments to facilitate evaluation of renal clearance, and exposure to fluid shear stress^[69, 80]. Jang and colleagues recapitulated the renal tubule by culturing human primary tubule cells on a collagen-type IV-coated porous membrane in a polydimethylsiloxane (PDMS)-based microfluidic device, that allows for exposure to a physiological fluid shear stress of 0.2 dyne·cm⁻²^[81]. Confluent monolayers demonstrated expression of tight junction protein ZO-1 and expression of Na,K-ATPase, which was restricted to the basolateral membrane, indicating maintained polarization of PTEC. Moreover, exposing cells to fluid shear stress increased ZO-1 expression, cell height, receptor-mediated endocytosis of albumin and activity of the Pgp efflux transporter.

Finally, PTEC exposed to fluid shear stress showed reduced leakage of LDH, which indicates that cells are more viable at baseline^[81]. A similar model based on primary renal cortex cells could be developed into a tubule-shaped architecture, further increasing physiological resemblance. Directed transport of PAH across the epithelial cell layer was observed, underlining that functional differentiation of proximal tubule cells is maintained in this model^[82]. As this kidney-on-a-chip model allowed for preservation of human PTEC characteristics, it demonstrates the value of increased physiological relevance of 3D culture systems. Its implementation potential for drug-induced toxicity screening in industry is, however, limited as these novel models usually lack high-throughput capacity.

Outline of the thesis

As current preclinical drug-induced nephrotoxicity studies lack predictive value, human-derived cell culture-based proximal tubule models with increased physiological relevance are required to provide a better platform for evaluating DDIs and drug-induced toxicity screening. Safety-related drug attrition in clinical phases of drug development can be reduced as a result, as well as the associated costs and use of animal models in preclinical studies. The aim of this thesis was to gain further insight into the role of drug transporters and endocytic receptors in drug-induced proximal tubule cytotoxicity, and to use this knowledge to develop advanced *in vitro* high-throughput renal toxicity screening models.

After this introduction, the development of such an advanced *in vitro* cell model is described in **Chapter 2**. Conditionally immortalized proximal tubule epithelial cell lines (ciPTEC) constitutively expressing OAT1 (ciPTEC-OAT1) or OAT3 (ciPTEC-OAT3) were generated. To determine their additional value, the contribution of OATs to DDIs and cytotoxicity induced by antiviral agents was tested. Building on these proximal tubule models that overexpress OAT1 or 3, the differential sensitivity to cisplatin, a chemotherapeutic drug that is typically handled by organic cation transporters, is studied in detail in **Chapter 3**. Using gene expression and an ASP⁺-based fluorescent transport assay, the mechanisms responsible for this observation are partly elucidated. Continuing on renal mechanisms of drug handling, the role of receptor mediated endocytosis in proximal tubule uptake and accumulation of antisense oligonucleotides (AONs) is unraveled in **Chapter 4**. To this end, low-molecular weight proteinuria was mimicked *in vitro* and trafficking of tagged AONs was evaluated by fluorescence microscopy. **Chapter 5** reviews the application of kidney-on-a-chip technology that potentially increases the physiological relevance and predictive

capacity of proximal tubule epithelial cells *in vitro*. An extensive overview of recent developments in kidney-on-a-chip platforms is provided, focusing on drug transporter function, receptor-mediated endocytosis and relevance for drug-induced nephrotoxicity screening. All knowledge gained in the preceding chapters of this thesis is united in **Chapter 6** that describes the development of such a kidney-on-a-chip device. Together, the 3D microfluidic system OrganoPlate® and the proximal tubule model ciPTEC-OAT1, represent a novel high-throughput *in vitro* screening platform for drug-drug interactions, as demonstrated by efflux transporters Pgp and MRP2/4 using fluorescence-based assays. A general discussion of the findings described in this thesis is presented in **Chapter 7**, describing the future and potential use of *in vitro* drug-induced DDI and toxicity screening models from both an academic and industrial perspective, followed by a summary of this thesis in **Chapter 8**.

References

1. Hoenig MP, Zeidel ML. Homeostasis, the milieu interieur, and the wisdom of the nephron. *Clin J Am Soc Nephrol.* 9, 1272-1281 (2014).
2. Nigam SK, Wu W, Bush KT, Hoenig MP, Blantz RC, Bhatnagar V. Handling of Drugs, Metabolites, and Uremic Toxins by Kidney Proximal Tubule Drug Transporters. *Clin J Am Soc Nephrol.* 10, 2039-2049 (2015).
3. Liangos O, Wald R, O'Bell JW, Price L, Pereira BJ, Jaber BL. Epidemiology and outcomes of acute renal failure in hospitalized patients: a national survey. *Clin J Am Soc Nephrol.* 1, 43-51 (2006).
4. Uchino S, Kellum JA, Bellomo R, Doig GS, Morimatsu H, Morgera S, Schetz M, et al. Acute renal failure in critically ill patients: a multinational, multicenter study. *Jama.* 294, 813-818 (2005).
5. Xue JL, Daniels F, Star RA, Kimmel PL, Eggers PW, Molitoris BA, Himmelfarb J, et al. Incidence and mortality of acute renal failure in Medicare beneficiaries, 1992 to 2001. *J Am Soc Nephrol.* 17, 1135-1142 (2006).
6. Mehta RL, Kellum JA, Shah SV, Molitoris BA, Ronco C, Warnock DG, Levin A. Acute Kidney Injury Network: report of an initiative to improve outcomes in acute kidney injury. *Crit Care.* 11, R31 (2007).
7. Bellomo R. Acute renal failure. *Semin Respir Crit Care Med.* 32, 639-650 (2011).
8. Perazella MA. Renal vulnerability to drug toxicity. *Clin J Am Soc Nephrol.* 4, 1275-1283 (2009).
9. Hall AM, Unwin RJ. The not so 'mighty chondrion': emergence of renal diseases due to mitochondrial dysfunction. *Nephron Physiol.* 105, p1-10 (2007).
10. George B, You D, Joy MS, Aleksunes LM. Xenobiotic transporters and kidney injury. *Adv Drug Deliv Rev.* 116, 73-91 (2017).
11. Budiman T, Bamberg E, Koepsell H, Nagel G. Mechanism of electrogenic cation transport by the cloned organic cation transporter 2 from rat. *J Biol Chem.* 275, 29413-29420 (2000).
12. Tsuda M, Terada T, Asaka J, Ueba M, Katsura T, Inui K. Oppositely directed H⁺ gradient functions as a driving force of rat H⁺/organic cation antiporter MATE1. *Am J Physiol Renal Physiol.* 292, F593-598 (2007).
13. Yonezawa A, Masuda S, Yokoo S, Katsura T, Inui K. Cisplatin and oxaliplatin, but not carboplatin and nedaplatin, are substrates for human organic cation transporters (SLC22A1-3 and multidrug and toxin extrusion family). *J Pharmacol Exp Ther.* 319, 879-886 (2006).
14. Meyer zu Schwabedissen HE, Verstuyft C, Kroemer HK, Becquemont L, Kim RB. Human multidrug and toxin extrusion 1 (MATE1/SLC47A1) transporter: functional characterization, interaction with OCT2 (SLC22A2), and single nucleotide polymorphisms. *Am J Physiol Renal Physiol.* 298, F997-f1005 (2010).
15. Tanihara Y, Masuda S, Sato T, Katsura T, Ogawa O, Inui K. Substrate specificity of MATE1 and MATE2-K, human multidrug and toxin extrusions/H(+)-organic cation antiporters. *Biochem Pharmacol.* 74, 359-371 (2007).
16. Tahara H, Kusuhara H, Endou H, Koepsell H, Imaoka T, Fuse E, Sugiyama Y. A species difference in the transport activities of H₂ receptor antagonists by rat and human renal organic anion and cation transporters. *J Pharmacol Exp Ther.* 315, 337-345 (2005).
17. Kauffhold M, Schulz K, Brejlik D, Gupta S, Henjakovic M, Krick W, Hagos Y, et al. Differential interaction of dicarboxylates with human sodium-dicarboxylate cotransporter 3 and organic anion transporters 1 and 3. *Am J Physiol Renal Physiol.* 301, F1026-1034 (2011).
18. Takeda M, Khamdang S, Narikawa S, Kimura H, Hosoyamada M, Cha SH, Sekine T, et al. Characterization of methotrexate transport and its drug interactions with human organic anion transporters. *J Pharmacol Exp Ther.* 302, 666-671 (2002).
19. El-Sheikh AA, van den Heuvel JJ, Koenderink JB, Russel FG. Interaction of nonsteroidal anti-inflammatory drugs with multidrug resistance protein (MRP) 2/ABCC2- and MRP4/ABCC4-mediated methotrexate transport. *J Pharmacol Exp Ther.* 320, 229-235 (2007).

20. Ho ES, Lin DC, Mendel DB, Cihlar T. Cytotoxicity of antiviral nucleotides adefovir and cidofovir is induced by the expression of human renal organic anion transporter 1. *J Am Soc Nephrol.* 11, 383-393 (2000).
21. Kohler JJ, Hosseini SH, Green E, Abuin A, Ludaway T, Russ R, Santoianni R, et al. Tenofovir renal proximal tubular toxicity is regulated by OAT1 and MRP4 transporters. *Lab Invest.* 91, 852-858 (2011).
22. Fujino H, Saito T, Ogawa S, Kojima J. Transporter-mediated influx and efflux mechanisms of pitavastatin, a new inhibitor of HMG-CoA reductase. *J Pharm Pharmacol.* 57, 1305-1311 (2005).
23. Windass AS, Lowes S, Wang Y, Brown CD. The contribution of organic anion transporters OAT1 and OAT3 to the renal uptake of rosuvastatin. *J Pharmacol Exp Ther.* 322, 1221-1227 (2007).
24. Hirano M, Maeda K, Matsushima S, Nozaki Y, Kusuhara H, Sugiyama Y. Involvement of BCRP (ABCG2) in the biliary excretion of pitavastatin. *Mol Pharmacol.* 68, 800-807 (2005).
25. Deng JW, Shon JH, Shin HJ, Park SJ, Yeo CW, Zhou HH, Song IS, et al. Effect of silymarin supplement on the pharmacokinetics of rosuvastatin. *Pharm Res.* 25, 1807-1814 (2008).
26. Cutler MJ, Urquhart BL, Velenosi TJ, Meyer Zu Schwabedissen HE, Dresser GK, Leake BF, Tirona RG, et al. In vitro and in vivo assessment of renal drug transporters in the disposition of mesna and dimesna. *J Clin Pharmacol.* 52, 530-542 (2012).
27. Masereeuw R, Russel FG. Regulatory pathways for ATP-binding cassette transport proteins in kidney proximal tubules. *Aaps j.* 14, 883-894 (2012).
28. Aleksunes LM, Goedken MJ, Rockwell CE, Thomale J, Manautou JE, Klaassen CD. Transcriptional regulation of renal cytoprotective genes by Nrf2 and its potential use as a therapeutic target to mitigate cisplatin-induced nephrotoxicity. *J Pharmacol Exp Ther.* 335, 2-12 (2010).
29. Atilano-Roque A, Aleksunes LM, Joy MS. Bardoxolone methyl modulates efflux transporter and detoxifying enzyme expression in cisplatin-induced kidney cell injury. *Toxicol Lett.* 259, 52-59 (2016).
30. Huang D, Wang C, Duan Y, Meng Q, Liu Z, Huo X, Sun H, et al. Targeting Oct2 and P53: Formononetin prevents cisplatin-induced acute kidney injury. *Toxicol Appl Pharmacol.* 326, 15-24 (2017).
31. Caetano-Pinto P, Jamalpoor A, Ham J, Goumenou A, Mommersteeg M, Pijnenburg D, Ruijtenbeek R, et al. Cetuximab Prevents Methotrexate-Induced Cytotoxicity in Vitro through Epidermal Growth Factor Dependent Regulation of Renal Drug Transporters. *Mol Pharm.* 14, 2147-2157 (2017).
32. Fukuda Y, Kaishima M, Ohnishi T, Tohyama K, Chisaki I, Nakayama Y, Ogasawara-Shimizu M, et al. Fluid shear stress stimulates MATE2-K expression via Nrf2 pathway activation. *Biochem Biophys Res Commun.* 484, 358-364 (2017).
33. Zhai XY, Nielsen R, Birn H, Drumm K, Mildnerberger S, Freudinger R, Moestrup SK, et al. Cubilin- and megalin-mediated uptake of albumin in cultured proximal tubule cells of opossum kidney. *Kidney Int.* 58, 1523-1533 (2000).
34. Nielsen R, Christensen EI, Birn H. Megalin and cubilin in proximal tubule protein reabsorption: from experimental models to human disease. *Kidney Int.* 89, 58-67 (2016).
35. Gibaldi M, Schwartz MA. Apparent effect of probenecid on the distribution of penicillins in man. *Clin Pharmacol Ther.* 9, 345-349 (1968).
36. Cundy KC, Petty BG, Flaherty J, Fisher PE, Polis MA, Wachsmann M, Lietman PS, et al. Clinical pharmacokinetics of cidofovir in human immunodeficiency virus-infected patients. *Antimicrob Agents Chemother.* 39, 1247-1252 (1995).
37. Somogyi A, Stockley C, Keal J, Rolan P, Bochner F. Reduction of metformin renal tubular secretion by cimetidine in man. *Br J Clin Pharmacol.* 23, 545-551 (1987).
38. Nakamura T, Yonezawa A, Hashimoto S, Katsura T, Inui K. Disruption of multidrug and toxin extrusion MATE1 potentiates cisplatin-induced nephrotoxicity. *Biochem Pharmacol.* 80, 1762-1767 (2010).
39. Guideline on the investigation of drug interactions. EMA. London (2012)

40. In Vitro Metabolism- and Transporter- Mediated Drug-Drug Interaction Studies, Guidance for Industry. FDA. Rockville, MD (2017).
41. Capdeville R, Buchdunger E, Zimmermann J, Matter A. Glivec (STI571, imatinib), a rationally developed, targeted anticancer drug. *Nat Rev Drug Discov.* 1, 493-502 (2002).
42. DiMasi JA, Grabowski HG, Hansen RW. Innovation in the pharmaceutical industry: New estimates of R&D costs. *J Health Econ.* 47, 20-33 (2016).
43. DiMasi JA, Hansen RW, Grabowski HG. The price of innovation: new estimates of drug development costs. *J Health Econ.* 22, 151-185 (2003).
44. Prasad V, Mailankody S. Research and Development Spending to Bring a Single Cancer Drug to Market and Revenues After Approval. *JAMA Intern Med.* 177, 1569-1575 (2017).
45. Mullard A. 2016 FDA drug approvals. *Nat Rev Drug Discov.* 16, 73-76 (2017).
46. Kola I, Landis J. Can the pharmaceutical industry reduce attrition rates? *Nat Rev Drug Discov.* 3, 711-715 (2004).
47. Guengerich FP. Mechanisms of drug toxicity and relevance to pharmaceutical development. *Drug Metab Pharmacokinet.* 26, 3-14 (2011).
48. Cook D, Brown D, Alexander R, March R, Morgan P, Satterthwaite G, Pangalos MN. Lessons learned from the fate of AstraZeneca's drug pipeline: a five-dimensional framework. *Nat Rev Drug Discov.* 13, 419-431 (2014).
49. Redfern WS, Ewart L, Hammond TG, Bialecki R, Kinter L, Lindgren S, Pollard CE, et al. Impact and frequency of different toxicities throughout the pharmaceutical life cycle. *The Toxicologist.* 114, 1 (2010).
50. Tiong HY, Huang P, Xiong S, Li Y, Vathsala A, Zink D. Drug-induced nephrotoxicity: clinical impact and preclinical in vitro models. *Mol Pharm.* 11, 1933-1948 (2014).
51. Astashkina AI, Mann BK, Prestwich GD, Grainger DW. Comparing predictive drug nephrotoxicity biomarkers in kidney 3-D primary organoid culture and immortalized cell lines. *Biomaterials.* 33, 4712-4721 (2012).
52. Shaw G, Morse S, Ararat M, Graham FL. Preferential transformation of human neuronal cells by human adenoviruses and the origin of HEK 293 cells. *Faseb j.* 16, 869-871 (2002).
53. Van der Hauwaert C, Savary G, Buob D, Leroy X, Aubert S, Flamand V, Hennino MF, et al. Expression profiles of genes involved in xenobiotic metabolism and disposition in human renal tissues and renal cell models. *Toxicol Appl Pharmacol.* 279, 409-418 (2014).
54. Jenkinson SE, Chung GW, van Loon E, Bakar NS, Dalzell AM, Brown CD. The limitations of renal epithelial cell line HK-2 as a model of drug transporter expression and function in the proximal tubule. *Pflugers Arch.* 464, 601-611 (2012).
55. Brown CD, Sayer R, Windass AS, Haslam IS, De Broe ME, D'Haese PC, Verhulst A. Characterisation of human tubular cell monolayers as a model of proximal tubular xenobiotic handling. *Toxicol Appl Pharmacol.* 233, 428-438 (2008).
56. Lash LH, Putt DA, Cai H. Membrane transport function in primary cultures of human proximal tubular cells. *Toxicology.* 228, 200-218 (2006).
57. Wilmer MJ, Saleem MA, Masereeuw R, Ni L, van der Velden TJ, Russel FG, Mathieson PW, et al. Novel conditionally immortalized human proximal tubule cell line expressing functional influx and efflux transporters. *Cell Tissue Res.* 339, 449-457 (2010).
58. Caetano-Pinto P, Janssen MJ, Gijzen L, Verscheijden L, Wilmer MJ, Masereeuw R. Fluorescence-Based Transport Assays Revisited in a Human Renal Proximal Tubule Cell Line. *Mol Pharm.* 13, 933-944 (2016).
59. Jansen J, Schophuizen CM, Wilmer MJ, Lahham SH, Mutsaers HA, Wetzels JF, Bank RA, et al. A morphological and functional comparison of proximal tubule cell lines established from human urine and kidney tissue. *Exp Cell Res.* 323, 87-99 (2014).

60. Mutsaers HA, Wilmer MJ, Reijnders D, Jansen J, van den Broek PH, Forkink M, Schepers E, et al. Uremic toxins inhibit renal metabolic capacity through interference with glucuronidation and mitochondrial respiration. *Biochim Biophys Acta.* 1832, 142-150 (2013).
61. Jansen J, Fedecostante M, Wilmer MJ, Peters JG, Kreuser UM, van den Broek PH, Mensink RA, et al. Bioengineered kidney tubules efficiently excrete uremic toxins. *Sci Rep.* 6, 26715 (2016).
62. Wieser M, Stadler G, Jennings P, Streubel B, Pfaller W, Ambros P, Riedl C, et al. hTERT alone immortalizes epithelial cells of renal proximal tubules without changing their functional characteristics. *Am J Physiol Renal Physiol.* 295, F1365-1375 (2008).
63. Aschauer L, Carta G, Vogelsang N, Schlatter E, Jennings P. Expression of xenobiotic transporters in the human renal proximal tubule cell line RPTEC/TERT1. *Toxicol In Vitro.* 30, 95-105 (2015).
64. Kandasamy K, Chuah JK, Su R, Huang P, Eng KG, Xiong S, Li Y, et al. Prediction of drug-induced nephrotoxicity and injury mechanisms with human induced pluripotent stem cell-derived cells and machine learning methods. *Sci Rep.* 5, 12337 (2015).
65. Narayanan K, Schumacher KM, Tasnim F, Kandasamy K, Schumacher A, Ni M, Gao S, et al. Human embryonic stem cells differentiate into functional renal proximal tubular-like cells. *Kidney Int.* 83, 593-603 (2013).
66. Crean D, Bellwon P, Aschauer L, Limonciel A, Moenks K, Hewitt P, Schmidt T, et al. Development of an in vitro renal epithelial disease state model for xenobiotic toxicity testing. *Toxicol In Vitro.* 30, 128-137 (2015).
67. Wilmes A, Bielow C, Ranninger C, Bellwon P, Aschauer L, Limonciel A, Chassaigne H, et al. Mechanism of cisplatin proximal tubule toxicity revealed by integrating transcriptomics, proteomics, metabolomics and biokinetics. *Toxicol In Vitro.* 30, 117-127 (2015).
68. Breslin S, O'Driscoll L. Three-dimensional cell culture: the missing link in drug discovery. *Drug Discov Today.* 18, 240-249 (2013).
69. Nieskens TT, Wilmer MJ. Kidney-on-a-chip technology for renal proximal tubule tissue reconstruction. *Eur J Pharmacol.* 790, 46-56 (2016).
70. DesRochers TM, Suter L, Roth A, Kaplan DL. Bioengineered 3D human kidney tissue, a platform for the determination of nephrotoxicity. *PLoS One.* 8, e59219 (2013).
71. Lawrence ML, Chang CH, Davies JA. Transport of organic anions and cations in murine embryonic kidney development and in serially-reaggregated engineered kidneys. *Sci Rep.* 5, 9092 (2015).
72. Takasato M, Er PX, Chiu HS, Maier B, Baillie GJ, Ferguson C, Parton RG, et al. Kidney organoids from human iPS cells contain multiple lineages and model human nephrogenesis. *Nature.* 526, 564-568 (2015).
73. Morizane R, Lam AQ, Freedman BS, Kishi S, Valerius MT, Bonventre JV. Nephron organoids derived from human pluripotent stem cells model kidney development and injury. *Nat Biotechnol.* 33, 1193-1200 (2015).
74. Weinbaum S, Duan Y, Satlin LM, Wang T, Weinstein AM. Mechanotransduction in the renal tubule. *Am J Physiol Renal Physiol.* 299, F1220-1236 (2010).
75. Praetorius HA. The primary cilium as sensor of fluid flow: new building blocks to the model. A review in the theme: cell signaling: proteins, pathways and mechanisms. *Am J Physiol Cell Physiol.* 308, C198-208 (2015).
76. Snouber LC, Letourneur F, Chafey P, Broussard C, Monge M, Legallais C, Leclerc E. Analysis of transcriptomic and proteomic profiles demonstrates improved Madin-Darby canine kidney cell function in a renal microfluidic biochip. *Biotechnol Prog.* 28, 474-484 (2012).
77. Choucha Snouber L, Jacques S, Monge M, Legallais C, Leclerc E. Transcriptomic analysis of the effect of ifosfamide on MDCK cells cultivated in microfluidic biochips. *Genomics.* 100, 27-34 (2012).
78. Raghavan V, Rbaibi Y, Pastor-Soler NM, Carattino MD, Weisz OA. Shear stress-dependent regulation of apical endocytosis in renal proximal tubule cells mediated by primary cilia. *Proc Natl Acad Sci U S A.* 111, 8506-8511 (2014).

79. Wilmer MJ, Ng CP, Lanz HL, Vulto P, Suter-Dick L, Masereeuw R. Kidney-on-a-Chip Technology for Drug-Induced Nephrotoxicity Screening. *Trends Biotechnol.* 34, 156-170 (2016).
80. Bhatia SN, Ingber DE. Microfluidic organs-on-chips. *Nat Biotechnol.* 32, 760-772 (2014).
81. Jang KJ, Mehr AP, Hamilton GA, McPartlin LA, Chung S, Suh KY, Ingber DE. Human kidney proximal tubule-on-a-chip for drug transport and nephrotoxicity assessment. *Integr Biol (Camb).* 5, 1119-1129 (2013).
82. Weber EJ, Chapron A, Chapron BD, Voellinger JL, Lidberg KA, Yeung CK, Wang Z, et al. Development of a microphysiological model of human kidney proximal tubule function. *Kidney Int.* 90, 627-637 (2016).
83. Bear R, Rintoul D. Urinary System. Web Page. OpenStax (2013). <http://cnx.org/contents/SKih6aFN@5/Urinary-System>.



Part I

2D Renal Proximal Tubule *In Vitro* Models to Evaluate Drug-Induced Kidney Injury



A Human Renal Proximal Tubule Cell Line with Stable Organic Anion Transporter 1 and 3 Expression Predictive for Antiviral Drug-Induced Toxicity

Tom TG Nieskens¹, Janny GP Peters¹, Marieke J Schreurs¹, Niels Smits¹, Rob Woestenenk², Katja Jansen¹, Thom K van der Made¹, Melanie Röring¹, Constanze Hilgendorf³, Martijn J Wilmer^{1*} and Rosalinde Masereeuw^{1,4*}

¹ Department of Pharmacology and Toxicology, Radboud university medical center, Nijmegen, The Netherlands

² Department of Laboratory Medicine - Laboratory of Hematology, Radboud university medical centre, Nijmegen, The Netherlands

³ AstraZeneca R&D, Innovative Medicines, Drug Safety and Metabolism, Sweden

⁴ Utrecht Institute for Pharmaceutical Sciences, Faculty of Science, Utrecht University, The Netherlands.

*Authors contributed equally

American Association of Pharmaceutical Sciences Journal. 18. 465-75 (2016)

Abstract

Drug-induced nephrotoxicity still hampers drug development, because current translation from *in vitro* or animal studies to human lack high predictivity. Often, renal adverse effects are recognized only during clinical stages of drug development. The current study aimed to establish a robust and a more complete human cell model suitable for screening of drug related interactions and nephrotoxicity. In addition to endogenously expressed renal organic cation transporters and efflux transporters, conditionally immortalized proximal tubule epithelial cells (ciPTEC) were completed by transduction of cells with the organic anion transporter (OAT) 1 or OAT3. Fluorescence-activated cell sorting upon exposure to the OAT substrate fluorescein successfully enriched transduced cells. A panel of organic anions was screened for drug-interactions in ciPTEC-OAT1 and ciPTEC-OAT3. The cytotoxic response to the drug-interactions with antivirals was further examined by cell viability assays. Upon subcloning, concentration-dependent fluorescein uptake was found with a higher affinity for ciPTEC-OAT1 ($K_m = 0.8 \pm 0.1 \mu\text{M}$) than ciPTEC-OAT3 ($K_m = 3.7 \pm 0.5 \mu\text{M}$). Co-exposure to known OAT1 and/or OAT3 substrates (*viz.* para-aminohippurate, estrone sulfate, probenecid, furosemide, diclofenac and cimetidine) in cultures spanning 29 passage numbers revealed relevant inhibitory potencies, confirming the robustness of our model for drug-drug interactions studies. Functional OAT1 was directly responsible for cytotoxicity of adefovir, cidofovir and tenofovir, while a drug-interaction with zidovudine was not associated with decreased cell viability. Our data demonstrate that human-derived ciPTEC-OAT1 and ciPTEC-OAT3 are promising platforms for highly predictive drug screening during early phases of drug development.

Introduction

The renal proximal tubules play a major role in eliminating waste products from the body, including drugs and their metabolites. Their active secretion and reabsorption mechanisms together with biotransformation capacity make proximal tubule cells especially sensitive to drug-induced toxicity and subsequent acute kidney injury (AKI)^[1]. Not surprisingly, nephrotoxicity is a significant cause for drug attrition during pharmaceutical development, often recognized only during clinical stages of development as translation from *in vitro* and animal studies to human lack high predictivity^[2,3].

An *in vitro* model with high predictive value for drug-induced nephrotoxicity should closely reflect the *in vivo* processes involved in renal drug handling. More specific, a robust cell-based model should include a proximal tubule epithelium stably expressing a broad range of functional transporters and metabolic enzymes that act in concert in renal drug elimination^[4]. This process may be affected in concomitant drug treatment, leading to clinically relevant drug-drug interactions (DDI). The renal elimination mechanism of xenobiotics can roughly be divided into two major pathways, viz. the organic anion and the organic cation system. As a first step in elimination of organic anions in humans, active tubular uptake is mediated by the organic anion transporter 1 (OAT1; *SLC22A6*) and organic anion transporter 3 (OAT3; *SLC22A8*) present at the, blood-facing, basolateral side^[5]. These transporters are characterized by their high affinity and capacity and, as a consequence, are major players in the development of drug-induced nephrotoxicity^[6]. After uptake, secretion of anionic compounds into the tubular lumen is facilitated by apically expressed efflux transporters, such as the multidrug resistance proteins 2 and 4 (MRP2 and -4; *ABCC2 and -4*) and breast cancer resistance protein (BCRP; *ABCG2*)^[7]. In parallel, renal elimination of organic cations in the human proximal tubular epithelium is facilitated by basolateral uptake, predominantly via the organic cation transporter 2 (OCT2; *SLC22A2*), and apical efflux via multidrug and toxin extrusion proteins 1 and 2-K (MATE1 and -2-K; *SLC47A1 and -2*)^[8] and P-glycoprotein (P-gp; *ABCB1*)^[9].

Renal drug transporters demonstrate a large overlap in substrate specificity, introducing redundancy in uptake mechanisms of proximal tubule cells and contributing to the relative high sensitivity of the tissue^[6, 10]. This especially counts for organic anions, as this class comprises the majority of drugs that are excreted by the kidneys. Drug-induced nephrotoxicity related to the proximal tubular epithelium by this class of compounds have been described broadly, including for the acyclic nucleotide phosphonates adefovir, cidofovir and tenofovir^[11, 12]. These antiretroviral

compounds are used for treatment of HIV, hepatitis B and cytomegalovirus infections and function as nucleotide analog reverse transcriptase inhibitors (NtRTIs)^[13]. The exact mechanism of antiviral-induced renal toxicity is still under debate^[14], but the involvement of OATs in the uptake of many antivirals has been widely acknowledged^[15-17]. To prevent NtRTIs-induced nephrotoxicity, their uptake can be inhibited by co-administration of an OAT1 inhibitor, such as probenecid^[18]. As with many other diseases, current antiviral therapy in HIV infections is based on polypharmacy. Increased plasma concentrations and systemic toxicity have been observed with didanosine co-administration of tenofovir in anti-HIV triple therapy, possibly by DDI at the site of OAT1 that limited renal excretion^[19]. Together, polypharmacy can optimize the life-span of infected patients, but this strategy simultaneously increases the risk for DDI and demands for personalized evaluation of the benefit/risk ratio for each drug^[20].

The aim of this study was to establish a robust human cell model that allows prediction of drug-induced nephrotoxicity and DDI of organic anions, with a focus on antivirals. We evaluated conditionally immortalized proximal tubule epithelial cells (ciPTEC) as a preclinical *in vitro* prediction model^[21]. This model already demonstrated to be highly predictive for studying DDI at the site of OCT2^[22], and to endogenously exhibit metabolic enzymes^[23] together with a panel of functional efflux transporters^[21, 24]. However, the expression of OAT1 and OAT3 was rapidly lost in culture. Here, these transporters were stably expressed in ciPTEC by transduction, followed by an elegant selection procedure using OAT transporter functionality, completing the relevant renal xenobiotic transporters in ciPTEC. The function of both transporters appeared to be stable upon prolonged culturing. These unique characteristics of the presented OAT containing human cell lines allowed screening for DDI using known pharmacological OAT1 and OAT3 substrates and/or inhibitors. Upon validation, we demonstrated that OAT mediated uptake in ciPTEC are key determinants in antiviral-induced cytotoxicity. These findings underscore that ciPTEC-OAT1 and ciPTEC-OAT3 are valuable tools for drug-induced toxicity screening.

Materials and Methods

Cell culture

Conditionally immortalized proximal tubule epithelial cells (ciPTEC) were developed as described by Wilmer et al. with informed consent of the donors in accordance with the approved guidelines of the Radboud Institutional Review Board^[21]. Cells were seeded 7 days prior to the experiment at their corresponding density (55,000 cells/

cm² for ciPTEC parent cells, 63,000 cells/cm² for ciPTEC-OAT1 and 82,000 cells/cm² for ciPTEC-OAT3) and grown for 1 day at 33°C and 5% v/v CO₂ to allow proliferation, enabled by the temperature-sensitive mutant of SV large T antigen (SV40T). Next, cells were cultured for 6 days at 37°C and 5% v/v CO₂ to stimulate differentiation and formation of an epithelial monolayer, described as ‘maturation’. Cells were cultured using Dulbecco’s modified eagle medium (DMEM HAM’s F12, Life Technologies, Paisly, UK), 5 µg/ml insulin, 5 µg/ml transferrin, 5 µg/ml selenium, 35 ng/ml hydrocortisone, 10 ng/ml epidermal growth factor (EGF), 40 pg/ml tri-iodothyronine (Sigma, St. Louis, USA) and 10% fetal calf serum (FCS, Greiner Bio One, Kremsmuenster, Austria). Medium was refreshed every second day, supplemented with 1% penicillin/streptomycin (pen/strep, Invitrogen, Carlsbad, USA) at 33°C and without pen/strep at the maturation temperature of 37°C. 3T3 mouse-fibroblast (3T3) cells were cultured at 37°C and used only as irradiated non-proliferating feeder cells for sub-cloning procedures upon transduction, as described^[21].

Vector construction

Vector construction was performed using Gateway Cloning Technology (Invitrogen), according to the manufacturer’s instructions. Commercially obtained vectors containing OAT1 (pENTR201-hOAT1, Harvard Plasmids HsCD00044153) and OAT3 (pENTR201-hOAT3, HsCD00044090) were transferred into a pLenti4/V5-DEST vector by LR recombinant reaction, resulting in expression vectors pLenti4/V5-EX-hOAT1 and pLenti4/V5-EX-hOAT3. The inducible CMV-TetO2 promoter was replicated from pcDNA5-FRT-TO (Invitrogen) using primers that introduce ClaI (forward ClaI-CMV-TetO2: GCCGCCATCGATGCCGCCGTTGACATTGATTATTGACT) and EcoRI restriction sites (reverse EcoRI-CMV-TetO2: GCGCGCAATTCGGCGGCCGAGGCTGGATCGGTCCCGG). The resulting PCR product (ClaI-CMV-TetO2-EcoRI) product was purified using the High Pure PCR Product Purification kit (Roche, Basel, Switzerland). Both PCR product and expression vectors were digested by ClaI and EcoRI (New England Biolabs, Ipswich, USA) for 1 hour at 37°C and, after purification, ligation was performed with a 1:3 (insert:vector) unit ratio using T4 ligase (Invitrogen) for 2 h at 37°C, resulting in the pLenti expression constructs (pLenti4/V5-EX-CMV-TetO2-hOAT1 and pLenti4/V5-EX-CMV-TetO2-hOAT3).

OAT transduction in ciPTEC

To obtain lentiviral particles containing the OAT constructs, lentiviral stock was produced by transfecting the pLenti expression constructs with packaging plasmid mix into the HEK293FT cell line using ViraPower Lentiviral Gateway Expression Systems (Invitrogen), according to the manufacturer’s instructions. ciPTEC were cultured to 50-70% confluency and exposed to lentiviral particles for 24 h. Both ciPTEC-OAT1 and

ciPTEC-OAT3 were selected and subcloned to obtain a homogeneous cell population. To this end, transduced ciPTEC-OAT3 cells were plated into 3 separate culture flasks (100, 300 and 900 cells) containing irradiated (30 Gy) non-proliferating 3T3-cells as described by Saleem et al^[25]. After 2-3 weeks, single cell colonies of ciPTEC-OAT3 were picked and cultured. Transduction efficiency for ciPTEC-OAT1 was lower than for ciPTEC-OAT3, making immediate subcloning difficult. Therefore, the heterogeneous cell population of ciPTEC-OAT1 was enriched by positive selection of fluorescein transporting cells. Only successfully transduced ciPTEC express functional OAT; hence, positive selection could be performed upon exposure to the OAT substrate fluorescein using BD FACSAria SORP flow cytometer (BD biosciences, San Jose, USA). 20 million ciPTEC-OAT1 cells were suspended in HBSS (Invitrogen) containing 1 μ M fluorescein and incubated for 10 min at 37°C before fluorescence-activated cell sorting (FACS). Enriched ciPTEC-OAT1 cells were subcloned as described for ciPTEC-OAT3. Both ciPTEC-OAT1 and ciPTEC-OAT3 were cultured for up to 30 passages after transduction to study stability of OAT1 and OAT3 expression.

OAT-mediated fluorescein uptake

To evaluate OAT transporter function and inhibition properties of several known OAT substrates, fluorescein uptake was measured by flow cytometry and multi-plate reader. Mature monolayers of sub-cloned ciPTEC spanning 29 passages were co-incubated with fluorescein (1 μ M, unless stated otherwise) and a test compound in HBSS for 10 min at 37°C. Compounds known for their inhibitory effect on OAT-mediated transport, para-aminohippuric acid (PAH), estrone sulfate, probenecid, furosemide, cimetidine, diclofenac, adefovir, cidofovir, tenofovir and zidovudine, were tested. The organic cation metformin was included as a negative control. All chemicals were obtained from Sigma, unless stated otherwise. Uptake was stopped by washing 3 times with ice-cold HBSS (4°C). For flow cytometry, samples were harvested following fluorescein exposure using trypsin-EDTA, washed, fixed using 0.5% paraformaldehyde and measured using FACS calibur (Becton Dickinson, Franklin Lakes, USA). For 96 well plate assay, cells were lysed by 200 μ l 0.1 M NaOH for 10 min at 37°C and fluorescence was measured (excitation 485 nm, emission 535 nm) using the multiplate reader Victor X3 (Perkin Elmer, Waltham, USA).

Viability assays

To evaluate toxicity induced by antivirals, viability of ciPTEC was evaluated by an MTT assay^[26]. Briefly, monolayers of ciPTEC (96-wells) were exposed to antivirals in serum-free medium (SFM) on day 6 of maturation. Cell toxicity was analyzed further in presence of MRP and BCRP efflux inhibitors MK571 (5 μ M) and KO143 (10 μ M). After incubation for 24, 48 and 72 h at 37°C, ciPTEC were washed and incubated with 0.5

mg/ml thiazolyl blue tetrazolium bromide (MTT, Sigma) for 3 h at 37°C in absence of antivirals. Formazan crystals formed in viable cells were dissolved in dimethyl sulfoxide (DMSO, Merck, Whitehouse Station, USA) and optical density was measured (560 nm, background at 670 nm was subtracted) using Benchmark Plus (Bio-Rad, Hercules, USA).

Gene expressions in ciPTEC

Total RNA was isolated from matured ciPTEC (6-well plates) spanning 10 passages for ciPTEC-OAT1 and 11 passages for ciPTEC-OAT3 using TRIzol (Life Technologies Europe BV) and chloroform extraction. cDNA was synthesized using M-MLV Reverse Transcriptase (Promega, Madison, USA), according to the manufacturer's instructions. The mRNA expression levels were evaluated using gene-specific primer-probe sets obtained from Life Technologies: OAT1 (*SLC22A6*, hs00537914), OAT3 (*SLC22A8*, hs00188599), GAPDH (hs99999905) and TaqMan Universal PCR Master Mix (Applied Biosystems). The quantitative PCR reactions were performed using CFX96-Touch Real Time PCR System (BioRad) and analyzed using BioRad CFX Manager (version 1.6). mRNA-levels for ciPTEC-OAT1 and ciPTEC-OAT3 were calculated using GAPDH as a reference gene and compared to gene expressions in human kidney homogenates in triplicate.

Data analysis

A Michaelis-Menten equation was combined with linear diffusion to fit fluorescein uptake data after background subtraction with GraphPad Prism (version 5.03). For calculation of IC_{50} values, log (concentration inhibitor) versus fluorescein uptake was plotted after background subtraction using GraphPad Prism. For MTT and fluorescein inhibition assays, data were normalized to the viability or activity of untreated control cells. Non-linear regression with variable slope constraining the top to 100% was used to fit the data after background subtraction with GraphPad Prism. Statistics was performed by two-way ANOVA (two-tailed, $\alpha=0.05$) using GraphPad Prism as well. All data is presented as mean \pm SEM of at least three separate experiments (n=3) performed in triplicate, unless stated otherwise.

Results

Functional OAT expression in ciPTEC

The absence of endogenous OAT1 and OAT3 expression in ciPTEC was demonstrated by exposure to fluorescein (1 μM) for 10 min, which did not increase the intracellular fluorescence intensity as measured by flow cytometry (Figure 2.1B, red line). Therefore, OAT transporters were introduced separately by lentiviral transduction. A schematic overview of the experimental approach is provided in Figure 2.1A. The transporter genes *SLC22A6* and *SLC22A8* were cloned under regulation of a CMV promoter and a TetO2 site to conditionally induce the expression. Remarkably, basal expression and function upon transduction of both OAT transporters was positive without tetracycline induction, and was not influenced by this inducer (data not shown). Fluorescein uptake capacity (without induction by tetracycline) was used to discriminate between successfully transduced cells and non-transduced cells, reflected by two sub-populations in the flow cytometer histogram (Figure 2.1C). When exposed to 1 μM fluorescein for 10 min, a small cell population accumulated the fluorescent substrate, which was immediately selected using FACS. The fraction of OAT1 positive cells selected (Figure 2.1D) accounted for only 8.3% of the total population. The enriched population accumulated fluorescein efficiently, and was sensitive to inhibition by para-aminohippuric acid, a known OAT1 substrate and/or inhibitors (Figure 2.1E). The ciPTEC-OAT1 population enriched by FACS and the non-enriched ciPTEC-OAT3 population were subcloned to obtain homogeneous cell populations with high functional OAT transporter expression, demonstrated by qPCR.

Expression levels of OAT1 and OAT3 in the respective cell lines were compared to gene expression levels in human kidney tissue homogenates, resulting in a ratio of 0.7 ± 0.2 and 0.14 ± 0.02 for OAT1 and OAT3, respectively. Intact tubular phenotype was demonstrated by functionally active OCT2, for which a drug-interaction with cimetidine was shown to be similar to the parent cell line (Figure S2.1).

Drug-interaction at the site of OAT1 and OAT3

Transport kinetics of OAT-mediated fluorescein transport was investigated further by studying the time and concentration dependent uptake of the substrate. Fluorescein uptake demonstrated partial saturation in OAT1 and OAT3 expressing cells (Figure 2.2A, B and D) for which a K_m and V_{max} value was determined taking a passive diffusion component k_d into account (Table 2.1). Fluorescein affinity was approximately 5-fold higher for OAT1 than for OAT3. Upon fluorescein exposure (10 min, 1 μM), confocal fluorescent imaging confirmed uptake in ciPTEC-OAT1 and ciPTEC-OAT3 (Figure 2.2C

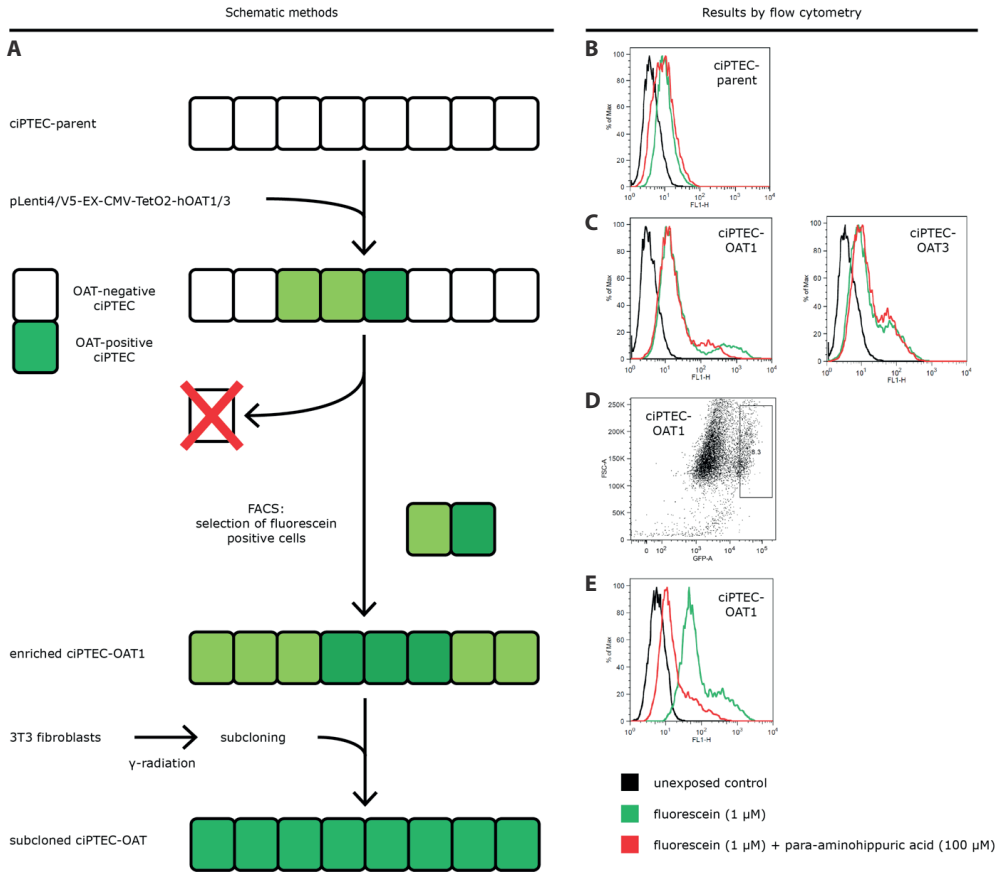


Figure 2.1 Schematic overview of transduction procedure to obtain ciPTEC-OAT1 and ciPTEC-OAT3. (A) CiPTEC parent was transduced with OAT1 or OAT3 lentiviral constructs and enriched by FACS using OATs' capacity to transport fluorescein. Further subcloning using radiated 3T3 fibroblasts as feeder cells resulted in a homogeneous ciPTEC-OAT1 or ciPTEC-OAT3 cell line. Histogram obtained by flow cytometry of (B) ciPTEC parent, (C) ciPTEC-OAT1 and ciPTEC-OAT3 exposed to fluorescein (1 μM, 10 min, green line), fluorescein and para-aminohippuric acid (100 μM, red line), or untreated cells (black line). Parent cells exposed to fluorescein did not show increased fluorescence intensity, while ciPTEC-OAT1 and ciPTEC-OAT3 both showed a sub-population with increased fluorescence indicative for OAT functionality, which is sensitive to para-aminohippuric acid-induced inhibition. (D) Scattered plot showing forward scatter (y-axis) and fluorescein intensity (x-axis) of transduced ciPTEC-OAT1 exposed to 1 μM fluorescein for 10 min. The population with high fluorescence intensity indicated by gate P1 (8.3% of total population) was sorted to enrich successfully transduced ciPTEC-OAT1. Transduction with OAT3 was more efficient than OAT1, represented by the larger positive subpopulation in Figure 2.1C, making the enrichment protocol redundant for ciPTEC-OAT3. (E) Histogram of enriched ciPTEC-OAT1 exposed to fluorescein (1 μM, 10 min) in presence (red line) or absence (green line) of competitor para-aminohippuric acid (100 μM) demonstrates increased fluorescence intensity compared to non-enriched ciPTEC, but a heterogeneous population sensitive to para-aminohippuric acid, pointing towards the requirement of subcloning of the enriched cells.

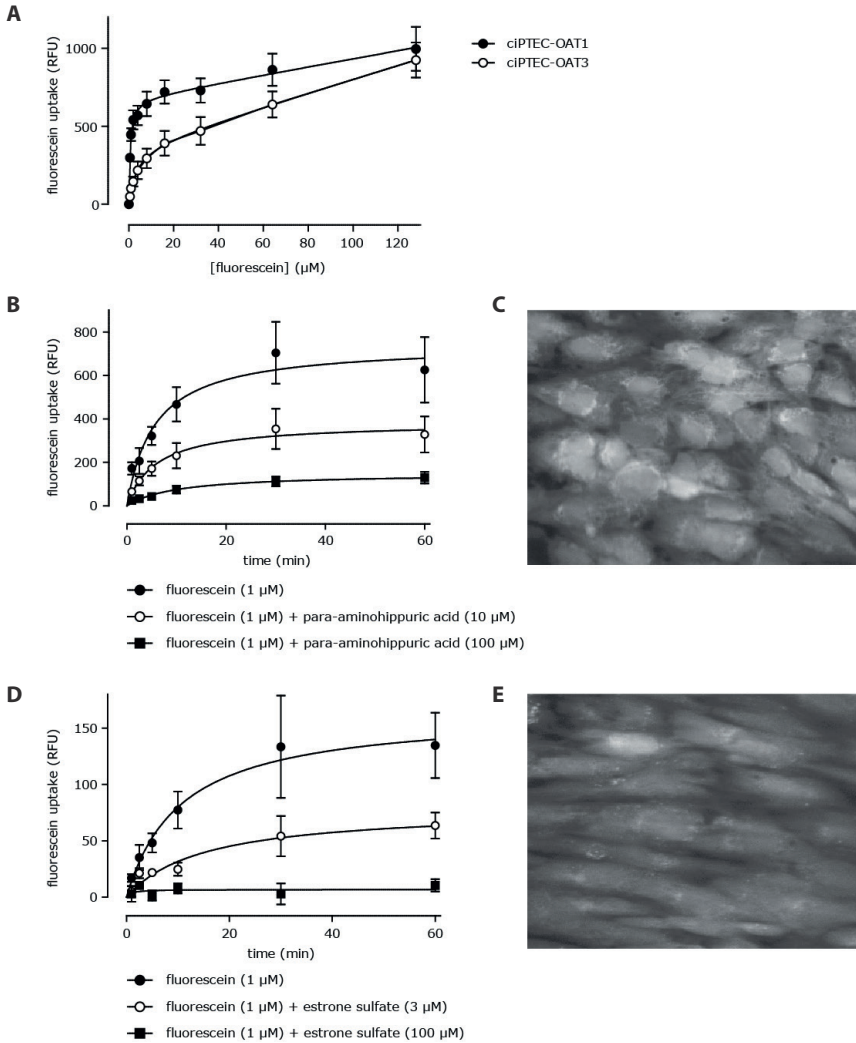


Figure 2.2 OAT-mediated fluorescein uptake in ciPTEC-OAT1 and ciPTEC-OAT3. (A) Concentration-dependent OAT1 and OAT3 mediated uptake of fluorescein after 10 min incubation in ciPTEC-OAT1 and ciPTEC-OAT3. The curve was fitted ($n=4$) according to a Michaelis-Menten model in combination with linear diffusion. (B, C) Fluorescein uptake ($1 \mu\text{M}$) by ciPTEC-OAT1 and (D, E) ciPTEC-OAT3 up to 60 min in absence or presence of two concentrations of the typical inhibitors para-aminohippuric acid (PAH, for ciPTEC-OAT1) or estrone sulfate (ES, for ciPTEC-OAT3). (B, D) The curves were fitted ($n=4$) to a standard saturation model after background subtraction. Analysis using two-way ANOVA indicated significantly decreased uptake curves in both ciPTEC-OAT1 ($10 \mu\text{M}$ and $100 \mu\text{M}$ PAH, $p<0.001$) and ciPTEC-OAT3 ($3 \mu\text{M}$ ES, $p<0.01$; $100 \mu\text{M}$ ES, $***p<0.001$). (C, E) Representative images of fluorescein uptake ($1 \mu\text{M}$) by ciPTEC-OAT1 (C) and ciPTEC-OAT3 (E) after 10 min (magnification 20x).

and E). To demonstrate the uptake was transporter mediated, specific inhibition of fluorescein uptake in presence of two concentrations para-aminohippuric acid (10 and 100 μM) and estrone sulfate (3 and 100 μM) in ciPTEC-OAT1 and ciPTEC-OAT3, was studied (Figure 2.2B and D). CiPTEC-OAT1 and ciPTEC-OAT3 were evaluated further by determination of IC_{50} values using concentration-dependent inhibition of fluorescein uptake in presence of para-aminohippuric acid, estrone sulfate, probenecid, furosemide, cimetidine and diclofenac (Figure 2.3, Table 2.2). Overall, IC_{50} values calculated in our models are in close agreement with previously reported values, although it should be noted that probe substrates may differ and influence IC_{50} values (Table 2.2). Further confirmation of specificity was obtained using metformin, not affecting OAT mediated fluorescein uptake in both ciPTEC-OAT1 and ciPTEC-OAT3, as metformin is an OCT substrate^[27]. The experiments depicted in Figure 3 were performed in cells spanning 29 passages after transduction. The small variations in these data and maintained fluorescein uptake indicate stable transduction and high robustness of transporter function in ciPTEC-OAT1 and ciPTEC-OAT3.

Table 2.1 Michaelis-Menten parameters for OAT-mediated fluorescein uptake in ciPTEC-OAT1 and ciPTEC-OAT3^a.

	ciPTEC-OAT1	ciPTEC-OAT3
K_m (μM)	0.8 \pm 0.1	3.7 \pm 0.5
V_{max} (RFU)	695 \pm 84	384 \pm 103
K_d (RFU \cdot L/ μmol)	2.4 \pm 1.2	4.3 \pm 0.9

^a Data are expressed as mean \pm SEM, n=4.

OATs mediate antiviral-induced toxicity

As toxicity of antivirals was reported to be associated with OAT1 and OAT3 mediated renal tubular uptake, we investigated their effects on OAT function and cell viability upon drug exposures. Concentration-dependent inhibition of fluorescein uptake via OAT1 was observed by adefovir, cidofovir, tenofovir and zidovudine, while OAT3 was only associated with zidovudine-fluorescein interactions (Figure 2.4, Table 2.3). Next, the DDI indices were determined. The United States Food and Drug Administration (FDA) draft a DDI guideline^[28] recommending to perform clinical DDI studies when the ratio between unbound plasma concentration and IC_{50} ($C_{\text{max,u}}/\text{IC}_{50}$) is higher than 0.1. For adefovir, cidofovir and zidovudine the IC_{50} value was less than 10 times the maximal free plasma concentration ($C_{\text{max,u}}/\text{IC}_{50}>0.1$), and, therefore, at clinically relevant plasma concentrations inhibition of OAT1 is likely and DDI with OAT1 transporter substrates were defined as clinically relevant in our study. Next,

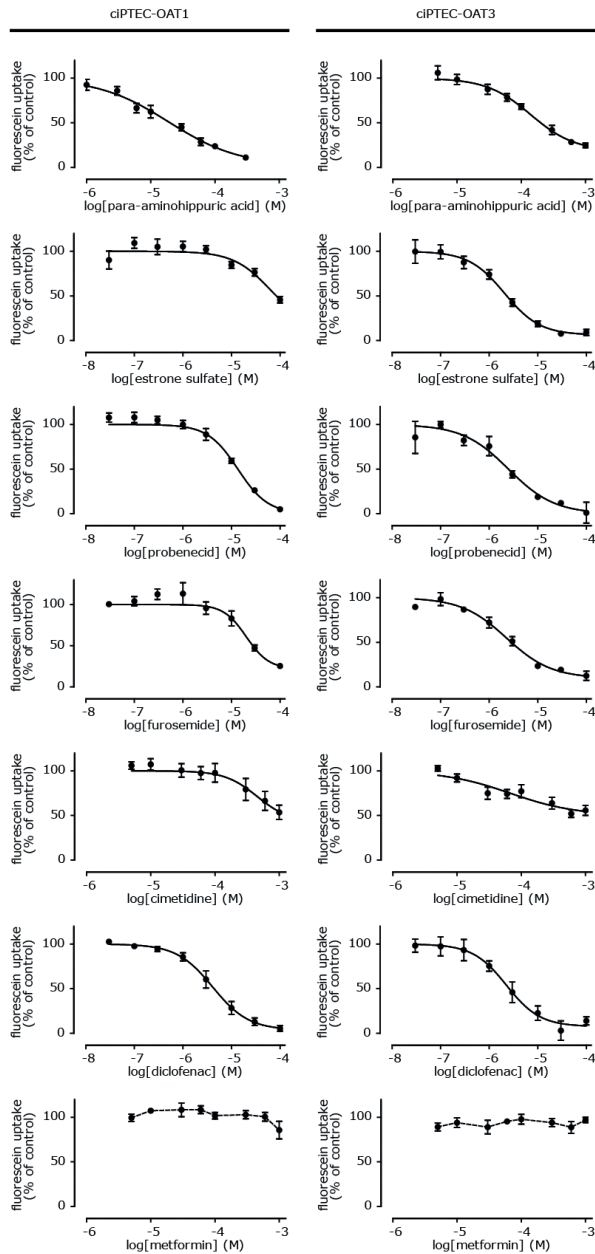


Figure 2.3 Inhibition of OAT-mediated fluorescein uptake by a panel of OAT-perpetrators. Fluorescein uptake (1 μ M) by ciPTEC-OAT1 and ciPTEC-OAT3 when co-incubated with para-aminhippuric acid, estrone sulfate, probenecid, furosemide, cimetidine, diclofenac and metformin for 10 min in HBSS at 37°C, relative to uptake without inhibitor. The line represents the fit according to a one-site competition model with variable slope, except for metformin. Values are derived from experiments performed at passage x+8, x+11, x+14 and x+29 upon transduction (n=4).

cytotoxicity caused by all four antivirals was evaluated after exposure of ciPTEC for 24-72 h to the drugs. As a measure of cytotoxicity, cell viability was analyzed by cellular dehydrogenase capacity, metabolizing MTT into purple formazan. In the parent ciPTEC, viability was not affected by any of the antivirals (48 hr, 1 mM), while adefovir, cidofovir and tenofovir significantly affected cell viability in ciPTEC-OAT1 and only tenofovir slightly decreased ciPTEC-OAT3 viability (Figure 2.5A). Antiviral-induced toxicity was evaluated in more detail, demonstrating a concentration- and time-dependent decrease in viability by adefovir, cidofovir and tenofovir in ciPTEC-OAT1, while the effect was less pronounced in ciPTEC-OAT3 (Figure 2.5B and Table 2.4). These findings indicate the direct involvement of the OAT transporters in antiviral-mediated nephrotoxicity, although IC_{50} values found in the current study are higher compared to those obtained in previous studies (Table 2.4). The cytotoxic effect of the antivirals correlated nicely with the inhibitory effect on fluorescein uptake, except for zidovudine. Despite a clear inhibition of fluorescein uptake by zidovudine, suggesting OAT-mediated uptake, this compound did not affect cell

Table 2.2 Inhibitory potencies of substrates and/or inhibitors of fluorescein uptake in ciPTEC-OAT1 and ciPTEC-OAT3 and a selection of reference values^a

	Current study		Literature		Substrate	Cell line	ref
	Cell line	IC_{50} (μ M)	IC_{50} (μ M)	K_i (μ M)			
para-aminohippuric acid	ciPTEC-OAT1	18 \pm 4	8.8	6.02	6-carboxyfluorescein	CHO-OAT1	[29]
					ochratoxin A	S2-OAT1	[49]
	ciPTEC-OAT3	152 \pm 3		19.6	ochratoxin A	S2-OAT3	[49]
				100	benzylpenicillin	HEK293-hOAT1	[50]
estrone sulfate	ciPTEC-OAT1	54 \pm 13	>100		PAH	S2-OAT1	[51]
	ciPTEC-OAT3	2.1 \pm 0.3	3.0		estrone sulfate	Xenopus-OAT3	[52]
probenecid	ciPTEC-OAT1	12.7 \pm 0.5		4.29	ochratoxin A	S2-OAT1	[49]
			6.3		6-carboxyfluorescein	CHO-OAT1	[29]
				12.1	PAH	S2-OAT1	[16]
	ciPTEC-OAT3	1.9 \pm 0.6	3.1		cimetidine	CHO-OAT3	[53]
			4.41	ochratoxin A	S2-OAT3	[49]	
furosemide	ciPTEC-OAT1	25 \pm 4	18		PAH	S2-OAT1	[54]
	ciPTEC-OAT3	2.3 \pm 0.4	7.31		estrone sulfate	S2-OAT3	[54]
			1.7		sitagliptin	CHO-OAT3	[53]
cimetidine ^b	ciPTEC-OAT1	654 \pm 291	492		PAH	S2-OAT1	[35]
	ciPTEC-OAT3	215 \pm 162	79		sitagliptin	CHO-OAT3	[53]
			53		estrone sulfate	Xenopus-OAT3	[55]
diclofenac	ciPTEC-OAT1	5 \pm 1	4.46		PAH	S2-OAT1	[56]
			4		adefovir	CHO-OAT1	[57]
	ciPTEC-OAT3	3 \pm 1	7.78		estrone sulfate	S2-OAT3	[56]

^aData are expressed as mean \pm SEM, n=4. ^bApparent IC_{50} value due to partial inhibition.

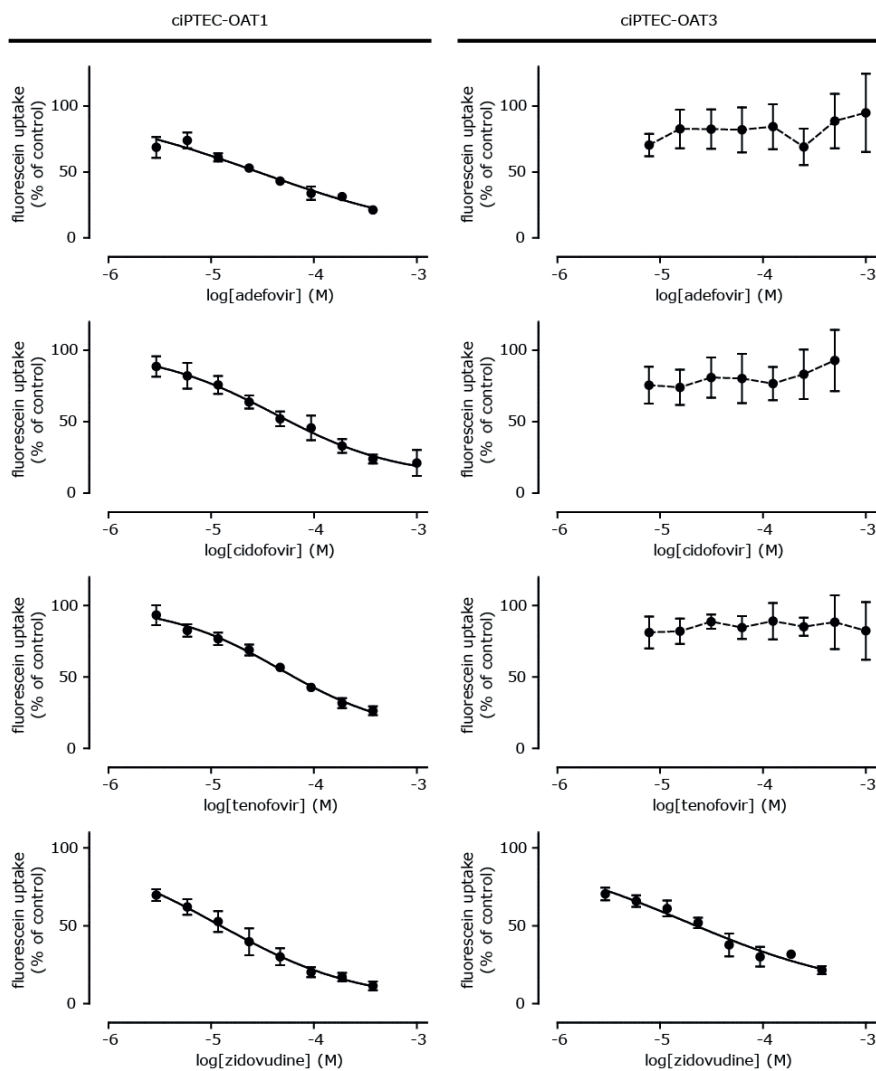


Figure 2.4 Inhibition of OAT-mediated fluorescein uptake by adefovir, cidofovir, tenofovir and zidovudine. Fluorescein uptake (1 μ M) by ciPTEC-OAT1 and ciPTEC-OAT3 when co-incubated with the antivirals for 10 min in HBSS at 37°C, relative to uptake without inhibitor. The line represents the fit according to a one-site competition model with variable slope ($n=4$).

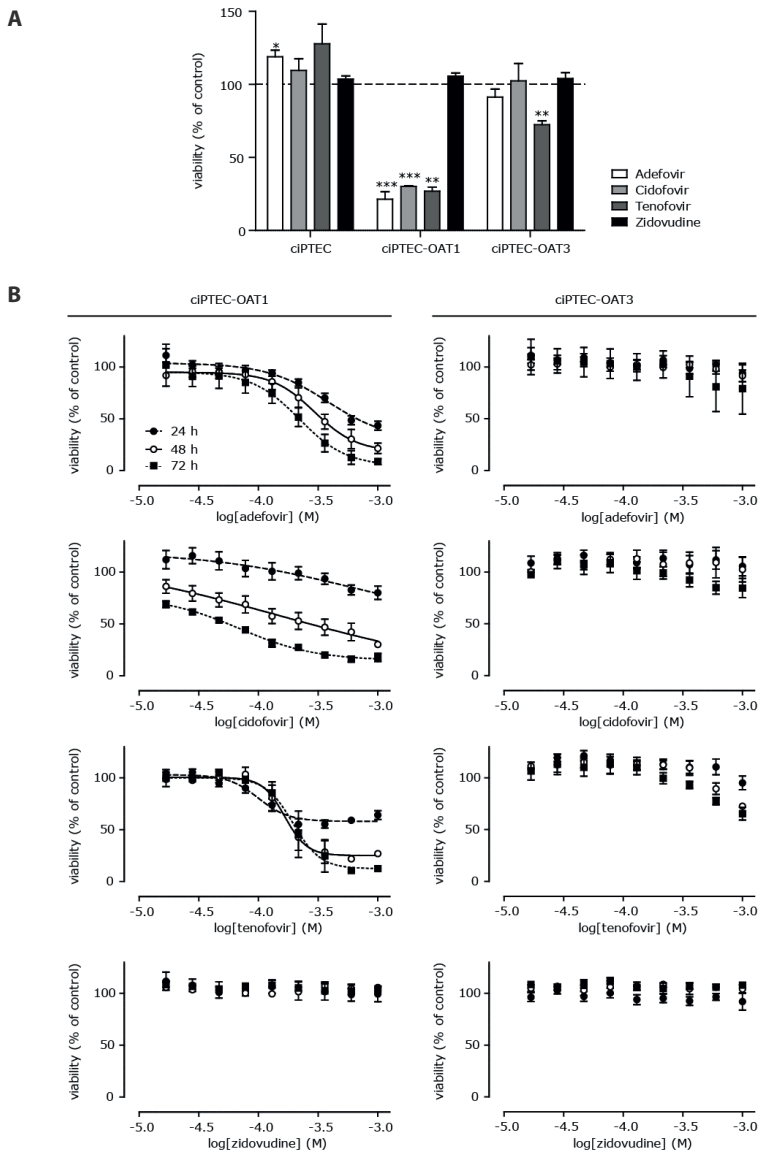


Figure 2.5 Antiviral-induced toxicity in ciPTEC-OAT1 and ciPTEC-OAT3. (A) Viability of ciPTEC parent, ciPTEC-OAT1 and ciPTEC-OAT3 after exposure to antiviral agent (1 mM) for 48 h in serum free medium relative to cell viability as measured with the MTT assay without exposure ($n=3$). ** $p<0.01$, *** $p<0.001$. (B) Viability of ciPTEC-OAT1 and ciPTEC-OAT3 upon tenofovir, adefovir, cidofovir or zidovudine exposure for 24, 48 and 72 h in serum free medium, relative to cell viability without exposure. The line represents the fit according to a one-site competition model with variable slope ($n\geq 3$).

viability as determined by the MTT assay. To investigate a potential protective effect via intact efflux transporters in ciPTEC, cells were exposed to zidovudine at $10 \times C_{max}$ (50 μM) in presence of MRP4 and BCRP inhibitors MK571 and KO143, respectively. This did not affect cell viability in ciPTEC, ciPTEC-OAT1 nor ciPTEC-OAT3, indicating that efflux transporters did not counteract intracellular exposure of zidovudine and thereby reduce the cytotoxic potential of zidovudine.

Table 2.3 Inhibitory potencies of antivirals on fluorescein uptake using ciPTEC-OAT1 and ciPTEC-OAT3 compared with a selection of reference values. In the current study, fluorescein inhibition by the model compounds was measured. For references, the competitive substrate is provided.

		Current study			Literature			DDI index		
	Cell line	IC ₅₀ (μM)	IC ₅₀ (μM)	K _m (μM)	Substrate	Cell line	Ref.	C _{max} (μM)	C _{max} /IC ₅₀	Ref.
adefovir	ciPTEC-OAT1	23±4	8.1	23.8	PAH	HeLa-OAT1	[30]	1.6	0.18	[58]
			28		6-carboxyfluorescein	CHO-OAT1	[29]	38.8	4.2	[59]
	N.A.	-	CHO-OAT1		[29]					
	ciPTEC-OAT3	N.A.								
cidofovir	ciPTEC-OAT1	71±34	60	58	6-carboxyfluorescein	CHO-OAT1	[29]	15.8	0.53	[60]
					-	CHO-OAT1	[29]	26.3	0.88	[61]
	N.A.									
tenofovir	ciPTEC-OAT1	42±8	29.3	33.8	PAH	HeLa-OAT1	[30]	0.52	0.014	[62]
					-		[36]	0.72	0.019	[63]
	N.A.									
zidovudine	ciPTEC-OAT1	14±7		45.9	-	S2-OAT1	[16]	5.5	0.55	[64]
									0.66	
	ciPTEC-OAT3	21±4	145		-	S2-OAT1	[16]	6.6	0.69	[64]
								0.83		

^a Data are expressed as mean±SEM, n=3. N.A., not applicable; PAH, para-aminohippurate; HeLa, human epitheloid cervix carcinoma cell; CHO, Chinese hamster ovary cell line; S2, SV40T immortalized mouse renal cell line.

Table 2.4 Inhibitory potencies of antivirals on cell viability as measured by MTT assay using ciPTEC-OAT1 and a selection of values as found in literature^a.

	ciPTEC-OAT1					
	Current study			Literature		
	24 h	48 h	72 h	48 h	120 h	Ref.
adefovir	462±52	303±38	230±37	0.22±0.08	1.4±0.7	[36, 38]
cidofovir ^b	613±384	130±58	69±2	0.5±0.2	3±1	[36, 38]
tenofovir	114±25	189±48	223±67	10±2	21±7	[36, 38]

^aData are expressed as μM (mean±SEM), n≥3. ^bApparent IC₅₀ value due to partial inhibition.

Discussion

To improve prediction of the nephrotoxic potential of novel chemical entities and to mechanistically understand the pathways associated with drug-induced toxicity, highly predictive and validated translational models are required. In the present report, we describe such a robust human-based cell model with intact proximal tubular characteristics. Stable OAT1 and OAT3 expression in the human renal cell line ciPTEC allowed studying reproducible DDI for a panel of model substrates and antiviral compounds. Functional OAT1 and OAT3 transport activity was demonstrated to be associated with drug-induced toxicity of the antivirals adefovir, cidofovir and tenofovir. These findings indicate that our model predicts drug-induced nephrotoxicity, and underscore that functional expression of influx transporters is pivotal in prediction of drug-induced renal toxicity.

Many reports related to studying drug-OAT interactions describe the use of non-polarized overexpression systems, such as Chinese hamster ovary (CHO) cells, the human cervical epitheloid carcinoma cell line HeLa, or human epithelial kidney (HEK) 293 cells, which are highly relevant for studying interactions at the single transporter level but might have a poor overall predictivity due to their simplicity^[29, 30]. Since proximal tubule cells are the main site of adverse drug effects in the kidney, this cell type is preferred for *in vitro* assays investigating drug-induced nephrotoxicity^[1]. Human primary proximal tubule cells reflect *in vivo* toxicological responses best, but lack reproducibility and robustness due to high donor-to-donor variability and limited availability. Moreover, primary cells lose their proximal tubular phenotype upon culturing, and OAT1-4, P-glycoprotein and MRP expressions were found to be rapidly decreased^[31, 32]. To extend the life span of human proximal tubular cells and to provide a robust model for drug screening, we and others have immortalized primary kidney cells, yet without demonstrating functional OATs^[21, 33], despite retained gene expressions^[34].

The current study demonstrates the first human model with stable expression of OAT1 and OAT3 for up to 10 and 11 passages, respectively, as analyzed by qPCR and functionality of OAT1 and OAT3 for up to 29 passages as analyzed by fluorescein uptake. Experimental values obtained for DDI of model compounds correlated well with published data, confirming PAH has a higher inhibitory potency for OAT1 compared to OAT3, whereas the inhibitory potencies of estrone sulfate, probenecid and furosemide were clearly higher for OAT3. The IC_{50} value of cimetidine in ciPTEC-OAT1 is, however, more than 5-fold higher as described earlier, whereas ciPTEC-OAT3 inhibition by cimetidine was found well within predetermined ranges^[35]. This

discrepancy may be explained by different substrates used in the studies, where the OAT1-substrate PAH used in earlier studies, has a lower affinity for OAT1 as compared to fluorescein used in the current study. Since tetracyclin-inducible expression of OAT1 and OAT3 in ciPTEC was not achieved, we hypothesize that random integration of the vector could have caused silencing of this particular promoter element. The effects of prototypic inhibitor compounds on drug transport are promising with respect to the application of ciPTEC as a tool to study drug-induced nephrotoxicity and the proof-of-concept was evaluated further with a selected panel of clinically relevant antivirals with various pharmacokinetic parameters.

DDIs are a major concern in anti-HIV therapy that includes co-administration of multiple antivirals. We evaluated adefovir, cidofovir, tenofovir and zidovudine DDI at the site of OAT1 and OAT3. The affinities of adefovir, cidofovir and tenofovir were higher for OAT1 than for OAT3, in agreement with previous studies in CHO cells overexpressing hOAT1 and hOAT3^[36]. The DDI index has been used to determine the potential of clinical DDI and drug-induced toxicities^[28, 37], and allows extrapolating *in vitro* observations to the clinical setting^[28, 37]. In our study, IC₅₀ values of less than 10 times the maximal free plasma concentration ($C_{\text{max,u}}/IC_{50} > 0.1$), were found for adefovir, cidofovir and zidovudine, indicating these antivirals are likely to inhibit OAT1 and OAT3 at clinically relevant concentrations.

Antiviral-induced nephrotoxicity was shown to be associated with OAT-mediated uptake and further evaluated in the current study^[11, 15, 36, 38]. We demonstrated that OAT1 or OAT3 expression is required for induction of toxicity by adefovir, cidofovir and tenofovir in ciPTEC. The relation between OAT1 transporter affinity and toxicity was described earlier using HeLa cells, transiently expressing hOAT1, in which cidofovir showed a higher affinity as well as a higher toxicity compared to tenofovir^[30]. In agreement, when the cytotoxic potential of NtRTIs in ciPTEC-OAT1 at 72 h of exposure was ranked, we found that cidofovir has the highest potency over tenofovir and adefovir^[36, 38]. On the other hand, the low potency of adefovir in our study contrasts to the cytotoxicity reported for other cell models^[35, 37]. In general, the toxic potency of the antivirals in ciPTEC is lower as compared to hOAT1-CHO and HEK-OAT1, which may be due to the presence of functional metabolic enzymes and an intact efflux machinery in ciPTEC^[36, 38, 39]. RNA expression of phase I enzymes CYP3A4, CYP4A11 and several UDP-glucuronosyltransferases (UGTs) in ciPTEC were found to be comparable to their expression levels in primary PTEC^[23, 32]. Protein expression of the efflux transporters Pgp and MRP4 was demonstrated, as well as functional efflux transport activity of Pgp, MRP4 and BCRP^[21, 24]. From these findings, we conclude that ciPTEC closely reflects the physiological situation, suggesting that our model is of higher predictive value

than single overexpression systems. Since MRP4 mediates the efflux of tenofovir, its functional presence in ciPTEC might explain the reduced cytotoxicity in our model as compared to overexpression systems lacking this transporter^[15, 39]. Future research should clarify this.

Activity of phase I and phase II metabolizing enzymes was demonstrated in ciPTEC of which the UGT2B7 subfamily might have been the cause of the tolerance for zidovudine observed in the present study^[23]. While adefovir, cidofovir and tenofovir are largely excreted unchanged by the kidneys, only 23% of zidovudine is eliminated via the urine without metabolic alterations^[40]. Zidovudine undergoes either phase II metabolism into the non-toxic 5'-zidovudine-O-glucuronide or the antiviral is phosphorylated resulting in mitochondrial toxicity^[12, 41]. As both glucuronidation and phosphorylation take place at the same functional group of zidovudine (5'-OH), the low toxicity of zidovudine suggests a favor for glucuronidation in ciPTEC. Although glucuronidation predominantly takes place in the liver, UGT2B7 expression in ciPTEC might contribute to zidovudine detoxification. Moreover, the toxic side effects of nucleoside analogues have been correlated with the kinetics of incorporation by the mitochondrial DNA polymerase, ranking zidovudine less toxic than tenofovir^[42]. As efflux inhibition of MRP4 and BCRP did not further reduce viability of ciPTEC upon exposure with zidovudine, the toxicity of this compound is likely not influenced by these efflux transporters. Differences in expression of metabolic enzymes and transporter activities between various cell lines used for toxicity studies should be taken into account when comparing functional readout parameters. Moreover, the broad presence of metabolic enzymes and transporters in our model as well as in freshly isolated PTECs increases their predictive potential, but complicates comparison with more simple models. Taken together, the combined expression of efflux transporters (MRP4, BCRP, MATE2-K and Pgp) with influx transporters (OAT1/3, OCT2 and SLCO4C1) and metabolic enzymes make ciPTEC suitable to study multiple steps involved in renal elimination and drug-induced nephrotoxicity.

The clinical relevance and impact on drug safety of OAT transporters are well acknowledged by regulatory authorities and the pharmaceutical industry^[43]. Both the FDA and the European Medicines Agency (EMA) have issued guidance documents, outlining that OAT interactions should be studied for new compounds^[28, 44]. Furthermore, the International Transporter Consortium (ITC) provided decision trees to determine whether a drug candidate may be a substrate (victim) or an inhibitor (perpetrator) of transporters involved in clinically relevant DDJ^[45]. Consequently, pharmaceutical industry started a quest for reliable and high-throughput *in vitro* models that mimic the human kidney with improved prediction of drug-induced

nephrotoxicity and a decrease in use of animals in research^[46]. Current preclinical tests for prediction of nephrotoxicity are mainly based on animal (rodent) models. These models provide information about systemic toxicity in living organisms, but they bear high costs, are time intensive and remain an ethical issue. Their clinical predictive value is limited due to inherent interspecies differences in drug disposition and emphasizes the urgent need for human based models that closely resemble the human kidney physiology^[6, 47]. Current innovations in *in vitro* models allowing cells to grow in polarized structures under flow conditions, in combination with high-throughput automated systems for toxicity read-outs, will become major steps forward in drug safety screening, for which the ciPTEC model may provide a suitable cellular basis^[48]. In general, application of ciPTEC as a predictive tool for drug-induced toxicity requires comparison with freshly isolated PTECs and further validation by extrapolation of *in vitro* data to clinical outcomes.

Conclusion

We present the first human PTEC model with stable expression and functionality of OAT1 and OAT3, allowing screening for drug-induced nephrotoxicity and DDI. The NtRTI drugs tenofovir, adefovir and cidofovir-induced nephrotoxicity and exhibited DDI indices at clinically relevant concentrations. These findings underscore that ciPTEC-OAT1 and ciPTEC-OAT3 are valuable tools for drug-induced toxicity screening that, upon systematic validation, could improve translation of *in vitro* findings to clinical research and might decrease the use of animal studies in the preclinical stages of drug development.

Acknowledgements

This work was partly supported by a collaboration research agreement from AstraZeneca, by a grant from the Dutch Kidney Foundation (grant nr. KJPB 11.023) and by the NephroTube project funded by NC3Rs (project no. 37497-25920). Authors declare no potential conflict of interest.

References

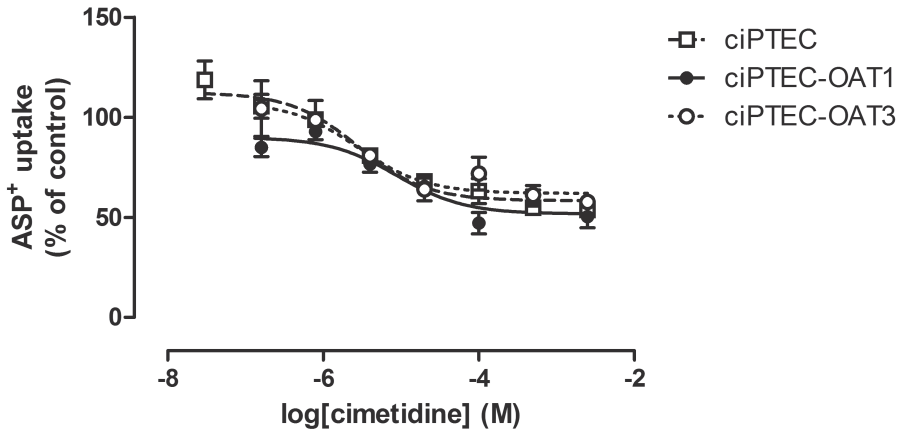
1. Tiong HY, Huang P, Xiong S, Li Y, Vathsala A, Zink D. Drug-induced nephrotoxicity: clinical impact and preclinical in vitro models. *Mol Pharm.* 11, 1933-1948 (2014).
2. Redfern WS, Ewart L, Hammond TG, Bialecki R, Kinter L, Lindgren S. Impact and frequency of different toxicities throughout the pharmaceutical life cycle. *The Toxicologist.* 1081 (2010).
3. Guengerich FP. Mechanisms of drug toxicity and relevance to pharmaceutical development. *Drug Metab Pharmacokinet.* 26, 3-14 (2011).
4. Gundert-Remy U, Bernauer U, Blomeke B, Doring B, Fabian E, Goebel C, Hessel S, et al. Extrahepatic metabolism at the body's internal-external interfaces. *Drug Metab Rev.* 46, 291-324 (2014).
5. Wang L, Sweet DH. Renal organic anion transporters (SLC22 family): expression, regulation, roles in toxicity, and impact on injury and disease. *AAPS J.* 15, 53-69 (2013).
6. Burckhardt G, Burckhardt BC. In vitro and in vivo evidence of the importance of organic anion transporters (OATs) in drug therapy. *Handb Exp Pharmacol.* 29-104 (2011).
7. Masereeuw R, Russel FG. Therapeutic implications of renal anionic drug transporters. *Pharmacol Ther.* 126, 200-216 (2010).
8. Motohashi H, Inui K. Organic cation transporter OCTs (SLC22) and MATEs (SLC47) in the human kidney. *AAPS J.* 15, 581-588 (2013).
9. Konig J, Muller F, Fromm MF. Transporters and drug-drug interactions: important determinants of drug disposition and effects. *Pharmacol Rev.* 65, 944-966 (2013).
10. Morrissey KM, Stocker SL, Wittwer MB, Xu L, Giacomini KM. Renal transporters in drug development. *Annu Rev Pharmacol Toxicol.* 53, 503-529 (2013).
11. Izzedine H, Harris M, Perazella MA. The nephrotoxic effects of HAART. *Nat Rev Nephrol.* 5, 563-573 (2009).
12. Lewis W, Day BJ, Copeland WC. Mitochondrial toxicity of NRTI antiviral drugs: an integrated cellular perspective. *Nat Rev Drug Discov.* 2, 812-822 (2003).
13. De Clercq E. Antiviral drugs in current clinical use. *J Clin Virol.* 30, 115-133 (2004).
14. Tourret J, Deray G, Isnard-Bagnis C. Tenofovir effect on the kidneys of HIV-infected patients: a double-edged sword? *J Am Soc Nephrol.* 24, 1519-1527 (2013).
15. Kohler JJ, Hosseini SH, Green E, Abuin A, Ludaway T, Russ R, Santoianni R, et al. Tenofovir renal proximal tubular toxicity is regulated by OAT1 and MRP4 transporters. *Lab Invest.* 91, 852-858 (2011).
16. Takeda M, Khamdang S, Narikawa S, Kimura H, Kobayashi Y, Yamamoto T, Cha SH, et al. Human organic anion transporters and human organic cation transporters mediate renal antiviral transport. *J Pharmacol Exp Ther.* 300, 918-924 (2002).
17. Cihlar T, Lin DC, Pritchard JB, Fuller MD, Mendel DB, Sweet DH. The antiviral nucleotide analogs didanosine and zalcitabine are novel substrates for human and rat renal organic anion transporter 1. *Mol Pharmacol.* 56, 570-580 (1999).
18. Lacy SA, Hitchcock MJ, Lee WA, Tellier P, Cundy KC. Effect of oral probenecid coadministration on the chronic toxicity and pharmacokinetics of intravenous didanosine in cynomolgus monkeys. *Toxicol Sci.* 44, 97-106 (1998).
19. Kearney BP, Flaherty JF, Shah J. Tenofovir disoproxil fumarate: clinical pharmacology and pharmacokinetics. *Clin Pharmacokinet.* 43, 595-612 (2004).
20. Vigouroux C, Bastard JP, Capeau J. Emerging clinical issues related to management of multiorgan comorbidities and polypharmacy. *Curr Opin HIV AIDS.* 9, 371-378 (2014).
21. Wilmer MJ, Saleem MA, Masereeuw R, Ni L, van der Velden TJ, Russel FG, Mathieson PW, et al. Novel conditionally immortalized human proximal tubule cell line expressing functional influx and efflux transporters. *Cell Tissue Res.* 339, 449-457 (2010).

22. Schophuizen CM, Wilmer MJ, Jansen J, Gustavsson L, Hilgendorf C, Hoenderop JG, van den Heuvel LP, et al. Cationic uremic toxins affect human renal proximal tubule cell functioning through interaction with the organic cation transporter. *Pflugers Arch.* 465, 1701-1714 (2013).
23. Mutsaers HA, Wilmer MJ, Reijnders D, Jansen J, van den Broek PH, Forkink M, Schepers E, et al. Uremic toxins inhibit renal metabolic capacity through interference with glucuronidation and mitochondrial respiration. *Biochim Biophys Acta.* 1832, 142-150 (2013).
24. Jansen J, Schophuizen CM, Wilmer MJ, Lahham SH, Mutsaers HA, Wetzels JF, Bank RA, et al. A morphological and functional comparison of proximal tubule cell lines established from human urine and kidney tissue. *Exp Cell Res.* 323, 87-99 (2014).
25. Saleem MA, O'Hare MJ, Reiser J, Coward RJ, Inward CD, Farren T, Xing CY, et al. A conditionally immortalized human podocyte cell line demonstrating nephrin and podocin expression. *J Am Soc Nephrol.* 13, 630-638 (2002).
26. Moghadasali R, Mutsaers HA, Azarnia M, Aghdami N, Baharvand H, Torensma R, Wilmer MJ, et al. Mesenchymal stem cell-conditioned medium accelerates regeneration of human renal proximal tubule epithelial cells after gentamicin toxicity. *Exp Toxicol Pathol.* 65, 595-600 (2013).
27. Kimura N, Masuda S, Tanihara Y, Ueo H, Okuda M, Katsura T, Inui K. Metformin is a superior substrate for renal organic cation transporter OCT2 rather than hepatic OCT1. *Drug Metab Pharmacokinet.* 20, 379-386 (2005).
28. Drug interaction studies - study design, data analysis, implications for dosing, and labeling recommendations. FDA. Silver Spring, MD (2012)
29. Cihlar T, Ho ES. Fluorescence-based assay for the interaction of small molecules with the human renal organic anion transporter 1. *Anal Biochem.* 283, 49-55 (2000).
30. Mandikova J, Volkova M, Pavek P, Cesnek M, Janeba Z, Kubicek V, Trejtnar F. Interactions with selected drug renal transporters and transporter-mediated cytotoxicity in antiviral agents from the group of acyclic nucleoside phosphonates. *Toxicology.* 311, 135-146 (2013).
31. Lash LH, Putt DA, Cai H. Membrane transport function in primary cultures of human proximal tubular cells. *Toxicology.* 228, 200-218 (2006).
32. Brown CD, Sayer R, Windass AS, Haslam IS, De Broe ME, D'Haese PC, Verhulst A. Characterisation of human tubular cell monolayers as a model of proximal tubular xenobiotic handling. *Toxicol Appl Pharmacol.* 233, 428-438 (2008).
33. Wieser M, Stadler G, Jennings P, Streubel B, Pfaller W, Ambros P, Riedl C, et al. hTERT alone immortalizes epithelial cells of renal proximal tubules without changing their functional characteristics. *Am J Physiol Renal Physiol.* 295, F1365-1375 (2008).
34. Aschauer L, Carta G, Vogelsang N, Schlatter E, Jennings P. Expression of xenobiotic transporters in the human renal proximal tubule cell line RPTEC/TERT1. *Toxicol In Vitro.* (2015).
35. Khamdang S, Takeda M, Shimoda M, Noshiro R, Narikawa S, Huang XL, Enomoto A, et al. Interactions of human- and rat-organic anion transporters with pravastatin and cimetidine. *J Pharmacol Sci.* 94, 197-202 (2004).
36. Cihlar T, Laflamme G, Fisher R, Carey AC, Vela JE, Mackman R, Ray AS. Novel nucleotide human immunodeficiency virus reverse transcriptase inhibitor GS-9148 with a low nephrotoxic potential: characterization of renal transport and accumulation. *Antimicrob Agents Chemother.* 53, 150-156 (2009).
37. Wang L, Sweet DH. Potential for food–drug interactions by dietary phenolic acids on human organic anion transporters 1 (SLC22A6), 3 (SLC22A8), and 4 (SLC22A11). *Biochem Pharmacol.* 84, 1088-1095 (2012).
38. Zhang X, Wang R, Piotrowski M, Zhang H, Leach KL. Intracellular concentrations determine the cytotoxicity of adefovir, cidofovir and tenofovir. *Toxicology in Vitro.* 29, 251-258 (2015).
39. Imaoka T, Kusuohara H, Adachi M, Schuetz JD, Takeuchi K, Sugiyama Y. Functional involvement of multidrug resistance-associated protein 4 (MRP4/ABCC4) in the renal elimination of the antiviral drugs adefovir and tenofovir. *Mol Pharmacol.* 71, 619-627 (2007).

40. Varma MV, Feng B, Obach RS, Troutman MD, Chupka J, Miller HR, El-Kattan A. Physicochemical determinants of human renal clearance. *J Med Chem.* 52, 4844-4852 (2009).
41. Blum MR, Liao SH, Good SS, de Miranda P. Pharmacokinetics and bioavailability of zidovudine in humans. *Am J Med.* 85, 189-194 (1988).
42. Lee H, Hanes J, Johnson KA. Toxicity of nucleoside analogues used to treat AIDS and the selectivity of the mitochondrial DNA polymerase. *Biochemistry.* 42, 14711-14719 (2003).
43. Nigam SK. What do drug transporters really do? *Nat Rev Drug Discov.* 14, 29-44 (2015).
44. Guideline on the investigation of drug interactions. EMA. London (2010)
45. International Transporter Consortium, Giacomini KM, Huang SM, Tweedie DJ, Benet LZ, Brouwer KL, Chu X, et al. Membrane transporters in drug development. *Nat Rev Drug Discov.* 9, 215-236 (2010).
46. McGuinness L. CRACK IT Challenge winners awarded £4.9 million to further their research. Web Page. National Centre for the Replacement, Refinement and Reduction of Animals in Research (2014). <https://www.nc3rs.org.uk/crackit-news/crack-it-challenge-winners-awarded-%C2%A349-million-further-their-research>.
47. Chu X, Bleasby K, Evers R. Species differences in drug transporters and implications for translating preclinical findings to humans. *Expert Opin Drug Metab Toxicol.* 9, 237-252 (2013).
48. Bhatia SN, Ingber DE. Microfluidic organs-on-chips. *Nat Biotechnol.* 32, 760-772 (2014).
49. Jung KY, Takeda M, Kim DK, Tojo A, Narikawa S, Yoo BS, Hosoyamada M, et al. Characterization of ochratoxin A transport by human organic anion transporters. *Life Sci.* 69, 2123-2135 (2001).
50. Deguchi T, Kusuvara H, Takadate A, Endou H, Otagiri M, Sugiyama Y. Characterization of uremic toxin transport by organic anion transporters in the kidney. *Kidney Int.* 65, 162-174 (2004).
51. Srimarong C, Jutabha P, Pritchard JB, Endou H, Chatsudhipong V. Interactions of stevioside and steviol with renal organic anion transporters in S2 cells and mouse renal cortical slices. *Pharm Res.* 22, 858-866 (2005).
52. Cha SH, Sekine T, Fukushima JI, Kanai Y, Kobayashi Y, Goya T, Endou H. Identification and characterization of human organic anion transporter 3 expressing predominantly in the kidney. *Mol Pharmacol.* 59, 1277-1286 (2001).
53. Chu XY, Bleasby K, Yabut J, Cai X, Chan GH, Hafey MJ, Xu S, et al. Transport of the dipeptidyl peptidase-4 inhibitor sitagliptin by human organic anion transporter 3, organic anion transporting polypeptide 4C1, and multidrug resistance P-glycoprotein. *J Pharmacol Exp Ther.* 321, 673-683 (2007).
54. Hasannejad H, Takeda M, Taki K, Shin HJ, Babu E, Jutabha P, Khamdang S, et al. Interactions of human organic anion transporters with diuretics. *J Pharmacol Exp Ther.* 308, 1021-1029 (2004).
55. Motohashi H, Uwai Y, Hiramoto K, Okuda M, Inui K. Different transport properties between famotidine and cimetidine by human renal organic ion transporters (SLC22A). *Eur J Pharmacol.* 503, 25-30 (2004).
56. Khamdang S, Takeda M, Noshiro R, Narikawa S, Enomoto A, Anzai N, Piyachaturawat P, et al. Interactions of human organic anion transporters and human organic cation transporters with nonsteroidal anti-inflammatory drugs. *J Pharmacol Exp Ther.* 303, 534-539 (2002).
57. Mulato AS, Ho ES, Cihlar T. Nonsteroidal anti-inflammatory drugs efficiently reduce the transport and cytotoxicity of adefovir mediated by the human renal organic anion transporter 1. *J Pharmacol Exp Ther.* 295, 10-15 (2000).
58. Barditch-Crovo P, Toole J, Hendrix CW, Cundy KC, Ebeling D, Jaffe HS, Lietman PS. Anti-human immunodeficiency virus (HIV) activity, safety, and pharmacokinetics of adefovir dipivoxil (9-²-(bis-pivaloyloxymethyl)-phosphonylmethoxyethyl]adenine) in HIV-infected patients. *J Infect Dis.* 176, 406-413 (1997).
59. Cundy KC, Barditch-Crovo P, Walker RE, Collier AC, Ebeling D, Toole J, Jaffe HS. Clinical pharmacokinetics of adefovir in human immunodeficiency virus type 1-infected patients. *Antimicrob Agents Chemother.* 39, 2401-2405 (1995).

60. Wachsman M, Petty BG, Cundy KC, Jaffe HS, Fisher PE, Pastelak A, Lietman PS. Pharmacokinetics, safety and bioavailability of HPMPC (cidofovir) in human immunodeficiency virus-infected subjects. *Antiviral Res.* 29, 153-161 (1996).
61. Cundy KC, Petty BG, Flaherty J, Fisher PE, Polis MA, Wachsman M, Lietman PS, et al. Clinical pharmacokinetics of cidofovir in human immunodeficiency virus-infected patients. *Antimicrob Agents Chemother.* 39, 1247-1252 (1995).
62. Kearney BP, Ramanathan S, Cheng AK, Ebrahimi R, Shah J. Systemic and renal pharmacokinetics of adefovir and tenofovir upon coadministration. *J Clin Pharmacol.* 45, 935-940 (2005).
63. Flynn PM, Mirochnick M, Shapiro DE, Bardeguet A, Rodman J, Robbins B, Huang S, et al. Pharmacokinetics and safety of single-dose tenofovir disoproxil fumarate and emtricitabine in HIV-1-infected pregnant women and their infants. *Antimicrob Agents Chemother.* 55, 5914-5922 (2011).
64. Moore KH, Raasch RH, Brouwer KL, Opheim K, Cheeseman SH, Eyster E, Lemon SM, et al. Pharmacokinetics and bioavailability of zidovudine and its glucuronidated metabolite in patients with human immunodeficiency virus infection and hepatic disease (AIDS Clinical Trials Group protocol 062). *Antimicrob Agents Chemother.* 39, 2732-2737 (1995).

Supplemental data



Supplemental Figure S2.1 Intact OCT2 transport after transduction procedures. ASP⁺ uptake (1 μ M) by ciPTEC parent, ciPTEC-OAT1 and ciPTEC-OAT3 when co-incubated with OCT2-substrate cimetidine for 60 min in HBSS at 37°C, relative to uptake without inhibitor. The lines represent the fit according to a one-site competition model. Values are expressed as mean \pm SEM, (ciPTEC, n=3; ciPTEC-OAT1, n=4; ciPTEC-OAT3, n=2). Analysis using Two-way ANOVA indicated significant inhibition of ASP⁺ uptake at OCT2 with cimetidine, resulted in similar IC₅₀ ($p>0.05$).



Expression of Organic Anion Transporter 1 or 3 In Human Kidney Proximal Tubule Cells Reduces Cisplatin Sensitivity

Tom TG Nieskens¹, Janny GP Peters¹, Dina Dabaghie¹, Daphne Korte¹, Katja Jansen², Alexander H Van Asbeck¹, Neslihan N Tavraz³, Thomas Friedrich³, Frans GM Russel¹, Rosalinde Masereeuw², Martijn J Wilmer¹

¹ Department of Pharmacology and Toxicology, Radboud Institute for Molecular Life Sciences, Radboudumc, Nijmegen, the Netherlands

² Div. Pharmacology, Utrecht Institute for Pharmaceutical Sciences, Utrecht, the Netherlands

³ Department of Physical Chemistry/Bioenergetics, Institute of Chemistry PC14, Technical University of Berlin, Berlin

Drug Metabolism and Disposition. 18. 592-599 (2018)

Abstract

Cisplatin is a cytostatic drug used for treatment of solid organ tumors. The main adverse effect is organic cation transporter 2 (OCT2)-mediated nephrotoxicity, observed in 30% of patients. The contribution of other renal drug transporters is elusive. Here, cisplatin-induced toxicity was evaluated in human-derived conditionally immortalized proximal tubule epithelial cells (ciPTEC) expressing renal drug transporters, including OCT2 and organic anion transporter 1 (OAT1) or 3 (OAT3). Parent ciPTEC demonstrated OCT2-dependent cisplatin toxicity (TC_{50} 34 ± 1 μM after 24 h exposure), as determined by cell viability. Over-expression of OAT1 and OAT3 resulted in reduced sensitivity to cisplatin (TC_{50} 45 ± 6 μM and 64 ± 11 μM after 24 h exposure, respectively). This effect was independent of OAT-mediated transport, as the OAT-substrates probenecid and diclofenac did not influence cytotoxicity. Decreased cisplatin sensitivity in OAT-expressing cells associated directly with a trend towards reduced intracellular cisplatin accumulation, explained by reduced OCT2 gene expression and activity. This was evaluated by V_{max} of the OCT2-model substrate ASP^+ (23.5 ± 0.1 min^{-1} , 13.1 ± 0.3 min^{-1} and 21.6 ± 0.6 min^{-1} in ciPTEC-parent, ciPTEC-OAT1 and ciPTEC-OAT3, respectively). While gene expression of cisplatin efflux transporter multidrug and toxin extrusion 1 (MATE1) was 16.2 ± 0.3 fold upregulated in ciPTEC-OAT1 and 6.1 ± 0.7 fold in ciPTEC-OAT3, toxicity was unaffected by the MATE substrate pyrimethamine, suggesting that MATE1 does not play a role in the current experimental set-up. In conclusion, OAT expression results in reduced cisplatin sensitivity in renal proximal tubule cells, explained by reduced OCT2-mediated uptake capacity. *In vitro* drug-induced toxicity studies should consider models that express both OCT and OAT drug transporters.

Introduction

The chemotherapeutic drug cisplatin is commonly used to treat solid organ tumours located in various tissues, including the head, neck, lung, testis, ovary and bladder. Nephrotoxicity is the main adverse effect of cisplatin, causing acute kidney injury (AKI) in 30% of patients^[1]. AKI is currently the dose-limiting factor in treatment with cisplatin and is characterized by dysfunction of the proximal tubule. Cisplatin continues to be prescribed, as less toxic alternatives including oxaliplatin, are suggested to have reduced anticancer potential^[2,3].

Proximal tubule epithelial cells mediate active excretion of xenobiotics and metabolites, and reabsorb low molecular weight proteins, such as β 2-microglobulin, and glucose and amino acids filtered by the glomerulus. To this end, proximal tubule cells express dedicated membrane spanning proteins^[4]. Influx of cisplatin in proximal tubule cells is critically mediated by organic cation transporter 2 (OCT2, *SLC22A2*)^[5-7] and ubiquitously expressed copper transporter 1 (CTR1, *SLC31A1*)^[8], both located in the proximal tubule epithelium at the basolateral membrane. Cisplatin is a substrate for efflux transporters multidrug and toxin extrusion 1 (MATE1, *SLC47A1*), and to a lesser extent MATE2-k (*SLC47A2*), both located at the apical membrane^[9,10]. The combined activity of influx and efflux transporters determines the amount of cisplatin accumulation, hence correlates to the drug's nephrotoxicity^[11]. Recent studies indicate that drug-drug interactions and interindividual genetic differences regarding OCT2 and MATE transporters may contribute to the nephrotoxic potential of cisplatin, underlining their concerted action is essential to maintain active clearance and avoid proximal tubule accumulation^[12,13].

Organic anion transporter 1 (OAT1, *SLC22A6*) and 3 (OAT3, *SLC22A8*) in proximal tubule cells play a main role in clearance of organic anions, including endogenous uremic toxins and a wide range of drugs^[4]. Recently, renal adverse effects of cisplatin were demonstrated to be reduced in an Oat1 knockout mouse model, while disposition of this drug is strongly associated with cation transporters^[14]. The mechanism is suggested to involve extra renal metabolism, yielding glutathione and cysteine conjugates that act as substrates for OAT transporters. Moreover, clinical studies demonstrated that cisplatin clearance was reduced upon co-treatment with OAT-inhibitor probenecid, consistent with a complete absence of renal adverse effects^[15,16]. As cisplatin transport is neither mediated by OAT1 nor OAT3, their role in cisplatin-induced nephrotoxicity remains to be elucidated.

The present study was designed to investigate the role of OATs in cisplatin-induced toxicity in conditionally immortalized proximal tubule cells (ciPTEC), a human-derived cell line manifesting proximal tubule characteristics (ciPTEC)^[17, 18]. In this cell line, we previously demonstrated functional apical absorption of albumin and phosphate, expression of OCT2, P-glycoprotein (Pgp, *ABCB1*), multidrug resistance-associated protein 4 (MRP4, *ABCC4*), breast cancer resistance protein (BCRP, *ABCG2*), and after stable transductions either OAT1 or OAT3 were reintroduced^[17-20]. In addition, ciPTEC express several UDP-glucuronosyltransferases and consume oxygen, suggesting intact mitochondrial energy production^[21, 22]. Therefore, ciPTEC is a relevant proximal tubule cell model with concerted action of different transport mechanisms, suitable for in vitro evaluation of drug-induced toxicity. The results of the present study show CTR1- and OCT2-dependent cisplatin-mediated toxicity in ciPTEC, which is alleviated in presence of active OAT1 or OAT3. Reduced sensitivity in OAT1- or OAT3-expressing cells was associated with a trend towards reduced cisplatin accumulation due to lower OCT2 uptake capacity. Since expression of OATs affects toxicity induced by drugs that are typically imported by OCTs, simultaneous expression of basolateral solute carrier transport proteins is important for in vitro drug-induced toxicity evaluation.

Methods and materials

Cell culture

Conditionally immortalized proximal tubule epithelial cells (ciPTEC-parent) were developed as described by Wilmer et al. with informed consent of the donors in accordance with the approved guidelines of the Radboud Institutional Review Board^[18]. ciPTEC-OAT1 and ciPTEC-OAT3 were derived from ciPTEC-parent cells and demonstrate constitutive expression of organic anion transporter 1 (OAT1) or 3 (OAT3), respectively, as described by Nieskens et al.^[17]. ciPTEC constitutively expressing eYFP (ciPTEC-eYFP) were developed by transduction of eYFP from the COX8-eYFP vector^[23] into the same pLenti4/V5-DEST vector as used for the OAT constructs, by LR recombinant reaction using Gateway Cloning Technology (Invitrogen, Carlsbad, USA) and resulting in expression vector pLenti4/V5-EX-CMV-TetO2-eYFP. Upon transduction as described for ciPTEC-OAT1 and -OAT3, ciPTEC-eYFP cells were selected for YFP fluorescence using BD FACSAria SORP flow cytometer (BD biosciences, San Jose, USA). Proliferating cell culture was maintained up to 90% confluency using T75 culture flasks (Greiner Bio-One, Kremsmünster, Germany) at 33°C and 5% v/v CO₂. Cells were seeded 7 or 8 days prior to the experiment in either T75 culture flasks (Greiner Bio-One), 12-well plates (Greiner Bio-One) or 96-well plates (Corning Life Sciences, New York, USA) with a seeding density of 55,000 cells/cm² for ciPTEC-parent,

63,000 cells/cm² for ciPTEC-OAT1 and 82,000 cells/cm² for ciPTEC-OAT3. Cells were subsequently incubated for 24 h at 33°C and 5% v/v CO₂ to stimulate proliferation, followed by 6 or 7 days at 37°C and 5% v/v CO₂ to allow differentiation and monolayer formation, referred to as maturation. Cells were cultured using Dulbecco's modified eagle medium (DMEM HAM's F12, Life Technologies, Paisly, UK), supplemented with 5 µg/ml insulin, 5 µg/ml transferrin, 5 µg/ml selenium, 35 ng/ml hydrocortisone, 10 ng/ml epidermal growth factor (EGF), 40 pg/ml tri-iodothyronine (Sigma, St. Louis, USA), and 10% fetal calf serum (FCS, Greiner Bio-One), and is referred to as complete medium (CM). Medium in which FCS was omitted, is referred to as serum free medium (SFM). The medium was refreshed every 2 to 3 days, supplemented with 1% penicillin/streptomycin (Invitrogen) only at 33°C.

Viability assay

To evaluate cisplatin-induced toxicity, viability of ciPTEC-parent, ciPTEC-OAT1 and ciPTEC-OAT3 was evaluated by an MTT assay^[24]. Briefly, ciPTEC were matured in 96-well plates, washed 3 times with SFM, and subsequently exposed to cisplatin (8.7-222 µM, Sigma) in SFM for 24 h. To evaluate the effect of competitive transport inhibitors on cisplatin-induced toxicity, cisplatin was co-exposed with probenecid (100 µM, Sigma), diclofenac (50 µM, Sigma), cimetidine (1.25 mM, Sigma) or pyrimethamine (10 and 100 nM, Sigma). For probenecid, a pre-exposure during ciPTEC maturation was additionally performed for 6 days in CM. Following cisplatin exposure, cells were washed 3 times with SFM and incubated with 0.5 mg/ml MTT (Sigma) in SFM for 3 h at 37°C. Formazan crystals formed in viable cells were dissolved in dimethyl sulfoxide (DMSO, Merck, New Jersey, USA) on a microplate shaker (VWR, Radnor, USA) for 1 h. Absorption was measured at 560 nm, subtracting the background at 670 nm, using the BioRad Benchmark Plus (BioRad, Hercules, USA). All values were normalized to unexposed control. Results were plotted with GraphPad Prism (version 5.03, GraphPad Software, San Diego, USA) using non-linear regression with four parameters (variable slope) on log-transformed x-values.

Cisplatin accumulation

To evaluate the effect of OCT2- and MATE-mediated transport on intracellular cisplatin accumulation, ciPTEC-parent, ciPTEC-OAT1 and ciPTEC-OAT3 were matured in T75 culture flasks, washed once in CM and exposed to cisplatin (250 µM, Sigma), with and without OCT2 and MATE substrates cimetidine (1.25 mM, Sigma) or pyrimethamine (100 nM, Sigma) in CM for 90 min. Cells were washed 3 times in HBSS (37°C), harvested using accutase (Invitrogen) and placed on ice. Cell suspensions were centrifuged at 1,500 rcf for 5 min (4°C) and cell pellets were resuspended in 200 µl nitric acid (100 mM, Merck). Lysates were obtained by applying 3 freeze-thaw

cycles of liquid nitrogen and a 37°C waterbath, followed by centrifugation at 10,000 rcf for 10 min (4°C). Cisplatin content of cell samples was evaluated using an atomic absorption spectrophotometer AAnalyst800 (Perkin Elmer, Waltham, USA) equipped with a transversally heated graphite tube atomizer and a platinum hollow cathode lamp (Photron, Melbourne, Australia), loaded with 20 µl of each sample, as described in detail before^[25, 26]. All values were corrected for blank (unexposed), normalized to ciPTEC-parent (for uninhibited control) or uninhibited control of each respective cell line (for competitive inhibitors) and results were plotted with GraphPad Prism (version 5.03, GraphPad Software).

Gene expression

To evaluate expression of drug transporter genes involved in cisplatin influx and efflux, ciPTEC-parent, ciPTEC-OAT1 and ciPTEC-OAT3 were matured in 12-well plates, washed 3 times and exposed to SFM for 24 h, before total RNA was isolated using the RNeasy Mini Kit (QIAGEN, Hilden, Germany), according to the manufacturer's instructions. When evaluating Nrf2 pathway induction, SFM was supplemented with 50 nM bardoxolone methyl (CDDO-Me, Sigma), cDNA was synthesized using M-MLV Reverse Transcriptase (Promega, Madison, USA), according to the manufacturer's instructions. mRNA expression levels of transporters were determined using gene-specific primer probe sets obtained from Life Technologies: OCT2 (*SLC22A2*, hs01010723_m1), MATE1 (*SLC47A1*, hs00217320_m1), MATE2-K (*SLC47A2*, hs00945650_m1), MRP2 (*ABCC2*, hs00166123_m1), *NQO1* (hs01045993_g1), *GCLC* (hs00155249_m1), *GAPDH* (hs99999905_m1) and TaqMan Universal PCR Master Mix (Applied Biosystems, Foster City, USA). Real-time qPCR reactions were performed using CFX96 Touch Real-Time PCR system (BioRad) according to the manufacturer's instructions, and analysed by CFX Manager software (version 1.6, BioRad). mRNA levels were calculated using *GAPDH* as reference gene and expressed as either $-\Delta\Delta C_t$ or fold change ($2^{-\Delta\Delta C_t}$) compared to ciPTEC-parent. Results were plotted with GraphPad Prism (version 5.03, GraphPad Software).

ASP accumulation

To evaluate the accumulation of hOCT2 model substrate ASP⁺^[27, 28]; ciPTEC-parent, ciPTEC-OAT1 and ciPTEC-OAT3 were matured in 96-well plates^[19]. Prior to the experiment, cells were washed 3 times in HEPES-Tris buffer, consisting of 132 mM NaCl, 4.2 mM KCl, 1 mM CaCl₂, 1 mM MgCl₂, 5.5 mM glucose, 10 mM Hepes, buffered to pH=7.4 using Tris pH=8.8. Next, cells were exposed to ASP⁺ (4-di-1-ASP⁺, 0.8-50 µM, Thermo Scientific, Waltham, USA) with and without cimetidine (1.25 mM, Sigma), pyrimethamine (10 and 100 nM, Sigma) or probenecid (100 µM, Sigma) for 1 h at 37°C. For probenecid, a pre-exposure during ciPTEC maturation was additionally

performed for 6 days in CM to study the effect of long-term OAT activity inhibition on ASP⁺ transporting proteins. After accumulation for 1 h, the fluorescent signal was measured (excitation 485 nm; emission 590 nm) using a Victor X3 plate reader (Perkin Elmer, Waltham, USA). Values were corrected for extracellular signal (empty wells with corresponding ASP⁺ concentration) and either presented as arbitrary units (for kinetic curves) or normalized to control (for competitive inhibitors). Results were plotted with GraphPad Prism (version 5.03, GraphPad Software) using Michaelis-Menten regression analysis for concentration-dependent transport rate curves.

Glutathione level

To evaluate total cellular glutathione level, ciPTEC were matured in 6-well plates and glutathione level was evaluated using the Glutathione Assay Kit (Sigma), according to the manufacturer's instructions. Briefly, cells were harvested using accutase (Invitrogen), washed with HBSS and deproteinized with 5% sulfosalicylic acid (Sigma). Lysates were obtained by applying 2 freeze-thaw cycles of liquid nitrogen and a 37°C water bath, followed by 5 min incubation on ice and centrifugation at 10,000 rcf for 10 min (4°C). Samples were measured undiluted and absorption was evaluated at 412 nm every min for 5 min, using the Benchmark Plus (BioRad). All values were corrected for blank, normalized to ciPTEC-parent and results were plotted with GraphPad Prism (version 5.03, GraphPad Software).

Data analysis and statistic

All data analysis and statistics were performed using GraphPad Prism (version 5.03, GraphPad Software) and presented as mean±S.E.M. of three independent experiments (n=3) performed in experimental triplicate, unless stated otherwise. For calculation of EC₅₀ values, log cisplatin concentration versus viability was plotted after background subtraction. Statistics were performed by Student's t-test (two-tailed, $\alpha=0.05$) or by two-way ANOVA (two-tailed, $\alpha=0.05$) using the Bonferroni post test ($p<0.05$), as indicated in the figures.

Results

The toxic potential of cisplatin was evaluated in parent ciPTEC by exposure for up to 72 h, which resulted in a concentration- and time-dependent loss in cell viability as measured via the MTT assay, presented in Figure 3.1A. To elucidate the role of influx transporter activity on cisplatin-induced toxicity, ciPTEC-parent was co-exposed to cisplatin in presence of the OCT2 substrate cimetidine or CTR1 substrate CuSO₄ for 24 h. Both substrates significantly attenuated toxicity of cisplatin, demonstrating their

involvement in uptake and related toxicity of the drug (Figure 3.1B). Next, cisplatin exposure to ciPTEC either expressing OAT1 or OAT3 demonstrated reduced sensitivity compared to ciPTEC-parent, reflected by increased TC_{50} values, for which the largest shift was observed for ciPTEC-OAT3 (Figure 3.1C, Table 3.1). The involvement of OAT-mediated transport in cisplatin-induced toxicity was investigated further by cisplatin exposure in the presence of OAT substrates probenecid and diclofenac. These did not affect the cytotoxicity after 24 h nor after 7 days of pre-exposure, suggesting that OAT-mediated influx is not directly involved in reducing cisplatin sensitivity, nor that OAT transport results in the induction of protective cellular changes on a long term (Table 3.1). It should be noted that 7-day exposure to competitive inhibitor solvent (DMSO, 0.1% v/v) slightly reduced cisplatin-induced toxicity, which may be explained by inactivation of the drug by prolonged exposure to DMSO (Table 3.1)^[29]. In order to avoid possible adaptive responses that may affect drug sensitivity, cisplatin preconditioning at shorter incubation times was not performed. Moreover, longer term exposures usually take place *in vivo* when patients are treated with cisplatin, making 24 or 48 h exposures clinically more relevant. To investigate the intracellular capacity to handle oxidative stress induced by cisplatin, total glutathione content was analysed in the three cell lines. No significant changes were observed in glutathione content between ciPTEC-parent, ciPTEC-OAT1 ($p=0.44$) and ciPTEC-OAT3 ($p=0.56$) (Supplemental Figure S3.1). As decreased sensitivity to cisplatin might be due to the transduction process used to over-express OAT1 or OAT3, we evaluated cisplatin sensitivity in ciPTEC expressing enhanced yellow fluorescent protein (ciPTEC-eYFP) generated by the same transduction methodology. No difference in toxicity ($p=0.53$) was observed between ciPTEC-eYFP (TC_{50} 39 ± 7 μ M) and ciPTEC-parent (TC_{50} 34 ± 1 μ M, Table 3.1), supporting our hypothesis that OAT protein expression is responsible for diminished cisplatin-sensitivity in OAT1 or OAT3 expressing cells and excluding nonspecific aberrations induced by the transduction methods.

The next step was to determine cisplatin accumulation in the three cell lines, which showed a reduced trend in ciPTEC-OAT1 ($p=0.29$) and ciPTEC-OAT3 ($p=0.12$) as compared to ciPTEC-parent after exposure to excess cisplatin concentrations for 90 min (Figure 3.2A). Hence, cisplatin accumulation in the cell lines was directly associated with their sensitivity to cisplatin as assessed by cell viability. This could be the result of decreased OCT2 expression levels or increased MATE1 and MATE2-k expression, which facilitate cisplatin influx and efflux, respectively. ciPTEC expressing OAT3 showed slightly but significantly decreased OCT2 (*SLC22A2*) gene expression of 0.4 ± 0.1 fold, while the 0.5 ± 0.1 fold reduction in ciPTEC-OAT1 was not significant. On the other hand, MATE1 (*SCL47A1*) was 16.2 ± 0.3 fold increased in ciPTEC-OAT1 and 6.1 ± 0.7 fold in ciPTEC-OAT3 (Figure 3.2B, C_t values are shown in Supplemental

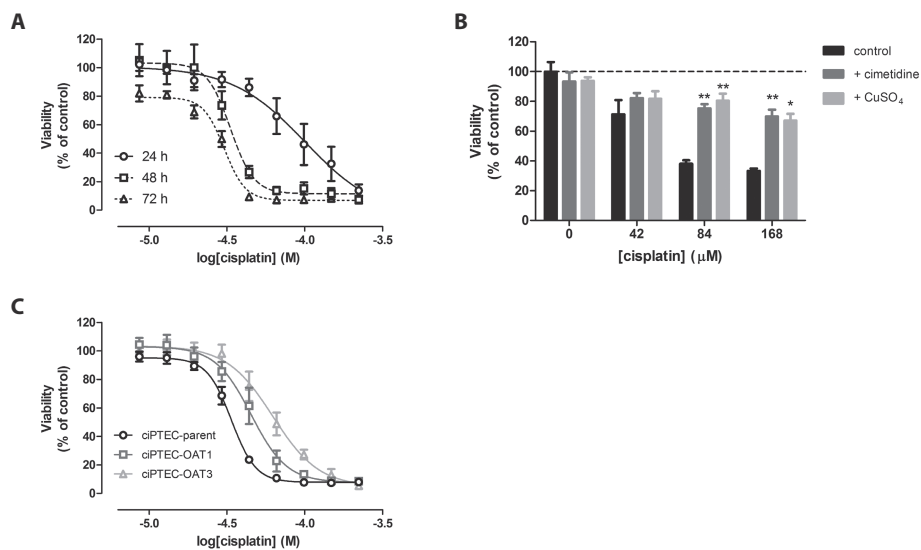


Figure 3.1 Cisplatin sensitivity in ciPTEC is reduced by OAT1 and OAT3 expression, and is dependent on OCT2- and CTR1-mediated transport. (A) Time and dose- dependent decrease in viability of ciPTEC-parent following exposure to cisplatin (8.7-222 μM) for 24, 48 or 72 h as determined by MTT assay (mean \pm S.E.M., n=3). (B) Decreased viability of ciPTEC-parent upon cisplatin exposure could be partially restored by competitive inhibition of OCT2 (cimetidine; 1.25 mM) or CTR1 (CuSO_4 ; 1.25 mM) for 24 h, determined by MTT assay (mean \pm S.E.M., n=3, * p <0.05, ** p <0.01; compared to control by Student's t-test). (C) Reduced sensitivity of ciPTEC-OAT1 and ciPTEC-OAT3 following exposure to cisplatin (8.7-222 μM) for 24 h compared to ciPTEC-parent, as determined by MTT assay (mean \pm S.E.M., n=3). Results are normalized to unexposed ciPTEC.

Table 3.1 Cisplatin-induced toxicity is independent of OAT-mediated transport in ciPTEC-OAT1 and ciPTEC-OAT3. TC_{50} values (represented in μM) calculated from MTT viability assays following cisplatin (8.7-222 μM) exposure for 24 h are not affected by 24 h (n=3) and 7 day (n=6) competitive inhibition of OAT (probenecid, 100 μM ; diclofenac, 50 μM) in ciPTEC-parent, ciPTEC-OAT1 and ciPTEC-OAT3 (mean TC_{50} \pm S.E.M., * p <0.05, *** p <0.001; compared to ciPTEC-parent, no significant differences were found for treatments by two-way ANOVA, N.D. is not determined).

	co-exposure (24 h)		co- and pre-exposure (7 days)	
	-	+	-	+
ciPTEC-parent				
probenecid	33 \pm 3	29 \pm 4	47 \pm 4	45 \pm 3
diclofenac	34 \pm 1	34 \pm 1	N.D.	N.D.
ciPTEC-OAT1				
probenecid	53 \pm 2*	49 \pm 3	45 \pm 6	45 \pm 6
diclofenac	45 \pm 6	45 \pm 4	N.D.	N.D.
ciPTEC-OAT3				
probenecid	92 \pm 8***	93 \pm 7***	80 \pm 2***	76 \pm 6***
diclofenac	64 \pm 11*	62 \pm 13*	N.D.	N.D.

Table S3.1). In addition, MATE2-k gene expression was increased in ciPTEC-OAT1, but decreased in ciPTEC-OAT3. Although MRP2 (*ABCC2*) expression has also been associated with reduced cisplatin sensitivity^[30], we did not find differential regulation of this drug transporter between the three cell lines studied (Supplemental Table S3.2). To evaluate the functional contribution of influx and efflux transporters further, cisplatin accumulation was analyzed in the presence of the competitive OCT2 inhibitor cimetidine and resulted in a reduction of intracellular cisplatin levels, that was significant for ciPTEC-OAT1, but not for ciPTEC-parent ($p=0.32$) or -OAT3 ($p=0.33$). Pyrimethamine did not affect cisplatin accumulation at concentrations for which it is a selective MATE1 substrate^[31], suggesting a limited role of MATE-mediated efflux in the current experimental conditions (Figure 3.2C). Competitive MATE inhibition by pyrimethamine did not affect cisplatin-induced toxicity following co-exposure for 24 h, again supporting the limited role of MATE in the current conditions (Table 3.2).

To study the influence of OAT expression on OCT2 protein activity in more detail, we investigated uptake of ASP^+ as specific substrate for the transporter in all ciPTEC cell lines in presence and absence of OCT2, MATE and OAT substrates. V_{max} of ASP^+ uptake was significantly reduced in ciPTEC-OAT1 ($13.1 \pm 0.3 \text{ min}^{-1}$) and ciPTEC-OAT3 ($21.6 \pm 0.6 \text{ min}^{-1}$) compared to ciPTEC-parent ($23.5 \pm 0.1 \text{ min}^{-1}$), suggesting that OCT2-mediated uptake capacity of ASP^+ is reduced in ciPTEC expressing OAT1 or OAT3 (Figure 3.3A, Table 3.3). As expected, competitive inhibition of OCT2 by cimetidine reduced ASP^+ accumulation (Figure 3.3B), while the competitive MATE inhibitor pyrimethamine did not affect ASP^+ accumulation, suggesting that ASP^+ is transported by OCT2 and not by MATE, which is in line with cisplatin accumulation assays (Figure 3.3C). Competitive OAT inhibition by probenecid did not affect ASP^+ accumulation after 24 h (Figure 3.3D), neither after 7 days (Figure 3.3E) of treatment, suggesting that OAT-mediated uptake did not regulate OCT2 transport capacity.

The Nrf2 pathway is known to attenuate cisplatin-mediated toxicity by regulation of cisplatin transporters^[32]. Therefore, the involvement of this pathway in the regulation of OCT2 and MATE transporters was evaluated in ciPTEC. Bardoxolone stimulated the Nrf2 pathway in ciPTEC parent, as assessed by increasing expression of both target genes *NQO1* and *GCLC* upon 24 h exposure by a factor of 6.1 ± 0.1 and 4.1 ± 0.2 , respectively (Figure 3.4A). This was accompanied by a 1.7 ± 0.2 fold increased MATE1, a 8.5 ± 0.6 fold increased MATE2-k and a 0.3 ± 0.1 fold decreased OCT2 expression, supporting the nephroprotective effect of Nrf2. A similar decrease in OCT2 expression was observed for ciPTEC-OAT1 and ciPTEC-OAT3, as described above. The involvement of Nrf2 in differential regulation of cisplatin transporters in ciPTEC-OAT1 and ciPTEC-OAT3 compared to ciPTEC-parent could however not be confirmed, as

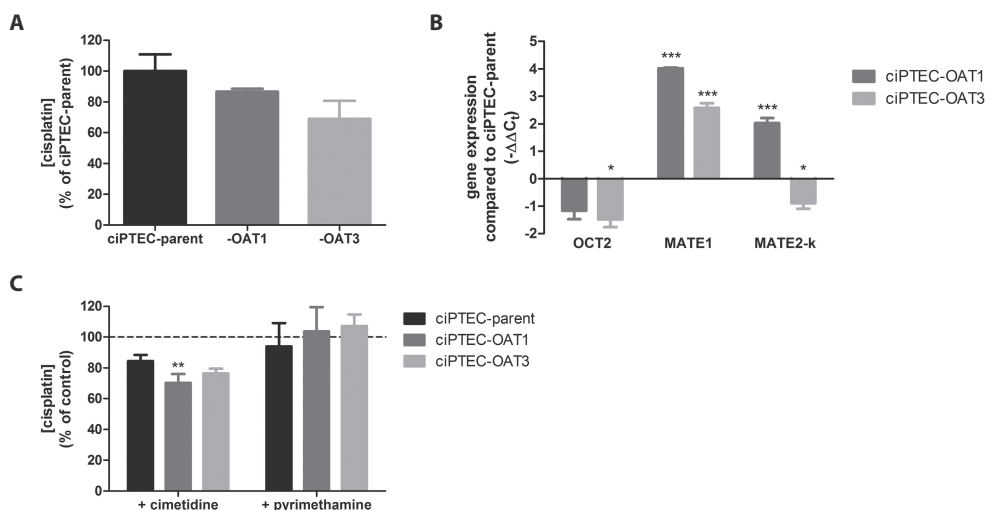


Figure 3.2 Decreased intracellular cisplatin accumulation and OCT2 gene expression in ciPTEC-OAT1 and ciPTEC-OAT3. (A) Whole-cell cisplatin content is decreased in ciPTEC-OAT1 and ciPTEC-OAT3 compared to ciPTEC-parent, following exposure to cisplatin (250 μ M) for 90 min. Results are normalized to ciPTEC-parent (mean \pm S.E.M., n=3, performed with 2 experimental replicates, no significant differences were found by one-way ANOVA). (B) Gene expression of OCT2 (*SLC22A2*) is decreased, while gene expression of MATE1 (*SLC47A1*) and MATE2-k (*SLC47A2*) is increased in ciPTEC-OAT1 and ciPTEC-OAT3 compared to ciPTEC-parent, using *GAPDH* as reference gene (mean \pm S.E.M., n=3, performed with 1 experimental replicate, * p <0.05, *** p <0.001; compared to ciPTEC-parent by one-way ANOVA). (C) Whole-cell cisplatin content is decreased by co-exposure to OCT2-substrate cimetidine (1.25 mM), but is not affected by co-exposure to MATE-substrate pyrimethamine (100 nM) during exposure to cisplatin for 90 min in ciPTEC-parent, ciPTEC-OAT1 and ciPTEC-OAT3. Results are normalized to control without substrate (mean \pm S.E.M., n=3, performed with 2 experimental replicates, ** p <0.01; compared to control by Student's t-test).

Table 3.2 Cisplatin-induced toxicity is independent of MATE-mediated transport in ciPTEC-parent, ciPTEC-OAT1 and ciPTEC-OAT3. TC_{50} values (represented in μ M) calculated from MTT viability assays following cisplatin (8.7-222 μ M) exposure for 24 h are not affected by competitive MATE inhibition (pyrimethamine, 10 and 100 nM) in ciPTEC-parent, ciPTEC-OAT1 and ciPTEC-OAT3 (mean TC_{50} , n=2).

	control		pyrimethamine	
			10 nM	100 nM
ciPTEC-parent	41		45	46
ciPTEC-OAT1	59		57	57
ciPTEC-OAT3	103		111	136

only the Nrf2 target *NQO1* was increased 2.7 ± 0.2 fold in ciPTEC-OAT1, while *GCLC* was neither upregulated in ciPTEC-OAT1 nor ciPTEC-OAT3 (Figure 3.4B). This illustrates that stimulation of Nrf2 via bardoxolone is distinct from the gene expression pattern observed in ciPTEC-OAT1 and ciPTEC-OAT3, indicating that the differences in OCT2 and MATE expression observed are not solely caused by Nrf2 pathway induction.

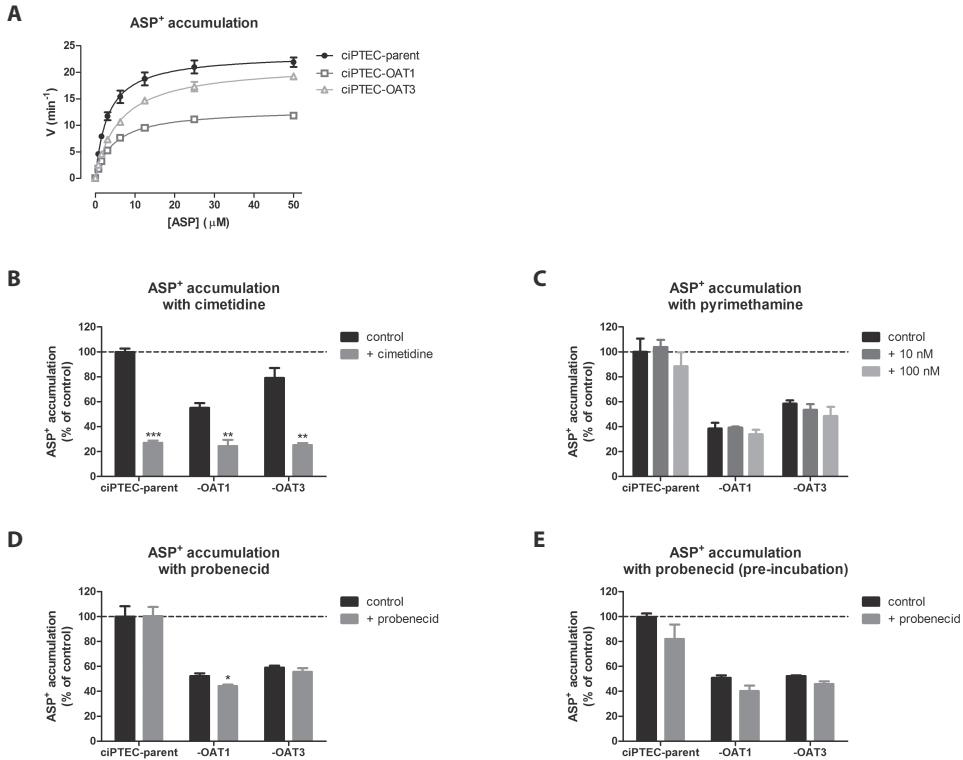


Figure 3.3 Reduced ASP⁺ accumulation reflects attenuated OCT2 transport capacity in ciPTEC-OAT1 and ciPTEC-OAT3. (A) ASP⁺ (0.8-50 μM) accumulation for 60 min is decreased in ciPTEC-OAT1 and ciPTEC-OAT3 compared to ciPTEC-parent, evaluated by intracellular fluorescence intensity after 60 min (mean±S.E.M., n=3). (B, C, D) ASP⁺ (3.1 μM) accumulation for 60 min in ciPTEC-parent, ciPTEC-OAT1 and ciPTEC-OAT3 is reduced by (B) competitive inhibition of OCT (cimetidine, 1.25 mM), but not affected by competitive inhibition of (C) MATE (pyrimethamine, 10 and 100 nM) or (D) OAT (probenecid, 100 μM), evaluated by intracellular fluorescence intensity. Results are normalized to unexposed ciPTEC-parent (mean±S.E.M., n=3, *p<0.05, **p<0.01, ***p<0.001; compared to control by Student's t-test). (E) ASP⁺ (3.1 μM) accumulation in for 60 min in ciPTEC-parent, ciPTEC-OAT1 and ciPTEC-OAT3 is not affected by 7-day competitive OAT inhibition (probenecid, 100 μM), evaluated by intracellular fluorescence intensity. Results are normalized to unexposed ciPTEC-parent (mean±S.E.M., n=2, no significant differences were found for treatment by Student's t-test).

Table 3.3 ASP⁺ accumulation is decreased in ciPTEC-OAT1 and ciPTEC-OAT3. K_m (represented in μM) and V_{max} values (represented in min^{-1}) calculated from Michaelis-Menten fitted ASP⁺ accumulation assays in ciPTEC-parent, ciPTEC-OAT1 and ciPTEC-OAT3 (mean \pm S.E.M., $n=3$, * $p<0.05$, ** $p<0.01$, *** $p<0.001$; compared to ciPTEC-parent by one-way ANOVA).

	K_m	V_{max}
ciPTEC-parent	2.3 ± 0.3	23.5 ± 0.1
ciPTEC-OAT1	$4.7 \pm 0.4^*$	$13.1 \pm 0.3^{***}$
ciPTEC-OAT3	$6.2 \pm 0.3^{***}$	$21.6 \pm 0.6^{**}$

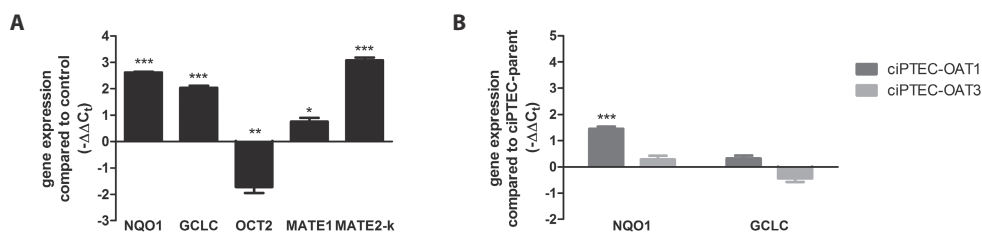


Figure 3.4 Nrf2 pathway activation by bardoxolone in ciPTEC-parent is associated with cisplatin transporter regulation, but is not increased in ciPTEC-OAT1 and -OAT3, compared to parent ciPTEC. (A) Gene expression of Nrf2 target genes *NQO1* and *GCLC* is increased after 24 h pre-exposure to bardoxolone (50 nM), which is associated with decreased *OCT2* (*SLC22A2*) gene expression, while gene expression of *MATE1* (*SLC47A1*) and *MATE2-k* (*SLC47A2*) is increased in parent ciPTEC, using *GAPDH* as reference gene (mean \pm S.E.M., $n=3$, performed with 1 experimental replicate, * $p<0.05$, ** $p<0.01$, *** $p<0.001$; compared to control by Student's t-test). (B) Gene expression of Nrf2 target genes *NQO1* and *GCLC* is not consistently increased in ciPTEC-OAT1 and ciPTEC-OAT3, compared to ciPTEC-parent, using *GAPDH* as reference gene (mean \pm S.E.M., $n=3$, performed with 1 experimental replicate, *** $p<0.001$; compared to ciPTEC-parent by one-way ANOVA).

Discussion

Cisplatin is a well-described nephrotoxicant, affecting the proximal tubule in particular. Here, we demonstrate that the human-derived proximal tubule epithelial cell model, ciPTEC, is sensitive to OCT2- and CTR1-mediated cisplatin-induced toxicity. Expression of OAT1 and OAT3 reduced ciPTEC sensitivity to cisplatin, which is independent of OAT transport activity, and is associated with a trend towards reduced intracellular cisplatin accumulation, explained by reduced OCT2-mediated uptake capacity.

The mechanism responsible for reduced cisplatin sensitivity in ciPTEC-OAT1 and ciPTEC-OAT3 involves reduced OCT2-dependent influx of the drug. ASP⁺ is a model substrate for OCT2 and was used to evaluate OCT2 transport capacity, which was decreased in ciPTEC expressing OAT. We can only speculate on how this is regulated, but this could involve the Nrf2 pathway, as Nrf2-null mice developed more extensive nephrotoxicity after cisplatin treatment compared to wild types^[33]. Nrf2-mediated signalling reduces expression of OCT2 in rat cortical tissue and MDCK cells, and increases expression of MATE1 in primary human proximal tubule cells, reducing renal cisplatin accumulation and toxicity^[32, 34, 35]. In ciPTEC-parent, the involvement of Nrf2 in down-regulation of OCT2 and upregulation of MATE1 could be confirmed supporting previous *in vivo* and *in vitro* studies^[32, 33]. Remarkably, we found a profound increase of MATE2-k gene expression, while the effect for MATE1 was less pronounced. Regulation of MATE2-k via Nrf2 was recently published when proximal tubule cells were exposed to flow^[36]. With respect to cisplatin-induced toxicity, OAT expression affected OCT2 and MATE1/2-k, for which the direct involvement of Nrf2 remains elusive as established target genes of this pathway were not consistently regulated. Therefore, the protective effect on cisplatin toxicity via bardoxolone-mediated Nrf-2 stimulation was not tested in the current study focusing on the differential effect of OAT expression. Alternatively, tyrosine kinase inhibitors reduced OCT2 activity and oxaliplatin-induced acute neuropathy *in vivo*, suggesting a role for tyrosine phosphorylation in regulation of OCT2^[37]. It is important to note that cisplatin sensitivity and accumulation were reduced most pronounced for ciPTEC-OAT3, while ASP⁺ accumulation was reduced mostly in ciPTEC-OAT1. This suggests that additional, non-elucidated cell protecting mechanisms in parallel of the Nrf2 pathway or tyrosine kinase activity might play a role in the protection against cisplatin toxicity.

In addition to drug transport function, OAT1 and OAT3 are associated with several metabolite pathways, including fatty acid, amino acid, nucleic acid, glucose, pyruvate and glutathione metabolism^[38, 39]. As a result, a hypothesis was postulated on the role of drug transporters in detecting and maintaining levels of endogenous metabolites, antioxidants, signalling molecules, hormones and nutrients^[40, 41]. OAT-mediated transport is bidirectional and therefore its activity influences the intracellular concentration of counter-transported compounds, including metabolites of the citric acid cycle, predominantly alpha-ketoglutarate^[42-44]. Reduced or competitively inhibited OAT function might therefore reduce energy metabolism, illustrated by reduced active transport of para-aminohippuric acid upon inhibition of mitochondrial ATP production^[45]. This, in turn, may affect drug-induced toxicity response in proximal tubules by pre-disposing redox state and supplementing or depleting the energy pool. Since reactive oxygen species (ROS) are key players in cisplatin-induced

nephrotoxicity, the proximal tubule redox state and cellular content of the ROS scavenger glutathione are highly important for sensitivity to drug-induced toxicity^[2, 3]. No significant differences in total glutathione content were observed among the ciPTEC cell lines, suggesting that redox metabolism is not directly affected by (lack of) OAT function in ciPTEC. The expression of OAT could have influenced the intracellular proton gradient thereby decreasing the membrane potential which drives transport by OCTs^[46, 47]. This might explain the increased K_m values for ASP⁺ accumulation in ciPTEC-OAT1 and ciPTEC-OAT3 as observed in the present study. Metabolomic analysis of compounds involved in energy production, especially of the citric acid cycle, may generate a more profound understanding of the role of OAT transporters in cellular homeostasis and drug sensitivity.

The present findings contradict previously reported publications, involving *in vivo* studies. Jacobs *et al.* suggested that cisplatin co-treatment with probenecid competitively inhibited OAT-mediated transport, thereby reducing the renal clearance of cisplatin and protecting patients from nephrotoxicity, even at dose-escalation^[15, 16]. In line with this, reduced cisplatin excretion and attenuated nephrotoxicity were observed in cisplatin-treated Oat1 knockout mice, and probenecid co-treated wild-type mice^[14]. The authors of the latter study suggested that cisplatin is converted into a highly reactive mercapturic acid metabolite, which is a substrate for OAT1 and OAT3, similar as described for cadmium and mercury^[48-50]. However, the first conversion step involves extra-renal conjugation of cisplatin to glutathione, generating a water soluble metabolite filtered by the glomerulus. Proximal tubule cells are therefore mainly apically exposed to the conjugated metabolite, suggesting limited involvement of basolaterally located OAT1 and OAT3. This indicates that current *in vitro* models underestimate the complexity of drug-induced renal injury. To account for the contribution of metabolism, our *in vitro* model could be extended to include pre-exposure of cisplatin to cultured hepatocytes or precision-cut liver slices^[51]. In contrast to studies in which OAT function contributes to nephrotoxicity, the beneficial effects of OAT-mediated transport on renal function have also been described. Ischemia reperfusion resulted in severe kidney injury in rats, which was accompanied by reduced expression of Oat1 and Oat3. Indomethacin prevented ischemia-induced downregulation of Oat1 and Oat3, while probenecid abolished indomethacin-mediated attenuation^[52]. As cisplatin-induced proximal tubule toxicity can induce a similar decrease of Oat1 and Oat3 expression^[53], investigating indomethacin-mediated regulation of OAT1 and OAT3, might provide an interesting mechanism that can explain reduced renal adverse effects.

Most *in vitro* models applied in drug-induced toxicity prediction lack human- and tissue-relevant expression of transporters and metabolizing enzymes^[54-57]. The proximal tubule model used here circumvents these issues as it demonstrates a tissue-specific expression profile in a human-derived stable cell line. To enable drug-induced toxicity evaluation of compounds that require influx by OAT transporters, OAT1 or OAT3 were re-introduced by lentiviral transfection of parent ciPTEC, generating ciPTEC-OAT1 and ciPTEC-OAT3^[17]. As this method may have induced genetic aberrations, a similar transduction process was performed with eYFP, to show that the transfection procedure did not significantly affect cisplatin sensitivity.

Functional MATE-mediated transport was lacking in our experimental conditions, illustrated by the inability of pyrimethamine to modulate ASP⁺ and cisplatin accumulation, and subsequent cisplatin-induced toxicity. This may be the result of limited polarization of ciPTEC under the current culture conditions, although activity of OCT2, OAT1 and OAT3 which are exclusively expressed at the basolateral membrane *in vivo*, was demonstrated. Although pyrimethamine is offered extracellularly, which may compromise inhibition of MATE-mediated cisplatin extrusion, MATE protein levels were below the limit of detection with Western blotting in ciPTEC (data not shown). Therefore, MATE transport function was not studied further in ciPTEC. Additional experiments using a polarized culture system could be used to enhance the expression levels and possibly transport activity of MATE1 and MATE2-k.

ASP⁺ and cisplatin have been described as MATE1-substrates *in vitro* and MATE1 has been shown to mediate efflux of cisplatin in rodents *in vivo*^[9, 10, 31, 58]. The driving force for MATE-mediated transport is a counter-directed gradient of H⁺^[59]. Transport of cisplatin was demonstrated upon intracellular acidification, resulting in a non-physiological outward-directed proton gradient and MATE-mediated influx^[9]. All experiments in ciPTEC were performed at a buffered pH of 7.4, thus lacking driving force for MATE. Important to consider is the limited cationic charge of cisplatin in buffers that contain a physiological chloride concentration, reflecting blood plasma, while it is twofold positively charged when exposed to low chloride, reflecting the cytoplasm^[60, 61]. Apparent transport affinities might be different for the neutral or charged form, possibly affecting accumulation of the drug and further increasing the mechanistic complexity of cisplatin-induced toxicity. In short, the *in vivo* contribution of MATE-mediated efflux to cisplatin-induced nephrotoxicity in humans remains to be elucidated. Evaluating cisplatin-induced toxicity in bi-compartmental Transwell® or 3D culture models that allow for mimicking of the pH gradient as experienced in the physiological proximal tubule, may help to elucidate the involvement of MATE in this process.

In conclusion, we demonstrated that expression of OAT1 or OAT3 in a human-derived proximal tubule epithelial cell model resulted in reduced sensitivity to cisplatin. This was independent of OAT transport function and most likely explained by a reduced OCT2-mediated influx capacity. As organic anion transporters influence sensitivity to drugs that are typically handled by organic cation transporters, reliable *in vitro* drug-induced nephrotoxicity evaluation requires simultaneous expression of basolateral solute carrier transport proteins.

Acknowledgements

This work was financially supported by a grant from the Dutch Kidney Foundation (grant nr. KJPB 11.023), by the CRACK-IT NephroTube Challenge funded by NC3Rs (project no. 37497-25920) and by the German Research Foundation (Cluster of Excellence "Unifying Concepts in Catalysis", EXC 314, Project Area E3). The authors declare no potential conflict of interest.

References

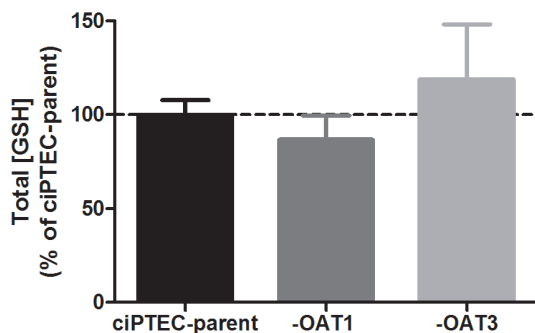
1. Hartmann JT, Kollmannsberger C, Kanz L, Bokemeyer C. Platinum organ toxicity and possible prevention in patients with testicular cancer. *Int J Cancer*. 83, 866-869 (1999).
2. Wang D, Lippard SJ. Cellular processing of platinum anticancer drugs. *Nat Rev Drug Discov*. 4, 307-320 (2005).
3. Manohar S, Leung N. Cisplatin nephrotoxicity: a review of the literature. *J Nephrol*. 31, 15-25 (2018).
4. Nigam SK, Wu W, Bush KT, Hoenig MP, Blantz RC, Bhatnagar V. Handling of Drugs, Metabolites, and Uremic Toxins by Kidney Proximal Tubule Drug Transporters. *Clin J Am Soc Nephrol*. 10, 2039-2049 (2015).
5. Ciarimboli G, Deuster D, Knief A, Sperling M, Holtkamp M, Edemir B, Pavenstadt H, et al. Organic cation transporter 2 mediates cisplatin-induced oto- and nephrotoxicity and is a target for protective interventions. *Am J Pathol*. 176, 1169-1180 (2010).
6. Ciarimboli G, Ludwig T, Lang D, Pavenstadt H, Koepsell H, Piechota HJ, Haier J, et al. Cisplatin nephrotoxicity is critically mediated via the human organic cation transporter 2. *Am J Pathol*. 167, 1477-1484 (2005).
7. Filipski KK, Mathijssen RH, Mikkelsen TS, Schinkel AH, Sparreboom A. Contribution of organic cation transporter 2 (OCT2) to cisplatin-induced nephrotoxicity. *Clin Pharmacol Ther*. 86, 396-402 (2009).
8. Pabla N, Murphy RF, Liu K, Dong Z. The copper transporter Ctr1 contributes to cisplatin uptake by renal tubular cells during cisplatin nephrotoxicity. *Am J Physiol Renal Physiol*. 296, F505-511 (2009).
9. Nakamura T, Yonezawa A, Hashimoto S, Katsura T, Inui K. Disruption of multidrug and toxin extrusion MATE1 potentiates cisplatin-induced nephrotoxicity. *Biochem Pharmacol*. 80, 1762-1767 (2010).
10. Yonezawa A, Masuda S, Yokoo S, Katsura T, Inui K. Cisplatin and oxaliplatin, but not carboplatin and nedaplatin, are substrates for human organic cation transporters (SLC22A1-3 and multidrug and toxin extrusion family). *J Pharmacol Exp Ther*. 319, 879-886 (2006).
11. Li Q, Guo D, Dong Z, Zhang W, Zhang L, Huang SM, Polli JE, et al. Ondansetron can enhance cisplatin-induced nephrotoxicity via inhibition of multiple toxin and extrusion proteins (MATEs). *Toxicol Appl Pharmacol*. 273, 100-109 (2013).
12. Chang C, Hu Y, Hogan SL, Mercke N, Gomez M, O'Bryant C, Bowles DW, et al. Pharmacogenomic Variants May Influence the Urinary Excretion of Novel Kidney Injury Biomarkers in Patients Receiving Cisplatin. *Int J Mol Sci*. 18, (2017).
13. Sauzay C, White-Koning M, Hennebelle I, Deluche T, Delmas C, Imbs DC, Chatelut E, et al. Inhibition of OCT2, MATE1 and MATE2-K as a possible mechanism of drug interaction between pazopanib and cisplatin. *Pharmacol Res*. 110, 89-95 (2016).
14. Hu S, Leblanc AF, Gibson AA, Hong KW, Kim JY, Janke LJ, Li L, et al. Identification of OAT1/OAT3 as Contributors to Cisplatin Toxicity. *Clin Transl Sci*. 10, 412-420 (2017).
15. Jacobs C, Coleman CN, Rich L, Hirst K, Weiner MW. Inhibition of cis-diamminedichloroplatinum secretion by the human kidney with probenecid. *Cancer Res*. 44, 3632-3635 (1984).
16. Jacobs C, Kaubisch S, Halsey J, Lum BL, Gosland M, Coleman CN, Sikic BI. The use of probenecid as a chemoprotector against cisplatin nephrotoxicity. *Cancer*. 67, 1518-1524 (1991).
17. Nieskens TT, Peters JG, Schreurs MJ, Smits N, Woestenenk R, Jansen K, van der Made TK, et al. A Human Renal Proximal Tubule Cell Line with Stable Organic Anion Transporter 1 and 3 Expression Predictive for Antiviral-Induced Toxicity. *Aaps j*. 18, 465-475 (2016).
18. Wilmer MJ, Saleem MA, Masereeuw R, Ni L, van der Velden TJ, Russel FG, Mathieson PW, et al. Novel conditionally immortalized human proximal tubule cell line expressing functional influx and efflux transporters. *Cell Tissue Res*. 339, 449-457 (2010).

19. Schophuizen CM, Wilmer MJ, Jansen J, Gustavsson L, Hilgendorf C, Hoenderop JG, van den Heuvel LP, et al. Cationic uremic toxins affect human renal proximal tubule cell functioning through interaction with the organic cation transporter. *Pflugers Arch.* 465, 1701-1714 (2013).
20. Jansen J, Schophuizen CM, Wilmer MJ, Lahham SH, Mutsaers HA, Wetzels JF, Bank RA, et al. A morphological and functional comparison of proximal tubule cell lines established from human urine and kidney tissue. *Exp Cell Res.* 323, 87-99 (2014).
21. Mutsaers HA, Wilmer MJ, Reijnders D, Jansen J, van den Broek PH, Forkink M, Schepers E, et al. Uremic toxins inhibit renal metabolic capacity through interference with glucuronidation and mitochondrial respiration. *Biochim Biophys Acta.* 1832, 142-150 (2013).
22. Schirris TJJ, Jansen J, Mihajlovic M, van den Heuvel LP, Masereeuw R, Russel FGM. Mild intracellular acidification by dexamethasone attenuates mitochondrial dysfunction in a human inflammatory proximal tubule epithelial cell model. *Sci Rep.* 7, 10623 (2017).
23. Koopman WJ, Visch HJ, Smeitink JA, Willems PH. Simultaneous quantitative measurement and automated analysis of mitochondrial morphology, mass, potential, and motility in living human skin fibroblasts. *Cytometry A.* 69, 1-12 (2006).
24. Mosmann T. Rapid colorimetric assay for cellular growth and survival: application to proliferation and cytotoxicity assays. *J Immunol Methods.* 65, 55-63 (1983).
25. Durr KL, Tavraz NN, Spiller S, Friedrich T. Measuring cation transport by Na,K- and H,K-ATPase in *Xenopus* oocytes by atomic absorption spectrophotometry: an alternative to radioisotope assays. *J Vis Exp.* e50201 (2013).
26. Eljack ND, Ma HY, Drucker J, Shen C, Hambley TW, New EJ, Friedrich T, et al. Mechanisms of cell uptake and toxicity of the anticancer drug cisplatin. *Metallomics.* 6, 2126-2133 (2014).
27. Pietruck F, Ullrich KJ. Transport interactions of different organic cations during their excretion by the intact rat kidney. *Kidney Int.* 47, 1647-1657 (1995).
28. Cetinkaya I, Ciarimboli G, Yalcinkaya G, Mehrens T, Velic A, Hirsch JR, Gorboulev V, et al. Regulation of human organic cation transporter hOCT2 by PKA, PI3K, and calmodulin-dependent kinases. *Am J Physiol Renal Physiol.* 284, F293-302 (2003).
29. Hall MD, Telma KA, Chang KE, Lee TD, Madigan JP, Lloyd JR, Goldlust IS, et al. Say no to DMSO: dimethylsulfoxide inactivates cisplatin, carboplatin, and other platinum complexes. *Cancer Res.* 74, 3913-3922 (2014).
30. Kawabe T, Chen ZS, Wada M, Uchiumi T, Ono M, Akiyama S, Kuwano M. Enhanced transport of anticancer agents and leukotriene C4 by the human canalicular multispecific organic anion transporter (cMOAT/MRP2). *FEBS Lett.* 456, 327-331 (1999).
31. Ito S, Kusuvara H, Kuroiwa Y, Wu C, Moriyama Y, Inoue K, Kondo T, et al. Potent and specific inhibition of mMate1-mediated efflux of type I organic cations in the liver and kidney by pyrimethamine. *J Pharmacol Exp Ther.* 333, 341-350 (2010).
32. Atilano-Roque A, Aleksunes LM, Joy MS. Bardoxolone methyl modulates efflux transporter and detoxifying enzyme expression in cisplatin-induced kidney cell injury. *Toxicol Lett.* 259, 52-59 (2016).
33. Aleksunes LM, Goedken MJ, Rockwell CE, Thomale J, Manautou JE, Klaassen CD. Transcriptional regulation of renal cytoprotective genes by Nrf2 and its potential use as a therapeutic target to mitigate cisplatin-induced nephrotoxicity. *J Pharmacol Exp Ther.* 335, 2-12 (2010).
34. Huang D, Wang C, Duan Y, Meng Q, Liu Z, Huo X, Sun H, et al. Targeting Oct2 and P53: Formononetin prevents cisplatin-induced acute kidney injury. *Toxicol Appl Pharmacol.* 326, 15-24 (2017).
35. Shu Y, Bello CL, Mangravite LM, Feng B, Giacomini KM. Functional characteristics and steroid hormone-mediated regulation of an organic cation transporter in Madin-Darby canine kidney cells. *J Pharmacol Exp Ther.* 299, 392-398 (2001).

36. Fukuda Y, Kaishima M, Ohnishi T, Tohyama K, Chisaki I, Nakayama Y, Ogasawara-Shimizu M, et al. Fluid shear stress stimulates MATE2-K expression via Nrf2 pathway activation. *Biochem Biophys Res Commun.* 484, 358-364 (2017).
37. Sprowl JA, Ong SS, Gibson AA, Hu S, Du G, Lin W, Li L, et al. A phosphotyrosine switch regulates organic cation transporters. *Nat Commun.* 7, 10880 (2016).
38. Ahn SY, Jamshidi N, Mo ML, Wu W, Eraly SA, Dnyanmote A, Bush KT, et al. Linkage of organic anion transporter-1 to metabolic pathways through integrated "omics"-driven network and functional analysis. *J Biol Chem.* 286, 31522-31531 (2011).
39. Wu W, Jamshidi N, Eraly SA, Liu HC, Bush KT, Palsson BO, Nigam SK. Multispecific drug transporter Slc22a8 (Oat3) regulates multiple metabolic and signaling pathways. *Drug Metab Dispos.* 41, 1825-1834 (2013).
40. Nigam SK. What do drug transporters really do? *Nat Rev Drug Discov.* 14, 29-44 (2015).
41. Bush KT, Wu W, Lun C, Nigam SK. The drug transporter OAT3 (SLC22A8) regulates endogenous metabolite flow through the gut-liver-kidney axis. *J Biol Chem.* 292, 15789-15803 (2017).
42. Kauffhold M, Schulz K, Brejcek D, Gupta S, Henjakovic M, Krick W, Hagos Y, et al. Differential interaction of dicarboxylates with human sodium-dicarboxylate cotransporter 3 and organic anion transporters 1 and 3. *Am J Physiol Renal Physiol.* 301, F1026-1034 (2011).
43. Burckhardt BC, Burckhardt G. Transport of organic anions across the basolateral membrane of proximal tubule cells. *Rev Physiol Biochem Pharmacol.* 146, 95-158 (2003).
44. Sweet DH, Chan LM, Walden R, Yang XP, Miller DS, Pritchard JB. Organic anion transporter 3 (Slc22a8) is a dicarboxylate exchanger indirectly coupled to the Na⁺ gradient. *Am J Physiol Renal Physiol.* 284, F763-769 (2003).
45. Nagai J, Yano I, Hashimoto Y, Takano M, Inui K. Efflux of intracellular alpha-ketoglutarate via p-aminohippurate/dicarboxylate exchange in OK kidney epithelial cells. *J Pharmacol Exp Ther.* 285, 422-427 (1998).
46. Budiman T, Bamberg E, Koepsell H, Nagel G. Mechanism of electrogenic cation transport by the cloned organic cation transporter 2 from rat. *J Biol Chem.* 275, 29413-29420 (2000).
47. Okuda M, Urakami Y, Saito H, Inui K. Molecular mechanisms of organic cation transport in OCT2-expressing *Xenopus* oocytes. *Biochim Biophys Acta.* 1417, 224-231 (1999).
48. Zalups RK. Molecular interactions with mercury in the kidney. *Pharmacol Rev.* 52, 113-143 (2000).
49. Zalups RK. Evidence for basolateral uptake of cadmium in the kidneys of rats. *Toxicol Appl Pharmacol.* 164, 15-23 (2000).
50. Cannon VT, Zalups RK, Barfuss DW. Amino acid transporters involved in luminal transport of mercuric conjugates of cysteine in rabbit proximal tubule. *J Pharmacol Exp Ther.* 298, 780-789 (2001).
51. Starokozhko V, Vatakuti S, Schievink B, Merema MT, Asplund A, Synnergren J, Aspegren A, et al. Maintenance of drug metabolism and transport functions in human precision-cut liver slices during prolonged incubation for 5 days. *Arch Toxicol.* 91, 2079-2092 (2017).
52. Schneider R, Meusel M, Betz B, Held C, Moller-Ehrlich K, Buttner-Herold M, Wanner C, et al. Oat1/3 restoration protects against renal damage after ischemic AKI. *Am J Physiol Renal Physiol.* 308, F198-208 (2015).
53. Liu T, Meng Q, Wang C, Liu Q, Guo X, Sun H, Peng J, et al. Changes in expression of renal Oat1, Oat3 and Mrp2 in cisplatin-induced acute renal failure after treatment of JBP485 in rats. *Toxicol Appl Pharmacol.* 264, 423-430 (2012).
54. Shaw G, Morse S, Ararat M, Graham FL. Preferential transformation of human neuronal cells by human adenoviruses and the origin of HEK 293 cells. *Faseb j.* 16, 869-871 (2002).
55. Van der Hauwaert C, Savary G, Buob D, Leroy X, Aubert S, Flamand V, Hennino MF, et al. Expression profiles of genes involved in xenobiotic metabolism and disposition in human renal tissues and renal cell models. *Toxicol Appl Pharmacol.* 279, 409-418 (2014).

56. Wilmer MJ, Ng CP, Lanz HL, Vulto P, Suter-Dick L, Masereeuw R. Kidney-on-a-Chip Technology for Drug-Induced Nephrotoxicity Screening. *Trends Biotechnol.* 34, 156-170 (2016).
57. Chu X, Bleasby K, Evers R. Species differences in drug transporters and implications for translating preclinical findings to humans. *Expert Opin Drug Metab Toxicol.* 9, 237-252 (2013).
58. Wittwer MB, Zur AA, Khuri N, Kido Y, Kosaka A, Zhang X, Morrissey KM, et al. Discovery of potent, selective multidrug and toxin extrusion transporter 1 (MATE1, SLC47A1) inhibitors through prescription drug profiling and computational modeling. *J Med Chem.* 56, 781-795 (2013).
59. Tsuda M, Terada T, Asaka J, Ueba M, Katsura T, Inui K. Oppositely directed H⁺ gradient functions as a driving force of rat H⁺/organic cation antiporter MATE1. *Am J Physiol Renal Physiol.* 292, F593-598 (2007).
60. Andersson A, Ehrsson H. Stability of cisplatin and its monohydrated complex in blood, plasma and ultrafiltrate—implications for quantitative analysis. *J Pharm Biomed Anal.* 13, 639-644 (1995).
61. Jennerwein M, Andrews PA. Effect of intracellular chloride on the cellular pharmacodynamics of cis-diamminedichloroplatinum(II). *Drug Metab Dispos.* 23, 178-184 (1995).

Supplemental data



Supplemental Figure S3.1 Glutathione content is similar in ciPTEC-parent, ciPTEC-OAT1 and ciPTEC-OAT3. Evaluation of whole-cell total glutathione content in ciPTEC-parent, ciPTEC-OAT1 and ciPTEC-OAT3. Results are normalized to ciPTEC-parent (mean±S.E.M., n=3; no significant differences were found by one-way ANOVA).

Supplemental Table S3.1 Gene expression of OCT2 and MATE1/2-k is differentially regulated between ciPTEC-parent, ciPTEC-OAT1 and ciPTEC-OAT3. C_t values (A.U.) of OCT2, MATE1 and MATE2-k derived from RT-qPCR assays following SFM exposure for 24 h are within the quantifiable range and are differentially regulated between ciPTEC-parent, ciPTEC-OAT1 and ciPTEC-OAT3 (mean C_t ±S.E.M., n=3).

	ciPTEC-parent	ciPTEC-OAT1	ciPTEC-OAT3
GAPDH	17.7 ± 0.1	17.9 ± 0.1	17.3 ± 0.1
OCT2 (SLC22A2)	33.6 ± 0.2	35.0 ± 0.4	34.8 ± 0.2
MATE1 (SLC47A1)	28.4 ± 0.3	24.6 ± 0.1	25.5 ± 0.1
MATE2-k (SLC47A2)	31.9 ± 0.3	30.1 ± 0.3	32.5 ± 0.3

Supplemental Table S3.2 Gene expression of MRP2 is not differentially regulated between ciPTEC-parent, ciPTEC-OAT1 and ciPTEC-OAT3. C_t values (A.U.) of MRP2 derived from RT-qPCR assays following SFM exposure for 24 h are not differentially regulated between ciPTEC-parent, ciPTEC-OAT1 and ciPTEC-OAT3 (mean C_t ±S.E.M., n=3).

	ciPTEC-parent	ciPTEC-OAT1	ciPTEC-OAT3
GAPDH	18.0 ± 0.2	18.2 ± 0.5	16.8 ± 0.4
MRP2 (ABCC2)	33.1 ± 0.6	33.2 ± 0.6	31.6 ± 0.3



Antisense Oligonucleotide Therapy Causes Transient Low Molecular Weight Proteinuria via Competitive Inhibition of Receptor-Mediated Endocytosis in Proximal Tubules

Manoe J Janssen^{1,2*}, Tom TG Nieskens^{1*}, Tessa AM Steevels³, Pedro Caetano-Pinto^{1,2}, Dirk den Braanker¹, Melissa Mulder³, Yolanda Ponstein³, Shaun Jones³, Sjef de Kimpe³, Rosalinde Masereeuw^{1,2}, Cathaline den Besten^{3*}, Martijn J Wilmer^{1*}

¹ Department of Pharmacology and Toxicology, Radboud University Medical Center, Radboud Institute for Molecular Life Sciences, Nijmegen, The Netherlands

² Utrecht Institute for Pharmaceutical Sciences, Faculty of Science, Utrecht University, The Netherlands., The Netherlands;

³ BioMarin Nederland B.V., Leiden, The Netherlands.

*Authors contributed equally

In preparation

Abstract

Despite their promising potential as therapeutic molecules, reports of mild urinary low molecular weight proteinuria during antisense oligonucleotide therapy warrant mechanistic safety assessment studies focusing on the kidney. Treatment of Duchenne Muscular Dystrophy patients with drisapersen, a modified 2'O methylribose phosphorothioate antisense oligonucleotide, was associated with a reversible increase in urinary alpha-1-microglobulin without further kidney injury in a clinical study. Here, we used human kidney cells to demonstrate that the observed low molecular weight proteinuria reflects a transient disturbance rather than a direct, nephrotoxic effect. Oligonucleotides were rapidly taken up in human-derived conditionally immortalized proximal tubule epithelial cells (ciPTEC) and accumulated intracellularly in a dose-dependent manner, without affecting cell viability when incubated for up to 7 days. The presence of oligonucleotides affected the absorption of alpha-1-microglobulin, albumin and receptor associated protein, most likely through competitive inhibition of receptor-mediated endocytosis. In addition, confocal microscopy showed accumulation of oligonucleotides stably captured in the lysosomes of proximal tubule cells. Therefore, we conclude that these phosphorothioate oligonucleotides compete with receptor-mediated endocytosis of low molecular weight proteins from the glomerular filtrate without inducing irreversible tubular cytotoxic effects.

Introduction

Single stranded antisense oligonucleotides are a promising therapeutic platform to treat a variety of genetic diseases, cancer and viral infections. To improve the drug-like properties of these molecules, the backbone structures of antisense oligonucleotides have been chemically modified. When the non-bridging oxygen atom in the phosphodiester is replaced by sulfur, the resulting phosphorothioate (PS) oligonucleotides demonstrate increased protein binding and resistance to endogenous nuclease breakdown^[1]. Addition of a methyl group to the 2' hydroxyl of the ribose moiety (2'-O-methyl; further referred to as 2'O Me) further improved nuclease resistance and target engagement^[1,2]. Antisense oligonucleotides are large, water soluble poly-anions and are cleared from the circulation by the kidney, with the unbound oligonucleotide being filtered by the glomerulus, followed by reabsorption into the proximal tubule epithelium. Due to the high nuclease resistance of synthetic antisense oligonucleotides, this results in accumulation of these compounds in the kidney, and when exceeding critical threshold levels, may become associated with tubule dysfunction in animals and in man^[3,4].

Preferential accumulation of antisense oligonucleotides in the kidney has been demonstrated in animal studies, and visualized microscopically by the presence of basophilic granules in the cytoplasm of proximal tubule epithelial cells (PTEC)^[5-7]. These basophilic granules are considered to reflect the physiological clearance mechanism of antisense oligonucleotides, and in the absence of associated degenerative changes, are not considered of toxicological importance. Dose and concentration dependent effects on renal PTEC have been well characterized and described for the class of PS 2'-O-methoxyethylribose (MOE) gapmer oligonucleotides, and in view of the similarities in physicochemical properties, these principles likely apply to related platform of 2'O Me-modified PS antisense oligonucleotides.

It has been hypothesized that antisense oligonucleotides are actively reabsorbed from the ultrafiltrate by receptor-mediated endocytosis in PTEC. This is supported by the observation of reversible low molecular weight proteinuria of alpha-1-microglobulin in a clinical trial of the 2'O Me-PS antisense oligonucleotide drisapersen treating Duchenne Muscular Dystrophy patients^[8]. In addition, uptake of antisense oligonucleotides was demonstrated to be saturable, which suggests that antisense oligonucleotides in the ultrafiltrate specifically bind to a receptor at the apical membrane^[9,10]. However, supporting evidence from mechanistic studies related to these *in vivo* findings is still lacking.

This study aims to unravel the mechanism of antisense oligonucleotide uptake by PTEC and their effect on kidney function, which is an important step in safety assessment. Here, cultures of human-derived conditionally immortalized proximal tubule cells (ciPTEC) demonstrated uptake of oligonucleotides and accumulation in the lysosomal compartment, without affecting cell viability when incubated for up to 7 days. Oligonucleotides did reduce the uptake of alpha-1-microglobulin, albumin and receptor associated protein, most likely through competitive inhibition of receptor-mediated endocytosis. Therefore, our data provide a molecular model for antisense oligonucleotide competitively inhibiting receptor-mediated endocytosis in PTEC without cytotoxic effects or irreversible tubule dysfunction.

Materials and Methods

Compounds

The oligonucleotides used in this study have a fully modified 2'O Me ribose PS backbone and were synthesized at BioMarin Nederland B.V. (Leiden, The Netherlands). Drisapersen (also known as PRO051) is a 20-mer with the sequence 5'- UCA AGG AAG AUG GCA UUU CU and targets dystrophin exon 51. AON1 is a 25-mer with the sequence 5'- UAU GAG UUU CUU CCA AAG CAG CCU C with 5'-methylated Cs. AON2 is a 24-mer with the sequence 5'- GAG UUU CUU CCA AAG CAG CCU CUC. The latter two AONs target dystrophin exon 55. The fluorophore-conjugated AONs, AON1-Texas red and drisapersen-Cy3, were synthesized by Biospring (Frankfurt, Germany) and BioMarin Nederland respectively.

Cell culture

CiPTEC were developed as previously described^[11]. In this model, cell proliferation is controlled by the expression of a temperature-sensitive mutant of SV large T antigen (SV40T), allowing cell expansion at 33°C and differentiation and formation of an epithelial monolayer at 37°C. Cells were seeded 7 days before the experiment at 55,000 cells/cm² and grown for 1 day at 33°C and 5 %v/v CO₂, followed by 6 days at 37°C and 5 % v/v CO₂ (cell maturation). Cells were cultured using Dulbecco's modified eagle medium (DMEM HAM's F12, Life Technologies, Paisly, UK), supplemented with 5 µg/ml insulin, 5 µg/ml transferrin, 5 µg/ml selenium, 35 ng/ml hydrocortisone, 10 ng/ml epidermal growth factor (EGF), 40 pg/ml tri- iodothyronine (Sigma, St. Louis, USA) and 10% fetal calf serum (FCS, Greiner Bio One, Kremsmuenster, Austria). To increase sensitivity of cubilin/megalín-mediated uptake, ciPTEC were incubated in culture medium without FCS, referred to as 'serum free medium' (SFM). Medium was refreshed every 2 to 3 days, supplemented with 1% penicillin/streptomycin (pen/

strep, Invitrogen, Carlsbad, USA) at 33°C and without pen/strep at the maturation temperature (37°C).

Antisense oligonucleotide uptake and determination of concentration by hybridization-ligation

To evaluate uptake of antisense oligonucleotides, monolayers of ciPTEC matured in 6-well plates for 7 days were washed with 1 ml HBSS (Invitrogen, Carlsbad, USA) and exposed to 0.35-11.5 µM AON1 or AON2 for 4 h or 24 h at 37°C. Samples were either harvested immediately, or subsequently incubated in SFM as recovery phase for 20 h (4 h exposure) or 48 h (24 h exposure) before harvesting. For harvesting, cells were washed 2 times with 2 ml HBSS at room temperature, and washed with 1 ml heparin (20 U/ml, Sigma, St. Louis, USA) at room temperature by shaking the plates gently, and washed with 2 ml HBSS at room temperature again. After complete aspiration of the supernatant, cells were lysed in 500 µl RLT buffer (Qiagen, Hilden, Germany) and incubated for 1 min at room temperature. Lysates were homogenized by pipetting up and down 3 times and antisense oligonucleotide content of 400 µl lysate was evaluated by the hybridization-ligation assay as described previously^[12]. In brief, after lysis using RLT buffer, ciPTEC incubated with AON1 or AON2 were stored at -80°C until analysis. ciPTEC lysates were diluted up to 1,000X in diluted control ciPTEC lysate (1% in PBS). A signal probe (containing the peptide for antibody recognition) and a template (complementary to antisense oligonucleotide and the probe) were sequentially added to cell lysates. A ligation step will take place only when both oligonucleotide and probe are bound to the template. After this step and washing away of the unbound signal probe, enzyme-linked antibodies were used to detect the amount of probe-antisense oligonucleotide.

Antisense oligonucleotide fluorescent imaging

To visualize the subcellular localization of antisense oligonucleotides in ciPTEC, cells were incubated for 4 and 24 h with fluorescently labeled oligonucleotides (AON1-Texas red or drisapersen-Cy3) in normal culture medium, in absence or presence of BSA-Alexa-Fluor[®]647 (ThermoFisher Scientific A34785, 5 µg/ml) or RAP-GST (recombinant protein produced in house, 2.5 µg/ml). After incubation cells were washed and incubated with Hoechst to stain the nucleus. Cells incubated with drisapersen-Cy3 and BSA-Alexa-Fluor[®]647 were imaged directly (live cells) whereas the cells incubated with AON1-Texas red and RAP-GST were first fixed (4% PFA for 15 min at RT) and permeabilised (0.1% Triton-X-100, 15 min at RT) before overnight incubation with anti-GST-ab (GE Healthcare 27457701, Goat polyclonal, 1:1600 in 1% BSA/PBS) and staining with a fluorescently labeled secondary ab (Alexa Fluor 488, Donkey anti goat, 1:500 in 1% BSA/PBS). Images were taken with a Yokogawa CV7000 confocal imager and analyzed using ImageJ.

A1M-FITC and BSA-FITC uptake determination by flow cytometry

To evaluate interaction at the megalin/cubilin receptor(s), monolayers of ciPTEC were grown in complete medium and matured for 6 days. All A1M-FITC and BSA-FITC experiments were performed in SFM to improve ligand uptake by the cells. Cells were washed and pre-incubated with SFM for 24 h at 37°C 5 %v/v CO₂. On day 8 after seeding, cells were washed with SFM and co-incubated in SFM with AON1 or AON2 (0.12, 1.15, 11.5 or 115 μM) or drisapersen (0.14, 1.35 or 13.5 μM), and BSA-FITC (0.73 μM) or A1M-FITC (3.85 μM; α1-microglobulin from antibodies-online.com, conjugated to FITC from Life Technologies) for 30 min, 2 h or 4 h at 37°C. A control set using BSA-FITC or A1M-FITC only was additionally incubated at 4°C. After co-incubation at 37°C, cells were washed 2 times with 500 μl HBSS and harvested using trypsin-EDTA (Invitrogen, Carlsbad, USA). The cell suspension was next washed using HBSS, fixed using 0.5% paraformaldehyde and analyzed on a FACS Calibur (Becton Dickinson, Franklin Lakes, USA).

RAP-GST binding and uptake

Protein cell surface binding and protein uptake was evaluated using the uptake of receptor associated protein (RAP) containing a glutathione S-transferase (GST) tag (RAP-GST). Cells were incubated with medium containing 0.38 μM RAP-GST at 4°C for cell surface binding or at 37°C for active protein uptake. After incubation cells were washed two times with medium, fixed in 4% PFA for 10 min, washed with PBS and permeabilized for 5 min using 0.1% Triton-X-100 in PBS. Next, cells were washed with PBS and incubated overnight with primary anti-GST antibody in 1% BSA/PBS (1:1600, GE Healthcare, 27457701). Uptake was visualized by 2 h incubation with fluorescently labeled secondary ab (1:500, Alexa Fluor 488) after which cells were washed with PBS and fluorescence (excitation 485 nm, emission 535 nm) was quantified using multiplate reader Victor X3 (Perkin Elmer, Waltham, USA) or using fluorescent microscopy.

Functional uptake assay upon long-term pre-incubation

To evaluate long-term antisense oligonucleotide induced effects on megalin/cubilin-mediated uptake capacity, BSA-FITC uptake capacity of ciPTEC was evaluated after extended pre-incubation. Briefly, monolayers of ciPTEC matured in 96-well plates for 7 days were exposed to 1.15 μM AON1 in complete culture medium for 7 days at 37°C 5 %v/v CO₂. Exposure medium was refreshed every day. After incubation for 7 days at 37°C, cells were washed 2 times with 100 μl SFM and incubated in SFM in absence of antisense oligonucleotides for 24 h at 37°C 5 %v/v CO₂. BSA-FITC uptake capacity was evaluated by washing cells with SFM and incubation with 0.15-7.3 μM BSA-FITC in SFM for 4 h at 37°C. Incubation was stopped by washing 3 times with ice-cold

(4°C) HBSS (Invitrogen, Carlsbad, USA) and fluorescence was immediately measured (excitation 485 nm, emission 535 nm) using the multiplate reader Victor X3 (Perkin Elmer, Waltham, USA).

Viability assay upon long-term pre-incubation

To evaluate toxicity induced by antisense oligonucleotides, viability of ciPTEC was evaluated by was determined by a standard spectrophotometric 3-(4,5-dimethylthiazole-2-yl)-2,5 diphenyltetrazolium bromide (MTT; Sigma) assay after extended pre-incubation with AON. Briefly, monolayers of ciPTEC matured in 96-well plates for 7 days were exposed to 1.15 μ M AON1 (in complete culture medium for 7 days at 37°C 5 %v/v CO₂). Exposure medium was refreshed every day. After incubation for 7 days at 37°C, cells were washed 2 times with 100 μ l SFM and subsequently MTT assay was performed immediately or cells were first incubated in SFM in absence of antisense oligonucleotides for 24 h at 37°C 5 %v/v CO₂, before MTT was performed. For MTT assay, cells were incubated with 0.5 mg/ml thiazolyl blue tetrazolium bromide (MTT, Sigma, St. Louis, USA) for 3 h at 37°C in absence of antisense oligonucleotides. Formazan crystals formed in viable cells were dissolved in dimethyl sulfoxide (DMSO, Merck, Whitehouse Station, USA) and optical density was measured (560 nm, background at 670 nm was subtracted) using Benchmark Plus (Bio-Rad, Hercules, USA).

Data analysis and statistics

For antisense oligonucleotide uptake assays, data are presented as lysate concentration and plotted with GraphPad Prism (version 6.07). Calibration curves of the analyzed antisense oligonucleotide were prepared by spiking a known amount of antisense oligonucleotide to diluted control cell lysate (1%) and used to quantify antisense oligonucleotide levels. All analyses were performed in duplicate. For A1M-FITC, BSA-FITC and RAP-GST uptake and inhibition assays, data are either presented as absolute fluorescence values or normalized to the activity of samples without antisense oligonucleotide and plotted after background subtraction with GraphPad Prism (version 6.07). For MTT viability assay, data were normalized to the viability of control cells and plotted with GraphPad Prism. Statistics was performed by one or two-way ANOVA (two-tailed, $\alpha=0.05$) using GraphPad Prism as well. All data are presented as mean \pm SD of at least two separate experiments (n=2) performed in triplicate, unless stated otherwise.

Results

To evaluate uptake and internalization of antisense oligonucleotides, ciPTEC were matured for 7 days and incubated with drisapersen or oligonucleotides with similar 2'O Me-PS chemistry but different nucleotide sequences, AON1 and AON2 (Figure 4.1A). Incubations for 4 h or 24 h at 37°C using concentrations ranging from 0.1x to 10x C_{max} of drisapersen in patient clinical trials^[8] showed that AON content in ciPTEC increased with longer exposure time and higher concentrations (Figure 4.1B,C). The recovery period of 20 h or 48 h following AON incubation did not reduce AON levels in the cell, indicating that the antisense oligonucleotides are stable inside the cells and are not degraded within this time period. Intracellular distribution was visualized with confocal microscopy using fluorescently labeled AONs (Figure 4.1D,E), which demonstrated that the AONs accumulate within the cell in a vesicular pattern, despite the presence of non-specific staining, suggesting uptake by endocytosis. In view of the reversible nature of the low molecular weight proteinuria observed in patients treated with drisapersen^[8], this adverse effect may be the result of competition for receptor-mediated endocytosis rather than a consequence of direct tubule toxicity. The membrane proteins megalin and cubilin at the apical side of the proximal tubule are responsible for this process by binding and uptake of alpha-1-microglobulin^[13, 14], RAP and albumin. RAP is a 39kDa chaperone protein that binds megalin with high affinity^[15, 16], while albumin is a large plasma protein ~68kD that in small amounts can pass the glomerular filter to be efficiently reabsorbed by the proximal tubule^[17, 18]. Co-localization of the antisense oligonucleotides with fluorescently labeled bovine serum albumin (BSA-Alexa-657) (Figure 4.1D) or RAP-GST (Figure 4.1E), confirmed that the uptake of antisense oligonucleotides in tubule cells occurs via the same endocytosis pathway.

To determine how antisense oligonucleotides affect receptor mediated endocytosis in proximal tubule cells, we examined the uptake of fluorescently labeled alpha-1-microglobulin (A1M-FITC) (Figure 4.2A-D), fluorescently labeled BSA (BSA-FITC) (Figure 4.2E-G), and RAP-GST (Figure 4.2H-L) in ciPTEC in the absence or presence of antisense oligonucleotides. At 37°C, A1M-FITC was actively taken up by ciPTEC over time (Figure 4.2A) and could be specifically inhibited by competition with excess unlabeled alpha-1-microglobulin (Figure 4.2B). When increasing concentrations of antisense oligonucleotides (AON1 or drisapersen) were added, A1M-FITC uptake was reduced in ciPTEC in a time- and concentration-dependent manner (Figure 4.2C-D), suggesting competitive interaction with the same receptor. Co-incubation with AON1 or AON2 also significantly inhibited BSA-FITC uptake (up to 50%) in ciPTEC at both 30 min and 4 h in a concentration-dependent manner (Figure 4.2E-G). The presence of

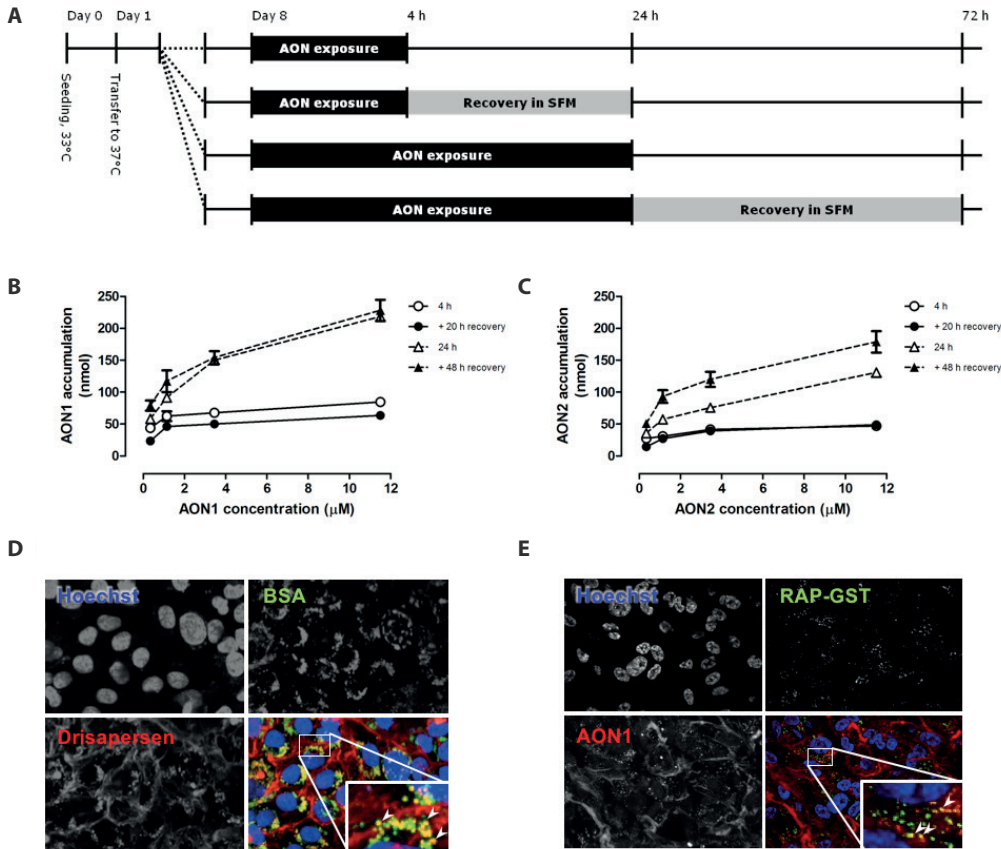
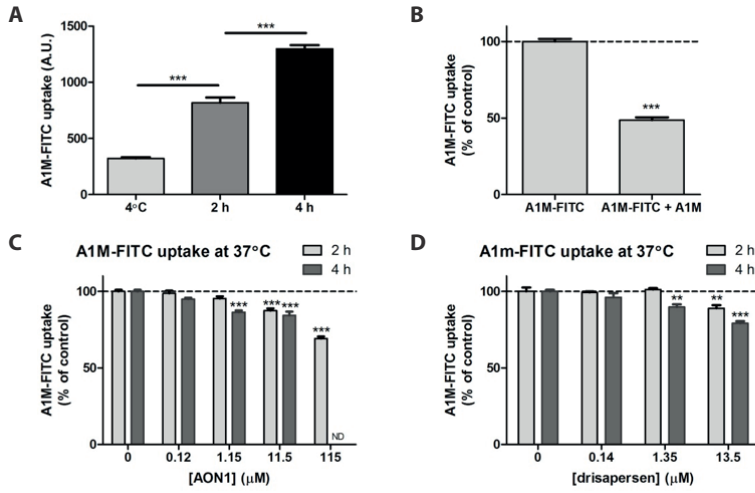
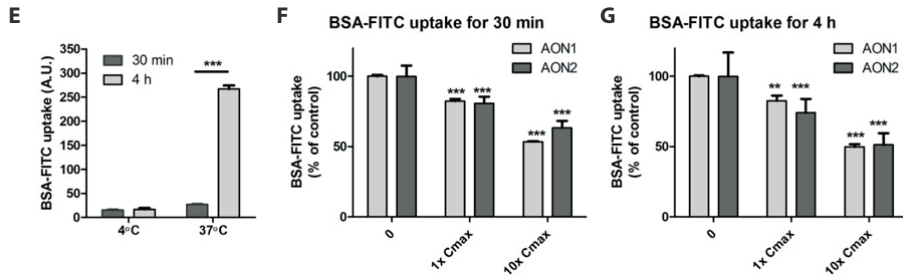


Figure 4.1 Endocytic uptake and limited degradation of antisense oligonucleotides in ciPTEC. (A) Schematic overview of the different AON incubation and recovery times in ciPTEC. Accumulation of AON1 (0.35-11.5 µM) (B) or AON2 (0.35-11.5 µM) (C) in ciPTEC when incubated for 4 h and 24 h at 37°C and harvested immediately, or when followed by a recovery period of 20 h and 48 h respectively (n=1). Uptake after 24 h of fluorescently labeled Drisapersen (in red) with BSA (green) (D), or fluorescently labeled AON1 (red) with RAP-GST (green) (E), nuclei are stained blue (Hoechst).

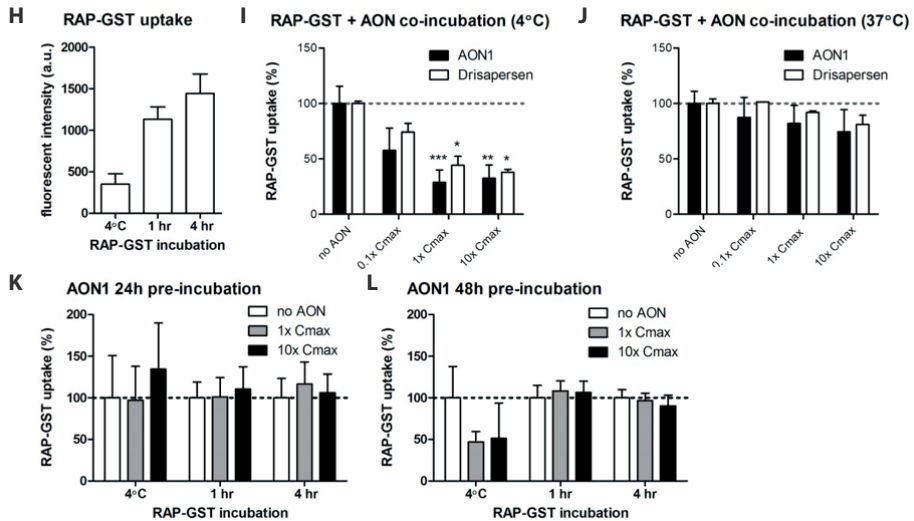
Alpha-1-microglobulin



BSA-FITC



RAP-GST



< **Figure 4.2 Antisense oligonucleotides compete with protein reabsorption in proximal tubular cells *in vitro*.** (A) A1M-FITC uptake by ciPTEC, for 2 h at 4°C, and for 2 h and 4 h at 37°C (n=2). (B) A1M-FITC uptake by ciPTEC incubated for 2 h at 37°C in the presence or absence of an equal concentration of unlabeled A1M (3.85 μ M) (n=2). (C-D) A1M-FITC (3.85 μ M) uptake by ciPTEC when co-incubated with different concentrations of (C) AON1 (0.12, 1.15, 11.5 and 115 μ M) or (D) drisapersen (0.14, 1.35 and 13.5 μ M) for 2 h and 4 h at 37°C, relative to uptake without antisense oligonucleotide, as evaluated by flow cytometry (n=2). (E) Fluorescent intensity after BSA-FITC uptake by ciPTEC when incubated at 4°C or 37°C for either 30 min or 4 h (n=2). (F,G) BSA-FITC uptake by ciPTEC when co-incubated with AON1 or AON2 for 30 min or 4 h at 37°C, as evaluated by flow cytometry (n=2). (H) RAP-GST cell surface binding (4°C for 30 min) and active uptake in proximal tubular cells (37°C at 1 and 4 h) in absence of antisense oligonucleotide. Co-incubation with either AON1 or drisapersen inhibited the cell surface binding of RAP-GST (30 min at 4°C) (I) and the active uptake of RAP-GST (4 h at 37°C) (J) in a concentration-dependent manner. Cells were pre-incubated with AON1 for 24 h (K) and 48 h (L) prior to analyzing RAP-GST endocytic capacity in absence of AON1. ND is not determined. **p<0.01, ***p<0.001. A.U.= arbitrary units

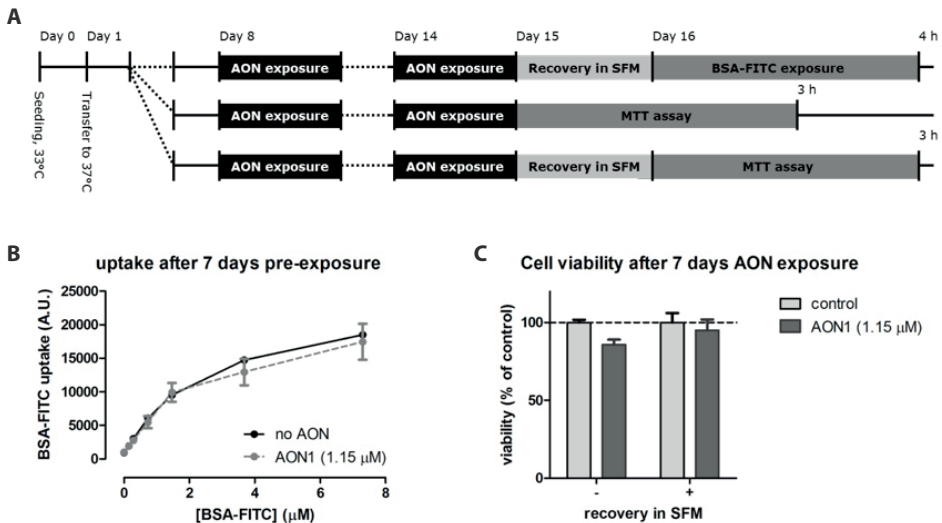


Figure 4.3 Long-term exposure to antisense oligonucleotides does not affect ciPTEC endocytosis capacity or result in cytotoxicity. (A) Schematic overview of ciPTEC pre-incubation with AON1, recovery and evaluation of BSA-FITC uptake capacity and MTT viability assay. (B) BSA-FITC (0.15-7.3 μ M) uptake by ciPTEC for 4 h at 37°C when pre-incubated with AON1 (1.15 μ M) for 7 days and subsequently recovered for 24 h, as evaluated by multiwell platerader (n=2). (C) Viability of ciPTEC after exposure to AON1 (1.15 μ M) for 7 days, with and without recovery, relative to cell viability without exposure (n=2).

antisense oligonucleotides also interfered with RAP-GST cell surface binding at 4°C (up to 70% reduction in binding) and inhibited active uptake of RAP-GST at 37°C (up to 25% reduction) (Figure 4.2H-J). To determine whether decreased RAP-GST uptake at 37°C was due to a non-specific cytotoxic response through AON accumulation, ciPTEC were pre-incubated only with AONs for 24 h or 48 h prior to incubation with the labelled substrate. This pre-incubation did not significantly inhibit the uptake of RAP-GST at 37 °C (Figure 4.2H,I), indicating that AON incubation directly competes with receptor binding capacity and has no cytotoxic effect that affects megalin/cubilin mediated endocytosis rate. Some residual inhibition was seen at 4°C after pre-incubation, which is likely due to occupation of ligand binding sites at the cell surface, which were not washed away at 4°C. Together these data indicate that antisense oligonucleotides directly compete with receptor-mediated protein reabsorption in ciPTEC, without adversely affecting the reabsorption capacity of the cells.

To evaluate long-term effects of renal proximal tubule exposure to antisense oligonucleotides, ciPTEC were pre-incubated with AON1 for 7 days, followed by 24 h recovery before BSA-FITC uptake capacity and cell viability were determined (Figure 4.3A). In the absence of AON1, BSA-FITC was internalized via endocytosis by ciPTEC in a concentration-dependent manner, reaching partial saturation at the highest concentrations. The 7-day pre-incubation with AON1 did not affect BSA uptake by ciPTEC (Figure 4.3B). In addition, cell viability was not significantly changed following 7-day exposure to AON1, both with and without 24 h recovery (Figure 4.3C). These results argue for intact endocytosis function in ciPTEC upon long-term exposure to antisense oligonucleotides, without causing irreversible cytotoxicity.

Discussion

Antisense oligonucleotide accumulation in renal proximal tubules has been observed widely, however, little is known about the cellular mechanism and potentially hazardous consequences. In this study, we investigated the effects of 2'O Me-PS oligonucleotides on epithelial reabsorption and cytotoxicity *in vitro*. Our data demonstrate that antisense oligonucleotides compete for receptor-mediated endocytosis with endogenous proteins and accumulate in the lysosomal compartment of the proximal tubule model ciPTEC. This did not affect endocytosis capacity or viability of PTEC after exposure for up to 7 days.

A clinical study in which patients with Duchenne muscular dystrophy were treated with the antisense oligonucleotide drisapersen that changes the splicing of the dystrophin gene (*DMD*) to correct its function, showed increased urinary alpha-1-microglobulin levels^[6]. But no signs of proximal tubule dysfunction (renal Fanconi's syndrome) were found and, moreover, urinary elevation of alpha-1-microglobulin was not progressive, as values moved towards normal after treatment. This transient proteinuria suggests a reversible interference with protein reabsorption in the proximal tubule^[6]. Although there are no indications that oligonucleotide treatment affected kidney function in patients with Duchenne muscular dystrophy^[19], rare cases of tubule nephrotoxicity have been reported^[3,20]. In both cases, (sub)chronic treatment with antisense oligonucleotides that demonstrate high renal clearance induced acute tubule necrosis which was reversible after drug discontinuation^[3, 20]. Pro-inflammatory immune responses, such as complement- and TLR-receptor activation have been observed more commonly in monkeys^[6,21] and rodents^[22-24], respectively, causing glomerulonephritis and vasculitis. In addition to base pair sequence and base modifications, backbone chemistry is the major contributor to pro-inflammatory effects^[23,25,26]. Since immune-mediated adverse effects present significant problems for clinical use if found, future studies should evaluate the immunomodulatory potential of the antisense oligonucleotides used in this study.

To understand the cellular mechanism and demonstrate a link between oligonucleotide treatment and proteinuria, we evaluated *in vitro* protein reabsorption by receptor-mediated endocytosis in human proximal tubule cells in the presence and absence of oligonucleotides. The ciPTEC model is human-derived and has functional basolateral and apical drug transporters, including OCT2, Pgp and MRPs, and intact receptor-mediated endocytosis, including expression of megalin and cubilin^[11, 27, 28]. These receptors play a pivotal role in reabsorption of low molecular weight protein in PTEC and mutations in these genes have been directly linked to proteinuria in both animal models and human disease^[29]. In line with this, saturation of the receptors can lead to competitive inhibition causing low molecular weight proteinuria, which was hypothesized here to be causative for the observed proteinuria upon oligonucleotide treatments. Alpha-1-microglobulin and, to a lower extent, albumin are both present in the glomerular filtrate and are fully reabsorbed by receptor-mediated endocytosis in PTEC. Incubation with antisense oligonucleotides indeed reduced the binding and uptake of megalin ligands alpha-1-microglobulin, albumin and the megalin-chaperone protein RAP. In contrast to co-incubation studies, pre-incubation with antisense oligonucleotide for 24 h and up to 7 days did not diminish protein reabsorption. This suggests a direct competition on the receptor level, rather than a reduction in proximal tubule reabsorption capacity due to intracellular oligonucleotide accumulation. The comparable effects of three

different 2'-O-Me PS antisense oligonucleotide indicate a common mechanism of 2'-O-Me PS antisense oligonucleotide-mediated interference with protein reabsorption. This finding is in line with literature that describes receptor-mediated endocytosis as high-capacity, but low-specificity uptake mechanism^[30]. The co-localization studies with albumin in endocytic vesicles further supported our hypothesis of receptor mediated uptake of oligonucleotides in proximal tubules, as reported in literature^[31].

The degradation of oligonucleotides in PTEC follows a first order kinetics and allows accumulation until a steady state is reached^[25]. Due to the modifications in the backbone of drisapersen, its degradation is strongly reduced, with a half-life of up to 2 weeks^[25]. Human PTEC also efficiently accumulated the oligonucleotides in the current study in a time and concentration dependent manner, but no cytotoxic effects were detected after 7 days exposure to antisense oligonucleotide at concentrations equivalent to peak plasma levels. Consistent with the long half-life of the oligonucleotides used, no significant degradation was seen at 20 h or 48 h exposure. Future studies should evaluate the long-term degradation of oligonucleotides in PTEC in relation to renal function.

In conclusion, our data indicate that 2'-O Me-PS antisense oligonucleotides, including drisapersen, directly compete with receptor-mediated endocytosis in PTEC and reduce the uptake of endogenous cubilin/megalin ligands such as alpha-1-microglobulin, explaining reversible low molecular weight proteinuria observed in treated patients.

Acknowledgements

This work was supported by a collaboration research agreement from BioMarin Nederland B.V., Leiden, the Netherlands. CdB, TS, YP, SJ and SdK are (former) employees of Biomarin Nederland B.V. All other authors declare no potential conflict of interest.

References

1. Bennett CF, Swayze EE. RNA targeting therapeutics: molecular mechanisms of antisense oligonucleotides as a therapeutic platform. *Annu Rev Pharmacol Toxicol.* 50, 259-293 (2010).
2. Crooke ST, Wang S, Vickers TA, Shen W, Liang XH. Cellular uptake and trafficking of antisense oligonucleotides. *Nat Biotechnol.* 35, 230-237 (2017).
3. Herrington WG, Talbot DC, Lahn MM, Brandt JT, Callies S, Nagle R, Winearls CG, et al. Association of long-term administration of the survivin mRNA-targeted antisense oligonucleotide LY2181308 with reversible kidney injury in a patient with metastatic melanoma. *Am J Kidney Dis.* 57, 300-303 (2011).
4. Voit T, Topaloglu H, Straub V, Muntoni F, Deconinck N, Campion G, De Kimpe SJ, et al. Safety and efficacy of drisapersen for the treatment of Duchenne muscular dystrophy (DEMAND II): an exploratory, randomised, placebo-controlled phase 2 study. *The Lancet Neurology.* 13, 987-996 (2014).
5. Geary RS, Norris D, Yu R, Bennett CF. Pharmacokinetics, biodistribution and cell uptake of antisense oligonucleotides. *Adv Drug Deliv Rev.* 87, 46-51 (2015).
6. Monteith DK, Horner MJ, Gillett NA, Butler M, Geary R, Burckin T, Ushiro-Watanabe T, et al. Evaluation of the renal effects of an antisense phosphorothioate oligodeoxynucleotide in monkeys. *Toxicol Pathol.* 27, 307-317 (1999).
7. Frazier KS. Antisense oligonucleotide therapies: the promise and the challenges from a toxicologic pathologist's perspective. *Toxicol Pathol.* 43, 78-89 (2015).
8. Goemans NM, Tulinius M, van den Akker JT, Burm BE, Ekhardt PF, Heuvelmans N, Holling T, et al. Systemic administration of PRO051 in Duchenne's muscular dystrophy. *N Engl J Med.* 364, 1513-1522 (2011).
9. van de Water FM, Boerman OC, Wouterse AC, Peters JG, Russel FG, Masereeuw R. Intravenously administered short interfering RNA accumulates in the kidney and selectively suppresses gene function in renal proximal tubules. *Drug Metab Dispos.* 34, 1393-1397 (2006).
10. Takakura Y, Oka Y, Hashida M. Cellular uptake properties of oligonucleotides in LLC-PK1 renal epithelial cells. *Antisense Nucleic Acid Drug Dev.* 8, 67-73 (1998).
11. Wilmer MJ, Saleem MA, Masereeuw R, Ni L, van der Velden TJ, Russel FG, Mathieson PW, et al. Novel conditionally immortalized human proximal tubule cell line expressing functional influx and efflux transporters. *Cell Tissue Res.* 339, 449-457 (2010).
12. Verhaart IE, van Vliet-van den Dool L, Sipkens JA, de Kimpe SJ, Kolfschoten IG, van Deutekom JC, Liefwaard L, et al. The Dynamics of Compound, Transcript, and Protein Effects After Treatment With 2OMePS Antisense Oligonucleotides in mdx Mice. *Mol Ther Nucleic Acids.* 3, e148 (2014).
13. Christensen EI, Birn H. Megalin and cubilin: multifunctional endocytic receptors. *Nat Rev Mol Cell Biol.* 3, 256-266 (2002).
14. Leheste JR, Rolinski B, Vorum H, Hilpert J, Nykjaer A, Jacobsen C, Aucouturier P, et al. Megalin knockout mice as an animal model of low molecular weight proteinuria. *Am J Pathol.* 155, 1361-1370 (1999).
15. Birn H, Vorum H, Verroust PJ, Moestrup SK, Christensen EI. Receptor-associated protein is important for normal processing of megalin in kidney proximal tubules. *J Am Soc Nephrol.* 11, 191-202 (2000).
16. Willnow TE, Rohlmann A, Horton J, Otani H, Braun JR, Hammer RE, Herz J. RAP, a specialized chaperone, prevents ligand-induced ER retention and degradation of LDL receptor-related endocytic receptors. *Embo j.* 15, 2632-2639 (1996).
17. Schwegler JS, Heppelmann B, Mildnerberger S, Silbernagl S. Receptor-mediated endocytosis of albumin in cultured opossum kidney cells: a model for proximal tubular protein reabsorption. *Pflugers Arch.* 418, 383-392 (1991).

18. Zhai XY, Nielsen R, Birn H, Drumm K, Mildenerger S, Freudinger R, Moestrup SK, et al. Cubilin- and megalin-mediated uptake of albumin in cultured proximal tubule cells of opossum kidney. *Kidney Int.* 58, 1523-1533 (2000).
19. Braat E, Hoste L, De Waele L, Gheysens O, Vermeersch P, Goffin K, Pottel H, et al. Renal function in children and adolescents with Duchenne muscular dystrophy. *Neuromuscul Disord.* 25, 381-387 (2015).
20. van Poelgeest EP, Swart RM, Betjes MG, Moerland M, Weening JJ, Tessier Y, Hodges MR, et al. Acute kidney injury during therapy with an antisense oligonucleotide directed against PCSK9. *Am J Kidney Dis.* 62, 796-800 (2013).
21. Henry SP, Beattie G, Yeh G, Chappel A, Giclas P, Mortari A, Jagels MA, et al. Complement activation is responsible for acute toxicities in rhesus monkeys treated with a phosphorothioate oligodeoxynucleotide. *Int Immunopharmacol.* 2, 1657-1666 (2002).
22. Agrawal S, Kandimalla ER. Role of Toll-like receptors in antisense and siRNA[corrected]. *Nat Biotechnol.* 22, 1533-1537 (2004).
23. Senn JJ, Burel S, Henry SP. Non-CpG-containing antisense 2'-methoxyethyl oligonucleotides activate a proinflammatory response independent of Toll-like receptor 9 or myeloid differentiation factor 88. *J Pharmacol Exp Ther.* 314, 972-979 (2005).
24. Wallace TL, Gamba-Vitalo C, Loveday KS, Cossum PA. Acute, multiple-dose, and genetic toxicology of AR177, an anti-HIV oligonucleotide. *Toxicol Sci.* 53, 63-70 (2000).
25. Engelhardt JA. Comparative Renal Toxicopathology of Antisense Oligonucleotides. *Nucleic Acid Ther.* 26, 199-209 (2016).
26. Stanton R, Sciabola S, Salatto C, Weng Y, Moshinsky D, Little J, Walters E, et al. Chemical modification study of antisense gapmers. *Nucleic Acid Ther.* 22, 344-359 (2012).
27. Caetano-Pinto P, Janssen MJ, Gijzen L, Verscheijden L, Wilmer MJ, Masereeuw R. Fluorescence-Based Transport Assays Revisited in a Human Renal Proximal Tubule Cell Line. *Mol Pharm.* 13, 933-944 (2016).
28. Gorvin CM, Wilmer MJ, Piret SE, Harding B, van den Heuvel LP, Wrong O, Jat PS, et al. Receptor-mediated endocytosis and endosomal acidification is impaired in proximal tubule epithelial cells of Dent disease patients. *Proc Natl Acad Sci U S A.* 110, 7014-7019 (2013).
29. Nielsen R, Christensen EI, Birn H. Megalin and cubilin in proximal tubule protein reabsorption: from experimental models to human disease. *Kidney Int.* 89, 58-67 (2016).
30. Eshbach ML, Weisz OA. Receptor-Mediated Endocytosis in the Proximal Tubule. *Annu Rev Physiol.* 79, 425-448 (2017).
31. Gonzalez-Barriga A, Nillessen B, Kranzen J, van Kessel IDG, Croes HJE, Aguilera B, de Visser PC, et al. Intracellular Distribution and Nuclear Activity of Antisense Oligonucleotides After Unassisted Uptake in Myoblasts and Differentiated Myotubes In Vitro. *Nucleic Acid Ther.* 27, 144-158 (2017).



Part II

Towards 3D Proximal Tubule *In Vitro* Models for Drug-Induced Toxicity Screening



Kidney-on-a-Chip Technology for Renal Proximal Tubule Tissue Reconstruction

Tom TG Nieskens¹ and Martijn J Wilmer¹

¹ Department of Pharmacology and Toxicology, Radboud Institute for Molecular Life Sciences,
Radboud University Medical Center, Nijmegen, The Netherlands

European Journal of Pharmacology. 790. 46-56 (2016)

Abstract

The renal proximal tubule epithelium is responsible for active secretion of endogenous and exogenous waste products from the body and simultaneous reabsorption of vital compounds from the glomerular filtrate. The complexity of this transport machinery makes investigation of processes such as tubular drug secretion a continuous challenge for researchers. Currently available renal cell culture models often lack sufficient physiological relevance and reliability. Introducing complex biological culture systems in a 3D microfluidic design improves the physiological relevance of *in vitro* renal proximal tubule epithelium models. Organ-on-a-chip technology provides a promising alternative, as it allows the reconstruction of a renal tubule structure. These microfluidic systems mimic the *in vivo* microenvironment including multi-compartmentalization and exposure to fluid shear stress. Increasing data supports that fluid shear stress impacts the phenotype and functionality of proximal tubule cultures, for which we provide an extensive background. In this review, we discuss recent developments of kidney-on-a-chip platforms with current and future applications. The improved proximal tubule functionality using 3D microfluidic systems is placed in perspective of investigating cellular signalling that can elucidate mechanistic aberrations involved in drug-induced kidney toxicity.

Introduction

The main physiological role of the kidneys is to clear endogenous waste products from the body. Exogenous drugs and toxins are often cleared via the same elimination route, making the kidney susceptible to drug-induced aberrations. Active cellular uptake of xenobiotics and metabolites by basolateral transport proteins contribute to the nephrotoxic potential of drugs^[1]. Renal sensitivity to drug-induced toxicity is further stimulated by the high fraction of cardiac output directed to the kidneys. This fraction is the driving force for renal filtration and tubular flow, resulting in high renal exposure to potential toxins^[1,2].

Early detection of adverse renal effects caused by lead compounds during drug development is seriously hampered by low predictive value of classical 2D cell culture models: compound attrition due to nephrotoxicity is only 2% in preclinical studies and rises to 9% in expensive clinical trials^[3]. Recent studies support that reconstruction of the physiological microenvironment increases the clinical relevance of renal *in vitro* models and can lead to enhanced *in vitro* predictivity of drug-induced renal adverse effects.

A kidney-on-a-chip is a microfluidic device that allows culturing of living renal cells in 3D channels. Microfluidic technology is able to mimic a complicated 3D kidney structure allowing tubule growth, enable compartmentalization, offer constant flow resulting in fluid shear stress, and can include many different cell types^[4]. By recreating the renal tubule microenvironment, *in vitro* cellular responses are likely to approach the *in vivo* situation better compared to 2D systems. This would improve drug-induced toxicity screening and provide a promising tool to study 3D kidney regeneration.

This review will focus on current developments and future perspectives of proximal tubule kidney-on-a-chip techniques, with an emphasis on pharmacological interactions, drug-induced nephrotoxicity and tubular regeneration. To this end, the function of proximal tubule cells and its relation to fluidic shear stress is discussed. Finally, the development of multi-organ-chips and possible applications for regenerative medicine will be highlighted.

Functionality of the proximal tubule epithelium

Reconstruction of a proximal tubule in a physiological relevant environment will substantially contribute to our understanding of renal physiology and pharmacology. To evaluate the quality of a cultured system in terms of functional characteristics, a clear understanding of the relevant transport mechanisms in the proximal tubular epithelium is required (Figure 5.1).

Receptor mediated endocytosis

Connected to Bowman's capsule, the proximal tubular lumen is exposed to the glomerular filtrate. The apical membrane of the proximal tubule forms a brush border and is extremely effective in the reabsorption of vital compounds that are freely filtered over the glomerular basement membrane. Low molecular weight proteins are largely reabsorbed from the glomerular filtrate via receptor mediated endocytosis. At the apical membrane, multi-ligand receptors megalin and cubilin bind low-molecular weight proteins in the glomerular filtrate with high capacity, which is followed by reabsorption via endocytosis^[5]. Low molecular weight proteinuria can consequently result from defects in this endocytic recycling machinery, for example caused by mutations in genes encoding transport proteins that are expressed at the lysosomal membranes. In the lysosomes, acidification results in dissociation of the receptor-ligand complex. Defects in receptor mediated endocytosis were reported for lysosomal transporter proteins chloride channel (CLC)-5 and cystinosin, which are associated with Dent's disease and nephropathic cystinosis, respectively^[6,7]. A kidney-on-a-chip platform with an apical fluid flow and intact endocytic machinery will be valuable in future research of such pathological conditions, moreover as endocytosis under flow conditions was demonstrated to be increased^[8-10].

Researchers often employed Opossum Kidney (OK) or Brown Norway rat yolk sac (BN-16) epithelial cells to study receptor mediated endocytosis, as these are known for their active megalin mediated endocytic machinery^[8, 11, 12]. Although expression of megalin and the endocytic capacity is relatively high in these animal derived cells, the use of a human renal epithelial cell line will be the preferred model for pathological and pharmacological studies. For example, the human kidney cell line (HKC)-8 cell line was used to demonstrate that albumin-induced apoptosis targets the mitochondria^[13] and endocytosis of albumin in HKC-8 could be stimulated by phosphorylation of endocytic adaptor disabled-2 (Dab2) via protein kinase B (Akt)^[14]. Albumin reabsorption was also increased in primary human kidney proximal tubule epithelial cells exposed to laminar apical flow in a microfluidic device, pointing towards the influence of a physiological environment on proximal tubular

function^[9]. A drawback of primary cells is the limited availability and batch-to-batch variations. The use of urine-derived proximal tubule epithelial cells allowed studying albumin uptake in cells isolated from patients with Dent's disease or nephropathic cystinosis that manifest with albuminuria. To obtain sufficient material, urine derived cells from healthy subjects and patients with mutations in the CTNS or CLC5 genes were conditionally immortalized using SV40 temperature sensitive large T antigen (SV40T) and human telomerase reverse transcriptase (hTERT)^[6, 15, 16]. These conditionally immortalized proximal tubule epithelial cells (ciPTEC) were used to demonstrate intact megalin dependent albumin and RAP reabsorption^[16, 17], while defects in albumin reabsorption via megalin and cubilin mediated endocytosis were demonstrated in ciPTEC derived from patients with Dent's disease and nephropathic cystinosis^[6, 18]. Together, studies using HKC-8 or ciPTEC can elucidate albumin handling in renal disease states such as acquired or inherited proteinuria. In respect of this review, the demonstration of fluidic shear stress affecting apical albumin handling in the proximal tubule epithelium supports that microfluidic devices should be used for future research focusing on receptor mediated endocytosis. Apical exposure to high levels of albumin under flow conditions can mimic albuminuria and microfluidic devices allow detailed (metabolic) analysis of the perfusion medium. In addition, urine-derived ciPTEC isolated from genetically well-characterized patients manifesting inherited low molecular weight proteinuria can be cultured in a kidney-on-a-chip to mimic these pathological conditions.

Transporter-mediated reabsorption

Next to receptor mediated endocytosis, apical membrane transporters of the solute carrier family (SLC) are responsible for the reabsorption of vital solutes from the glomerular filtrate, like phosphate (NaPi-IIa, *SLC34A1*, NaPi-IIc, *SLC34A3*), amino acids (members of the *SLC1*, *SLC7*, *SLC36*, *SLC38* and *SLC43*), and glucose (GLUT2, *SLC2A2*; *SGLT1*, *SLC5A1*; *SGLT2*, *SLC5A2*). Similar to increased albumin uptake under flow conditions, Jang and colleagues demonstrated that laminar flow in a microfluidic device increased the expression of *SGLT2*, resulting in improved reabsorption of glucose^[9], again supporting the role of fluidic shear stress on apical transport function.

Transporter-mediated secretion: drug transporters

The proximal tubule epithelium facilitates renal secretion of waste compounds and xenobiotics that are not freely filtered by the glomerulus due to their charge, size or because they are protein-bound. This transcellular transport from blood into the urine depends on drug transporters acting in concert at the basolateral and apical membrane^[19]. These polyspecific membrane transporters enable efficient clearance of different classes of compounds, viz. organic cations and organic anions. Generally, drug

transporters are categorized depending on their driving force: membrane transporters using the electrochemical gradient belong to the SLC family, while transporters coupled to ATP hydrolysis belong to the ATP binding cassette transporters (ABC). At the renal proximal tubule basolateral membrane, organic cation transporter 2 (OCT2; *SCL22A2*) and organic anion transporters 1 (OAT1; *SLC22A6*) and 3 (OAT3; *SLC22A8*) mediate elimination of waste compounds and xenobiotics from the circulatory system into the proximal tubule epithelium^[20]. It should be noted that these metabolic waste products, often called uremic toxins (e.g. indoxyl sulfate or kynurenic acid) accumulate in chronic kidney disease^[21]. Next to metabolic waste products, renal elimination of many pharmaceutical compounds is very efficient and compete for the same excretion pathways^[22]. This complicates the use of pharmaceuticals in chronic kidney disease as drugs potentially compete with accumulating uremic toxins at the site of drug transporters, hence, drug serum levels can be elevated.

Removal of drugs and waste compounds from the circulatory system make the proximal tubular epithelium an important target for drug-induced kidney toxicity. For example, the dosing of the anti-neoplastic agent cisplatin, often used as a first treatment option against solid tumors, is limited due to the risk of nephrotoxicity associated with OCT2 transport activity^[23]. The group of Ciarimboli used HEK293 cells over-expressing human OCT2 to demonstrate the specific involvement of OCT2 in drug-drug-interactions of cisplatin with cimetidine. Other studies employed isolated human proximal tubules from kidney tissue in which OCT2 transport function was demonstrated by analyzing internalization of fluorescent probe 4-(4-dimethylamino) styryl-N-methylpyridinium (ASP⁺) over the basolateral membrane^[24]. As these studies are technically challenging and inter-experimental variations are relatively high, human ciPTEC stably expressing functional OCT2 might be more suitable for high-throughput drug screening^[25]. Further improvements could be achieved when such stable cell lines are cultured under flow conditions in a 3D tubule structure with an apical and basal compartment in order to approach the *in vivo* situation.

Intracellular accumulation of substrates internalized via basolateral transport, is prevented at physiological conditions by efficient efflux into the proximal tubule lumen via ABC and SLC transporters present on the apical membrane or via intracellular metabolism. The most widely studied ABC transporter is probably p-glycoprotein (Pgp or MDR1; *ABCB1*), which gene expression was up regulated in multidrug-resistant clones of human leukemia and ovarian carcinoma cells^[26]. Later studies demonstrated the broad expression of this drug transporter on epithelia of many tissues such as blood-brain barrier, the kidney, intestine, testis and placenta, underscoring their protective role against toxins^[27]. More recently, cell-based

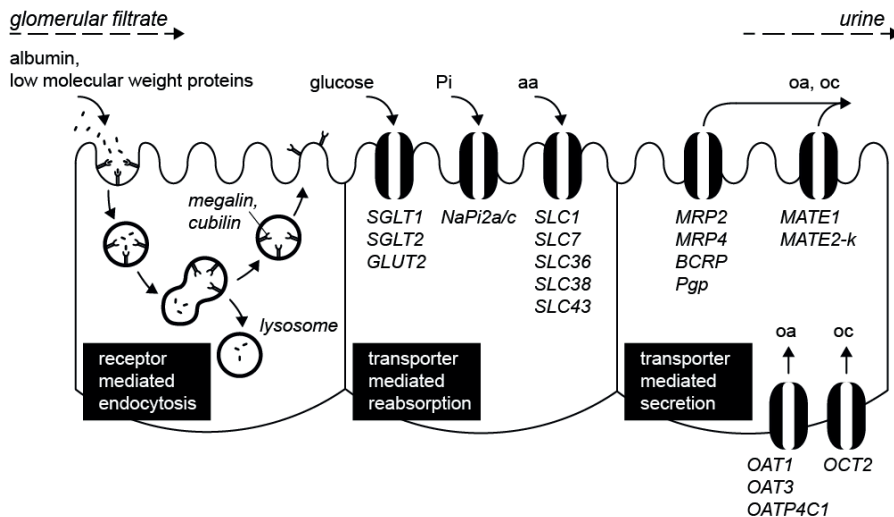


Figure 5.1 Reabsorption and secretion by renal proximal tubule epithelial cells. Megalin and cubilin mediate endocytosis of low molecular weight proteins from the luminal side of the tubule. Apical transport proteins (SGLT, GLUT, NaPi, and SLC) mediate reabsorption of essential serum components, such as glucose, inorganic phosphate (Pi) and amino acids (aa) from the glomerular filtrate. Transcellular transport of organic anions (oa) and organic cations (oc) requires transporter mediated influx at the basolateral membrane and transporter mediated efflux at the apical membrane, acting in concert to facilitate selective renal elimination of waste compounds or drugs.

assays investigating the concerted action of basolaterally expressed OCT2 with apically expressed multidrug and toxin extrusion transporters 1 (MATE1; *SLC47A1*) and MATE2-K (*SLC47A2*) in Madin Darby Canine Kidney cells (MDCK) opened new avenues, including predictive renal clearance studies in pre-clinical stages of drug development^[28,29]. The advantage of using such double-transfected MDCK cells is the formation of a tight epithelial monolayer with a high transepithelial electrochemical resistance (TEER). Consequently, active trans-epithelial transport is relatively easily exceeding the passive diffusion component. Strikingly, MDCK cells have commonly a TEER of $>300 \text{ Ohm cm}^{-1}$ while primary proximal tubule cells present a TEER of approximately 75 Ohm cm^{-1} when grown on semi-permeable filter supports^[30]. Future studies in microfluidic platforms seeded with human proximal tubule cells should take these differences in TEER values into account as this challenges trans-epithelial transport assays using physiologic models.

Next to organic cation secretion, the renal epithelium efficiently eliminates organic anions from the circulatory system. Similar to the adverse effects observed with organic cation drug-interactions, co-administration of organic anions can also result

in drug-induced nephrotoxicity. For example, nucleotide analog reverse transcriptase inhibitors (NtRTIs) such as adefovir, cidofovir and tenofovir are related to drug-induced nephrotoxicity associated with OAT activity^[31,32]. Many researchers have used Chinese Hamster Ovary (CHO) cells as a model to over-express OAT1 or OAT3 and demonstrate cytotoxicity of organic anions^[33-35]. Although CHO-OAT1 has proven to be relevant for studying drug interactions at the site of OAT for over a decade, the deficiency of the cooperating apical efflux transporters multidrug resistance-associated proteins 2 (MRP2; *ABCC2*), and 4 (MRP4; *ABCC4*) and breast cancer resistance protein (BCRP; *ABCG2*) make incorporation in a kidney-on-a-chip not useful. The use of primary proximal tubules cultured directly on semi-permeable inserts with intact organic anion influx and efflux transporters allowed to study transepithelial transport of p-amino hippurate, however, OAT expression was rapidly decreased^[30]. Recently, our group demonstrated stable expression of OAT1 and OAT3 in transfected ciPTEC that endogenously expressed functional MRP and BCRP transport as well^[17,32].

Fluid shear stress induces intracellular signalling in the proximal tubule epithelium

The kidneys play a major role in the excretion of waste products, for which 25% of cardiac output is directed to the kidneys resulting in approximately 180 L of glomerular filtrate entering the renal tubule lumen daily^[2]. Consequently, epithelial cells lining the renal tubule are exposed to an apical fluid shear stress calculated to be approximately 1 dyne·cm⁻²^[10]. Renal tubule cells 'sense' apical fluid shear stress by a single sensory organelle known as the primary cilium^[36]. Cilium-mediated signal transduction contributes to differentiation of the renal tubule epithelial tissue.

The renal non-motile primary cilium is a thin organelle (with a diameter of 0.25 µm) typically protruding 2 to 3 µm from the apical membrane into the tubule lumen^[37]. It is present as a single structure on almost all renal cells, except for the intercalated cells of the collecting duct^[37]. In short, it consists out of 9 circumferentially arranged doublet tubulin-based microtubules enclosed by an extension of the cell membrane. Cilia were demonstrated to gradually bend in response to fluid shear stress over the apical membrane or by direct modulation using a micropipette in cultured MDCK cells^[38]. The intracellular Ca²⁺ concentration increased accordingly, requiring Ca²⁺ influx from the apical compartment (Figure 5.2). The response to fluid shear stress was completely abolished when the primary cilium was chemically removed by exposing MDCK cells to chloral hydrate for 68 hours^[39]. However, completely removing the cilium via this method likely results in a-specific effects such as affected proliferation,

since the cilium is anchored to the cytoskeleton via the basal body, which acts as microtubule-organizing centre during mitosis^[37]. Targeting structural cilium proteins or cilium-mediated signal transduction pathways provide a more specific approach to investigate cilium function. Essential for the structure and signal transduction of primary cilia are polycystic kidney disease 1 (*PKD1*) and -2 (*PKD2*) genes encoding the proteins polycystin 1 (PC1) and transient receptor potential channel 2 (*TRPP2*). Loss-of-function mutations in these genes were identified to cause autosomal dominant polycystic kidney disease (ADPKD)^[40, 41]. Affecting 1 in 1000, ADPKD is the most common cause of inherited kidney disease in human adults^[42]. It is clinically characterized by progressive formation of fluid-filled cysts in the kidney, pancreas and liver, together with cardiovascular symptoms^{c[42]}.

PC1 and TRPP2 are transmembrane proteins that interact at the primary cilium to form a protein complex (Figure 5.2)^[43]. In response to fluid shear stress, PC1 is activated resulting in the opening of the TRPP2 channel which allows a localized Ca^{2+} influx^[44].

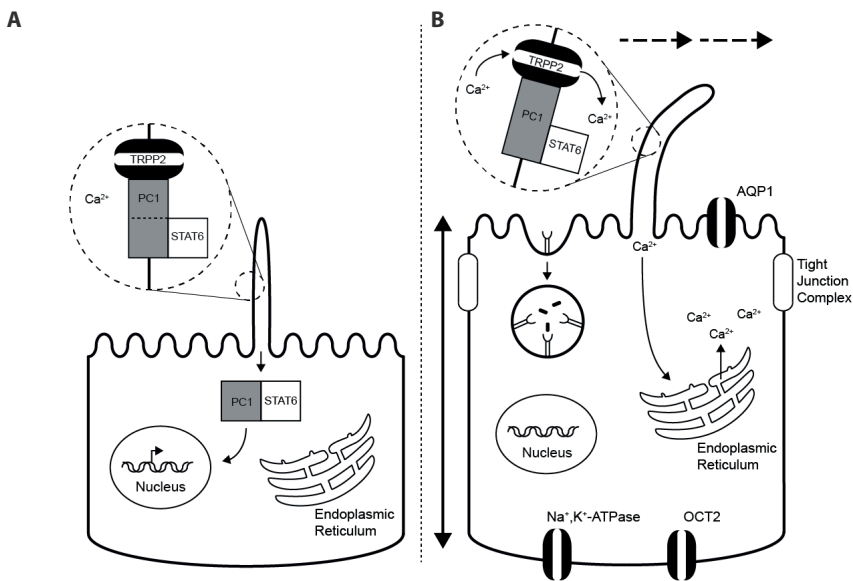


Figure 5.2 Cilium-mediated signal transduction in renal proximal tubule epithelial cells. (A) In absence of fluid shear stress, the Ca^{2+} channel of the PC1-TRPP2 protein complex is closed. The PC1 C-terminus undergoes proteolytic cleavage and translocates together with STAT6 to the nucleus to function as nuclear transcription factor. (B) In presence of fluid shear stress, the primary cilium bends causing the PC1-TRPP2 protein complex to act as channel for extracellular Ca^{2+} . This causes a local rise in intracellular Ca^{2+} concentration, possibly further propagated by a Ca^{2+} release from the endoplasmic reticulum. Cilium-mediated signalling leads to increased cell volume, receptor-mediated endocytosis, expression of tight-junction protein complexes at apical focal adhesion points and polarized expression of AQP1, OCT2 and Na,K-ATPase.

The signal is then further propagated by triggering release of intracellular Ca^{2+} from the ER, mediated by the ryanodine receptor. In addition to Ca^{2+} dependent signals, PC1 was shown to regulate multiple pathways that could explain cyst formation observed in ADPKD. Expression of PC1 induces the JAK-STAT pathway, inducing cell-cycle arrest, which is absent when mutations prevent formation of the PC1-TRPP2 protein complex^[45]. In addition, the C-terminal tail of PC1 was found to interact with nuclear transcription factor STAT6, which co-localizes with the primary cilium under fluidic conditions (Figure 5.2)^[46]. When apical fluid shear stress is absent, the C-terminus of PC1 undergoes proteolytic cleavage and translocates together with STAT6 to the nucleus where it functions as transcription factor, possibly mediating signal transduction. PC1 also interacts with tuberlin, which is a regulator of mTOR kinase activity^[47]. In tubule epithelial cells isolated from cysts of ADPKD patients, the mTOR pathway was stimulated, providing a possible mechanism for increased cell growth observed in cyst formation^[47, 48].

Evolution of renal culture systems towards 3D

2D cultures have been used to study renal physiology, pharmacology and pathology for over 50 years. Such 2D models have the advantage to be relatively simple and low in cost and form the basis of our current knowledge in cellular mechanisms (Figure 5.3). However, 2D cell cultures do not reproduce the *in vivo* microenvironment of the nephron, which likely contributes to the functionally differentiated state of cells. To this end, different approaches have been initiated to increase the physiological relevance of *in vitro* culture systems, including incorporation of extracellular matrix and application of fluid shear stress.

3D spheroids embedded in a matrix

To better mimic the *in vivo* situation, 3D renal culture models were developed that incorporate extracellular matrix (ECM) (Figure 5.3). ECM in the kidney consists of various types of collagen, glycosaminoglycans, laminin and fibronectin that connect to integrin proteins located in the plasma membrane of cells. The basolateral side of renal tubule epithelial cells faces ECM mainly composed of collagen type IV which dictates the 3D structure of the renal tubule and allows for integrin-mediated signalling, regulating cell adhesion, differentiation and regeneration^[49]. To mimic the basement membrane *in vitro*, commercially available Matrigel is commonly used. It is derived from Engelbreth-Holm-Swarm mouse tumour cells and consists of collagen IV, laminin, perlecan and growth factors, which are also found in the basement membrane^[50]. When single MDCK cells are embedded within Matrigel, fluid-filled spheroids will develop by proliferation, polarization and subsequent lumen formation

in a step-by-step process^[51]. Initially, membrane proteins are randomly distributed over the plasma membrane. ECM components, in particular laminin, provide a strong basolateral signal, resulting in translocation of apical membrane targeted proteins to the membrane opposite from the ECM and finally cause the formation of a polarized cell^[52,53]. Tight junction complexes consisting of claudin, occludin and zonula occludens 1 (ZO-1) proteins are formed and physically separate the apical from the basolateral membrane^[54]. The final step in lumen formation by MDCK cells in Matrigel involves the apical expression of podocalyxin. This glycosylated molecule carries a highly negative charge and results in dissociation of cell-cell interactions, except at tight junctions, allowing the formation of a fluid-filled lumen^[55,56]. Increased resistance to chemotherapeutic drugs was demonstrated in 3D spheroid models of breast cancer cell lines MEC (mammary epithelial cell) HMT3522 and MCF-7 (Michigan cancer foundation-7) breast cancer cells cultured in Matrigel when compared to standard 2D monolayer cultures. These findings point towards the effect of ECM and 3D structures on the pharmacological response^[57,58].

Micro-engineered 3D kidney rudiments

While MDCK cells form relatively simple spheroids when cultured in ECM, other cell types are able to form more advanced 3D tubule-like structures, demonstrating higher similarity to the *in vivo* kidney (Figure 5.3). DesRochers and colleagues have reported an *in vitro* system in which human telomerase reverse transcriptase (hTERT)-immortalized human renal cortical (NKi-2) cells were cultured in a 1:1 mixture of Matrigel and rat tail collagen I^[59]. A 3D interconnected tubular structure was formed within 2 weeks and could be maintained for up to 8 weeks. These tissues expressed epithelial cell marker E-cadherin (*CDH1*) and proximal tubule cell marker γ -glutamyltransferase 1 (GGT1, *GGT1*), demonstrated Na⁺-dependent glucose transport and stained positive for expression of transporters OAT1 and OAT4. NKi-2 cells expressed mRNA transcripts for MRP2, MRP4 and MRP5 and the endocytosis receptor megalin (*LRP2*), suggesting its potential application in drug interaction studies. The 3D tubule structures were exposed to well-known nephrotoxic drugs cisplatin, gentamicin and doxorubicin and viability was evaluated by leakage of cytoplasmic lactate dehydrogenase (LDH), reflecting membrane integrity. Cisplatin was found to demonstrate similar LD₅₀ values for both 2D and 3D cultures. For gentamicin and doxorubicin however, the 3D tissue culture models were demonstrated to be significantly more sensitive^[59]. An even more complex system with multiple cell types was reported by Lawrence and colleagues, who developed functional kidney rudiments *in vitro* from renal progenitor cells^[60]. Single cell suspensions of isolated murine epithelial ureteric bud surrounded by condensed mesenchyme at embryonic day 11.5, are capable of producing rudimentary engineered kidneys^[61]. The tubule structures are organized

around a single collecting duct that demonstrate cortical and medullary zones and form morphologically distinct structures, such as loops of Henle. Transport function was elegantly evaluated using fluorescent substrates. Uptake of the fluorescent anion 6-carboxyfluorescein could be inhibited by OAT substrate probenecid, indicating OAT-specific transport. Efflux of 6-carboxyfluorescein, inhibited by MRP inhibitor MK571, indicated MRP-specific transport. Uptake of the fluorescent cation DAPI was inhibited by OCT substrates metformin and cimetidine, indicating OCT-specific transport^[60]. While murine-derived kidney rudiments recapitulate the *in vivo* kidney in terms of 3D microenvironment and interactions between multiple cell types, their predictivity for human clinical drug toxicity and pharmacological interaction studies is relatively low^[62]. Kidney rudiments derived from human pluripotent stem cells (hPSC) do not have this limitation. Freedman and colleagues demonstrated that undifferentiated hPSC first develop into spheroids when cultured between two layers of diluted Matrigel. Subsequent inhibition of glycogen synthetase kinase-3b (GSK3b) leads to development of convoluted, translucent tubular organoids^[63]. Treatment with nephrotoxic drugs cisplatin and gentamicin induced expression of kidney injury molecule-1 (KIM-1) at the luminal surface of tubules, suggesting this culture system can be used to study clinically-relevant biomarkers. In addition, endocytosis activity was demonstrated using rhodamine-labelled dextran accumulation in tubular lumens, which was reduced in presence of endocytosis inhibitor latrunculin B.

A disadvantage of most spheroid and micro engineered cultures is that they rely on ECM, such as Matrigel, with varying composition of different batches (Figure 5.3). In addition, sizes and distribution through the gel are not uniform and the luminal fluid is not easily accessible for sampling or differential control of exposure conditions to apical and basolateral membranes^[64]. Moreover, spheroid, organoid and engineered kidney cultures are not exposed to fluid shear stress, unlike the physiological renal lumen. These issues make spheroid and micro engineered cultures not suitable for high-throughput screening of drug-induced toxicity. Kidney-on-a-chip devices may reintroduce these physiologically important characteristics of renal tissue.

Reconstruction of the physiological microenvironment in a kidney-on-a-chip

An organ-on-a-chip is a microfluidic device that allow 3D cultures of living cells in perfused channels on a micro scale. The aim is to recreate a physiologically relevant niche for a particular cell type or tissue to such an extent, that cellular responses are more *in vivo*-like compared to standard 2D tissue culture. Important features include


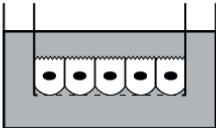
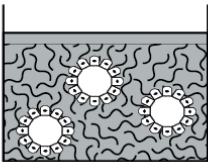
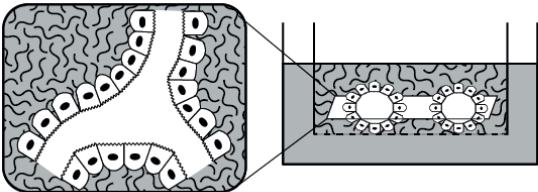
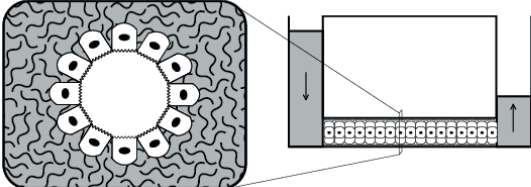
Tissue culture model	Advantages	Disadvantages
<p>Two-dimensional monolayer</p> 	<ul style="list-style-type: none"> • Coating with ECM • Easily accessible • Low in cost • Compatible with HTS 	<ul style="list-style-type: none"> • 2D • No transepithelial transport • No fluid shear stress • No polarization
<p>Two-dimensional monolayer on Transwell™ insert</p> 	<ul style="list-style-type: none"> • Easily accessible • Cell polarization • Transepithelial transport studies • Coating with ECM 	<ul style="list-style-type: none"> • 2D • No fluid shear stress
<p>ECM-embedded spheroid</p> 	<ul style="list-style-type: none"> • Cell polarization • ECM signaling • Compatible with HTS 	<ul style="list-style-type: none"> • No fluid shear stress • Lumen is not easily accessible • Non-uniform spheroid size • Non-uniform distribution
<p>Bioengineered (rudimentary) organs</p> 	<ul style="list-style-type: none"> • Cell polarization • 3D tubule formation • ECM signaling • Multiple cell types 	<ul style="list-style-type: none"> • No fluid shear stress • Lumen is not easily accessible • Low throughput • Relatively high cost
<p>Organ-on-a-chip (microfluidic devices)</p> 	<ul style="list-style-type: none"> • Cell polarization • ECM signaling • 3D tubule formation • Multiple cell types • Fluid shear stress • Perfusate analysis 	<ul style="list-style-type: none"> • No standardization • High-throughput screening may be possible in the future • Relatively high cost • Laborious

Figure 5.3 Evolution of 3D culture models. Overview of 2D and 3D tissue culture models, including advantages and disadvantages. ECM, extra cellular matrix; HTS, high throughput screening.

dimensional and structural architecture, fluid shear stress, mechanical forces and the ability to culture multiple cell types, preferably in multiple compartments^[4]. In the simplest example a ‘chip’ consists of one single microfluidic channel lined with cells of one cell type, cultured immediately on the structural surface (Figure 5.3). Using perfusion by gravity or active pumping systems, cells can be exposed to a fluid shear stress similar to what is experienced in the physiological tissue. Due to the channel’s micrometer size, fluid flow in microfluidic systems is exclusively

laminar: turbulence is minimal or absent. In a more advanced system, two parallel channels can be separated by a porous membrane or by PhaseGuide™ technology to create membrane-free parallel channels, which allows compartmentalization for transcellular transport studies^[9, 65]. When combined with different cell types, parallel channels allow for studying cell-cell interactions^[66]. In addition, mechanical forces as experienced by cells located in the lung and gut for example, can be incorporated by culturing cells on an elastic surface^[67, 68]. Eventually, serially linking of chambers that are lined with cells representing different organs may be used to mimic inter-organ interactions and advance towards a 'human-on-a-chip' model^[69, 70].

Material and production process of organ-on-a-chip devices

Microfluidic devices are often produced of poly-dimethylsiloxane (PDMS) and the process requires molding and/or photolithographic etching techniques^[71]. Briefly, the structural outline of the organ-on-a-chip system originates from a computer assisted photo mask, which is projected over a silicon base covered with a thin layer of photosensitive material. By applying ultraviolet light and dissolving the exposed material, the inverse pattern of the chip is fabricated. By subsequently pouring the liquid polymer PDMS on the etched surface, the layout of the chip is created^[72]. Hollow channels result from fixing the PDMS to a flat surface, such as plastic or glass. The chip interior can be coated with cell type specific ECM prior to the addition of cells in suspension^[73].

The advantages of using PDMS are its biocompatibility, its permeability to gas and its optical clarity, allowing evaluation of cellular responses by live imaging. Moreover, the design of PDMS-based microfluidic devices allows for a controlled fluid shear stress. On the contrary, PDMS absorbs small organic compounds such as drugs, which poses problems for toxicological and pharmacological studies as the final exposure to the cells is equivocal^[74]. This drawback can be circumvented by inert plastic or glass^[65, 75].

Fluid shear stress affects renal phenotype

Next to the design and fabrication, renal cell functionality determines the potential applications of a chip. Efficient excretion of metabolites and xenobiotics is dependent on cellular transport activity and renal metabolism. Commonly used renal cell models, such as OK cells, LLC-PK1, HK-2 and MDCK cells, lack functional differentiation that limits their application for drug-induced injury testing and drug interaction studies^[76-78]. Remarkably, transcriptomic and proteomic analysis in MDCK cells cultured on a fibronectin-coated surface PDMS-based biochip exposed to fluid shear stress revealed increased expression of phase I enzymes (i.e. *CYP1B1*), phase II enzymes (i.e. *GSTA3* and *GSTT1*), and ABC transporters (*ABCC4* and *ABCC5*), as well as SLC transporters (*SLC20A1*, *SLC37A2*, *SLC23A2*

and *SLC7A11*)^[79]. MDCK cells cultured in the kidney-on-a-chip demonstrated a reduction in inflammatory responses by modulating the nuclear factor (erythroid-derived 2)-like 2 (Nrf-2), ataxia telangiectasia mutated (ATM), tumour protein p53 and nuclear factor kappa-light-chain-enhancer of activated B cells (NF-κB) pathways, and reduced integrin-related gene expression in response to treatment with the antineoplastic drug ifosfamide^[80]. Despite the drawbacks in terms of pharmacological relevance, the MDCK cell line was successfully used to demonstrate the influence of fluid shear stress on cellular physiology^[62].

Raghavan and colleagues have evaluated uptake of FITC-labelled albumin via receptor mediated endocytosis in OK cells, LLC-PK1 and MDCK cells, while applying a physiological fluid shear stress of 0.1 dyne·cm⁻²^[10,81]. Compared to static conditions, an increase of albumin uptake in OK and LLC-PK1 cells was observed with a concomitant increase in intracellular Ca²⁺ concentration (Figure 5.2)^[10]. These findings are consistent with the current models of cilia-mediated signal transduction induced by fluid shear stress and underline the importance when evaluating renal tubule transport function.

Multi-compartmentalization combined with fluid shear stress

The current golden standard to study transepithelial transport of drugs and their metabolites via influx and efflux transporters is to culture epithelial cells on semi-permeable membrane supports. Exposure to fluid shear stress is in this setup difficult if not impossible to control. Jang and colleagues therefore applied PDMS-based microfluidic techniques in combination with a similar porous polyester membrane^[82]. When primary rat inner medullary collecting duct (IMCD) cells were cultured on fibronectin-coated membranes and were exposed to fluid shear stress of 1 dyne·cm⁻², renal epithelial polarization was improved: cell height increased by 3-fold, expression of aquaporin 2 (AQP2) was restricted to the apical membrane and Na,K-ATPase was restricted to the basolateral membrane. In addition, reorganization of the cytoskeleton was stimulated as long bundles and networks without a distinction of the cell periphery transformed into thick actin fibres at the cell periphery. Moreover, E-cadherin localization was restricted under fluid shear stress to narrow areas where cells interact, reflecting formation of tight junction protein complexes^[82]. When primary human kidney proximal tubule cells were cultured on collagen IV-coated membranes in the same microfluidic device and fluid shear stress was adjusted to 0.2 dyne·cm⁻², renal epithelial characteristics were improved to a similar extend^[9]. While tight junction protein ZO1 was expressed under both static and fluidic conditions, fluid shear stress increased cell height by 2-fold, expression of Na,K-ATPase was restricted to the basolateral membrane, expression of AQP1 was increased and a significant increase in the amount of ciliated cells was observed (Figure 5.2). To limit the effect of

semi-permeable membranes that create multiple culture compartments, membrane-free microfluidic devices are developed that separate the ECM compartment from the medium perfusion compartment using the PhaseGuide™ technology^[65, 75]. Fluid shear stress in the OrganoPlate® is achieved without pumps and associated tubing systems, allowing for increased throughput in a standard well plate format. These characteristics allow for high-throughput toxicity studies on kidney epithelial tubules with basal and apical compartments.

Next to obvious phenotypic alterations, multi-compartmentalized systems open the ability to study renal clearance in transepithelial transport assays and investigate the toxicological response upon basolateral or apical exposures under fluid shear stress. Pgp efflux activity was increased under fluidic conditions, indicating an improved protection against toxicants^[9]. Further, the toxic response to basolaterally exposed cisplatin was partially ameliorated by fluid shear stress, as measured by lactate dehydrogenase (LDH) release. Under static conditions, the effect of the cisplatin-induced insult was still observed after a 4-day recovery period, while cells under fluidic conditions were completely recovered. These findings indicate that fluid shear stress may enhance the regenerative capacity of renal proximal tubule cells and underscores the importance of a dynamic culture system for regenerative medicine studies.

Applications of kidney-on-a-chip: current and future developments

Recent advances in organ-on-a-chip technology open new applications. The ability for high throughput screening have gained attention at the pharmaceutical industry, while the improvements in the physiological environment are of interest for fundamental studies with clinical relevance or even clinical applications.

Kidney-on-a-chip in drug development

A current challenge in drug development is to bridge the gap between preclinical systems and the clinical situation. Kidney-on-a-chip devices improve the physiological relevance of culture conditions, allowing evaluation of disease processes that develop within 4 to 6 weeks, the timeframe in which the recapitulated tissue remains viable^[9]. The improved complexity of such culture devices could further improve prediction and reduce animal experiments upon careful validation in the future. Microfluidic devices are promising for studying drug-induced toxicity and drug interaction studies^[9, 59, 60, 80]. In addition, microfluidic devices have the potential for high-throughput and multiplex biomarker screening, using live cell fluorescent imaging or analysis of the perfusion medium.

However, using kidney-on-a-chip devices for high-throughput nephrotoxicity screening still faces important challenges^[4]. First of all, the chip-system should be technically and biologically reproducible in order to be implemented in drug screening programs. Differentiation and formation of tight monolayers, ECM composition and fluid shear stress in each individual kidney-on-a-chip should be robust, demanding high quality of both the biological and non-biological materials. Next, microfluidic channels should be fabricated using a biocompatible, low-cost and preferably inert non-absorptive material with the ability of mass-production. Suitable materials may include poly (methyl methacrylate), polystyrene and polycarbonate^[63]. Finally, kidney-on-a-chip models should be validated against established nephrotoxicity assays with approved read-outs. End-point measurements need to be translated to clinical observations, which requires *in vitro* to *in vivo* extrapolation (IVIVE). Validation requires compounds for which *in vitro*, animal and clinical data are available, and should demonstrate whether 3D renal models exceed sensitivity and specificity of existing 2D *in vitro* and animal models. Despite the remaining challenges, future drug development can benefit from kidney-on-a-chip technology by increased predictivity and reduced animal experiments, resulting in safer drugs entering clinical studies.

Kidney-on-a-chip in kidney replacement therapy

While development of kidney-on-a-chip technology is currently driven towards toxicological and pharmacological studies, it may have potential as the functional unit in bioartificial kidneys. Renal replacement therapy using haemodialysis has been applied in the clinic for many years, drastically improving the prognosis of patients with acute and chronic kidney disease^[84]. However, current dialysis only replaces glomerular filtration and compounds known as uremic toxins accumulate in patients suffering from chronic kidney disease^[84]. Improvement of current dialysis treatment is therefore required for which the development of bioartificial kidney devices are explored^[21, 85]. These include the incorporation of a 'living membrane' supporting the growth of renal tubule epithelial cells on a synthetic microfluidic scaffold^[86, 87]. Current approaches rely on culturing renal tubule progenitor cells^[88] or ciPTEC on semi-permeable hollow-fibre membranes coated with ECM proteins^[87]. When ciPTEC were grown on collagen IV coated polyethersulfone hollow fibre membranes, OCT2 transport function was demonstrated using live confocal microscopy by uptake of fluorescent substrate ASP⁺, and subsequent inhibition by cimetidine^[89]. Such transport function in living cells cultured on hollow-fibres can contribute to selective excretion of waste products, such as uremic toxins, when incorporated in a bioartificial kidney^[21]. An initial phase I/II clinical trial using bioartificial kidneys harbouring renal tubule cells supported that this approach can lead to an improvement of survival in patients suffering from AKI^[90]. Shen and colleagues cultured HK-2 and MDCK cells

on polyethylene glycol (PEG)-based curved hollow fibres with inside diameters of 1200, 800 and 400 μm ^[91]. Curvature was demonstrated to induce activity of metabolic enzymes GGT and alkaline phosphatase, promote transport of glucose and increase MRP2-mediated efflux of 5-carboxyfluorescein diacetate^[91]. The next step in the development of the bioartificial kidney is to miniaturize it into a wearable device, for which microfluidic technology could open new opportunities^[92]. A microfluidic-based bioartificial kidney in combination with a microfluidic haemofilter would allow active secretion of uremic solutes in addition to continuous clearance of small solutes. Microfluidic techniques approach the physiological environment with functional tubule epithelial cells, including compartmentalization required for excretion under complete control over fluidic parameters. The capacity of such an application requires efficient elimination of uremic toxins, such as indoxyl sulfate or kynurenic acid, in order to decrease elevated serum levels in patients with CKD towards physiologic levels. Experimentally determined clearance rates of a sub-set of uremic toxins using a microfluidic device can demonstrate the feasibility of such an application, taking into account that size, time and flow rate are limited. Therefore, kidney-on-a-chip technology could aid in the development of miniaturized bioartificial renal devices.

Kidney-on-a-chip to investigate epithelial repair mechanisms

Rudiment kidney cultures demonstrate improved spatial heterogeneity compared to traditionally cell cultures, and are therefore ideal to study regenerative medicine that involves cells at different stages of differentiation. Kidney-on-a-chip technology encompassing tubule structures may be suitable to investigate self-organized epithelial repair mechanisms and in particular the role of fluid shear stress in this process, which can be controlled experimentally.

As the adult human kidney is unable to initiate de novo nephron formation, kidney repair after an ischemia-induced or drug-induced insult depends on repair of damaged nephrons by cellular regeneration. Surviving epithelial cells at or near the site of insult will replace the injured or lost neighbour tubule cells by dedifferentiation, proliferation, migration and redifferentiation^[93-95]. Interestingly, the pathways involved in dedifferentiation and proliferation observed in epithelial repair are overlapping to some extent with those associated with the formation of cysts in PKD, such as mTOR, STAT6, canonical Wnt signalling and planar cell polarity pathways, suggesting the involvement of primary cilia and fluid shear stress in this process^[46, 47, 96]. Cilium length is reported to increase from $\sim 3 \mu\text{m}$ in a healthy renal tubule cell to more than 10 μm in cells of injured nephrons, and tubule cells exposed to fluid shear stress reduces lengthening of the primary cilium^[97, 98]. Since microfluidic devices allow for controlled exposure to laminar fluidic shear stress and can recapitulate other renal

niche characteristics, kidney-on-a-chip may be a helpful tool to investigate the role of cilia-mediated signalling in epithelial repair.

Multi-organ-on-a-chip models in drug development

Drug-metabolism in the liver can significantly influence renal adverse effects. Certain drugs, such as cyclosporine A and tetrafluoroethylene, are metabolised by the liver and this can either suppress or enhance nephrotoxicity^[99, 100]. To study the effects of liver-mediated drug-metabolism on nephrotoxicity, a kidney-on-a-chip linked to a liver-on-a-chip may provide a suitable platform.

A liver-on-a-chip device with high *in vivo* relevance was developed by Midwoud and colleagues^[101]. Precision-cut liver slices were wedged between a polycarbonate and PDMS membrane, allowing distribution of both culture medium and oxygen, and placed into a microfluidic PDMS-based device. These precision-cut liver slices were remained functionally for at least 24 h, sufficient for active compound metabolism^[101]. While liver tissue from rats was used for this study, human-derived tissue or human-derived hepatocyte cell lines would allow investigating human-relevant drug metabolism, drug clearance, drug interactions and drug-induced liver toxicity^[71]. By guiding the perfusate of such a liver-on-a-chip to a kidney-on-a-chip, the effect of liver metabolites on the kidney could be evaluated.

Multi-organ-chips are reported that support *in vitro* growth of tissue derived from four different organs with the aim to fully recapitulate human pharmacokinetics^[69, 70]. A highly advanced model developed by Maschmeyer and colleagues incorporates human primary cells or human-derived cell lines representing the intestine epithelium, hepatocytes, isolated skin and renal proximal tubule cells^[69]. The device was fabricated of PDMS and all tissues were maintained on a polyester membrane with 1 µm pores, with fluid on both sides representing a blood circuit or excretion circuit in case of the kidney compartment. A physiological tissue-to-fluid ratio was obtained and fluid shear stress in both circuits was controlled by peristaltic pumps. Co-cultures were viable for up to 28 days, with a stable glucose balance. Glucose concentration was lowest in the excretory circuit of the kidney culture compartment, suggesting intact physiological glucose reabsorption in proximal tubule cells, further supported by active sodium-coupled glucose transporter *SLC5A2* mRNA expression^[69]. Another multi-compartmental 3D microfluidic system incorporated cells that resembled liver, lung, kidney and fat tissue^[70]. Tissue culture compartments were separated from fluidic channels by small openings, called micropillars, and were linked in a closed loop, requiring the use of a common culture medium. Functionality of the different monolayer cultures was demonstrated by albumin secretion (liver), pentoxeresorufin

O-dealkylase activity (lung), γ -glutamyltransferase activity (kidney) and adiponectin secretion (fat tissue)^[70]. In conclusion, these advanced microfluidic devices are the next step towards 'human-on-a-chip' technology with high potential to investigate absorption, distribution, metabolism and excretion kinetics *in vitro*, enhancing the efficiency of drug development.

Conclusions

In conclusion, microfluidic technology supports long-term *in vitro* survival, differentiation and function of renal proximal tubule cells. A kidney-on-a-chip recreates the physiologically relevant renal microenvironment, including the 3D structure, extracellular matrix and apical fluid shear stress. Organ-on-a-chip technology has the potential to culture multiple cell types for development towards a human-on-a-chip or advanced techniques such as renal replacement or studying renal repair mechanisms. Together, the 3D design and microenvironment of a microfluidic renal device provide researchers with a valuable tool in the fields of pharmacology, toxicology and physiology for which recent developments are just the start of a new era in cell culturing.

Acknowledgements

This work was supported financially by NC3Rs (NephroTube Challenge; project no. 37497-25920). Authors declare no potential conflict of interest.

References

1. Cummings BS, Schnellmann RG: Pathophysiology of nephrotoxic cell injury. In: Schrier RW, Philadelphia PA, eds. *Diseases of the Kindey and Urogenital Tract*: Lippincott Williams and Wilkinson, 2001; 1071-1136.
2. Richards IS. *Principles and Practice of Toxicology in Public Health*. Sudbury, Massachusetts: Jones and Bartlett Publishers, (2008).
3. Redfern WS, Ewart L, Hammond TG, Bialecki R, Kinter L, Lindgren S. Impact and frequency of different toxicities throughout the pharmaceutical life cycle. *The Toxicologist*. 1081 (2010).
4. Wilmer MJ, Ng CP, Lanz HL, Vulto P, Suter-Dick L, Masereeuw R. Kidney-on-a-Chip Technology for Drug-Induced Nephrotoxicity Screening. *Trends Biotechnol*. 34, 156-170 (2016).
5. Nielsen R, Christensen EI, Birn H. Megalin and cubilin in proximal tubule protein reabsorption: from experimental models to human disease. *Kidney Int*. 89, 58-67 (2016).
6. Gorvin CM, Wilmer MJ, Piret SE, Harding B, van den Heuvel LP, Wrong O, Jat PS, et al. Receptor-mediated endocytosis and endosomal acidification is impaired in proximal tubule epithelial cells of Dent disease patients. *Proc Natl Acad Sci U S A*. 110, 7014-7019 (2013).
7. Wilmer MJ, Emma F, Levchenko EN. The pathogenesis of cystinosis: mechanisms beyond cystine accumulation. *Am J Physiol Renal Physiol*. 299, F905-916 (2010).
8. Ferrell N, Ricci KB, Groszek J, Marmorstein JT, Fissell WH. Albumin handling by renal tubular epithelial cells in a microfluidic bioreactor. *Biotechnol Bioeng*. 109, 797-803 (2012).
9. Jang KJ, Mehr AP, Hamilton GA, McPartlin LA, Chung S, Suh KY, Ingber DE. Human kidney proximal tubule-on-a-chip for drug transport and nephrotoxicity assessment. *Integr Biol (Camb)*. 5, 1119-1129 (2013).
10. Raghavan V, Rbaibi Y, Pastor-Soler NM, Carattino MD, Weisz OA. Shear stress-dependent regulation of apical endocytosis in renal proximal tubule cells mediated by primary cilia. *Proc Natl Acad Sci U S A*. 111, 8506-8511 (2014).
11. Lima WR, Parreira KS, Devuyst O, Caplanusi A, N'Kuli F, Marien B, Van Der Smissen P, et al. ZONAB promotes proliferation and represses differentiation of proximal tubule epithelial cells. *J Am Soc Nephrol*. 21, 478-488 (2010).
12. Vegt E, van Eerd JE, Eek A, Oyen WJ, Wetzels JF, de Jong M, Russel FG, et al. Reducing renal uptake of radiolabeled peptides using albumin fragments. *J Nucl Med*. 49, 1506-1511 (2008).
13. Erkan E, Devarajan P, Schwartz GJ. Mitochondria are the major targets in albumin-induced apoptosis in proximal tubule cells. *J Am Soc Nephrol*. 18, 1199-1208 (2007).
14. Koral K, Li H, Ganesh N, Birnbaum MJ, Hallows KR, Erkan E. Akt recruits Dab2 to albumin endocytosis in the proximal tubule. *Am J Physiol Renal Physiol*. 307, F1380-1389 (2014).
15. Wilmer MJ, Kluijtmans LA, van der Velden TJ, Willems PH, Scheffer PG, Masereeuw R, Monnens LA, et al. Cysteamine restores glutathione redox status in cultured cystinotic proximal tubular epithelial cells. *Biochim Biophys Acta*. 1812, 643-651 (2011).
16. Wilmer MJ, Saleem MA, Masereeuw R, Ni L, van der Velden TJ, Russel FG, Mathieson PW, et al. Novel conditionally immortalized human proximal tubule cell line expressing functional influx and efflux transporters. *Cell Tissue Res*. 339, 449-457 (2010).
17. Caetano-Pinto P, Janssen MJ, Gijzen L, Verscheijden L, Wilmer MJ, Masereeuw R. Fluorescence-Based Transport Assays Revisited in a Human Renal Proximal Tubule Cell Line. *Mol Pharm*. 13, 933-944 (2016).
18. Ivanova EA, De Leo MG, Van Den Heuvel L, Pastore A, Dijkman H, De Matteis MA, Levchenko EN. Endo-lysosomal dysfunction in human proximal tubular epithelial cells deficient for lysosomal cystine transporter cystinosin. *PLoS One*. 10, e0120998 (2015).
19. Nigam SK, Wu W, Bush KT, Hoening MP, Blantz RC, Bhatnagar V. Handling of Drugs, Metabolites, and Uremic Toxins by Kidney Proximal Tubule Drug Transporters. *Clin J Am Soc Nephrol*. 10, 2039-2049 (2015).

20. Koepsell H. The SLC22 family with transporters of organic cations, anions and zwitterions. *Mol Aspects Med.* 34, 413-435 (2013).
21. Duranton F, Cohen G, De Smet R, Rodriguez M, Jankowski J, Vanholder R, Argiles A. Normal and pathologic concentrations of uremic toxins. *J Am Soc Nephrol.* 23, 1258-1270 (2012).
22. Varma MV, Feng B, Obach RS, Troutman MD, Chupka J, Miller HR, El-Kattan A. Physicochemical determinants of human renal clearance. *J Med Chem.* 52, 4844-4852 (2009).
23. Ciarimboli G, Ludwig T, Lang D, Pavenstadt H, Koepsell H, Piechota HJ, Haier J, et al. Cisplatin nephrotoxicity is critically mediated via the human organic cation transporter 2. *Am J Pathol.* 167, 1477-1484 (2005).
24. Pietig G, Mehrens T, Hirsch JR, Cetinkaya I, Piechota H, Schlatter E. Properties and regulation of organic cation transport in freshly isolated human proximal tubules. *J Biol Chem.* 276, 33741-33746 (2001).
25. Schophuizen CM, Wilmer MJ, Jansen J, Gustavsson L, Hilgendorf C, Hoenderop JG, van den Heuvel LP, et al. Cationic uremic toxins affect human renal proximal tubule cell functioning through interaction with the organic cation transporter. *Pflugers Arch.* 465, 1701-1714 (2013).
26. Shen DW, Fojo A, Chin JE, Roninson IB, Richert N, Pastan I, Gottesman MM. Human multidrug-resistant cell lines: increased *mdr1* expression can precede gene amplification. *Science.* 232, 643-645 (1986).
27. Staud F, Ceckova M, Micuda S, Pavek P. Expression and function of p-glycoprotein in normal tissues: effect on pharmacokinetics. *Methods Mol Biol.* 596, 199-222 (2010).
28. Sato T, Masuda S, Yonezawa A, Tanihara Y, Katsura T, Inui K. Transcellular transport of organic cations in double-transfected MDCK cells expressing human organic cation transporters hOCT1/hMATE1 and hOCT2/hMATE1. *Biochem Pharmacol.* 76, 894-903 (2008).
29. Tsuda M, Terada T, Ueba M, Sato T, Masuda S, Katsura T, Inui K. Involvement of human multidrug and toxin extrusion 1 in the drug interaction between cimetidine and metformin in renal epithelial cells. *J Pharmacol Exp Ther.* 329, 185-191 (2009).
30. Brown CD, Sayer R, Windass AS, Haslam IS, De Broe ME, D'Haese PC, Verhulst A. Characterisation of human tubular cell monolayers as a model of proximal tubular xenobiotic handling. *Toxicol Appl Pharmacol.* 233, 428-438 (2008).
31. Izzedine H, Harris M, Perazella MA. The nephrotoxic effects of HAART. *Nat Rev Nephrol.* 5, 563-573 (2009).
32. Nieskens TT, Peters JG, Schreurs MJ, Smits N, Woestenenk R, Jansen K, van der Made TK, et al. A Human Renal Proximal Tubule Cell Line with Stable Organic Anion Transporter 1 and 3 Expression Predictive for Antiviral-Induced Toxicity. *Aaps j.* 18, 465-475 (2016).
33. Ho ES, Lin DC, Mendel DB, Cihlar T. Cytotoxicity of antiviral nucleotides adefovir and cidofovir is induced by the expression of human renal organic anion transporter 1. *J Am Soc Nephrol.* 11, 383-393 (2000).
34. Hotchkiss AG, Gao T, Khan U, Berrigan L, Li M, Ingraham L, Pelis RM. Organic Anion Transporter 1 Is Inhibited by Multiple Mechanisms and Shows a Transport Mode Independent of Exchange. *Drug Metab Dispos.* 43, 1847-1854 (2015).
35. Ingraham L, Li M, Renfro JL, Parker S, Vapurcuyan A, Hanna I, Pelis RM. A plasma concentration of alpha-ketoglutarate influences the kinetic interaction of ligands with organic anion transporter 1. *Mol Pharmacol.* 86, 86-95 (2014).
36. Praetorius HA. The primary cilium as sensor of fluid flow: new building blocks to the model. A review in the theme: cell signaling: proteins, pathways and mechanisms. *Am J Physiol Cell Physiol.* 308, C198-208 (2015).
37. Rodat-Despoix L, Delmas P. Ciliar functions in the nephron. *Pflugers Arch.* 458, 179-187 (2009).
38. Praetorius HA, Spring KR. Bending the MDCK cell primary cilium increases intracellular calcium. *J Membr Biol.* 184, 71-79 (2001).
39. Praetorius HA, Spring KR. Removal of the MDCK cell primary cilium abolishes flow sensing. *J Membr Biol.* 191, 69-76 (2003).

40. Qian F, Watnick TJ, Onuchic LF, Germino GG. The molecular basis of focal cyst formation in human autosomal dominant polycystic kidney disease type I. *Cell*. 87, 979-987 (1996).
41. Mochizuki T, Wu G, Hayashi T, Xenophontos SL, Veldhuisen B, Saris JJ, Reynolds DM, et al. PKD2, a gene for polycystic kidney disease that encodes an integral membrane protein. *Science*. 272, 1339-1342 (1996).
42. Simms RJ. Autosomal dominant polycystic kidney disease. *Bmj*. 352, i679 (2016).
43. Hanaoka K, Qian F, Boletta A, Bhunia AK, Piontek K, Tsiokas L, Sukhatme VP, et al. Co-assembly of polycystin-1 and -2 produces unique cation-permeable currents. *Nature*. 408, 990-994 (2000).
44. Nauli SM, Alenghat FJ, Luo Y, Williams E, Vassilev P, Li X, Elia AE, et al. Polycystins 1 and 2 mediate mechanosensation in the primary cilium of kidney cells. *Nat Genet*. 33, 129-137 (2003).
45. Bhunia AK, Piontek K, Boletta A, Liu L, Qian F, Xu PN, Germino FJ, et al. PKD1 induces p21(waf1) and regulation of the cell cycle via direct activation of the JAK-STAT signaling pathway in a process requiring PKD2. *Cell*. 109, 157-168 (2002).
46. Low SH, Vasanth S, Larson CH, Mukherjee S, Sharma N, Kinter MT, Kane ME, et al. Polycystin-1, STAT6, and P100 function in a pathway that transduces ciliary mechanosensation and is activated in polycystic kidney disease. *Dev Cell*. 10, 57-69 (2006).
47. Shillingford JM, Murcia NS, Larson CH, Low SH, Hedgepeth R, Brown N, Flask CA, et al. The mTOR pathway is regulated by polycystin-1, and its inhibition reverses renal cystogenesis in polycystic kidney disease. *Proc Natl Acad Sci U S A*. 103, 5466-5471 (2006).
48. Polak P, Hall MN. mTOR and the control of whole body metabolism. *Curr Opin Cell Biol*. 21, 209-218 (2009).
49. Combes AN, Davies JA, Little MH. Cell-cell interactions driving kidney morphogenesis. *Curr Top Dev Biol*. 112, 467-508 (2015).
50. Kleinman HK, Martin GR. Matrigel: basement membrane matrix with biological activity. *Semin Cancer Biol*. 15, 378-386 (2005).
51. Schluter MA, Margolis B. Apical lumen formation in renal epithelia. *J Am Soc Nephrol*. 20, 1444-1452 (2009).
52. Martin-Belmonte F, Yu W, Rodriguez-Fraticelli AE, Ewald AJ, Werb Z, Alonso MA, Mostov K. Cell-polarity dynamics controls the mechanism of lumen formation in epithelial morphogenesis. *Curr Biol*. 18, 507-513 (2008).
53. Yu W, Datta A, Leroy P, O'Brien LE, Mak G, Jou TS, Matlin KS, et al. Beta1-integrin orients epithelial polarity via Rac1 and laminin. *Mol Biol Cell*. 16, 433-445 (2005).
54. Wang Q, Margolis B. Apical junctional complexes and cell polarity. *Kidney Int*. 72, 1448-1458 (2007).
55. Cheng HY, Lin YY, Yu CY, Chen JY, Shen KF, Lin WL, Liao HK, et al. Molecular identification of canine podocalyxin-like protein 1 as a renal tubulogenic regulator. *J Am Soc Nephrol*. 16, 1612-1622 (2005).
56. Bryant DM, Roignot J, Datta A, Overeem AW, Kim M, Yu W, Peng X, et al. A molecular switch for the orientation of epithelial cell polarization. *Dev Cell*. 31, 171-187 (2014).
57. Weaver VM, Lelievre S, Lakins JN, Chrenek MA, Jones JC, Giancotti F, Werb Z, et al. beta4 integrin-dependent formation of polarized three-dimensional architecture confers resistance to apoptosis in normal and malignant mammary epithelium. *Cancer Cell*. 2, 205-216 (2002).
58. Pogany G, Timar F, Olah J, Harisi R, Polony G, Paku S, Bocsi J, et al. Role of the basement membrane in tumor cell dormancy and cytotoxic resistance. *Oncology*. 60, 274-281 (2001).
59. DesRochers TM, Suter L, Roth A, Kaplan DL. Bioengineered 3D human kidney tissue, a platform for the determination of nephrotoxicity. *PLoS One*. 8, e59219 (2013).
60. Lawrence ML, Chang CH, Davies JA. Transport of organic anions and cations in murine embryonic kidney development and in serially-reaggregated engineered kidneys. *Sci Rep*. 5, 9092 (2015).
61. Sebinger DD, Unbekandt M, Ganeva VV, Ofenbauer A, Werner C, Davies JA. A novel, low-volume method for organ culture of embryonic kidneys that allows development of cortico-medullary anatomical organization. *PLoS One*. 5, e10550 (2010).

62. Chu X, Bleasby K, Evers R. Species differences in drug transporters and implications for translating preclinical findings to humans. *Expert Opin Drug Metab Toxicol.* 9, 237-252 (2013).
63. Freedman BS, Brooks CR, Lam AQ, Fu H, Morizane R, Agrawal V, Saad AF, et al. Modelling kidney disease with CRISPR-mutant kidney organoids derived from human pluripotent epiblast spheroids. *Nat Commun.* 6, 8715 (2015).
64. Sodunke TR, Turner KK, Caldwell SA, McBride KW, Reginato MJ, Noh HM. Micropatterns of Matrigel for three-dimensional epithelial cultures. *Biomaterials.* 28, 4006-4016 (2007).
65. van Duinen V, Trietsch SJ, Joore J, Vulto P, Hankemeier T. Microfluidic 3D cell culture: from tools to tissue models. *Curr Opin Biotechnol.* 35, 118-126 (2015).
66. Novik E, Maguire TJ, Chao P, Cheng KC, Yarmush ML. A microfluidic hepatic coculture platform for cell-based drug metabolism studies. *Biochem Pharmacol.* 79, 1036-1044 (2010).
67. Huh D, Matthews BD, Mammoto A, Montoya-Zavala M, Hsin HY, Ingber DE. Reconstituting organ-level lung functions on a chip. *Science.* 328, 1662-1668 (2010).
68. Kim HJ, Huh D, Hamilton G, Ingber DE. Human gut-on-a-chip inhabited by microbial flora that experiences intestinal peristalsis-like motions and flow. *Lab Chip.* 12, 2165-2174 (2012).
69. Maschmeyer I, Lorenz AK, Schimek K, Hasenberg T, Ramme AP, Hubner J, Lindner M, et al. A four-organ-chip for interconnected long-term co-culture of human intestine, liver, skin and kidney equivalents. *Lab Chip.* 15, 2688-2699 (2015).
70. Zhang C, Zhao Z, Abdul Rahim NA, van Noort D, Yu H. Towards a human-on-chip: culturing multiple cell types on a chip with compartmentalized microenvironments. *Lab Chip.* 9, 3185-3192 (2009).
71. Bhatia SN, Ingber DE. Microfluidic organs-on-chips. *Nat Biotechnol.* 32, 760-772 (2014).
72. Duffy DC, McDonald JC, Schueller OJ, Whitesides GM. Rapid Prototyping of Microfluidic Systems in Poly(dimethylsiloxane). *Anal Chem.* 70, 4974-4984 (1998).
73. Folch A, Ayon A, Hurtado O, Schmidt MA, Toner M. Molding of deep polydimethylsiloxane microstructures for microfluidics and biological applications. *J Biomech Eng.* 121, 28-34 (1999).
74. Toepke MW, Beebe DJ. PDMS absorption of small molecules and consequences in microfluidic applications. *Lab Chip.* 6, 1484-1486 (2006).
75. Jang M, Neuzil P, Volk T, Manz A, Kleber A. On-chip three-dimensional cell culture in Phaseguides improves hepatocyte functions in vitro. *Biomicrofluidics.* 9, 034113 (2015).
76. Jenkinson SE, Chung GW, van Loon E, Bakar NS, Dalzell AM, Brown CD. The limitations of renal epithelial cell line HK-2 as a model of drug transporter expression and function in the proximal tubule. *Pflugers Arch.* 464, 601-611 (2012).
77. Racusen LC, Monteil C, Sgrignoli A, Lucskay M, Marouillat S, Rhim JG, Morin JP. Cell lines with extended in vitro growth potential from human renal proximal tubule: characterization, response to inducers, and comparison with established cell lines. *J Lab Clin Med.* 129, 318-329 (1997).
78. Van der Hauwaert C, Savary G, Buob D, Leroy X, Aubert S, Flamand V, Hennino MF, et al. Expression profiles of genes involved in xenobiotic metabolism and disposition in human renal tissues and renal cell models. *Toxicol Appl Pharmacol.* 279, 409-418 (2014).
79. Snouber LC, Letourneur F, Chafey P, Broussard C, Monge M, Legallais C, Leclerc E. Analysis of transcriptomic and proteomic profiles demonstrates improved Madin-Darby canine kidney cell function in a renal microfluidic biochip. *Biotechnol Prog.* 28, 474-484 (2012).
80. Choucha Snouber L, Jacques S, Monge M, Legallais C, Leclerc E. Transcriptomic analysis of the effect of ifosfamide on MDCK cells cultivated in microfluidic biochips. *Genomics.* 100, 27-34 (2012).
81. Raghavan V, Rbaibi Y, Pastor-Soler NM, Carattino MD, Weisz OA. Correction for Raghavan et al., Shear stress-dependent regulation of apical endocytosis in renal proximal tubule cells mediated by primary cilia. *Proc Natl Acad Sci U S A.* (2016).
82. Jang KJ, Suh KY. A multi-layer microfluidic device for efficient culture and analysis of renal tubular cells. *Lab Chip.* 10, 36-42 (2010).

83. van Midwoud PM, Janse A, Merema MT, Groothuis GM, Verpoorte E. Comparison of biocompatibility and adsorption properties of different plastics for advanced microfluidic cell and tissue culture models. *Anal Chem.* 84, 3938-3944 (2012).
84. Fleming GM. Renal replacement therapy review: past, present and future. *Organogenesis.* 7, 2-12 (2011).
85. Jansen J, Fedecostante M, Wilmer MJ, van den Heuvel LP, Hoenderop JG, Masereeuw R. Biotechnological challenges of bioartificial kidney engineering. *Biotechnol Adv.* 32, 1317-1327 (2014).
86. Humes HD, MacKay SM, Funke AJ, Buffington DA. Tissue engineering of a bioartificial renal tubule assist device: in vitro transport and metabolic characteristics. *Kidney Int.* 55, 2502-2514 (1999).
87. Schophuizen CM, De Napoli IE, Jansen J, Teixeira S, Wilmer MJ, Hoenderop JG, Van den Heuvel LP, et al. Development of a living membrane comprising a functional human renal proximal tubule cell monolayer on polyethersulfone polymeric membrane. *Acta Biomater.* 14, 22-32 (2015).
88. Humes HD, Krauss JC, Cieslinski DA, Funke AJ. Tubulogenesis from isolated single cells of adult mammalian kidney: clonal analysis with a recombinant retrovirus. *Am J Physiol.* 271, F42-49 (1996).
89. Jansen J, De Napoli IE, Fedecostante M, Schophuizen CM, Chevtchik NV, Wilmer MJ, van Asbeck AH, et al. Human proximal tubule epithelial cells cultured on hollow fibers: living membranes that actively transport organic cations. *Sci Rep.* 5, 16702 (2015).
90. Humes HD, Weitzel WF, Bartlett RH, Swaniker FC, Paganini EP, Luderer JR, Sobota J. Initial clinical results of the bioartificial kidney containing human cells in ICU patients with acute renal failure. *Kidney Int.* 66, 1578-1588 (2004).
91. Shen C, Meng Q, Zhang G. Increased curvature of hollow fiber membranes could up-regulate differential functions of renal tubular cell layers. *Biotechnol Bioeng.* 110, 2173-2183 (2013).
92. Humes HD, Buffington D, Westover AJ, Roy S, Fissell WH. The bioartificial kidney: current status and future promise. *Pediatr Nephrol.* 29, 343-351 (2014).
93. Bonventre JV. Dedifferentiation and proliferation of surviving epithelial cells in acute renal failure. *J Am Soc Nephrol.* 14 Suppl 1, S55-61 (2003).
94. Humphreys BD, Czerniak S, DiRocco DP, Hasnain W, Cheema R, Bonventre JV. Repair of injured proximal tubule does not involve specialized progenitors. *Proc Natl Acad Sci U S A.* 108, 9226-9231 (2011).
95. Humphreys BD, Valerius MT, Kobayashi A, Mugford JW, Soeung S, Duffield JS, McMahon AP, et al. Intrinsic epithelial cells repair the kidney after injury. *Cell Stem Cell.* 2, 284-291 (2008).
96. Patel V, Li L, Cobo-Stark P, Shao X, Somlo S, Lin F, Igarashi P. Acute kidney injury and aberrant planar cell polarity induce cyst formation in mice lacking renal cilia. *Hum Mol Genet.* 17, 1578-1590 (2008).
97. Iomini C, Tejada K, Mo W, Vaananen H, Piperno G. Primary cilia of human endothelial cells disassemble under laminar shear stress. *J Cell Biol.* 164, 811-817 (2004).
98. Wang L, Weidenfeld R, Verghese E, Ricardo SD, Deane JA. Alterations in renal cilium length during transient complete ureteral obstruction in the mouse. *J Anat.* 213, 79-85 (2008).
99. Duncan JI, Heys SD, Thomson AW, Simpson JG, Whiting PH. Influence of the hepatic drug-metabolizing enzyme-inducer phenobarbitone on cyclosporine nephrotoxicity and hepatotoxicity in renal-allografted rats. *Transplantation.* 45, 693-697 (1988).
100. Odum J, Green T. The metabolism and nephrotoxicity of tetrafluoroethylene in the rat. *Toxicol Appl Pharmacol.* 76, 306-318 (1984).
101. van Midwoud PM, Groothuis GM, Merema MT, Verpoorte E. Microfluidic biochip for the perfusion of precision-cut rat liver slices for metabolism and toxicology studies. *Biotechnol Bioeng.* 105, 184-194 (2010).



Screening of Drug-Transporter Interactions in a 3D Microfluidic Renal Proximal Tubule on a Chip

Jelle Vriend¹, Tom TG Nieskens¹, Marianne K Vormann², Bartholomeus T van den Berge¹, Angelique van den Heuvel², Frans GM Russel¹, Laura Suter-Dick³, Henriëtte L Lanz², Paul Vulto², Rosalinde Masereeuw⁴, Martijn J Wilmer^{1*}

¹ Department of Pharmacology and Toxicology, Radboud Institute for Molecular Life Sciences, Radboud University Medical Center, Nijmegen, The Netherlands

² Mimetas BV, Leiden, The Netherlands

³ University of Applied Sciences Northwestern Switzerland, School of Life Sciences, Muttenz, Switzerland

⁴ Div. Pharmacology, Utrecht Institute for Pharmaceutical Sciences, Utrecht, The Netherlands

American Association of Pharmaceutical Sciences Journal 20. 87 (2018)

Abstract

Drug-transporter interactions could impact renal drug clearance and should ideally be detected in early stages of drug development to avoid toxicity-related withdrawals in later stages. This requires reliable and robust assays for which current high-throughput screenings have, however, poor predictability. Kidney-on-a-chip platforms have the potential to improve predictability, but often lack compatibility with high-content detection platforms. Here, we combined conditionally immortalized proximal tubule epithelial cells overexpressing organic anion transporter 1 (ciPTEC-OAT1) with the microfluidic titerplate OrganoPlate to develop a screenings assay for renal drug-transporter interactions. In this platform, apical localization of F-actin and intracellular tight-junction protein zonula occludens-1 (ZO-1) indicated appropriate cell polarization. Gene expression levels of the drug transporters organic anion transporter 1 (OAT1; *SLC22A6*), organic cation transporter 2 (OCT2; *SLC22A2*), P-glycoprotein (P-gp; *ABCB1*) and multidrug resistance-associated protein 2 and 4 (MRP2/4; *ABCC2/4*) were similar levels to 2D static cultures. Functionality of the efflux transporters P-gp and MRP2/4 was studied as proof-of-concept for 3D assays using calcein-AM and 5-chloromethylfluorescein-diacetate (CMFDA), respectively. Confocal imaging demonstrated a 4.4 ± 0.2 -fold increase in calcein accumulation upon P-gp inhibition using PSC833. For MRP2/4, a 3.0 ± 0.2 -fold increased accumulation of glutathione-methylfluorescein (GS-MF) was observed upon inhibition with a combination of PSC833, MK571 and KO143. Semi-quantitative image processing methods for P-gp and MRP2/4 was demonstrated with corresponding Z'-factors of 0.1 ± 0.3 and 0.4 ± 0.1 , respectively. In conclusion, we demonstrate a 3D microfluidic PTEC model valuable for screening of drug-transporter interactions that further allows multiplexing of endpoint read-outs for drug-transporter interactions and toxicity.

Introduction

Excretion of metabolic waste products and drugs from blood into the urine takes place in the kidney and is a result of glomerular filtration, active tubular secretion and reabsorption. It has been estimated that about one third of the commonly used drugs and compounds tested in clinical trials are being (partially) removed via the urine without further metabolism^[1,2]. Renal clearance thus is a pivotal parameter to take into account during drug disposition studies in drug development.

Active tubular secretion of drugs in the kidney takes place mainly by the proximal tubule epithelial cells (PTEC) of the nephron, and involves transporters^[3]. Uptake from blood to PTEC is mediated by members of the solute carrier (SLC) transporter family, such as organic cation transporter 2 (OCT2/*SLC22A2*) and organic anion transporter 1 and 3 (OAT1/*SLC22A6*; OAT3/*SLC22A8*). To complete elimination via urine from compounds internalized via SLC-mediated transport over the basolateral membrane, a range of drug transporters is expressed at the apical membrane of PTEC. This energy demanding process is facilitated by transporters classified in the ATP-binding cassette (ABC)-transporter family, such as P-glycoprotein (P-gp/*ABCB1*), breast cancer resistance protein (BCRP/*ABCG2*) and multidrug resistance-associated proteins 2 and 4 (MRP2/*ABCC2*; MRP4/*ABCC4*). Other drug transporters present at the apical membrane are the multidrug and toxin extrusion proteins 1 and 2-k (MATE1/*SLC47A1*; MATE2-k/*SLC47A2*). In drug development, investigating interactions with a sub-set of drug transporters is recommended by the regulatory agencies, such as the United States Food and Drug Administration (FDA) and the European Medicines Agency (EMA)^[4,5]. Clinical studies have shown drug-transporter interactions with e.g. digoxin, ritonavir or valsopodar (PSC833) and with tenofovir via P-gp and MRP2/4, respectively^[6-8].

In the past decade, multiple renal immortalized cell lines have been established, allowing *in vitro* screening of nephrotoxicity and renal drug transporters. Conditionally immortalized proximal tubule epithelial cells (ciPTEC) are derived from a healthy volunteer and manifest a stable expression and functionality of OCT2, P-gp and MRP4^[9]. Further transduction resulted in stable expression and functionality of OAT1 or OAT3^[10]. Multiple studies have shown the potential of ciPTEC for studying drug transport and drug-induced toxicity cultured under conventional static conditions, often referred to as two-dimensional (2D) cell culture^[10-13]. In addition, transepithelial barrier function, polarization and transport of cations and anions have been demonstrated in ciPTEC cultured in a three-dimensional (3D) model using a tailor-made hollow fiber membrane system exposed to flow^[13,14]. Benefits of 3D microfluidic

models incorporating fluid shear stress (FSS) and cell-extracellular matrix (ECM) interactions are often referred to as organ-on-a-chip or microphysiological systems. Using PTEC, kidney-on-a-chip platforms have been demonstrated to improve proximal tubule characteristics, such as increased expression of tight-junction protein zonula occludens-1 (ZO-1) and increased number of ciliated cells^[15]. Kidney-on-a-chip platforms could therefore advance predictability of large *in vitro* screenings, also referred to as high-throughput screening (HTS), which are typically employed during early phases in drug development.

The current study focuses on implementing a kidney-on-a-chip platform for the determination of drug-transporter interactions during drug development. To this end, we culture human ciPTEC-OAT1 in a microfluidic titerplate, the OrganoPlate, that enables 3D culture under FSS. The OrganoPlate consists of 40 or 96 chips and is based upon a 384-well microtiter plate format^[16, 17]. Flow is induced by passive leveling by gravity of medium in medium channel inlets and outlets of chips, creating a bi-directional flow. Using this platform, we assessed stability in drug transporter expression and functionality via fluorescence based 3D drug efflux assays to evaluate P-gp and MRP2/4 transporter activities. In addition, we set up a user-friendly data analysis method using open-source software compatible with HTS. This approach resulted in a 3D microfluidic PTEC model suitable for HTS of drug-transporter interactions.

Materials & Methods

Cell culture

ciPTEC-OAT1 were obtained as described previously^[9, 10]. Briefly, cells were retrieved from urine from a healthy volunteer in compliance with the guidelines of the Radboud Institutional Review Board and conditionally immortalized via transduction with the temperature-sensitive mutant of SV large T antigen (SV40T) and human telomerase reverse transcriptase (hTERT)^[9]. Transduction of OAT1 in ciPTEC was performed using lentiviral particles containing genes encoding for human OAT1^[10].

Cells were sub-cultured at a dilution of 1:2 to 1:6 at 33°C and 5% (v/v) CO₂ to allow proliferation and were used from passage number 48 to 60 for experiments. Cells were cultured in a 1:1 mixture of Dulbecco's modified eagle medium (DMEM) and Ham's F-12 Nutrient Mixture without phenol red (DMEM HAM's F12, Life Technologies, Paisley, UK) and supplemented with insulin (5 µg/ml, Sigma-Aldrich, Zwijndrecht, The Netherlands), transferrin (5 µg/ml, Sigma-Aldrich), selenium (5 ng/ml, Sigma-

Aldrich), hydrocortisone (36 ng/ml, Sigma-Aldrich), epidermal growth factor (10 ng/ml, Sigma-Aldrich), tri-iodothyrene (40 pg/ml, Sigma-Aldrich), 1% (v/v) penicillin/streptomycin (Life Technologies) and 10% (v/v) fetal calf serum (FCS, Greiner Bio One, Kremsmuenster, Austria), further referred to as PTEC complete medium.

For 2D static cell culture, cells were seeded at 55,000 cells/cm² in 6-well plates and cultured for one day at 33°C 5% (v/v) CO₂ without penicillin/streptomycin to allow proliferation. Then, cells were cultured for seven days at 37°C 5% (v/v) CO₂ to induce maturation into confluent cell mono layers. Cells were harvested on day eight after seeding.

For 3D FSS cell culture, a 400 µm two-lane OrganoPlate (Mimetas, Leiden, The Netherlands) was used for culturing ciPTEC-OAT1 in a microfluidic platform. Prior to seeding, 50 µl of Hank's balanced salt solution (HBSS, Life Technologies) was added to the observation window (Figure 6.1A). An ECM mix containing collagen I (4 mg/ml, AMSbio Cultrex 3D Collagen I Rat Tail), sodium bicarbonate (3.7 mg/ml, Sigma-Aldrich) and HEPES (100 mM, Life Technologies) was prepared and 2 µl was added to the gel channel^[17]. Then, the OrganoPlate was placed at 37°C 5% (v/v) CO₂ for 30 min to allow polymerization of the ECM. Proliferating cells were harvested from a culture flask using accutase (Sigma-Aldrich), centrifuged (300 x g, 5 min) and then resuspended in PTEC complete medium. Per chip, 40,000 cells in a suspension of 2 µl were seeded in the medium channel inlet (Figure 6.1A,B). In chips used for background correction of fluorescent signal, 2 µl of medium was used. The OrganoPlate was then placed vertically at 33°C 5% (v/v) CO₂ for 30 min with the gel channel facing down to allow cells to attach to the ECM (Figure 6.1B). Next, 30 µl of PTEC complete medium was added to the medium channel inlet. The OrganoPlate was oriented horizontally again at 33°C 5% (v/v) CO₂ for four to six hours. Upon addition of another 30 µl PTEC complete medium to the medium channel inlet, 60 µl PTEC complete medium was added to the medium channel outlet. CiPTEC-OAT1 in the OrganoPlate was cultured at 33°C 5% (v/v) CO₂ to allow proliferation without any FSS for three days. Medium was supplemented with 1% (v/v) penicillin/streptomycin when culturing at 33°C.

At day three after seeding, medium channels were refreshed with PTEC complete medium without penicillin/streptomycin and the OrganoPlate was placed on an interval rocker platform (angled at -7° or +7° from base, 8 min interval) at 37°C 5% (v/v) CO₂ to allow the cells to mature under FSS induced by a bi-directional flow (Figure 6.1B,C). Experiments in the OrganoPlate were performed on day eight after seeding, unless states otherwise. Medium was refreshed every two to three days.

For long-term cell culture of ciPTEC-OAT1 in the OrganoPlate, chips were pre-coated (30 min, 37°C) prior to seeding with L-3,4-dihydroxydiphenylalanine (L-DOPA, 2 mg/ml in 10 mM Tris pH 8.5, Sigma-Aldrich) as earlier described^[18]. Cells were then cultured at 33°C on an interval rocker, as above described, for 20 days.

Immunofluorescence staining of ciPTEC-OAT1 in the OrganoPlate

At day 8 and 20 after seeding, PTEC complete medium was aspirated from the medium channel and cells were fixated with 3.7% (w/v) formaldehyde (Sigma-Aldrich) in HBSS. The plate was incubated for 15 min at room temperature. For all described incubation and wash steps, 50 µl was added to the inlet and outlet of the medium channel, and plate was placed at angle to allow perfusion, unless stated otherwise. Fixative was aspirated and medium channels were washed twice with washing solution (4% (v/v) FCS in HBSS). Then, cells were permeabilized by adding 0.3% (v/v) Triton-X100 (Sigma-Aldrich) in HBSS and incubated for 10 min at room temperature. Cells were subsequently washed with washing solution and then incubated with blocking solution (2% (v/v) FCS, 2% (w/v) bovine serum albumin (BSA, Sigma-Aldrich), 0.1% (v/v) Tween-20 (Sigma-Aldrich) in HBSS) for 45 min at room temperature. Primary and secondary antibodies were diluted in blocking solution and perfusion during incubation was allowed by adding 30 µl to the medium channel inlet and 10 µl to the outlet. Primary antibodies against zonula occludens-1 (ZO-1, 1:125, rabbit, ThermoFisher), a tight-junction protein; acetylated-tubulin (clone 6-11B-1, 1:1000, mouse, Sigma-Aldrich), a constituent of the primary cilium; and pericentrin (1:500, rabbit, Abcam), a centrosome marker, were used and incubated for 60 min at room temperature. Next, cells were washed three times with washing solution and then incubated with secondary antibodies Alexa Fluor® 488 goat anti-rabbit (1:250, Life Technologies or Abcam), Alexa Fluor® 488 goat anti-mouse (1:250, Life Technologies), and Alexa Fluor® 647 goat anti-rabbit (1:250, Life Technologies) for 30 min at room temperature. Cells were then washed three times, followed by addition of probes in the last wash step to stain F-actin and nuclei with ActinRed 555 (2 drops/ml in HBSS, Life Technologies) and DRAQ5 (1:1000 in HBSS, Abcam) or DAPI (300 nM in HBSS, Life Technologies), respectively. Fluorescent images of the ZO-1 staining were acquired with a Leica TCS SP5 laser point confocal microscope (Leica, Wetzlar, Germany) or a Zeiss LSM880 confocal scanning microscope (Carl Zeiss, Jena, Germany) using a 20X objective. Z-stacks were acquired using a 2 µm interval over a 200-220 µm range. To investigate polarization of the PTEC monolayer of ciPTEC-OAT1 in the OrganoPlate, fluorescent images were acquired of acetylated-tubulin and pericentrin staining with a Zeiss LSM880 confocal scanning microscope using a 40X water immersion objective. A range of 45 µm was imaged using a 0.88 µm interval between Z-stacks. Images were adjusted for windows and level, and then 3D images were reconstructed in Fiji (version 1.51n)^[19].

Gene expression of ciPTEC-OAT1

Cells were harvested from 6-well plates using accutase, and then RNA was extracted using the RNeasy Mini kit (Qiagen, Venlo, the Netherlands). RLT lysis buffer was added to the cell pellet and RNA was then extracted according to the protocol provided by the manufacturer.

RNA from cells in the OrganoPlate was isolated using the RNeasy Micro kit (Qiagen). From each chip, RNA was isolated by adding 50 μ l and 25 μ l RLT lysis buffer to the medium channel inlet and outlet, respectively. Cell lysates of two chips were then pooled and RLT lysis buffer was added up to a volume of 350 μ l. The extracted RNA was purified following the manufacturer's protocol.

M-MLV Reverse Transcriptase (Promega, Madison, USA) was used to synthesize complementary DNA (cDNA) according to the manufacturer's protocol. Human kidney cortex material was used as reference. Tissues unsuitable for transplantation were obtained for research purposes from three donors, who gave permission and which was registered in the Dutch Donor registry. RNA isolation and cDNA synthesis were performed as previously described^[20]. The expression levels of mRNA were quantified using gene-specific primer-probe sets from Applied Biosystems (Bleiswijk, The Netherlands): *GAPDH* (hs99999905_m1), *HPRT1* (hs02800695_m1), *SLC22A6* (hs00537914_m1), *ABCB* (hs01067802_m1), *ABCC2* (hs00166123_m1), *ABCC4* (hs00195260_m1), *SLC22A2* (hs01010723_m1) and TaqMan Universal polymerase chain reaction (PCR) Master Mix. Quantitative PCR reactions were carried out using CFX96-Touch Real-Time PCR System (BioRad, Veenendaal, The Netherlands) and analyzed with BioRad CFX Manager (version 3.1). Expression levels of *GAPDH* were used as reference gene.

3D drug efflux assays in the OrganoPlate

Functionality of P-gp and MRP2/4 was assessed based upon accumulation of substrates, as previously described for ciPTEC in 2D (Figure 6.1C)^[12]. Prior to measuring efflux activity of P-gp and MRP2/4 in the OrganoPlate, medium channel inlet and outlets were washed with 50 μ l KHH at 37°C. Medium channels were then perfused two times. Then, cells were exposed to substrates with or without inhibitors or corresponding vehicle for one hour at 37°C.

For P-gp activity assessments, calcein-AM (2 μ M, Life Technologies) was used as substrate and PSC833 (10 μ M, Tocris, Bristol, UK) was used as inhibitor. Calcein-AM and PSC833 were dissolved in DMSO (Sigma-Aldrich). All dilutions were prepared in Krebs-Henseleit buffer (Sigma-Aldrich) supplemented with HEPES (10 mM, Sigma-Aldrich) and adjusted to pH 7.4 (KHH).

Chloromethylfluorescein-diacetate (CMFDA, 1.25 μM , Molecular Probes) was used to study MRP2/4 activity. A combination of PSC833 (10 μM), KO143 (10 μM , Sigma-Aldrich) and MK571 (10 μM , Sigma-Aldrich) was used to inhibit efflux of CMFDA and GS-MF via P-gp, BCRP and MRP2/4, respectively. CMFDA and KO143 were dissolved in DMSO, while MK571 was dissolved in Milli-Q water, requiring appropriate vehicle controls. All dilutions were prepared in KHH.

After substrate incubations, cell nuclei were stained with Hoechst33342 by first washing with KHH, followed by staining with Hoechst33342 (10 $\mu\text{g/ml}$, Molecular Probes) for 10 min at room temperature. Cells were co-incubated with PSC833 (10 μM), KO143 (10 μM) and MK571 (10 μM) during staining with Hoechst33342 to inhibit all efflux transport processes. Subsequently, cells were washed and efflux of calcein-AM and GS-MF was arrested by adding ice-cold KHH to medium channel. FSS in medium channel during experiment and washing was assured by adding 80 μl to the medium channel inlet and 20 μl to the medium channel outlet.

Fluorescent imaging in the OrganoPlate

Fluorescence of intracellular accumulation of calcein or GS-MF and Hoechst33342 in ciPTEC-OAT1 cultured in the OrganoPlate were imaged *in situ* using a Becton Dickinson (BD) Pathway 855 high-throughput microscope (BD Bioscience, Breda, The Netherlands) using a 10X objective (Figure 6.1C). The BD Pathway 855 microscope was compatible with the two-lane OrganoPlate and allowed to acquire images of the observation window of each chip using two different fluorescent dyes with wide-field microscopy and spinning disk confocal microscopy at room temperature. A macro was developed to acquire fluorescent and bright-field images using BD AttoVision (version 1.6, BD Bioscience). Z-height was determined per experiment by determining the top and bottom of multiple chips in the OrganoPlate visually. The average Z-height was used as starting point for acquiring five Z-planes with a 10 μm interval, covering 50 μm in Z-direction, generating focused images of cells cultured against ECM. First, calcein and GS-MF fluorescence images were acquired (488 nm excitation and 520 nm emission filters) with exposure time and gain set at 0.5 sec and 100, respectively. Hoechst33342 images were acquired subsequently (360 nm excitation filter and 435 nm emission filter), with exposure time and gain set at 0.01 sec and 100, respectively. Afterwards, bright-field images of each chip were acquired using an exposure time of 0.02 sec.

Image processing

An image analysis method (Figure 6.1C) was set up to analyze the full data set using custom made macros in Fiji (version 1.51n). Initially, the region of interest (ROI) was selected from bright-field images in which the gel channel, medium channel and the phase guide were clearly visible, by focusing at the interface of ECM and medium. The same area size was used for all images. All raw fluorescence images (uncompressed 12-bit TIFF) were cropped based upon the interface selection and converted from a pixel to μm scale. Then, the raw fluorescence images were corrected for background noise by subtracting images of chips with ECM without any cells exposed to either calcein-AM or CMFDA. Background corrected images were saved to an uncompressed 16-bit TIFF file and the average intensity was calculated (see macro in Supplemental data). In parallel, a mask was created for each image using 17 threshold algorithms available in Fiji (Supplemental Table S6.1) to automatically determine localization of intracellular accumulated fluorescent calcein or GS-MF. Upon running a median image filter (radius size five pixels), a cell selection mask was created via the selected algorithm to create a binary image. Pixels from the edges of the cell selection mask in the binary image were removed using 'erode' in Fiji. The binary image represented a cell selection and was used to analyze fluorescence intensity of each Z-stack per chip.

As part of the image quality control (QC), only in-focus images of cells cultured at the ECM and medium interface were selected and reviewed by three independent observers (Figure 6.1C). An image was defined as out-of-focus if no in-focus cell in the ROI were scored by at least two of the three observers.

Manual interventions, such as determination of out-of-focus images are not compatible with HTS. Therefore, selected image QC metrics were established to automatically exclude out-of-focus images: focus score, image correlation and power log-log slope (PLLS), which all have been described in literature for image analysis^[21-24]. An image QC method was set up using these image QC metrics in CellProfiler (version 2.2.0)^[25, 26]. For the focus score, the deviation of pixel intensity was assessed upon normalization per image. The correlation of the gray scale value of neighboring pixel was evaluated for image correlation. Pixel size for image correlation and focus score was empirically based upon the area of the observed intracellular accumulation of calcein or GS-MF and set at 20, 50, 100, 200, 500 pixels. For the PLLS, the slope of power spectral density versus the spatial frequency, both on a log scale, was plotted. All images were automatically binned based upon the image QC metrics in GraphPad Prism (version 5.03). Multiple cut-off values were compared per image QC metric. The efficiency of the automated image QC metrics was compared to visually reviewing of out-of-focus scoring as described earlier, which was defined as ground truth. For all image QC metrics, the precision and

recall rates were determined, as well as the harmonic mean of the precision and recall rates, also known as F-score. Precision, recall and F-score were calculated as follows:

$$F - score = \frac{2 * precision * recall}{precision + recall}$$

Where precision is:

$$precision = \frac{true\ positives}{true\ positives + false\ positives}$$

And recall is:

$$recall = \frac{true\ positives}{true\ positives + false\ negatives}$$

Average intensities of visual observation in-focus images were calculated per chip (Figure 6.1C). Two to eight chips were analyzed per condition and repeated in at least three independent experiments. All groups were checked for outliers using Grubbs' test for outliers (using a significance level of $\alpha=0.05$) and finally normalized to average fluorescence intensity in vehicle condition per experiment.

The Z'-factor was used to index the thresholding algorithms and overall intensity per image and condition to assess quality and optimize the data analysis methods. The Z'-factor has been described as statistical parameter in HTS assays taking in account the variation between a signal in maximum response, the positive control, and minimum response, the negative control^[27]. Hence, the Z'-factor can be used as guideline to optimize semi-quantitative methods in order to improve discrimination between the positive and negative controls. Mean and standard deviation (SD) were determined for the positive control, inhibitor condition, and negative control, vehicle condition, to calculate the Z'-factor per experiment as follows:

$$Z' - factor = 1 - \frac{3(\sigma\ positive\ control + \sigma\ negative\ control)}{|\mu\ positive\ control - \mu\ negative\ control|}$$

Statistical data analysis

All statistics were performed using GraphPad Prism (version 5.03). Data is presented as mean \pm SEM of at least three independent experiments ($n=3$) and considered to be significantly different if $p<0.05$ using an unpaired two-tailed Student's t-test, unless stated otherwise.

Results

PTEC's formed a 3D tubular structure in the OrganoPlate

Upon seeding ciPTEC-OAT1 against the ECM in the two-lane OrganoPlate, cells formed a monolayer that migrated towards the top and bottom of the medium channel, creating a tubule-like structure at day eight after seeding (Figure 6.2A, Supplemental Figure S6.1). PTEC tubules could be cultured up to 20 days in the OrganoPlate (Supplemental Figure S6.2). ZO-1, a tight-junction protein, was localized between the cells in the monolayer of the PTEC tubules (Figure 6.2B), indicative for polarization. Staining of the centrosome, or pericentrin, and acetylated-tubulin, showed apical expression of single cilia per cell (Figure 6.2C, Supplemental Figure S6.3). Some migration of ciPTEC-OAT1 from the medium channel into the ECM was observed, likely influencing the monolayer integrity. Although the majority of cilia were mainly expressed at the apical side of the tubules, some cilia were observed on single cells that migrated into the ECM (Supplemental Figure S6.3).

Drug transporter gene expression in ciPTEC-OAT1 cultured in the OrganoPlate

Drug transporter gene expression levels in ciPEC-OAT1 cultured in 2D static (6-well plate) and under FSS (OrganoPlate) were compared (Figure 6.3). Expression levels of SLC transporters OAT1 and OCT2 and ABC transporters P-gp, MRP2/4 were found to be similar in ciPTEC-OAT1 cultured in the OrganoPlate as compared to 2D cultures. This indicates a maintained phenotype of ciPTEC-OAT1 when cultured in the OrganoPlate. Only expression levels of HPRT1, here assessed to be used as a reference gene, were lower in ciPTEC-OAT1 cultured in the OrganoPlate and, consequently, not valid as reference gene. On the other hand, reference gene GAPDH was stably expressed in ciPTEC-OAT1 cultured both in 6-well plate and in the OrganoPlate with corresponding Ct values of 19.7 ± 0.1 and 19.6 ± 0.1 , respectively. It is important to note that drug transporter gene expression levels presented here were derived from cells both located in the perfused channels, as well as the medium channel inlet and outlets. As the latter cells are not exposed to laminar flow, nor were cultured in 3D, gene expression profiling was based on a hybrid population and should be regarded as qualitative measurement.

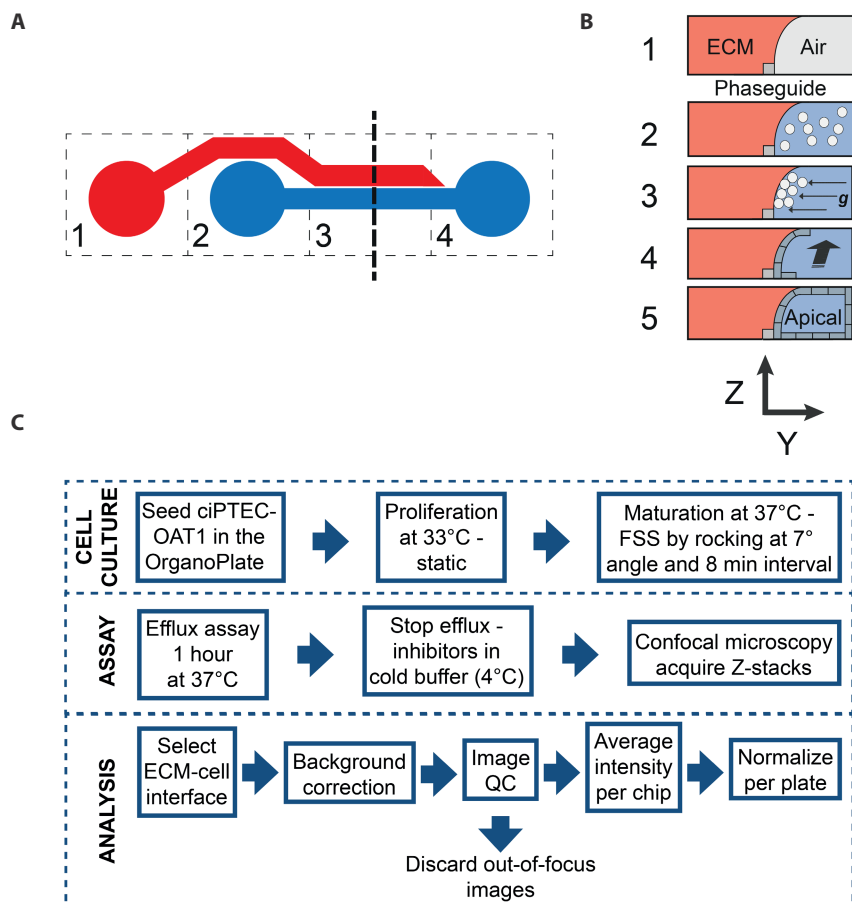


Figure 6.1 Overview of two-lane OrganoPlate and cell culture, assay and image analysis protocol.

(A) Schematic overview of a two-lane OrganoPlate consisting of a gel channel (red) and medium channel (blue) and covering four wells of a 384-wells plate. Four wells are named 1 = gel channel inlet, 2 = medium channel inlet, 3 = observation window, and 4 = medium channel outlet. Dotted line indicates position of cross-sectional overview. (B) Cross-sectional overview of culture protocol of ciPTEC-OAT1 in the OrganoPlate: 1 = addition of ECM to the gel channel creating two membrane-free compartments because of the phase guide; 2 = seeding of ciPTEC-OAT1; 3 = by placing the plate vertically, cells are allowed to attach to ECM by gravity; 4 = ciPTEC-OAT1 is allowed to mature under FSS; 5 = two compartments are created per chip consisting of an extracellular matrix (ECM) and an apical channel (medium channel). (C) Culture conditions and assay details of 3D P-gp, MRP2/4 drug efflux assay specified. Image analysis in Fiji contained background correction, image QC (visual observation) and normalization. Z stacks per chip were acquired using 10- μ m intervals between each Z stack resulting in a total number of five Z stacks per chip. Cells on ECM and medium interface were selected for further analysis and calculation of the average intensity of Z stacks per chip.

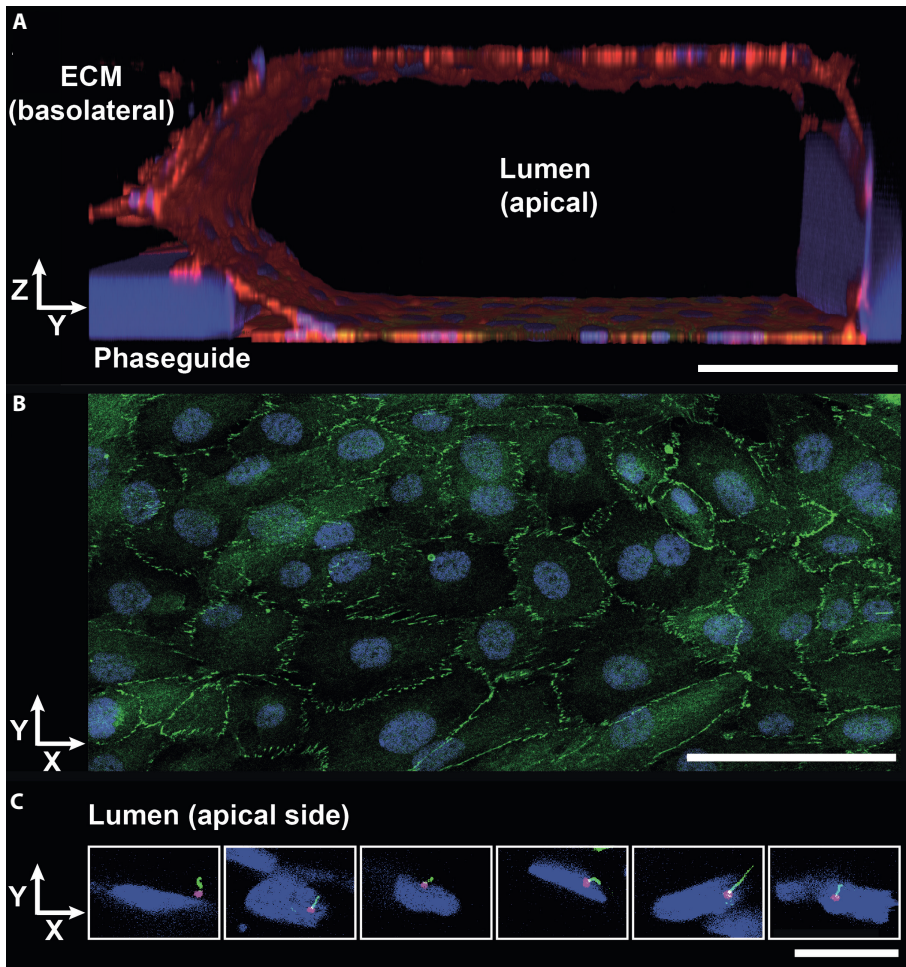


Figure 6.2 Immunofluorescence staining of ciPTEC-OAT1 in OrganoPlate. (A) Three-dimensional (3D) view of ciPTEC-OAT1 in OrganoPlate with F-actin (red) and nuclei (DAPI, blue) showing the formation of tubule structures after 8 days of seeding. The phase guide is visible as blue bar at the left side of the image. The lumen at the apical side and the extracellular matrix (ECM) are indicated. Scale bar represents 100 μm . (B) Staining of nuclei (DAPI, blue) and zonula occludens (ZO-1, green). Expression of ZO-1 visible between cell monolayer on top of PTEC tubules. Scale bar represents 100 μm . (C) Representative images of single cells attached to the extracellular matrix (ECM) selected from the tubular ciPTECOAT1 structures in the OrganoPlate, showing staining of nuclei (DAPI, blue) and primary cilia with pericentrin (magenta) and acetylated tubulin (green). Most cilia face towards the lumen (apical side), demonstrating polarization of the tubules. Scale bar represents 20 μm .

Table 6.1 mRNA expression in human kidney cortex and ciPTEC-OAT1 cultured in 2D static or in the OrganoPlate^a

	dCt			Relative expression ciPTEC-OAT1 vs. hKidney	
	hKidney	ciPTEC-OAT1		6-well	OrganoPlate
		6-well	OrganoPlate		
HPRT1	4.2 ± 0.2	6.1 ± 0.1	6.9 ± 0.1	27.6%	15.8%
OAT1	-0.7 ± 0.5	2.2 ± 0.2	3.1 ± 0.7	11.5%	7.4%
OCT2	4.8 ± 0.3	17.5 ± 0.6	17.8 ± 0.3	0.017%	0.012%
P-gp	4.8 ± 0.5	7.6 ± 0.1	8.9 ± 0.7	12.9%	6.3%
MRP2	3.0 ± 0.6	14.18 ± 0.04	14.0 ± 0.1	0.037%	0.043%
MRP4	3.7 ± 0.1	6.3 ± 0.1	6.6 ± 0.4	17.0%	14.2%

^a mRNA expression of drug transporters of three independent experiment performed at least in duplicate. Gene expression levels were normalized to GAPDH, used as reference gene. Ct values of GAPDH in human kidney (hKidney), ciPTEC-OAT1 in 6-well and in the OrganoPlate were 25.6 ± 0.7, 19.7 ± 0.1 and 19.6 ± 0.1, respectively.

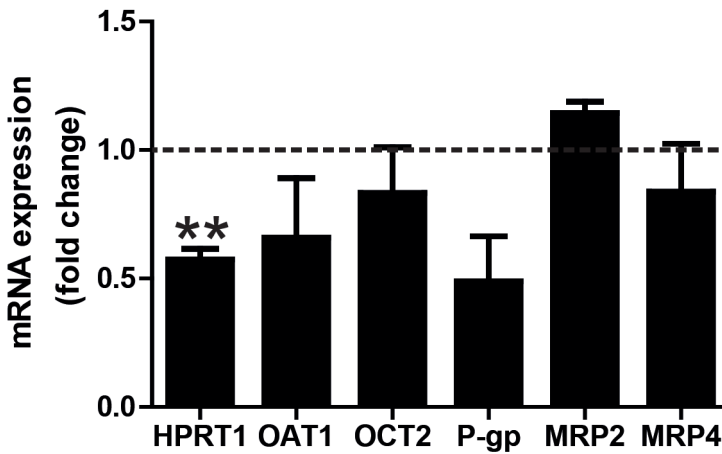


Figure 6.3 The HPRT1, OAT1, OCT2, P-gp, MRP2, and MRP4 expression levels in matured ciPTEC-OAT1 cultured under FSS (OrganoPlate). Gene expression levels were normalized to GAPDH, used as reference gene, and here calculated a fold difference compared to gene expression levels in 2D static cell culture (6-well plate). **p < 0.01 compared to mRNA expression in ciPTEC-OAT1 cultured in a 6-well plate

In addition, expression levels of ciPTEC-OAT1 cultured in 6-well plate or in the OrganoPlate were compared to expression levels in human kidney cortex samples (Table 6.1). In human kidney cortex, OAT1 is most abundantly expressed relative to expression levels of other drug transporters assessed here (rank order OAT1>MRP2>MRP4>OCT2>P-gp). Expression of OAT1 was also abundantly expressed in ciPTEC-OAT1 when cultured either in a 6-well plate or in the OrganoPlate, although a different relative expression was observed (rank order OAT1>MRP4>P-gp>MRP2>OCT2).

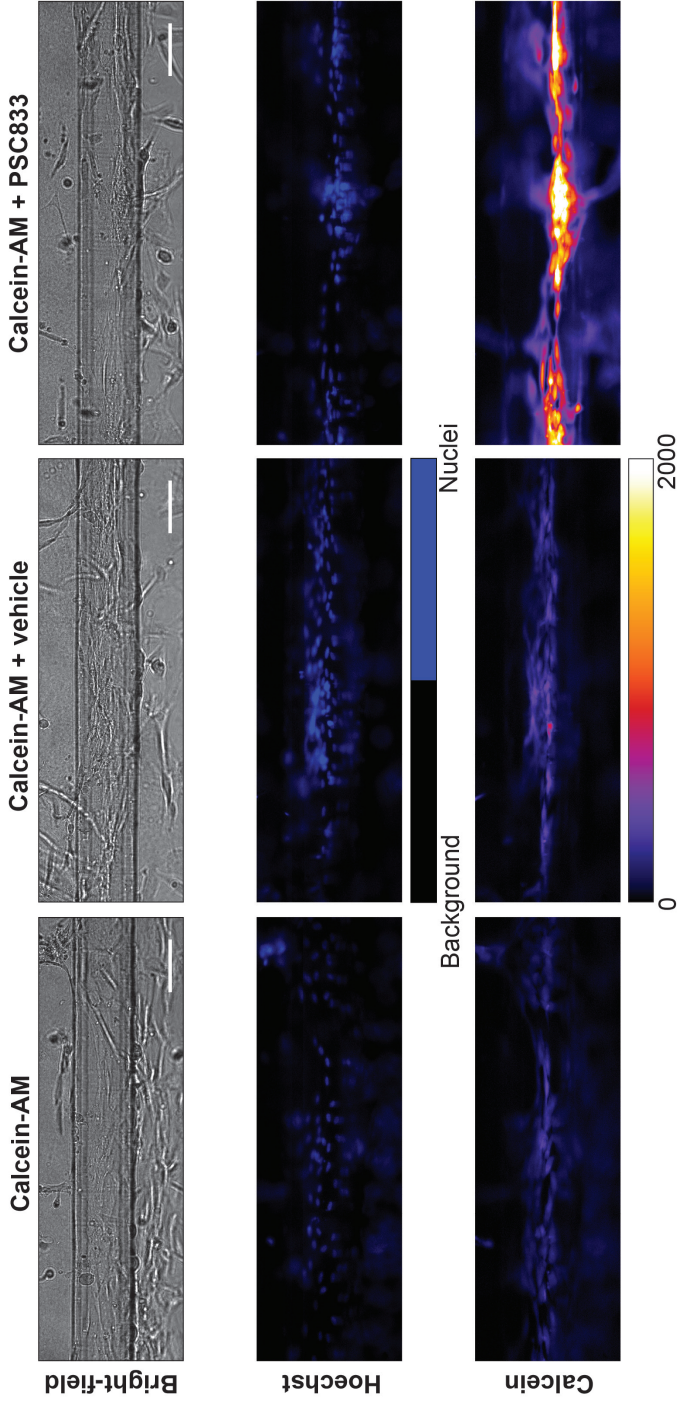
Fluorescence-based drug efflux assays in 3D tubule structures

We set up 3D efflux assays for P-gp and MRP2/4 as proof-of-concept to demonstrate transport activity in 3D microfluidic PTEC model. The first step in our image analysis included the selection of the ROI per chip, which included cells at the ECM and medium interface. As shown in Figure 6.4A, the gel channel, medium channel and the phase guide were clearly visible. The bright-field images were used to objectively choose the ROI per chip. Cell layers formed at the ECM were demonstrated by the Hoechst staining (Figure 6.4A).

P-gp shows the highest affinity for uncharged and positively charged compounds^[28,29]. Calcein-AM was used as substrate to study P-gp efflux activity in ciPTEC-OAT1 cultured in the OrganoPlate. Calcein-AM can freely diffuse through the cell membrane and is a substrate with high affinity for P-gp. Intracellularly, calcein-AM is metabolized through esterase activity into the fluorescent calcein. Slight accumulation of calcein was observed in the control and vehicle incubated tubules upon incubation with calcein-AM (Figure 6.4A), which was strongly enhanced upon co-incubation with PSC833, suggesting inhibition of P-gp (Figure 6.4A and Figure 6.5A).

MRP2/4 show highest affinity for negatively charged compounds in the kidney^[30-33]. To study MRP2/4 activity, 5-chloromethylfluorescein-diacetate (CMFDA), which enters the cell via diffusion, was used. CMFDA is then metabolized to the fluorescent 5-chloromethylfluorescein (CMF) via esterase activity and then further metabolized into carboxylfluorescein-glutathione (GS-MF) through direct interaction with glutathione (GSH) or via transferase activity. CMF is completely transferred into GS-MF during incubation time used here^[12]. GS-MF is predominantly a substrate for MRP2/4, although some selectivity was demonstrated for BCRP and P-gp^[12]. We therefore used a combination of inhibitors, as described in the materials and methods section. In the control and vehicle tubules, minor accumulation of GS-MF was visible. After co-incubation with an inhibitor cocktail of PSC833, KO143 and MK571, a higher fluorescence intensity was demonstrated as compared to vehicle control, indicating

A



B

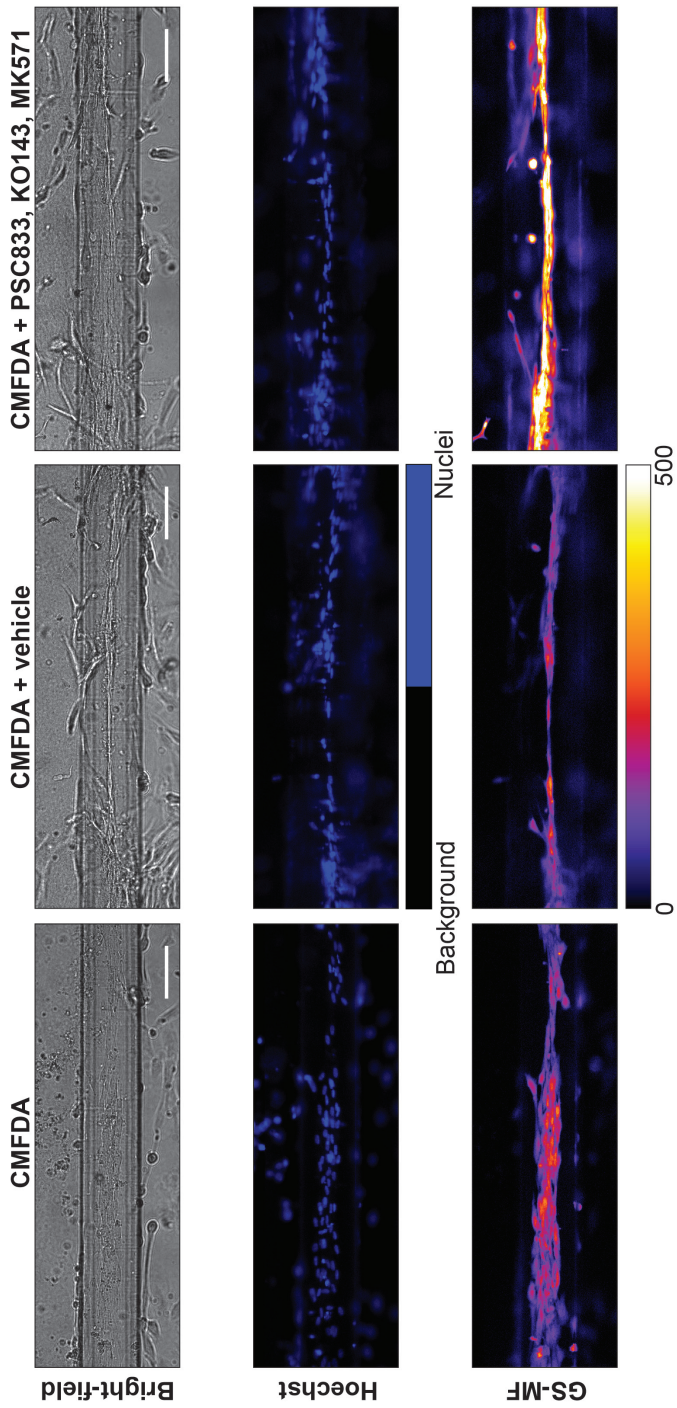


Figure 6.4 Representative bright-field and fluorescent images of Hoechst and calcein or GS-MF. A cell monolayer is formed at the phase guide is clearly visible in the center of the bright-field images. The ECM and medium channel are positioned above and below the phase guide, respectively. Hoechst staining was used to improve cell monolayer visibility. (A) Accumulation of calcein was visible in control, vehicle, and PSC833-treated tubules. Accumulation of calcein was increased upon PSC833-mediated inhibition of P-gp. (B) Intracellular accumulation of GS-MF in control, vehicle, treated, and in presence of inhibitor cocktail (consisting of PSC833, KO143 and MK571). Accumulation of GS-MF was increased upon incubation with the cocktail. For visualization, gray values for bright-field, Hoechst, calcein, and GS-MF images were set from 250 to 1000, 0 to 500, 0 to 2000, and 0 to 500, respectively. Gray scale of calcein and GS-MF fluorescent images were converted to look-up table (LUT) color fire to enhance contrast. Calibration bar of LUT shows level of intensity of calcein or GS-MF. Scale bar in bright-field images represents 100 μm . See Figure 6.5 for quantification of the signals.

active MRP2/4 in ciPTEC-OAT1 cultured in the OrganoPlate. Signal intensity was stable for at least 25 min for both calcein and GS-MF (data not shown).

Image QC and image analysis

Setting up a proper image QC could reduce the variation caused by factors such as out-of-focus images, signal-to-noise ratio and cell density. In-focus images of the cell layer between ECM and medium interfaces were acquired in the majority of chips. Available image QC metrics in CellProfiler were applied to obtain an automated and fast image QC of our data set.

Each image was visually evaluated to be in-focus or out-of-focus. Of all images acquired for the 3D P-gp drug efflux assay (n=245, from four different experiments), 14.3% (n=35) were assigned to be out-of-focus. For the 3D MRP2/4 drug efflux assay, 21.7% (n=52) of all images (n=240, from four different experiments) were assigned to be out-of-focus. The visually evaluated in-focus and out-of-focus images were defined as ground truth.

Means of image QC metrics of in-focus and out-of-focus images were compared for the two transporter assays as defined for P-gp (Supplemental Table S6.2) and MRP2/4 (Supplemental Table S6.3). By calculating the F-score per image QC metric, the false negatives, true and false positives were incorporated and compared with the ground truth. Focus score showed an F-score of 0.46, the highest F-score of all image QC metrics determined for the 3D P-gp drug efflux assay, the recall and precision score obtained were 0.33 and 0.77, respectively (Supplemental Table S6.2). For the 3D MRP2/4 drug efflux assay, using focus score with a pixel size 200 resulted in an F-score of 0.53, the highest F-score for this assay, with corresponding precision and recall scores of 0.36 and 0.94, respectively (Supplemental Table S6.3). For both assays low precision scores were obtained, because of a high number of false positives compared to true positives, leading to low F-scores.

To demonstrate proof-of-concept, further analysis was based on the visually determined out-of-focus images by three observers, since the image QC metrics determined here were less optimal to distinguish in-focus and out-of-focus images for our data set. Visually reviewed out-of-focus images were excluded from further calculations from this point.

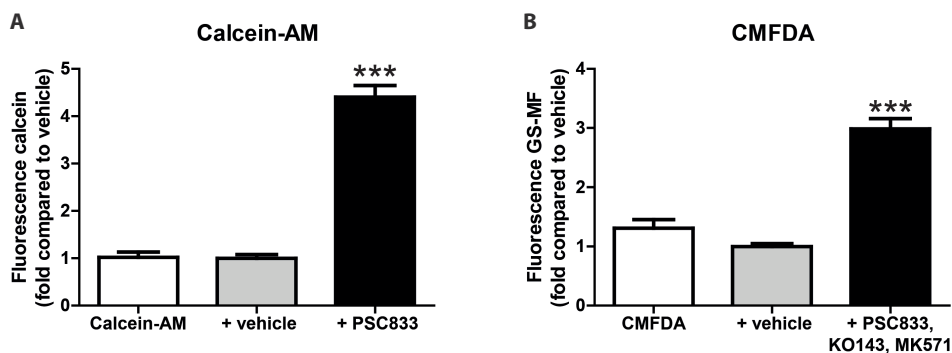


Figure 6.5 Average intensity measured per condition and chip is shown for control, solvent-treated and inhibitor-treated conditions. (A) Fold difference in calcein or in (B) GS-MF fluorescence. Values were normalized to vehicle per experiment. No threshold algorithm was used. Significant differences of the means were compared to vehicle using one-way ANOVA followed by Dunnett's multi comparison post hoc test. *** $p < 0.001$ compared to vehicle.

Table 6.2 Fold difference in fluorescence intensity for the 3D P-gp drug efflux assay compared to vehicle using different threshold algorithm available in Fiji and corresponding calculated Z'-factors

	CMFDA ^a	CMFDA + vehicle ^a	CMFDA + PSC833, KO143, MK571 ^a	Z'-factor ^b
No threshold	1.0 ± 0.1	1.0 ± 0.1	4.4 ± 0.2***	0.1 ± 0.3
Default	0.5 ± 0.1	1.0 ± 0.1	5.3 ± 0.6***	-2 ± 1
Huang	0.5 ± 0.1	1.0 ± 0.1	4.4 ± 0.5***	-0.5 ± 0.2
IJ_IsoData	0.5 ± 0.1	1.0 ± 0.1	4.8 ± 0.6***	-2 ± 1
Intermodes	0.6 ± 0.1	1.0 ± 0.1	4.7 ± 0.7***	-2 ± 1
IsoData	0.5 ± 0.1	1.0 ± 0.1	5.1 ± 0.6***	-2 ± 1
Li	0.6 ± 0.1	1.0 ± 0.1	4.4 ± 0.5***	-0.2 ± 0.3
MaxEntropy	0.6 ± 0.1	1.0 ± 0.1	4.1 ± 0.5***	-1 ± 1
Mean	0.8 ± 0.1	1.0 ± 0.1	5.0 ± 0.4***	-0.1 ± 0.3
MinError	0.5 ± 0.1	1.0 ± 0.1	4.8 ± 0.6***	-2 ± 1
Minimum	0.6 ± 0.1	1.0 ± 0.1	4.6 ± 0.7***	-2 ± 1
Moments	0.8 ± 0.1	1.0 ± 0.1	3.5 ± 0.6***	3 ± 2
Otsu	0.5 ± 0.1	1.0 ± 0.1	5.0 ± 0.6***	-0.1 ± 0.4
Percentile	0.7 ± 0.1	1.0 ± 0.1	3.6 ± 0.5***	-0.5 ± 0.6
RenyiEntropy	0.6 ± 0.1	1.0 ± 0.1	4.0 ± 0.5***	-1 ± 1
Shanbhag	0.6 ± 0.1	1.0 ± 0.1	4.6 ± 0.7***	-2 ± 1
Triangle	0.7 ± 0.1	1.0 ± 0.1	4.0 ± 0.4***	-2 ± 1

^aValues were normalized to vehicle per experiment. Significant differences of the means were compared to vehicle using one-way ANOVA followed by Dunnett's multi comparison post-hoc test. *** $p < 0.01$ compared to vehicle. ^bAverage Z'-factor as calculated in four independent experiments.

Table 6.3 Fold difference in fluorescence intensity for the 3D MRP2/4 drug efflux assay compared to vehicle using different threshold algorithm available in Fiji and corresponding calculated Z'-factors

	CMFDA ^a	CMFDA + vehicle ^a	CMFDA + PSC833, K0143, MK571 ^a	Z'-factor ^b
No threshold	1.3 ± 0.1	1.00 ± 0.05	3.0 ± 0.2***	0.4 ± 0.1
Default	1.3 ± 0.2	1.0 ± 0.1	5.1 ± 0.7***	-0.4 ± 0.2
Huang	1.2 ± 0.2	1.0 ± 0.1	3.9 ± 0.5***	-0.6 ± 0.1
IJ_IsoData	1.3 ± 0.2	1.0 ± 0.1	4.2 ± 0.6***	-0.70 ± 0.05
Intermodes	1.2 ± 0.1	1.0 ± 0.1	3.7 ± 0.3***	-0.4 ± 0.2
IsoData	1.3 ± 0.2	1.0 ± 0.1	4.6 ± 0.6***	-0.5 ± 0.2
Li	1.3 ± 0.2	1.00 ± 0.05	4.0 ± 0.4***	-0.7 ± 0.2
MaxEntropy	1.2 ± 0.1	1.0 ± 0.1	3.7 ± 0.4***	-0.3 ± 0.3
Mean	1.4 ± 0.2	1.0 ± 0.1	3.4 ± 0.3***	-0.4 ± 0.4
MinError	1.3 ± 0.2	1.0 ± 0.1	4.2 ± 0.6***	-0.70 ± 0.05
Minimum	0.9 ± 0.2	1.0 ± 0.1	3.7 ± 0.3***	-0.2 ± 0.1
Moments	1.2 ± 0.2	1.0 ± 0.1	4.1 ± 0.5***	-0.3 ± 0.3
Otsu	1.3 ± 0.2	1.00 ± 0.04	4.5 ± 0.6***	-0.5 ± 0.1
Percentile	1.6 ± 0.3	1.0 ± 0.1	2.9 ± 0.3***	-1.4 ± 0.2
RenyiEntropy	1.2 ± 0.1	1.0 ± 0.1	3.6 ± 0.3***	-0.3 ± 0.2
Shanbhag	0.8 ± 0.2	1.0 ± 0.1	4.0 ± 0.7***	-5 ± 5
Triangle	1.4 ± 0.2	1.0 ± 0.04	3.2 ± 0.2***	-0.2 ± 0.1

^aValues were normalized to vehicle per plate. Significant differences of the means were compared to vehicle using one-way ANOVA followed by Dunnett's multi comparison post-hoc test. ***p<0.01 compared to vehicle. ^bAverage Z'-factor as calculated in four independent experiments.

Fluorescence intensity in image and average per chip

Fluorescence intensities per image were determined in Fiji to perform semi-quantitative analysis of P-gp and MRP2/4 drug efflux activities (Table 6.2 and 6.3). Masking using thresholding algorithms was applied to create a selection area incorporating the intracellular accumulation of calcein or GS-MF, and compared to the intensity of the entire image. A higher intensity after co-incubation with inhibitor(s) was observed for all semi-quantitative methods used in both drug efflux assays (Table 6.2 and 6.3). No differences between vehicle-treated and control were observed in the drug efflux assays.

Z'-factor was calculated per experiment to compare and optimize the semi-quantitative analysis methods. Thresholding algorithm and the intensity of the entire image were compared in Table 6.2 and 6.3. Z'-factors are only meaningful when they fall within a range of $-1 < Z' \leq 1$, which is the case for the majority of the thresholding

algorithms^[27]. Remarkably, when using algorithm threshold Moments for the 3D P-gp drug efflux assay, the mean of the negative control (vehicle treatment) was higher than the mean of positive control (PSC833) treatment in two experiments, resulting in $Z' > 1$. Without using a thresholding algorithm, this resulted in Z' -factor values of 0.1 ± 0.3 and 0.4 ± 0.1 for the 3D P-gp and MRP2/4 drug efflux assays, respectively. For all analysis methods, a significant increase in fluorescence intensity was found upon transport inhibition for both assays, however, thresholding algorithms resulted in large standard deviations. In general, Z' -factor values were < 0 when using a thresholding algorithm, because of an overlap in fluorescence intensity between the groups, indicating that image analysis using threshold algorithms as presented here is not suitable for HTS^[27]. Thresholding algorithms included more steps in the semi-quantitative analysis macro in Fiji (see Supplemental data), which increased the processing time per image, and Z' -factors were lower compared to the intensity of the entire image. Therefore, measuring intensity in the entire image showed the most reliable results.

Upon establishing a valid semi-quantitative image analysis method for both assays, the average fluorescence intensities per chip were calculated, as shown in Figure 6.5. PSC833-mediated inhibition of P-gp resulted in a 4.4 ± 0.2 -fold increase fluorescence intensity compared to vehicle treated tubules (Figure 6.5A). For the 3D MRP2/4 drug efflux assay, in tubules co-incubated with PSC833, KO143 and MK571 led to a 3.0 ± 0.2 -fold increased compared to vehicle (Figure 6.5B). Both assays demonstrate function of P-gp and MRP2/4 and the possibility to semi-quantify renal drug interaction via increased fluorescence intensity.

Discussion

In this study, we developed a 3D microfluidic PTEC model demonstrated to be suitable for the evaluation of renal drug interactions with efflux transporters. The system has high potential for early drug screening due to its medium to high-throughput features and compatibility with high-content imaging platforms as shown in the current study on 3D efflux assays as well as demonstrated by Vormann et al.^[34] and Suter-Dick et al.^[35]. We cultured the human conditionally immortalized cell line ciPTEC-OAT1 in the OrganoPlate exposed to FSS induced by leveling, creating a 3D microfluidic PTEC model. The OrganoPlate enabled the formation of polarized tubule-like structures in a 96-well format.

A polarized epithelium was obtained upon culturing of ciPTEC-OAT1 in the OrganoPlate and showed apical expression of cilia, in line with an earlier publication of a perfusable printed 3D PTEC^[36]. Furthermore, gene expression levels of OAT1 (*SLC22A6*), OCT2 (*SLC22A2*), P-gp (*ABCB1*), MRP2 (*ABCC2*) and MRP4 (*ABCC4*) were confirmed. Representative monolayers were formed and functional activity and drug interactions for P-gp and MRP2/4 was demonstrated by means of fluorescence-based transport assays. Open source imaging software was used to analyze fluorescence to make this platform user friendly and suitable for screening of larger data sets.

Basal PTEC characteristics were shown to be improved in kidney-on-a-chip platforms, likely because of inclusion of a physiological FSS and cell-ECM interaction^[15, 36, 37]. Interestingly, enhanced P-gp efflux activity and transepithelial transport of para-aminohippurate (PAH) was demonstrated^[15,38]. Microfluidic kidney models could advance lead optimization at early stages of drug development and are an emerging technology to study drug-transporter interactions and toxicity^[39]. Future efforts demonstrating the improvements of such microfluidic 3D PTEC models as compared to regular 2D static culture should include a validation study with a compound library focusing on sensitivity and specificity using nephrotoxic and non-nephrotoxic compounds. Complexity and lack of compatibility with HTS of current kidney-on-a-chip models are a major drawback as opposed to 2D static cell culture in a multiwell setting required for drug screening purposes. Most published kidney-on-a-chip models use complex pump-driven single chip systems that frustrate experiments relying on multiple test conditions^[15, 36, 38, 40-42]. The 3D microfluidic PTEC model presented here consisted of 96 chips on one plate and physiological FSS that is induced by leveling, without the need for external components. Therefore, it has high potential for HTS settings and could relatively easily be implemented in current disposition studies in drug development.

In vitro toxicity screening at early phases of drug discovery benefits from its compatibility for HTS and low costs. Freshly isolated human primary PTEC are the golden standard for *in vitro* screenings when it comes to intact drug transporter functionality and resemblance to the human kidney. However, expression levels decrease within days after seeding and such studies are limited for their low reproducibility^[43, 44]. Vesicles and over-expression of drug transporters in immortalized cell lines are powerful tools as well to evaluate such drug-transporter interactions, but often lack human PTEC characteristics that could link drug-transporter interactions to clinically relevant toxicological read-outs^[45-49]. Human-derived immortalized renal cell models such as human embryonic kidney 293 (HEK 293) and human kidney 2 (HK 2) cells have shown to be a valuable tool in screenings in drug development, but have low or no endogenous expression of relevant drug transporters^[50, 51]. To overcome

these limitations, we have developed ciPTEC-OAT1 with proven suitability for nephrotoxicity and drug-transporter interactions studies^[10-14]. The broad range of drug transporter expression in ciPTEC-OAT1 provides a strong basis for highly predictive renal drug interaction studies. The inter-complexity and overlap in substrates of renal drug transporters, rather than through one drug transporter, is incorporated because of this broad range of drug transporter expression. This resembles a more physiological, *in vivo*-like, mechanism of renal drug handling. Gene expression levels of drug transporters in ciPTEC-OAT1 assessed here were lower compared to levels observed in samples of the human renal cortex, in accordance with other renal cell lines^[50]. Functionality of OAT1, OCT2, BCRP, P-gp and MRP2/4 in ciPTEC 2D cell culture has been demonstrated in multiple studies^[9, 10, 12-14].

Establishing highly predictive renal *in vitro* models for nephrotoxicity and renal drug-transporter interactions could refine and, ultimately, replace animal experiments. Besides the ethical issues, animal testing is expensive and not always translatable because of species differences. Following this study, future research should be directed to develop a method that allows *in vitro-in vivo* extrapolation of data, using experimental input from the 3D microfluidic PTEC model in accordance to Kunze et al.^[52]. Such extrapolation could demonstrate the added value and potential of our model to replace current animal studies now used for renal drug handling screenings.

Influx drug transporters should be evaluated in parallel to drug transporter efflux activity to obtain a reliable prediction on renal excretion. Uptake via OCT2 and OAT1/3 has been demonstrated in ciPTEC using uptake of fluorescent substrates^[9, 10]. Using ciPTEC-OAT1, transepithelial transport of the uremic toxins indoxyl sulfate and kynurenic acid could be indirectly demonstrated when cells were cultured on hollow fiber membranes, thereby forming a renal epithelial tubule^[13]. Expanding the platform with a third lane that includes a perfusable basolateral compartment together with a perfusable apical compartment in a 3D microfluidic platform could be used to study transepithelial transport or organic cations and anion in detail, as shown by Vormann et al.^[34]. Other potential applications for the three-compartmental system are the incorporation of other segments of the renal tubules or co-culture with vascular endothelial cells, as recently was demonstrated^[42, 53].

In the current study, accumulation of fluorescence in the chips was evaluated from five z-stacks with a 10 μm interval per chip. This approach resulted in a variation of image focus per chip and per experiment. To reduce variability per stack, an image QC was introduced. We used a visually determination of in-focus and out-of-focus images. In our study, image QC metrics tested, such as PLLS, resulted in low precision

and corresponding F-scores because of overlapping means of image QC metric between in-focus and out-of-focus images assessed. Optimizing imaging in the OrganoPlate by using autofocus could reduce the number of out-of-focus images and improve image QC metric outcome. In addition, by acquiring more Z-stacks per chip, chances of obtaining in-focus images increase. A proper image QC is key in reliably screening larger data sets typical for HTS, and should therefore be optimized for each setting. Measuring fluorescence intensity in the entire image as compared to using thresholding algorithms provided the most optimal semi-quantification of efflux activity. Corresponding Z'-scores were within an acceptable range ($0.5 > Z' > 0$) where standard deviation bands of positive and negative controls were separated^[27]. Aforementioned improvements in confocal imaging could further increase separation of standard deviations from controls.

Conclusion

To conclude, we present a 3D microfluidic PTEC model including most important renal drug transporters in a platform consisting of 96 chips. Multiplexing of different endpoint read-outs and testing multiple conditions in one plate allows this platform to be suitable for medium to high-throughput screenings and compatible with most high-content imaging platforms.

Acknowledgements

This project was supported by the NephroTube project funded by the National Center for the Replacement, Refinement and Reduction of Animals in Research (NC3Rs), under the Crack-it challenge 15 (Nephrotube) project no. 37497-25920. The authors thank Johan van der Vlag (department Nephrology, Radboud University Medical Center, Nijmegen, The Netherlands) for supplying the human kidney cortex tissues. The authors thank Dr. Miriam Schmidts for kindly providing antibodies for acetylated-tubulin and pericentrin. The authors also thank Professor Dr. Hans Tanke from the department of Molecular Cell Biology at the Leiden University Medical Center (LUMC) and the microscopic imaging center at Radboud University Medical Center for using the imaging facilities. The authors thank Renata Škovroňová and Christiaan Stuuut for their assistance with imaging processing.

Additional information

All experiments described in this article comply with the Radboud Institutional Review Board. OrganoPlate and PhaseGuide are a registered trademark of Mimetas BV. The authors MKV, AvdH, HLL and PV are employees of Mimetas BV.

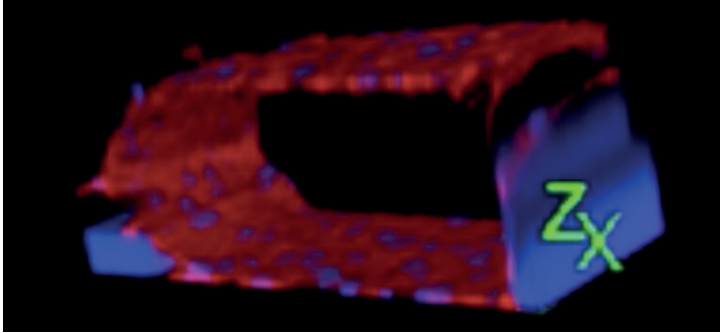
References

1. Morrissey KM, Stocker SL, Wittwer MB, Xu L, Giacomini KM. Renal transporters in drug development. *Annu Rev Pharmacol Toxicol.* 53, 503-529 (2013).
2. Varma MV, Feng B, Obach RS, Troutman MD, Chupka J, Miller HR, El-Kattan A. Physicochemical determinants of human renal clearance. *J Med Chem.* 52, 4844-4852 (2009).
3. Ivanyuk A, Livio F, Biollaz J, Buclin T. Renal Drug Transporters and Drug Interactions. *Clin Pharmacokinet.* 56, 825-892 (2017).
4. EMA. Guideline on the Investigation of drug interactions (CPMP/EWP/560/95/Rev. 1). In: EMA; 2012.
5. FDA. In Vitro Metabolism- and Transporter-Mediated Drug-Drug interaction Studies. Guidance for Industry (draft). In: FDA; 2017. p. 13-19.
6. Ding R, Tayrouz Y, Riedel KD, Burhenne J, Weiss J, Mikus G, Haefeli WE. Substantial pharmacokinetic interaction between digoxin and ritonavir in healthy volunteers. *Clin Pharmacol Ther.* 76, 73-84 (2004).
7. Kovarik JM, Rigaudy L, Guerret M, Gerbeau C, Rost KL. Longitudinal assessment of a P-glycoprotein-mediated drug interaction of valsopodar on digoxin. *Clin Pharmacol Ther.* 66, 391-400 (1999).
8. Likanonsakul S, Suntisuklappon B, Nitiyanontakij R, Prasithsirikul W, Nakayama EE, Shioda T, Sangsajja C. A Single-Nucleotide Polymorphism in ABCB4 Is Associated with Tenofovir-Related Beta2-Microglobulinuria in Thai Patients with HIV-1 Infection. *Plos One.* 11, (2016).
9. Wilmer MJ, Saleem MA, Masereeuw R, Ni L, van der Velden TJ, Russel FG, Mathieson PW, et al. Novel conditionally immortalized human proximal tubule cell line expressing functional influx and efflux transporters. *Cell Tissue Res.* 339, 449-457 (2010).
10. Nieskens TT, Peters JG, Schreurs MJ, Smits N, Woestenenk R, Jansen K, van der Made TK, et al. A Human Renal Proximal Tubule Cell Line with Stable Organic Anion Transporter 1 and 3 Expression Predictive for Antiviral-Induced Toxicity. *AAPS J.* 18, 465-475 (2016).
11. Caetano-Pinto P, Jamalpoor A, Ham J, Goumenou A, Mommersteeg M, Pijnenburg D, Ruijtenbeek R, et al. Cetuximab Prevents Methotrexate-Induced Cytotoxicity in Vitro through Epidermal Growth Factor Dependent Regulation of Renal Drug Transporters. *Mol Pharm.* 14, 2147-2157 (2017).
12. Caetano-Pinto P, Janssen MJ, Gijzen L, Verscheijden L, Wilmer MJ, Masereeuw R. Fluorescence-Based Transport Assays Revisited in a Human Renal Proximal Tubule Cell Line. *Mol Pharm.* 13, 933-944 (2016).
13. Jansen J, Fedecostante M, Wilmer MJ, Peters JG, Kreuser UM, van den Broek PH, Mensink RA, et al. Bioengineered kidney tubules efficiently excrete uremic toxins. *Sci Rep.* 6, 26715 (2016).
14. Jansen J, De Napoli IE, Fedecostante M, Schophuizen CM, Chevtchik NV, Wilmer MJ, van Asbeck AH, et al. Human proximal tubule epithelial cells cultured on hollow fibers: living membranes that actively transport organic cations. *Sci Rep.* 5, 16702 (2015).
15. Jang KJ, Mehr AP, Hamilton GA, McPartlin LA, Chung S, Suh KY, Ingber DE. Human kidney proximal tubule-on-a-chip for drug transport and nephrotoxicity assessment. *Integr Biol (Camb).* 5, 1119-1129 (2013).
16. Trietsch SJ, Naumovska E, Kurek D, Setyawati MC, Vormann MK, Wilschut KJ, Lanz HL, et al. Membrane-free culture and real-time barrier integrity assessment of perfused intestinal epithelium tubes. *Nat Commun.* 8, 262 (2017).
17. Wevers NR, van Vught R, Wilschut KJ, Nicolas A, Chiang C, Lanz HL, Trietsch SJ, et al. High-throughput compound evaluation on 3D networks of neurons and glia in a microfluidic platform. *Sci Rep.* 6, 38856 (2016).

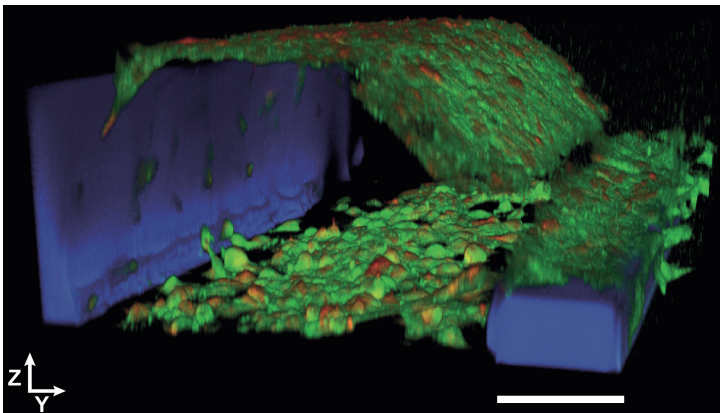
18. Schophuizen CM, De Napoli IE, Jansen J, Teixeira S, Wilmer MJ, Hoenderop JG, Van den Heuvel LP, et al. Development of a living membrane comprising a functional human renal proximal tubule cell monolayer on polyethersulfone polymeric membrane. *Acta Biomater.* 14, 22-32 (2015).
19. Schindelin J, Arganda-Carreras I, Frise E, Kaynig V, Longair M, Pietzsch T, Preibisch S, et al. Fiji: an open-source platform for biological-image analysis. *Nat Methods.* 9, 676-682 (2012).
20. Tutakhel OA, Jelen S, Valdez-Flores M, Dimke H, Piersma SR, Jimenez CR, Deinum J, et al. Alternative splice variant of the thiazide-sensitive NaCl cotransporter: a novel player in renal salt handling. *Am J Physiol Renal Physiol.* 310, F204-216 (2016).
21. Sun Y, Duthaler S, Nelson BJ. Autofocusing in computer microscopy: selecting the optimal focus algorithm. *Microsc Res Tech.* 65, 139-149 (2004).
22. Groen FCA, Young IT, Lighthart G. A Comparison of Different Focus Functions for Use in Autofocus Algorithms. *Cytometry.* 6, 81-91 (1985).
23. Haralick RM. Statistical and Structural Approaches to Texture. *Proceedings of the IEEE.* 67, 786-804 (1979).
24. Field DJ, Brady N. Visual sensitivity, blur and the sources of variability in the amplitude spectra of natural scenes. *Vision Res.* 37, 3367-3383 (1997).
25. Carpenter AE, Jones TR, Lamprecht MR, Clarke C, Kang IH, Friman O, Guertin DA, et al. CellProfiler: image analysis software for identifying and quantifying cell phenotypes. *Genome Biol.* 7, R100 (2006).
26. Kametsky L, Jones TR, Fraser A, Bray MA, Logan DJ, Madden KL, Ljosa V, et al. Improved structure, function and compatibility for CellProfiler: modular high-throughput image analysis software. *Bioinformatics.* 27, 1179-1180 (2011).
27. Zhang JH, Chung TD, Oldenburg KR. A Simple Statistical Parameter for Use in Evaluation and Validation of High Throughput Screening Assays. *J Biomol Screen.* 4, 67-73 (1999).
28. Aller SG, Yu J, Ward A, Weng Y, Chittaboina S, Zhuo R, Harrell PM, et al. Structure of P-glycoprotein reveals a molecular basis for poly-specific drug binding. *Science.* 323, 1718-1722 (2009).
29. Cascorbi I. P-glycoprotein: tissue distribution, substrates, and functional consequences of genetic variations. *Handb Exp Pharmacol.* 261-283 (2011).
30. Chen ZS, Tiwari AK. Multidrug resistance proteins (MRPs/ABCCs) in cancer chemotherapy and genetic diseases. *FEBS J.* 278, 3226-3245 (2011).
31. Masereeuw R, Russel FG. Therapeutic implications of renal anionic drug transporters. *Pharmacol Ther.* 126, 200-216 (2010).
32. van Aubel RA, Smeets PH, Peters JG, Bindels RJ, Russel FG. The MRP4/ABCC4 gene encodes a novel apical organic anion transporter in human kidney proximal tubules: putative efflux pump for urinary cAMP and cGMP. *J Am Soc Nephrol.* 13, 595-603 (2002).
33. Smeets PH, van Aubel RA, Wouterse AC, van den Heuvel JJ, Russel FG. Contribution of multidrug resistance protein 2 (MRP2/ABCC2) to the renal excretion of p-aminohippurate (PAH) and identification of MRP4 (ABCC4) as a novel PAH transporter. *J Am Soc Nephrol.* 15, 2828-2835 (2004).
34. Vormann MK, Gijzen L, Hutter S, Boot L, Nicolas A, van den Heuvel A, Vriend J, et al. Nephrotoxicity and Kidney Transport Assessment on 3D Perfused Proximal Tubules. *Aaps j.* 20, 90 (2018).
35. Suter-Dick L, Mauch L, Ramp D, Caj M, Vormann MK, Hutter S, Lanz HL, et al. Combining Extracellular miRNA Determination with Microfluidic 3D Cell Cultures for the Assessment of Nephrotoxicity: a Proof of Concept Study. *Aaps j.* 20, 86 (2018).
36. Homan KA, Kolesky DB, Skylar-Scott MA, Herrmann J, Obuobi H, Moisan A, Lewis JA. Bioprinting of 3D Convulated Renal Proximal Tubules on Perfusable Chips. *Sci Rep.* 6, 34845 (2016).
37. Secker PF, Luks L, Schlichenmaier N, Dietrich DR. RPTEC/TERT1 cells form highly differentiated tubules when cultured in a 3D matrix. *ALTEX.* (2017).

38. Weber EJ, Chapron A, Chapron BD, Voellinger JL, Lidberg KA, Yeung CK, Wang Z, et al. Development of a microphysiological model of human kidney proximal tubule function. *Kidney Int.* 90, 627-637 (2016).
39. Wilmer MJ, Ng CP, Lanz HL, Vulto P, Suter-Dick L, Masereeuw R. Kidney-on-a-Chip Technology for Drug-Induced Nephrotoxicity Screening. *Trends Biotechnol.* 34, 156-170 (2016).
40. Frohlich EM, Alonso JL, Borenstein JT, Zhang X, Arnaout MA, Charest JL. Topographically-patterned porous membranes in a microfluidic device as an in vitro model of renal reabsorptive barriers. *Lab Chip.* 13, 2311-2319 (2013).
41. Gao X, Tanaka Y, Sugii Y, Mawatari K, Kitamori T. Basic structure and cell culture condition of a bioartificial renal tubule on chip towards a cell-based separation microdevice. *Anal Sci.* 27, 907-912 (2011).
42. Vedula EM, Alonso JL, Arnaout MA, Charest JL. A microfluidic renal proximal tubule with active reabsorptive function. *PLoS One.* 12, e0184330 (2017).
43. Lash LH, Putt DA, Cai H. Membrane transport function in primary cultures of human proximal tubular cells. *Toxicology.* 228, 200-218 (2006).
44. Brown CD, Sayer R, Windass AS, Haslam IS, De Broe ME, D'Haese PC, Verhulst A. Characterisation of human tubular cell monolayers as a model of proximal tubular xenobiotic handling. *Toxicol Appl Pharmacol.* 233, 428-438 (2008).
45. Karlsson JE, Heddle C, Rozkov A, Rotticci-Mulder J, Tuvesson O, Hilgendorf C, Andersson TB. High-activity p-glycoprotein, multidrug resistance protein 2, and breast cancer resistance protein membrane vesicles prepared from transiently transfected human embryonic kidney 293-epstein-barr virus nuclear antigen cells. *Drug Metab Dispos.* 38, 705-714 (2010).
46. El-Sheikh AA, Greupink R, Wortelboer HM, van den Heuvel JJ, Schreurs M, Koenderink JB, Masereeuw R, et al. Interaction of immunosuppressive drugs with human organic anion transporter (OAT) 1 and OAT3, and multidrug resistance-associated protein (MRP) 2 and MRP4. *Transl Res.* 162, 398-409 (2013).
47. Wittgen HG, van den Heuvel JJ, van den Broek PH, Dinter-Heidorn H, Koenderink JB, Russel FG. Cannabinoid type 1 receptor antagonists modulate transport activity of multidrug resistance-associated proteins MRP1, MRP2, MRP3, and MRP4. *Drug Metab Dispos.* 39, 1294-1302 (2011).
48. Fahrmayr C, Konig J, Auge D, Mieth M, Munch K, Segrestaa J, Pfeifer T, et al. Phase I and II metabolism and MRP2-mediated export of bosentan in a MDCKII-OATP1B1-CYP3A4-UGT1A1-MRP2 quadruple-transfected cell line. *Br J Pharmacol.* 169, 21-33 (2013).
49. Gartzke D, Fricker G. Establishment of optimized MDCK cell lines for reliable efflux transport studies. *J Pharm Sci.* 103, 1298-1304 (2014).
50. Jenkinson SE, Chung GW, van Loon E, Bakar NS, Dalzell AM, Brown CD. The limitations of renal epithelial cell line HK-2 as a model of drug transporter expression and function in the proximal tubule. *Pflugers Arch.* 464, 601-611 (2012).
51. Astashkina AI, Mann BK, Prestwich GD, Grainger DW. Comparing predictive drug nephrotoxicity biomarkers in kidney 3-D primary organoid culture and immortalized cell lines. *Biomaterials.* 33, 4712-4721 (2012).
52. Kunze A, Huwyler J, Poller B, Gutmann H, Camenisch G. In vitro-in vivo extrapolation method to predict human renal clearance of drugs. *J Pharm Sci.* 103, 994-1001 (2014).
53. Musah S, Mammoto A, Ferrante TC, Jeanty SSF, Hirano-Kobayashi M, Mammoto T, Roberts K, et al. Mature induced-pluripotent-stem-cell-derived human podocytes reconstitute kidney glomerular-capillary-wall function on a chip. *Nat Biomed Eng.* 1, (2017).
54. Vriend J, Nieskens TTG, Vormann MK, van den Berge BT, van den Heuvel A, Russel FGM, Suter-Dick L, et al. Screening of Drug-Transporter Interactions in a 3D Microfluidic Renal Proximal Tubule on a Chip. *Aaps j.* 20, 87 (2018).

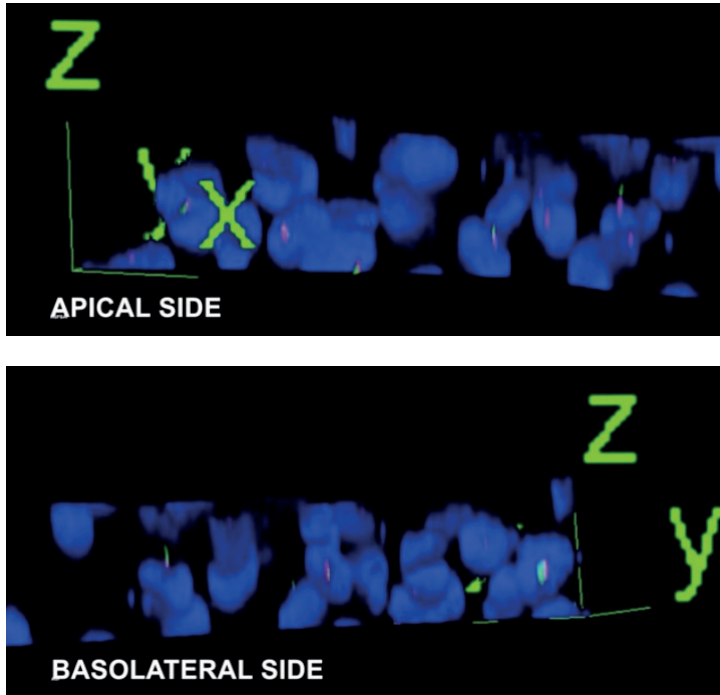
Supplemental data



Supplemental Figure S6.1 Rotation of 360° of tubules at day 8 after seeding. Immunofluorescence staining with F-actin (red) and nuclei (DAPI, blue) in ciPTEC-OAT1 in the OrganoPlate. Available online^[54].



Supplemental Figure S6.2 Long-term culture of 20 days of ciPTEC-OAT1. Immunofluorescence staining of F-actin (red), tight-junction protein zonula occludens (ZO-1, green), nuclei (DRAQ5, blue) in ciPTEC-OAT1 in the OrganoPlate, stained at day 20 after seeding. Scale bar represents 100 μm .



Supplemental Figure S6.3 Cilia staining in ciPTEC-OAT1 demonstrates polarized tubular structures. Immunofluorescence staining of nuclei (DAPI, blue) and cilia by means of staining pericentrin (magenta) and acetylated-tubulin (green) in ciPTEC-OAT1 in the OrganoPlate at day 8 after seeding. Z stacks displayed as volume and 360° rotation of cell monolayer attached to the extracellular matrix (ECM). Rotation starts viewing from lumen (apical side) and rotates to viewing point from ECM (basolateral side) and back with the viewing point from lumen. Clearly visible is that cilia were mainly demonstrated on apical side, facing the lumen of the tubules. Cilia are also observed on few cells that migrated into the ECM. Available online^[54].

Supplemental Table S6.1 Thresholding algorithms available in Fiji (version 1.51n) and used in image analysis described in this paper

Default	IsoData	MinError	Percentile
Huang	Li	Minimum	RenyiEntropy
IJ_IsoData	MaxEntropy	Moments	Shanbhag
Intermodes	Mean	Otsu	Triangle

Supplemental Table S6.2 Image QC metrics focus score, image correlation and PLSS of 3D P-gp drug efflux assay^a

Metrics	Pixel size	In focus	Out of focus	Cut-off	Precision	Recall	F-score
Focus score	-	$3.0 \times 10^{-3} \pm 0.3 \times 10^{-3}$	$4.2 \times 10^{-4} \pm 0.8 \times 10^{-4}****$	0	0.33	0.77	0.46
	500	$3.8 \times 10^{-4} \pm 0.8 \times 10^{-4}$	$2 \times 10^{-5} \pm 1 \times 10^{-5}$	0	0.18	0.97	0.30
	200	$2.8 \times 10^{-3} \pm 0.5 \times 10^{-3}$	$7 \times 10^{-4} \pm 5 \times 10^{-4}$	0	0.17	0.94	0.29
	100	$5.8 \times 10^{-3} \pm 0.7 \times 10^{-3}$	$2 \times 10^{-3} \pm 1 \times 10^{-3}*$	0	0.23	0.94	0.36
	50	$7.7 \times 10^{-3} \pm 0.9 \times 10^{-3}$	$7 \times 10^{-4} \pm 4 \times 10^{-4}***$	0	0.23	0.94	0.37
	20	$5.0 \times 10^{-3} \pm 0.8 \times 10^{-3}$	$3 \times 10^{-4} \pm 2 \times 10^{-4}**$	0	0.22	0.91	0.36
Image correlation	500	0.20 ± 0.01	0.23 ± 0.03	0.55	0.15	1.00	0.25
	200	0.27 ± 0.01	0.27 ± 0.03	0.60	0.15	1.00	0.26
	100	0.35 ± 0.01	0.33 ± 0.04	0.20	0.20	0.43	0.27
	50	0.45 ± 0.01	0.41 ± 0.04	0.20	0.25	0.43	0.32
	20	0.63 ± 0.01	$0.51 \pm 0.04***$	0.3	0.45	0.40	0.42
PLLS	-	-1.90 ± 0.02	-1.94 ± 0.09	-2.2	0.23	0.43	0.30

^aData is of spinning disk confocal microscopy images of calcein (n=245) from four independent experiments. In-focus and out-of-focus images were determined visually, using criteria as described in the methods section, and defined as ground truth. Per image QC metric, cut-off values and its corresponding F-scores were calculated. The best achievable F-score is displayed in this table. *p<0.05 compared to in-focus, **p<0.01 compared to in-focus, ***p<0.001 compared to in focus images.

Supplemental Table S6.3 Image QC metrics focus score, image correlation and PLSS of 3D MRP2/4 drug efflux assay^a

Metrics	Pixel size	In focus	Out of focus	Cut-off	Precision	Recall	F-score
Focus score	-	$7.2 \times 10^{-4} \pm 0.5 \times 10^{-4}$	$2.2 \times 10^{-4} \pm 0.2 \times 10^{-4}^{***}$	2×10^{-4}	0.39	0.73	0.51
	500	$8 \times 10^{-5} \pm 1 \times 10^{-5}$	$1.1 \times 10^{-5} \pm 0.3 \times 10^{-5}^{***}$	0	0.30	0.83	0.44
	200	$5.7 \times 10^{-4} \pm 0.7 \times 10^{-4}$	$6 \times 10^{-5} \pm 2 \times 10^{-5}^{***}$	0	0.38	0.87	0.53
	100	$1.4 \times 10^{-3} \pm 0.2 \times 10^{-3}$	$8 \times 10^{-5} \pm 3 \times 10^{-5}^{**}$	0	0.30	0.92	0.46
	50	$9 \times 10^{-4} \pm 1 \times 10^{-4}$	$4 \times 10^{-5} \pm 1 \times 10^{-5}^{***}$	0	0.33	0.92	0.48
	20	$2.7 \times 10^{-4} \pm 0.4 \times 10^{-4}$	$9 \times 10^{-6} \pm 3 \times 10^{-6}^{***}$	0	0.36	0.94	0.52
Image correlation	500	0.19 ± 0.01	0.15 ± 0.02	0.1	0.33	0.62	0.43
	200	0.25 ± 0.01	$0.18 \pm 0.02^{**}$	0.15	0.31	0.65	0.42
	100	0.33 ± 0.01	$0.24 \pm 0.03^{**}$	0.15	0.38	0.48	0.43
	50	0.43 ± 0.01	$0.32 \pm 0.03^{***}$	0.3	0.36	0.62	0.45
	20	0.60 ± 0.01	$0.43 \pm 0.03^{***}$	0.4	0.45	0.56	0.50
PLLS	-	-1.89 ± 0.02	-1.87 ± 0.06	-2.3	0.53	0.31	0.39

^aData is of spinning disk confocal microscopy images of GS-MF (n=240) from four independent experiments. In-focus and out-of-focus images were determined visually, using criteria as described in the methods section, and defined as ground truth. Per image QC metric, cut-off values and its corresponding F-scores were calculated. The best achievable F-score is displayed in this table. *p<0.05 compared to in-focus, **p<0.01 compared to in-focus, ***p<0.001 compared to in focus images.

Macro to measure fluorescence intensity

Note: different algorithm thresholds can be used to measure intensity

```
macro "Measure intensity Alexa488, no thresholding algorithm" {
  nameImg=getTitle();
  setOption("BlackBackground", true);
  run("Set Measurements...", "area mean standard modal min centroid center perimeter
  bounding fit shape feret's integrated median skewness kurtosis area_fraction stack
  display redirect=None decimal=3");
  selectWindow(nameImg);
  run("Measure");
  selectWindow(nameImg);
  close();
}
```

```
macro "Measure intensity Alexa488 with thresholding algorithm" {
  nameImg=getTitle();
  setOption("BlackBackground", true);
  run("Duplicate...", "title=Mask");
  selectWindow("Mask");
  run("Median...", "radius=5");
  algorithm = "add name threshold here";
  run("Auto Threshold", "method=" + algorithm + " dark");
  run("Convert to Mask");
  run("Erode");
  run("Create Selection");
  roiManager("Add");
  roiManager("select", 0);
  selectWindow("Mask");
  close();
  run("Set Measurements...", "area mean standard modal min centroid center perimeter
  bounding fit shape feret's integrated median skewness kurtosis area_fraction stack
  display redirect=None decimal=3");
  selectWindow(nameImg);
  roiManager("Select", 0);
  roiManager("Measure");
  selectWindow(nameImg);
  close();
}
```



General Discussion

Introduction

The first phase in drug development often concerns the identification of a lead compound for the biological target of interest, using high-throughput screening of large chemical libraries. Adverse effects of candidate drugs are commonly evaluated only in late pre-clinical stages, following optimization of pharmacokinetics and pharmacodynamics, and are traditionally regarded as the ‘final hurdles’ before clinical trials can be initiated. At this point, the remaining drug candidates are tested using rodent and non-rodent animal models, while 2D cell culture models are applied in screening for specific organ toxicity. These current preclinical models are, however, insufficiently capable of predicting drug-induced kidney injury, resulting in undesirably high clinical attrition of potential drugs^[1]. Laboratory animals and humans intrinsically differ in physiology and therefore responses in animal toxicological studies are not always applicable to human drug toxicity. The reason why existing *in vitro* models perform suboptimal, may be reflected in the use of oversimplified and insufficiently differentiated cell lines and the neglect of renal micro environmental cues^[2-4]. The lack of predictive value results in approximately 50% of drug candidates having unknown harmful effects while entering clinical trials with harmful effects, leading to costly and ethically compromised late-stage drug withdrawals^[1]. To improve the success rate of drug development, harmful compounds need to be eliminated at early phases, without the risk of excluding false-positives. To this end, *in vitro* toxicity studies and drug-drug interaction (DDI) evaluations should be implemented at earlier stages of the drug development pipeline, employing models with high predictive value for humans.

***In vitro* models for drug-induced renal proximal tubule toxicity screening**

The most important and ongoing challenge for *in vitro* disease modeling in general, including drug-induced toxicity research, is to find a reliable and sustainable source of human-derived cells that phenotypically represent their *in vivo* counterpart^[5]. Drug-induced renal toxicity commonly affects the proximal tubule epithelium. Therefore, the phenotype of cultured proximal tubule epithelial cells (PTEC) is decisive for drug sensitivity and faithful replication of the mechanisms responsible for toxicity induction. Renal models generally consist of either freshly isolated or cryopreserved primary renal cortex cells, immortalized proximal tubule cell lines or induced pluripotent stem cell (iPSC)-derived renal cells. Each of these models has unique advantages and disadvantages, which are summarized below.

Primary renal tubule cells phenotypically resemble their *in vivo* counterpart best in terms of morphology, polarization, drug transporter function and biomarkers. As such, primary cells demonstrate the best replication of drug-induced toxicity mechanisms^[6, 7]. While they can be cryopreserved to be readily available, their expansion capacity in culture is low, resulting in the need for multiple donors. While the observed differences between donors lead the way for personalized medicine, this does not contribute to experimental reproducibility.

Induced pluripotent stem cell (iPSC), on the other hand, can be cultured for extended passages and are capable of differentiation into renal cells, theoretically generating an unlimited cell source^[8]. Usually skin fibroblasts are the source of these cells but they can be generated from any nucleated cell type, and can consecutively be differentiated into tissues relevant for drug-induced toxicity evaluation, including proximal tubule-like cells^[9, 10]. Accumulating evidence in literature underlines the influence of inter-individual genetic differences on drug responses and drug-induced toxicity, giving rise to a personalized medicine approach^[11, 12]. Most adverse effects only occur in a subset of treated individuals, which are most likely underrepresented in clinical trials. Experimental models representing subgroups of the general population may identify individuals at increased risk for developing adverse effects, including children, elderly and patients for which the drug is intended, but also individuals suffering from chronic kidney disease or diabetes mellitus. Being able to generate renal proximal tubule cell models derived from any individual will pave the way towards personalized medicine. At present, these cell models have been successfully applied in kidney organoid cultures for toxicity evaluation, suggesting intact function including drug transporter activity, but it remains to be elucidated how the *in vitro* phenotypes of individual iPSC-derived cells compare to their *in vivo* counterparts^[10]. In addition, modeling subpopulations or disease states *in vitro* likely requires reproducing affected physiological parameters. While further progress is needed to fully mature the techniques involved, iPSC-derived tissues are likely to be implemented in the evaluation of drug-induced toxicity and DDIs in a personalized approach.

Immortalized cell lines can overcome some of the limitations mentioned above and therefore have been adapted for industrial screening applications. The phenotypes of human-derived renal cell lines are well-characterized and include retained PTEC morphology, in some cases polarization, and demonstrate enhanced proliferative capacity compared to primary PTEC. However, reduced drug transporter function and renal biomarker expression may cause these cells to be hampered by low predictivity^[13, 14]. Several suitable human-derived proximal tubule cell lines were established that have retained proximal tubule characteristics rather well, including

ciPTEC and RPTEC/TERT1. Recently, the genome of both cell lines has been edited to over-express transport proteins that were initially lost in the immortalization process, like OAT1 and OAT3 for ciPTEC^[15], and OAT1 and OCT2 for RPTEC/TERT1 [ATCC-LGC Standards, Wesel, Germany].

As we demonstrated in **Chapter 2** for ciPTEC, expression of OATs results in regained sensitivity for clinically relevant nephrotoxic antiretroviral agents, such as adefovir and tenofovir. Compared to earlier studies employing OAT over-expressing cell lines of non-renal origin, ciPTEC-OAT1 remarkably demonstrated reduced sensitivity to the antiretroviral drugs tested. Although we used a relatively insensitive endpoint, the main reason for this observation is most likely the presence of active ABC (efflux) transporters, including MRP4. The *in vitro* capacity of MRP4 to transport adefovir and tenofovir has been known for several years^[16, 17], while evidence for the clinical implications of MRP4-mediated transport of antiretrovirals was only reported recently. For example, several single nucleotide polymorphisms in *ABCC4* have been identified that predispose for tenofovir-induced nephrotoxicity^[18, 19]. In the clinical setting, DDIs with MRP4 could have the same effect, but this has not been observed consistently^[20, 21]. Expression of MRP4 is retained in ciPTEC, which provides a good platform to study modulation of proximal tubule efflux as approach to reduce antiretroviral-induced acute kidney injury (AKI). Mitochondria are the primary target of renal toxicity by antiretrovirals. Impairment of these organelles especially affects the PTEC as they are rich in mitochondria and dependent on aerobic, OXPHOS-mediated ATP production to supply the energy required for active transport processes and metabolism^[22]. The mechanism of adefovir toxicity involves inhibition of mitochondrial DNA polymerase- γ leading to a decrease in mitochondrial DNA (mtDNA) replication and expression of mitochondrial OXPHOS proteins, ultimately resulting in reduced ATP production^[23]. The mechanism for tenofovir may be different as *in vitro* studies suggested that depletion of mtDNA and cytotoxicity is lower compared to similar antiretroviral drugs^[24, 25], while it caused severe AKI in the clinic, associated with morphological aberrations and swollen mitochondria^[26]. Unknown additional mitochondrial targets may be responsible for the observed tenofovir-induced adverse effects in PTEC. OAT1-overexpressing ciPTEC may be a suitable model to study these mechanisms in more detail.

Expression of OATs in PTEC models also offers the opportunity to investigate the indirect contribution of OAT-mediated transport to drug-induced toxicity. In **Chapter 3**, we showed that expression of OAT1 and OAT3 reduced ciPTEC sensitivity to cisplatin, a cytostatic drug that is handled by organic cation transporters. The observation could be explained by reduced activity of the influx transporter OCT2, although we can only

speculate about the involved regulatory pathways. OAT transport function is closely related to energy metabolism since these transporters exchange dicarboxylates, preferentially the citric acid cycle intermediates α -ketoglutarate, glutarate, succinate and fumarate^[27]. Therefore, metabolic changes due to loss of OAT expression in PTEC models may affect *in vitro* prediction of drug-induced toxicity. Using metabolomics and microarray data from OAT1 and OAT3 knockout mice, it was possible to generate an extended metabolic network focused on these transporters, indicating their importance in glycolysis, citric acid cycle, fatty acid and lipid, pyruvate, NAD, flavonoid, amino acid, vitamin, and (cyclic) nucleotide metabolism^[28-31]. In line with these observations, drug transporters are postulated to be involved in the regulation of endogenous metabolism and metabolic homeostasis^[32]. Considering drug-induced toxicity, DDIs with OATs may affect energy metabolism and could contribute to adverse drug effects, especially in tissues with high OAT expression, such as the kidney proximal tubule epithelium. A better understanding of the endogenous roles of drug transporters will shed light on their influence on physiological and disease metabolism, and possibly on adverse drug effects and predisposing factors we do not yet understand.

Biomarkers for drug-induced renal proximal tubule toxicity screening

To enable *in vitro* to *in vivo* extrapolation of renal adverse effects, human-derived cell culture models should allow analysis of clinically relevant biomarkers. Classical readouts of toxicity used in regular 2D assays as evaluated in **Chapters 2 and 3** focus on acute toxicity and reflect membrane integrity, like lactate dehydrogenase (LDH) and propidium iodide (PI), or metabolic activity, like reduction of MTT and intracellular ATP concentration. Biochemical markers for membrane integrity and energy metabolism are widely applied, but are not specific to the kidney and, therefore, have limited translational value^[33, 34]. In addition, evaluating general cytotoxicity by studying membrane integrity and ATP metabolism may underestimate renal injury in the clinic, which involves more subtle, functional changes, such as proteinuria. This was illustrated in **Chapter 4**, as uptake of antisense oligonucleotides (AON's) in ciPTEC resulted in competition with low-molecular weight proteins for receptor-mediated endocytosis, mimicking proteinuria *in vitro*, while cytotoxicity for AON's was not observed. Quantification of kidney-specific proteins like kidney injury molecule 1 (KIM-1) and their gene expression profiles allows for *in vitro* to *in vivo* extrapolation. KIM-1 is a transmembrane glycoprotein involved in tubular regeneration and is increasingly expressed in dedifferentiated proximal tubule epithelial cells after

ischemic or toxic injury^[35,36]. Upon tubule cell damage, the ectodomain of KIM-1 is shed into the urine and abundance increases over 100-fold, significantly outperforming serum creatinine as biomarker in rat models of kidney injury^[36]. This response has been validated for tubular toxicity induced by well-established nephrotoxicants, such as cisplatin and aminoglycoside antibiotics in rodents^[36,37], although additional clinical evaluation is required^[34]. Biomarkers with similar *in vitro* to *in vivo* translation potential include the cytosolic protein NGAL (neutrophil gelatinase-associated lipocalin), cystatin C, cytokines involved in renal immune responses, such as IL-6 and IL-8; and possibly heme oxygenase 1 (HO-1)^[33,38]. In addition, several miRNAs, including miR-21, miR-155 and miR-18a, may see future application as renal-specific biomarkers, as these are released into the urine upon drug-induced tubule epithelial injury, similar to KIM-1^[39]. Implementation of renal-specific biomarkers will improve our mechanistic understanding of drug-induced kidney injury and will be crucial for translation of renal adverse effects to the clinic.

Fluid shear stress in renal proximal tubule function

A growing body of evidence in literature shows that increased reproduction of the physiological microenvironment, including luminal flow, improves *in vitro* renal proximal tubule characteristics and, therefore, may enhance predictive value of these models, as discussed in **Chapter 5**. Replicating the characteristic microenvironment of kidneys improves the differentiation of human primary PTEC as evaluated by epithelial polarization, indicated by increased cell height, basolateral expression of Na⁺/K⁺-ATPase and apical expression of AQP1^[2,40,41]. Regarding evaluation of drug-induced toxicity and DDIs, fluid shear stress (FSS) has been shown to enhance Pgp and MATE2-k transport function and receptor-mediated endocytosis in proximal tubule cells^[2,4,42].

Primary cilia have been postulated to regulate the activity of drug transporters and endocytosis receptors in response to FSS, but conclusive evidence for this relation has not been produced. Primary cilia are immotile, microtubule-based organelles that are responsible for transduction of flow-mediated signaling in epithelial cells. This role is supported in *in vitro* tubule models by an increased number of ciliated cells and length of primary cilia after exposure to FSS^[2,43-45]. Hence, to investigate the role of primary cilia in flow-mediated regulation of drug transporters, a deciliated clone of ciPTEC was generated by CRISPR/Cas9 genome editing technology. The target sequence selected was located in the *KIF3A* gene (Figure 7.1A, underlined), because its disruption should prevent the formation of the primary cilia cellular membrane^[46,47]. The *KIF3A* gene in

cilia-depleted and parent ciPTEC was sequenced, confirming the introduction of a genomic frame shift mutation (Figure 7.1A), resulting in knock-out of KIF3A protein in ciPTEC^{KIF3A^{-/-}}, while it was clearly expressed in ciPTEC parent in both proliferating (33°C) and maturing (37°C) cultures (Figure 7.1B). Finally, cilia-depleted and parent ciPTEC were stained for acetylated tubulin and peri-centrin to confirm the presence of primary cilia in ciPTEC-parent (indicated by the white arrows) and the successful inhibition of ciliogenesis in ciPTEC^{KIF3A^{-/-}} (Figure 7.1C). While cilia formation was prevented in ciPTEC^{KIF3A^{-/-}}, the downstream signaling pathways should be preserved, in contrast to methods using chemically removal of cilia by chloral hydrate that possibly compromises pathways and metabolic processes^[45, 48]. In addition to flow regulation, primary cilia are known to be involved in cell differentiation and proliferation through Wnt and Hedgehog signaling pathways^[49]. Therefore, cilia are also postulated to play a role in epithelial repair mechanisms following drug-induced insults^[50]. Together, the ciPTEC model and its cilia-depleted counterpart are currently available as tools to investigate the mechanism of cilia-mediated signaling in the human proximal tubule.

Kidney-on-a-chip for drug-induced renal proximal tubule toxicity and DDI screening

A luminal flow that is regulated, equally distributed (laminar) and pulsatile within the physiological range will better mimic the renal tubule physiological microenvironment *in vitro*. The most promising technique to generate proximal tubule cultures with increased physiological relevance and investigate the effect of FSS is a microfluidic device, also called kidney-on-a-chip, as discussed in **Chapter 5**. Microfluidic devices enable the *in vitro* culture of cells in a perfused channel with micrometer dimensions, in order to recreate the physiologically relevant niche of the cell type in question, hence, potentially increasing differentiation status and function. The force of FSS that is applied in current *in vitro* models ranges from 0.2 to 1 dyne-cm⁻², and most likely resembles the force as experienced *in vivo* by a normal human PTEC^[51]. In addition to flow, microfluidic models support replication of the extracellular matrix (ECM), eg. by coating with collagen type IV. Furthermore, it may include multiple compartments that stimulate polarization of PTEC with formation of distinct apical and basolateral membranes and access to their bounding compartments^[2, 40, 41, 44, 52]. Combining these technologies with a human-derived PTEC model provides a promising basis for developing advanced renal drug-induced toxicity testing models. In **Chapter 6** we demonstrated proof-of-principle for ciPTEC using fluorescent-based assays to evaluate transport activity of Pgp and MRP2/4 in a microfluidic device. The microtiterplate OrganoPlate[®] used in our study allows culturing of ciPTEC-OAT1 on collagen type I in

a perfused channel with a tubule-like structure. Additional studies should point out if the increased physiological relevance of this novel model translates into a higher predictive value for drug-induced renal toxicity in humans.

The future position and complexity of renal microfluidic devices in drug development will be reflected by their need as pre-clinical evaluation tools that partly replace animal testing and reduce adverse events during clinical trials. Current examples of kidney-on-a-chip systems that demonstrate high complexity and physiological resemblance can easily be applied in mechanistic studies^[53-55]. Such studies are most likely to be performed in late-phase pre-clinical studies, if the number of compounds to be tested is relatively low (less than 10), and clinically more relevant models are required^[54]. This application may benefit from the experimental designs of current microfluidic devices, which allows a fit-for-purpose solution^[55]. Additional advantages of current systems include the optical transparency, which allows for real-time and high-resolution analysis; a reduction in expensive cell culture reagents and drug compounds due to small volumes; and the possibility to culture multiple cell types, representing interacting tissues or even organs^[53]. Microfluidic devices are, moreover, a suitable approach to comply with the principles of 3Rs, being reduction, refinement and replacement of animals in research. Despite the promising and tempting leap forward in physiological relevance and drug sensitivity of *in vitro* cultures of proximal tubule cells, several challenges remain to be solved before microfluidic devices can be implemented in pharmaceutical industry. The ongoing challenges will be discussed point-by-point in the following paragraphs and are summarized in Figure 7.2.

Kidney models that demonstrate an increased complexity and physiological resemblance are generally not compatible with automated screening. High content screening (HCS) employs automated imaging and analysis to ideally evaluate multiple toxicological endpoints, which increases throughput and improves mechanistic insight at the same time^[56]. An essential requirement is multiplexing of fluorescent dyes probing cellular functions like membrane integrity and mitochondrial membrane potential, to enable analysis by algorithms and automation compatibility. Such an approach was used previously in the liver-derived HepG2 cell line, which resulted in a sensitivity of around 50% and less than 10% false positives in drug-induced hepatotoxicity screening^[57]. Similar predictive values were found in a study evaluating drug-induced toxicity in cultured primary human PTEC in which 129 phenotypic parameters were derived from 4 combined fluorescent probes using machine-learning algorithms^[58]. The combination of HCS and microfluidic devices might further improve drug-induced nephrotoxicity screening. Consequently, designing microfluidic devices with HCS and automation will be an essential asset for future

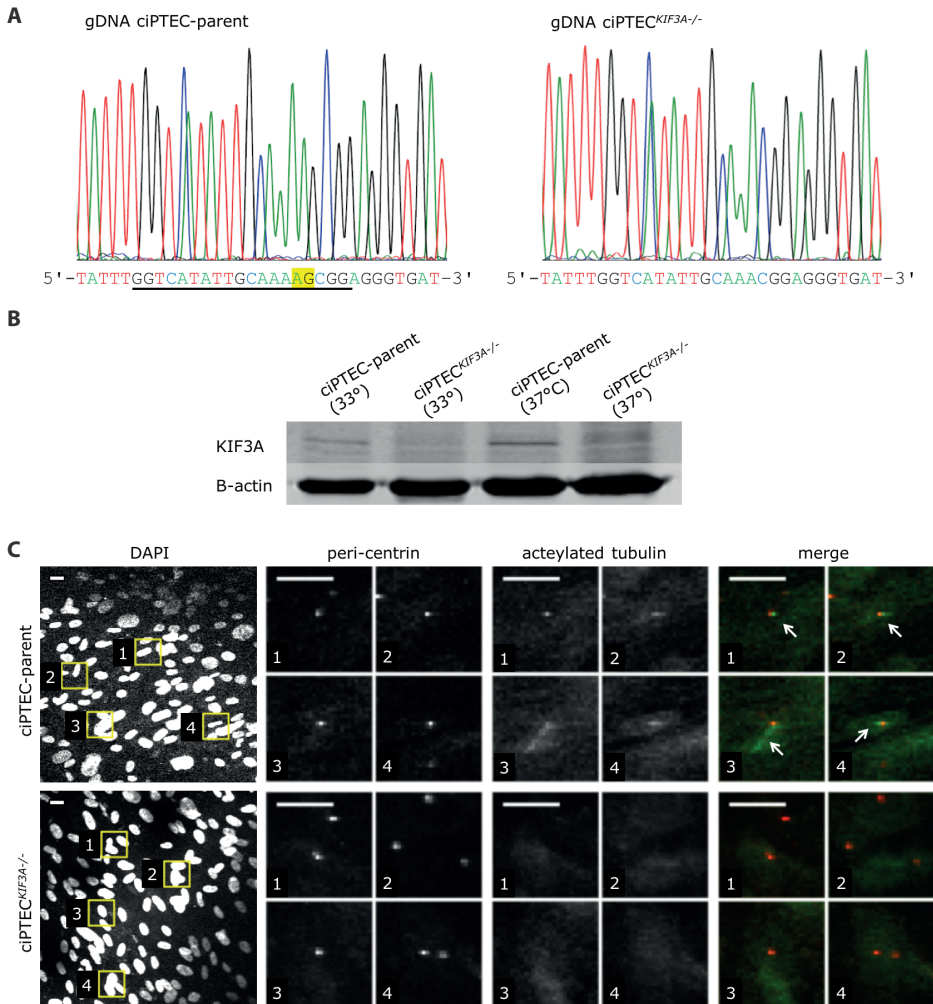


Figure 7.1 Absence of KIF3A protein and cilia in ciPTEC^{KIF3A^{-/-}} confirms the successful knock-out of KIF3A in ciPTEC. (A) Sequenced genomic DNA of ciPTEC-parent and ciPTEC^{KIF3A^{-/-}} demonstrating the loss of 2 base pairs, demonstrating a successful frame shift mutation in the *KIF3A* gene. *KIF3A* genomic RNA target sequence used to guide CRISPR/Cas9 to the *KIF3A* gene is underlined. (B) KIF3A protein (80 kDa) expression is present in ciPTEC-parent and is lacking in ciPTEC^{KIF3A^{-/-}}, suggesting successful knock-out of *KIF3A* at both 33°C and 37°C using β -actin (42 kDa) as loading control (n=3, representative images are used) (C) Confocal immunofluorescent images confirm the presence of primary cilia (indicated by the white arrows) specific acetylated tubulin (green) in ciPTEC-parent and the absence in ciPTEC^{KIF3A^{-/-}}, while the basal body specific peri-centrin (red) is present in both cell lines (n=1, scale bar indicates 20 μ m).

drug screening devices. In **Chapter 6** we have shown compatibility of a semi high-throughput microfluidic device with automated image capture and analysis, suitable for screening purposes. The future of renal toxicity screening will probably consist of a tiered approach with increasing complexity and physiological resemblance as compounds progress through the phases of development, reducing the throughput capacity along the way. An overview of *in vitro* approaches in order of increasing complexity was presented in **Chapter 5**, including the most important advantages and disadvantages of each system. Regular 2D cell culture of immortalized PTEC are suitable to identify overtly toxic compounds, while microfluidic-based proximal tubule tissue provides the cell physiological cues to mechanistically study adverse effects of drug candidates, which is required at more advanced stages of drug development^[55].

Another important limitation of *in vitro* safety evaluation models is the diversity of toxicological mechanisms and cellular targets that need to be represented. Animal models inherently demonstrate a higher integrative physiological value than any *in vitro* system currently available, illustrated by the role of hepatic metabolism in the uptake and nephrotoxicity of cisplatin^[59]. Combining a liver-on-a-chip and a kidney-on-a-chip in one model would include the toxic effects of drug metabolites to be investigated, as was shown for ifosfamide, and could be part of the solution for modeling the processes involved in cisplatin-induced nephrotoxicity^[60]. Multi-organ cultures are promising tools for toxicity studies that involve drugs administered as prodrugs and/or undergo extensive metabolism that could account for toxicity. It is, however, important to implement the correct scaling between the different organotypic cultures incorporated, and developing a common culture medium is an ongoing challenge in this field^[53,54]. For now, we should be aware that even in models demonstrating the highest degree of physiological resemblance technically possible, only a subset of the entire variation of cell types, tissues and organs of a human body is represented, which may still be insufficient to account for many of the toxic mechanisms that we do not yet understand. Nevertheless, better identification and recapitulation of off-target toxicities with *in vitro* models will be a necessary step in improving the drug safety evaluation process.

The materials used to produce microfluidic devices, such as polydimethylsiloxane (PDMS), polycarbonate and polyester have several advantages. They allow a flexible design, are not expensive and are optically clear, enabling real-time analysis by microscopy. On the other hand, these synthetic materials do not resemble the *in vivo* ECM, requiring coatings to enable cell adhesion^[53]. Moreover, PDMS absorb hydrophobic drug molecules, which leads to a reduction in their effective

concentration and thereby underestimation of the toxic potential^[61]. Oxidizing a thin layer of PDMS on the inside of the device, creates a layer of silicon dioxide on the surface, that limits binding^[62]. Future and more standardized microfluidic devices will most likely be developed with more inert materials, such as the OrganoPlate[®] that is composed of glass^[63,64]. Cell adherence can be improved by coating the inner surface of microfluidic channels with ECM components that resemble the physiological environment, such as collagen type I and IV, laminin and fibronectin^[65]. As this increases costs, reduces manufacturing capacity and implies the persistent need for animal-derived materials, successful industrial application may see the use of biocompatible synthetic hydrogels in the near future. They can be modified to closely mimic the ECM surrounding the cell type of interest, including ciPTEC^[66], enhancing attachment and possibly study toxic responses or kidney regeneration *in vitro*^[67].

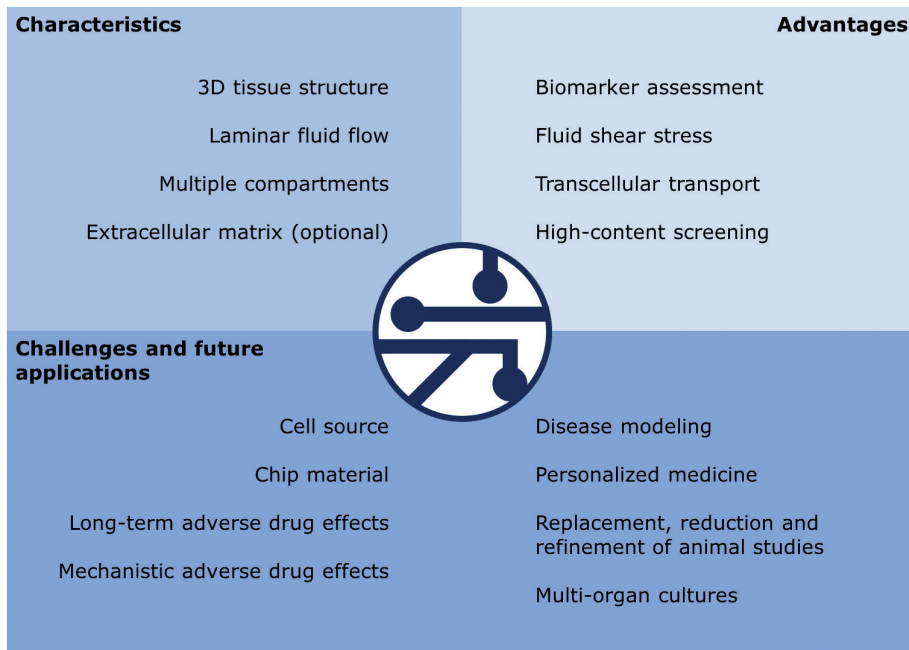


Figure 7.2 Overview of the inherent characteristics of microfluidic devices, the advantages and opportunities these devices offer and the challenges and future applications of this advanced culture method. The lines at the center of this figure represent microfluidic channels in general and are for illustrative purposes only.

Finally, microfluidic-based tissue technology can only achieve its full potential for drug safety evaluation upon proper validation and full implementation in the drug development processes^[53-55]. Validation of drug-induced responses can be achieved best by using a well-defined set of nephrotoxic and non-nephrotoxic agents, for which both *in vitro* and *in vivo* data are readily available. Comparing the responses to known nephrotoxic drugs and drug candidates that failed because of toxicity observed with available animal data and regular culture systems, will be crucial to demonstrate the additional predictive capability of the newly developed *in vitro* model. To accommodate this process, organ-on-a-chip developers, and partners from pharmaceutical industry and regulatory agencies should team up to form consortia that provide an integrated testing platform for novel microfluidic devices. An international network that is already in place is the Crack-it NephroTube Challenge, initiated by the National Centre for the Replacement, Refinement and Reduction of Animals in Research (NC3Rs), in which pharmaceutical industry, academia and companies developing microfluidic devices are brought together. The first results of this effort are described in **Chapter 6** of this thesis, in which the proximal tubule model ciPTEC-OAT1 and the microfluidic OrganoPlate[®] were combined for renal DDI studies. Currently, this international consortium performs a screen of 12 nephrotoxic compounds and 15 different biomarkers, as the first step towards validating this renal microfluidic culture device and its compatibility with industrial high content equipment. Another example is the National Centre for Advancing Translation Sciences (NCATS) at the National Institutes of Health, which has recently started to evaluate intra- and inter-laboratory reproducibility, robustness and shipping of microfluidic-based tissue culture devices^[54]. Continuous dialog with the international regulatory agencies, such as EMA and FDA, is needed to develop guidelines for the use of novel organ-on-a-chip systems in early safety toxicology. In turn, this enables a discussion to ultimately reduce and refine animal studies in drug-induced toxicity evaluation of candidate therapeutic drugs. It is important to note here that culture models usually require animal-derived serum, which may compromise their promise to reduce animal burden. Some culture models, including selected proximal tubule cell lines, are readily compatible with serum-free media. As formulations are improving, it may soon be possible to extend these towards cultures that have not yet made this transition. In order for microfluidic devices to become commercially interesting, the feasibility of technical implementation into the currently existing drug development process will play a key role and needs a focus on the end-users^[68]. Therefore, kidney-on-a-chip devices should ideally be packaged into off-the-shelf applications, accompanied by reliable and reproducible assays, and be compatible to some degree with conventional culture methodologies, that will ease automated handling, analysis and data extraction^[53].

***In silico* models for drug-drug interaction screening**

In silico modeling of DDIs has gained much interest over recent years and has been applied to identify, predict and explain DDIs with higher capacity as compared to *in vitro* experiments^[69, 70]. Computational approaches like protein-based pharmacophore modeling, combines structural information of the target protein and drug molecule and uses molecular docking methods to predict *in silico* ligand–protein interactions. This type of computational modeling is hampered however, as this method requires determination of the crystal structure of renal drug transporters in a useful conformation, binding to each substrate or inhibitor involved, with sufficient resolution. This is available for several mammalian drug transporters, including Pgp^[71] and MRP2^[72]. Chemical pharmacophore modeling, on the other hand, evaluates molecular descriptors related to binding affinity and substrate specificity and identifies features common among substrates and inhibitors. This strategy was first used to identify aromatic, ether and amine functional groups shared among Pgp substrates^[73]. In addition, substrates for the SLC transporters have been investigated, elucidating that OATs seem to have higher preference for planar molecules, while OCTs tend to transport compounds with more 3D-shaped structures^[74]. Further, substrates of OAT3 are usually more cationic or zwitterionic in character compared to substrates for OAT1^[74]. For MATE1, chemical pharmacophore models suggested that the presence of an aromatic ring and sufficient hydrophobicity are important features of inhibitors^[75]. Chemical pharmacophore modeling is currently applied for predicting the substrate or inhibition capacity of new chemical entities in drug discovery. However, a vast database containing chemical structures of substrates, inhibitors and non-interacting compounds of the target of interest is required to feed the algorithm^[76]. Recent validation of chemical-based pharmacophore modeling has indicated that its predictions are as of yet only valid for extrapolation between compounds with very similar structures, although 3D pharmacophore modeling can enhance its performance^[77]. Therefore, *in vitro* models are still required to evaluate DDIs, such as those developed in **Chapters 2 and 6**. Finally, physiologically-based pharmacokinetic (PBPK) modeling forms a separate class of *in silico* prediction methods, as it estimates the concentration of drugs in plasma and tissues over time under varying physiological and pharmacological conditions, including co-medication^[70]. PBPK software platforms such as SimCYP may be used to predict organ and tissue exposure to the drug of interest, which can serve as a starting point for *in vitro* toxicity studies. A slowly growing amount of information on drug-protein interactions may increase the application of computational DDI screening in early phases of the drug development process in the future. Similar to DDIs, it might be possible in the future to understand how toxicity arises from certain chemical features using *in silico* methods, which would allow chemical adjustment

of lead molecules into safer alternatives^[78]. Early attempts are made for the liver as target organ, modelling crucial pathways involved in toxicity induction, including glutathione status, mitochondrial (dys)function, energy balance, cellular life cycle, cell death and parts of the innate immune system^[79]. Due to the complexity of the biology involved, future validation will demonstrate to what extent computational models will be able to predict drug-induced nephrotoxicity.

Conclusions

In conclusion, the high incidence of renal adverse effects observed in the final stages of drug development underlines the limitations of current pre-clinical models for drug-induced toxicity testing. PTEC cultures demonstrating relevant drug transporters and metabolism, combined with analysis of renal specific biomarkers, have the potential to improve the predictive value of *in vitro* drug-induced toxicity testing and reduce safety-related drug attrition in the clinic. Microfluidic devices can further increase the physiological relevance, possibly aided by *in silico* predictions in the future. Depending on the research question, models with different degrees of complexity are available that range from those suitable for relatively simple screening purposes to detailed mechanistic investigations. Organ-on-a-chip models have, therefore, the capacity to shift the paradigm of toxicology from the traditional 'final hurdle' before clinical evaluation is initiated, to a continuous process that aims to reduce the toxic potential of novel drugs in every step of the of drug development pipeline.

References

1. Cook D, Brown D, Alexander R, March R, Morgan P, Satterthwaite G, Pangalos MN. Lessons learned from the fate of AstraZeneca's drug pipeline: a five-dimensional framework. *Nat Rev Drug Discov.* 13, 419-431 (2014).
2. Jang KJ, Mehr AP, Hamilton GA, McPartlin LA, Chung S, Suh KY, Ingber DE. Human kidney proximal tubule-on-a-chip for drug transport and nephrotoxicity assessment. *Integr Biol (Camb).* 5, 1119-1129 (2013).
3. Racusen LC, Monteil C, Sgrignoli A, Lucskay M, Marouillat S, Rhim JG, Morin JP. Cell lines with extended in vitro growth potential from human renal proximal tubule: characterization, response to inducers, and comparison with established cell lines. *J Lab Clin Med.* 129, 318-329 (1997).
4. Raghavan V, Rbaibi Y, Pastor-Soler NM, Carattino MD, Weisz OA. Shear stress-dependent regulation of apical endocytosis in renal proximal tubule cells mediated by primary cilia. *Proc Natl Acad Sci U S A.* 111, 8506-8511 (2014).
5. Tiong HY, Huang P, Xiong S, Li Y, Vathsala A, Zink D. Drug-induced nephrotoxicity: clinical impact and preclinical in vitro models. *Mol Pharm.* 11, 1933-1948 (2014).
6. Brown CD, Sayer R, Windass AS, Haslam IS, De Broe ME, D'Haese PC, Verhulst A. Characterisation of human tubular cell monolayers as a model of proximal tubular xenobiotic handling. *Toxicol Appl Pharmacol.* 233, 428-438 (2008).
7. Lash LH, Putt DA, Cai H. Drug metabolism enzyme expression and activity in primary cultures of human proximal tubular cells. *Toxicology.* 244, 56-65 (2008).
8. Takasato M, Er PX, Chiu HS, Maier B, Baillie GJ, Ferguson C, Parton RG, et al. Kidney organoids from human iPS cells contain multiple lineages and model human nephrogenesis. *Nature.* 526, 564-568 (2015).
9. Kaminski MM, Tomic J, Kresbach C, Engel H, Klockenbusch J, Muller AL, Pichler R, et al. Direct reprogramming of fibroblasts into renal tubular epithelial cells by defined transcription factors. *Nat Cell Biol.* 18, 1269-1280 (2016).
10. Kandasamy K, Chuah JK, Su R, Huang P, Eng KG, Xiong S, Li Y, et al. Prediction of drug-induced nephrotoxicity and injury mechanisms with human induced pluripotent stem cell-derived cells and machine learning methods. *Sci Rep.* 5, 12337 (2015).
11. Little MH, Kairath P. Regenerative medicine in kidney disease. *Kidney Int.* 90, 289-299 (2016).
12. Wyatt CM, Dubois N. In vitro generation of renal tubular epithelial cells from fibroblasts: implications for precision and regenerative medicine in nephrology. *Kidney Int.* 91, 265-267 (2017).
13. Jenkinson SE, Chung GW, van Loon E, Bakar NS, Dalzell AM, Brown CD. The limitations of renal epithelial cell line HK-2 as a model of drug transporter expression and function in the proximal tubule. *Pflugers Arch.* 464, 601-611 (2012).
14. Van der Hauwaert C, Savary G, Buob D, Leroy X, Aubert S, Flamand V, Hennino MF, et al. Expression profiles of genes involved in xenobiotic metabolism and disposition in human renal tissues and renal cell models. *Toxicol Appl Pharmacol.* 279, 409-418 (2014).
15. Zou C, McDaniel R, Romero L, Shapiro BA, Annesi C, Turner E, Chase B. A New Human Renal Solute Carrier Uptake Model for Drug Toxicity Studies. Web Page. American Type Culture Collection Cell Systems (2017). <https://www.lgcstandards-atcc.org/~media/92E2CAEAC89E41929099740F8A549B21.ashx>.
16. Imaoka T, Kusuhara H, Adachi M, Schuetz JD, Takeuchi K, Sugiyama Y. Functional involvement of multidrug resistance-associated protein 4 (MRP4/ABCC4) in the renal elimination of the antiviral drugs adefovir and tenofovir. *Mol Pharmacol.* 71, 619-627 (2007).

17. Kohler JJ, Hosseini SH, Green E, Abuin A, Ludaway T, Russ R, Santoianni R, et al. Tenofovir renal proximal tubular toxicity is regulated by OAT1 and MRP4 transporters. *Lab Invest.* 91, 852-858 (2011).
18. Likanonsakul S, Suntuksakul B, Nitiyanontakij R, Prasithsirikul W, Nakayama EE, Shioda T, Sangsajja C. A Single-Nucleotide Polymorphism in ABCC4 Is Associated with Tenofovir-Related Beta2-Microglobulinuria in Thai Patients with HIV-1 Infection. *PLoS One.* 11, e0147724 (2016).
19. Salvaggio SE, Giacomelli A, Falvella FS, Oreni ML, Meraviglia P, Atzori C, Clementi EGI, et al. Clinical and genetic factors associated with kidney tubular dysfunction in a real-life single centre cohort of HIV-positive patients. *BMC Infect Dis.* 17, 396 (2017).
20. Rokx C, Alshangi H, Verbon A, Zietse R, Hoorn EJ, Rijnders BJ. Renal Toxicity of Concomitant Exposure to Tenofovir and Inhibitors of Tenofovir's Renal Efflux Transporters in Patients Infected With HIV Type 1. *J Infect Dis.* 213, 561-568 (2016).
21. Suzuki S, Nishijima T, Kawasaki Y, Kurosawa T, Mutoh Y, Kikuchi Y, Gatanaga H, et al. Effect of Tenofovir Disoproxil Fumarate on Incidence of Chronic Kidney Disease and Rate of Estimated Glomerular Filtration Rate Decrement in HIV-1-Infected Treatment-Naive Asian Patients: Results from 12-Year Observational Cohort. *AIDS Patient Care STDS.* 31, 105-112 (2017).
22. Dykens JA, Will Y. The significance of mitochondrial toxicity testing in drug development. *Drug Discov Today.* 12, 777-785 (2007).
23. Tanji N, Tanji K, Kambham N, Markowitz GS, Bell A, D'Agati V D. Adefovir nephrotoxicity: possible role of mitochondrial DNA depletion. *Hum Pathol.* 32, 734-740 (2001).
24. Birkus G, Hitchcock MJ, Cihlar T. Assessment of mitochondrial toxicity in human cells treated with tenofovir: comparison with other nucleoside reverse transcriptase inhibitors. *Antimicrob Agents Chemother.* 46, 716-723 (2002).
25. Cihlar T, Birkus G, Greenwalt DE, Hitchcock MJ. Tenofovir exhibits low cytotoxicity in various human cell types: comparison with other nucleoside reverse transcriptase inhibitors. *Antiviral Res.* 54, 37-45 (2002).
26. Herlitz LC, Mohan S, Stokes MB, Radhakrishnan J, D'Agati VD, Markowitz GS. Tenofovir nephrotoxicity: acute tubular necrosis with distinctive clinical, pathological, and mitochondrial abnormalities. *Kidney Int.* 78, 1171-1177 (2010).
27. Kauffhold M, Schulz K, Breljak D, Gupta S, Henjakovic M, Krick W, Hagos Y, et al. Differential interaction of dicarboxylates with human sodium-dicarboxylate cotransporter 3 and organic anion transporters 1 and 3. *Am J Physiol Renal Physiol.* 301, F1026-1034 (2011).
28. Ahn SY, Jamshidi N, Mo ML, Wu W, Eraly SA, Dnyanmote A, Bush KT, et al. Linkage of organic anion transporter-1 to metabolic pathways through integrated "omics"-driven network and functional analysis. *J Biol Chem.* 286, 31522-31531 (2011).
29. Bush KT, Wu W, Lun C, Nigam SK. The drug transporter OAT3 (SLC22A8) and endogenous metabolite communication via the gut-liver-kidney axis. *J Biol Chem.* 292, 15789-15803 (2017).
30. Liu HC, Jamshidi N, Chen Y, Eraly SA, Cho SY, Bhatnagar V, Wu W, et al. An Organic Anion Transporter 1 (OAT1)-centered Metabolic Network. *J Biol Chem.* 291, 19474-19486 (2016).
31. Wu W, Jamshidi N, Eraly SA, Liu HC, Bush KT, Palsson BO, Nigam SK. Multispecific drug transporter Slc22a8 (Oat3) regulates multiple metabolic and signaling pathways. *Drug Metab Dispos.* 41, 1825-1834 (2013).
32. Nigam SK. What do drug transporters really do? *Nat Rev Drug Discov.* 14, 29-44 (2015).
33. Vaidya VS, Ferguson MA, Bonventre JV. Biomarkers of acute kidney injury. *Annu Rev Pharmacol Toxicol.* 48, 463-493 (2008).
34. Kane-Gill SL, Smithburger PL, Kashani K, Kellum JA, Frazee E. Clinical Relevance and Predictive Value of Damage Biomarkers of Drug-Induced Kidney Injury. *Drug Saf.* 40, 1049-1074 (2017).
35. Bailly V, Zhang Z, Meier W, Cate R, Sanicola M, Bonventre JV. Shedding of kidney injury molecule-1, a putative adhesion protein involved in renal regeneration. *J Biol Chem.* 277, 39739-39748 (2002).

36. Vaidya VS, Ramirez V, Ichimura T, Bobadilla NA, Bonventre JV. Urinary kidney injury molecule-1: a sensitive quantitative biomarker for early detection of kidney tubular injury. *Am J Physiol Renal Physiol.* 290, F517-529 (2006).
37. Vaidya VS, Ozer JS, Dieterle F, Collings FB, Ramirez V, Troth S, Muniappa N, et al. Kidney injury molecule-1 outperforms traditional biomarkers of kidney injury in preclinical biomarker qualification studies. *Nat Biotechnol.* 28, 478-485 (2010).
38. Adler M, Ramm S, Hafner M, Muhlich JL, Gottwald EM, Weber E, Jaklic A, et al. A Quantitative Approach to Screen for Nephrotoxic Compounds In Vitro. *J Am Soc Nephrol.* 27, 1015-1028 (2016).
39. Saikumar J, Hoffmann D, Kim TM, Gonzalez VR, Zhang Q, Goering PL, Brown RP, et al. Expression, circulation, and excretion profile of microRNA-21, -155, and -18a following acute kidney injury. *Toxicol Sci.* 129, 256-267 (2012).
40. Vedula EM, Alonso JL, Arnaout MA, Charest JL. A microfluidic renal proximal tubule with active reabsorptive function. *PLoS One.* 12, e0184330 (2017).
41. Weber EJ, Chapron A, Chapron BD, Voellinger JL, Lidberg KA, Yeung CK, Wang Z, et al. Development of a microphysiological model of human kidney proximal tubule function. *Kidney Int.* 90, 627-637 (2016).
42. Fukuda Y, Kaishima M, Ohnishi T, Tohyama K, Chisaki I, Nakayama Y, Ogasawara-Shimizu M, et al. Fluid shear stress stimulates MATE2-K expression via Nrf2 pathway activation. *Biochem Biophys Res Commun.* 484, 358-364 (2017).
43. Rodat-Despoix L, Delmas P. Ciliar functions in the nephron. *Pflugers Arch.* 458, 179-187 (2009).
44. Schophuizen CMS, Hoenderop JGJ, Van den Heuvel LP, Masereeuw R. Towards a Bioartificial Kidney - Insights in uptake and elimination of cationic solutes by proximal tubule epithelial cells. Nijmegen: Radboud University Nijmegen; 2016.
45. Praetorius HA, Spring KR. Removal of the MDCK cell primary cilium abolishes flow sensing. *J Membr Biol.* 191, 69-76 (2003).
46. Hoang-Minh LB, Deleyrolle LP, Nakamura NS, Parker AK, Martuscello RT, Reynolds BA, Sarkisian MR. PCM1 Depletion Inhibits Glioblastoma Cell Ciliogenesis and Increases Cell Death and Sensitivity to Temozolomide. *Transl Oncol.* 9, 392-402 (2016).
47. Hoang-Minh LB, Deleyrolle LP, Siebzehrubel D, Ugartemendia G, Futch H, Griffith B, Breunig JJ, et al. Disruption of KIF3A in patient-derived glioblastoma cells: effects on ciliogenesis, hedgehog sensitivity, and tumorigenesis. *Oncotarget.* 7, 7029-7043 (2016).
48. Mohammed SG, Arjona FJ, Latta F, Bindels RJM, Roepman R, Hoenderop JGJ. Fluid shear stress increases transepithelial transport of Ca²⁺ in ciliated distal convoluted and connecting tubule cells. *Faseb j.* 31, 1796-1806 (2017).
49. Berbari NF, O'Connor AK, Haycraft CJ, Yoder BK. The primary cilium as a complex signaling center. *Curr Biol.* 19, R526-535 (2009).
50. Deane JA, Ricardo SD. Emerging roles for renal primary cilia in epithelial repair. *Int Rev Cell Mol Biol.* 293, 169-193 (2012).
51. Weinbaum S, Duan Y, Satlin LM, Wang T, Weinstein AM. Mechanotransduction in the renal tubule. *Am J Physiol Renal Physiol.* 299, F1220-1236 (2010).
52. Jansen J, Fedecostante M, Wilmer MJ, Peters JG, Kreuser UM, van den Broek PH, Mensink RA, et al. Bioengineered kidney tubules efficiently excrete uremic toxins. *Sci Rep.* 6, 26715 (2016).
53. Esch EW, Bahinski A, Huh D. Organs-on-chips at the frontiers of drug discovery. *Nat Rev Drug Discov.* 14, 248-260 (2015).
54. Ewart L, Fabre K, Chakilam A, Dragan Y, Duignan DB, Eswaraka J, Gan J, et al. Navigating tissue chips from development to dissemination: A pharmaceutical industry perspective. *Exp Biol Med (Maywood).* 242, 1579-1585 (2017).
55. Low LA, Tagle DA. Tissue chips - innovative tools for drug development and disease modeling. *Lab Chip.* 17, 3026-3036 (2017).

56. Persson M, Hornberg JJ. Advances in Predictive Toxicology for Discovery Safety through High Content Screening. *Chem Res Toxicol.* 29, 1998-2007 (2016).
57. Persson M, Loye AF, Mow T, Hornberg JJ. A high content screening assay to predict human drug-induced liver injury during drug discovery. *J Pharmacol Toxicol Methods.* 68, 302-313 (2013).
58. Su R, Xiong S, Zink D, Loo LH. High-throughput imaging-based nephrotoxicity prediction for xenobiotics with diverse chemical structures. *Arch Toxicol.* 90, 2793-2808 (2016).
59. Hu S, Leblanc AF, Gibson AA, Hong KW, Kim JY, Janke LJ, Li L, et al. Identification of OAT1/OAT3 as Contributors to Cisplatin Toxicity. *Clin Transl Sci.* 10, 412-420 (2017).
60. Choucha-Snouber L, Aninat C, Grsicom L, Madalinski G, Brochot C, Poleni PE, Razan F, et al. Investigation of ifosfamide nephrotoxicity induced in a liver-kidney co-culture biochip. *Biotechnol Bioeng.* 110, 597-608 (2013).
61. Berthier E, Young EW, Beebe D. Engineers are from PDMS-land, Biologists are from Polystyrenia. *Lab Chip.* 12, 1224-1237 (2012).
62. Wong I, Ho CM. Surface molecular property modifications for poly(dimethylsiloxane) (PDMS) based microfluidic devices. *Microfluid Nanofluidics.* 7, 291-306 (2009).
63. Lanz HL, Saleh A, Kramer B, Cairns J, Ng CP, Yu J, Trietsch SJ, et al. Therapy response testing of breast cancer in a 3D high-throughput perfused microfluidic platform. *BMC Cancer.* 17, 709 (2017).
64. Wevers NR, van Vught R, Wilschut KJ, Nicolas A, Chiang C, Lanz HL, Trietsch SJ, et al. High-throughput compound evaluation on 3D networks of neurons and glia in a microfluidic platform. *Sci Rep.* 6, 38856 (2016).
65. Cooke MJ, Phillips SR, Shah DS, Athey D, Lakey JH, Przyborski SA. Enhanced cell attachment using a novel cell culture surface presenting functional domains from extracellular matrix proteins. *Cytotechnology.* 56, 71-79 (2008).
66. Weber HM, Tsurkan MV, Magno V, Freudenberg U, Werner C. Heparin-based hydrogels induce human renal tubulogenesis in vitro. *Acta Biomater.* 57, 59-69 (2017).
67. Jansen K, Schuurmans CCL, Jansen J, Masereeuw R, Vermonden T. Hydrogel-Based Cell Therapies for Kidney Regeneration: Current Trends in Biofabrication and In Vivo Repair. *Curr Pharm Des.* 23, 3845-3857 (2017).
68. Junaid A, Mashaghi A, Hankemeier T, Vulto P. An end-user perspective on Organ-on-a-Chip: Assays and usability aspects. *Current Opinion in Biomedical Engineering.* 1, 15-22 (2017).
69. Ai N, Fan X, Ekins S. In silico methods for predicting drug-drug interactions with cytochrome P-450s, transporters and beyond. *Adv Drug Deliv Rev.* 86, 46-60 (2015).
70. Ekins S, Polli JE, Swaan PW, Wright SH. Computational modeling to accelerate the identification of substrates and inhibitors for transporters that affect drug disposition. *Clin Pharmacol Ther.* 92, 661-665 (2012).
71. Li J, Jaimes KF, Aller SG. Refined structures of mouse P-glycoprotein. *Protein Sci.* 23, 34-46 (2014).
72. Jackson SM, Manolaridis I, Kowal J, Zechner M, Taylor NMI, Bause M, Bauer S, et al. Structural basis of small-molecule inhibition of human multidrug transporter ABCG2. *Nat Struct Mol Biol.* 25, 333-340 (2018).
73. Poongavanam V, Haider N, Ecker GF. Fingerprint-based in silico models for the prediction of P-glycoprotein substrates and inhibitors. *Bioorg Med Chem.* 20, 5388-5395 (2012).
74. Liu HC, Goldenberg A, Chen Y, Lun C, Wu W, Bush KT, Balac N, et al. Molecular Properties of Drugs Interacting with SLC22 Transporters OAT1, OAT3, OCT1, and OCT2: A Machine-Learning Approach. *J Pharmacol Exp Ther.* 359, 215-229 (2016).
75. Xu Y, Liu X, Wang Y, Zhou N, Peng J, Gong L, Ren J, et al. Combinatorial Pharmacophore Modeling of Multidrug and Toxin Extrusion Transporter 1 Inhibitors: a Theoretical Perspective for Understanding Multiple Inhibitory Mechanisms. *Sci Rep.* 5, 13684 (2015).
76. Ekins S, Clark AM, Wright SH. Making Transporter Models for Drug-Drug Interaction Prediction Mobile. *Drug Metab Dispos.* 43, 1642-1645 (2015).

77. Jiang L, Rizzo RC. Pharmacophore-based similarity scoring for DOCK. *J Phys Chem B*. 119, 1083-1102 (2015).
78. Hornberg JJ, Mow T. How can we discover safer drugs? *Future Med Chem*. 6, 481-483 (2014).
79. Shoda LK, Woodhead JL, Siler SQ, Watkins PB, Howell BA. Linking physiology to toxicity using DILIsym(R), a mechanistic mathematical model of drug-induced liver injury. *Biopharm Drug Dispos*. 35, 33-49 (2014).



Summary

Summary

This thesis describes the development of advanced renal proximal tubule epithelial cell (PTEC) culture models to study the mechanisms of drug-induced toxicity and drug-drug interactions (DDIs), and to evaluate their potential for *in vitro* drug-induced toxicity screenings.

The excretory function of the kidney is vital to human health. In addition to glomerular filtration, PTEC express multiple drug transporters and endocytosis receptors that mediate the selective excretion of waste products and reabsorption of nutrients. Drug transporters facilitate influx and efflux of drug compounds and are major determinants of PTEC drug sensitivity. In fact, one in five cases of acute kidney injury (AKI) is caused by nephrotoxicity of therapeutic drugs, indicating that evaluation of renal adverse effects in drug development lacks predictive value for humans. **Chapter 1** describes that animal models and most PTEC models have poor translational value for clinical drug studies because of species differences in transporter expression and lack of functional differentiation in the cell models. The conditionally immortalized proximal tubule epithelial cell line (ciPTEC) is an exception, since it demonstrates endogenous expression of drug transporters and endocytosis receptors. This thesis aimed to develop advanced *in vitro* cell culture models based on ciPTEC, that reflect differentiated human renal PTEC enabling the investigation of the mechanisms by which drugs induce nephrotoxicity, with a focus on renal drug handling and drug-drug interactions (DDIs).

Expression of physiologically relevant drug transporters in *in vitro* models is crucial for sensitive drug-induced toxicity evaluation. Primary proximal tubule cells rapidly lose their epithelial phenotype upon culturing, including loss of expression of OAT transporters, as is the case for ciPTEC. Therefore, developed ciPTEC constitutively expressing OAT1 (ciPTEC-OAT1) or OAT3 (ciPTEC-OAT3) as is described in **Chapter 2**. Lentiviral transfection of vectors containing either OAT-gene coupled to a cytomegalovirus promoter, resulted in successful expression that was confirmed by qPCR. Organic anion transport function was demonstrated by the active uptake of the fluorescent OAT1/3 model substrate fluorescein, and competitive inhibition by the OAT1/3 substrates para-aminohippuric acid, estrone sulfate, probenecid and diclofenac. In addition, OAT1 DDIs could be confirmed for the antiretroviral agents adefovir, cidofovir, tenofovir and zidovudine. For the first three compounds, the crucial role of OAT transport function in antiretroviral-induced toxicity was shown by the renal proximal tubule models ciPTEC-OAT1 and ciPTEC-OAT3, which exhibited increased sensitivity to these substrates.

Renal toxicity induced by the chemotherapeutic cisplatin is mainly mediated by OCT2 influx activity, which is endogenously expressed in ciPTEC. In **Chapter 3**, we showed that overexpression of OAT1 or OAT3 in ciPTEC reduced PTEC sensitivity to cisplatin, which was associated with reduced intracellular cisplatin accumulation. This observation was explained further by decreased gene expression and transport capacity of OCT2, demonstrated by reduced accumulation of the fluorescent OCT2 model substrate ASP⁺. Despite a profound increase in *MATE1* gene expression in ciPTEC-OAT1 and ciPTEC-OAT3, known to mediate cisplatin efflux, no functional contribution to cisplatin accumulation, ASP⁺ accumulation, or cisplatin-induced toxicity was found. Together, the results suggest that expression of OATs is also important for the evaluation of toxicity induced by drugs that are typically cleared by organic cation transporters, underlining the need for *in vitro* models that express both organic anion and cation drug transporters for the evaluation of drug-induced renal toxicity.

Receptor-mediated endocytosis is important for the proximal tubule reabsorption of low-molecular weight proteins and is the major uptake pathway of nucleotides, peptides, proteins but also (nephrotoxic) aminoglycoside antibiotics, such as gentamicin. In **Chapter 4**, we demonstrated that antisense oligonucleotides (AONs) competitively inhibit receptor-mediated endocytosis of α 1-microglobulin and albumin in ciPTEC, which can explain transient low-molecular weight proteinuria at pharmacologically relevant concentrations. Uptake of AONs was visualized using fluorescent tags, showing accumulation in vesicular-like structures over time. Interestingly, prolonged treatment with AONs at pharmacologically relevant concentrations did not affect ciPTEC viability or albumin uptake capacity. This shows that uptake of AONs in PTEC is facilitated by receptor-mediated endocytosis and compromises protein reabsorption, but does not induce direct toxic responses.

Monolayer cultures of proximal tubule cells may benefit from renal microenvironmental cues to help retain, or even regain, their epithelial differentiation status. **Chapter 5** reviews the use of 3D renal proximal tubule tissue reconstruction as advanced models for drug-induced toxicity screening, including kidney-on-a-chip. Culturing proximal tubule cells in a 3D microfluidic device allows for recapitulation of a tubule structure, multi-compartmentalization and exposure to fluid shear stress (FSS), which increases the physiological relevance of the model. Recent examples of kidney-on-a-chip models suggest that signals from the microenvironment increase proximal tubule transport functionality, which improves the sensitivity and response of PTEC to drug-induced injury and their predictive capacity. Future applications of kidney-on-a-chip devices include drug development and investigating the

contribution of FSS to renal epithelial cell differentiation and epithelial repair mechanisms.

While microfluidic devices are capable of increasing the physiological relevance of renal tubule cultures, this implicitly increases the complexity of the systems involved, which is accompanied by a lack of automation compatibility and reduced throughput. **Chapter 6** describes the development of a novel kidney-on-a-chip system that is suitable for high-throughput *in vitro* screening of DDIs. The platform combines the ciPTEC-OAT1 model with the 3D microfluidic system OrganoPlate®. This device is derived from the regular culture plate format and allows independent gravitational-based perfusion of its culture channels, allowing simultaneous culturing and automated fluorescent imaging of renal chips in parallel, while maintaining high-throughput compatibility. Gene expression and function of the efflux transporters Pgp and MRP2/4 was demonstrated in this device for ciPTEC-OAT1, using fluorescence-based assays coupled to automated image analysis and data extraction. This suggests that major limitations of microfluidic devices can be overcome, including lack of automation and throughput, paving the way for application of kidney-on-a-chip systems in industry.

Finally, **Chapter 7** provides a general discussion on the findings in this thesis and describes the role of advanced renal *in vitro* models in current and future drug-induced toxicity and DDI screening. In the future, induced pluripotent stem cell-derived renal cultures may replace immortalized cell lines as cell source, paving the way for personalized medicine in which clinically-relevant biomarkers will play a pivotal role. Apical fluid flow is an emerging microenvironmental factor that can increase PTEC differentiation. A ciPTEC model lacking its flow-sensing organelle, the primary cilium, is proposed as a tool to evaluate the contribution of flow-induced cilia-mediated signaling to drug transporter activity and drug sensitivity of *in vitro* PTEC models.

In conclusion, the *in vitro* models and techniques described in this thesis have increased the mechanistic insight into drug-induced adverse effects to the renal proximal tubule. Future applications of these advanced models in drug-induced toxicity and DDI screening have the potential to improve pre-clinical safety of candidate drugs in drug development and reduce animal experimentation.



Samenvatting

Samenvatting

Dit proefschrift beschrijft de *in vitro*-ontwikkeling van geavanceerde proximale tubulusepithelcelkweken (PTEC). Met deze modellen kunnen bijwerkingen van medicijnen op de nier mechanistisch worden onderzocht. Ook kunnen de modellen worden ingezet om bijwerkingen die de nierfunctie aantasten al vroeg tijdens de ontwikkeling van potentiële geneesmiddelen op te sporen.

De uitscheiding van afvalstoffen via de nieren is essentieel om gezond te blijven. De PTEC hebben verschillende transporteiwitten die zorgen voor de actieve uitscheiding van afvalstoffen vanuit het bloed naar de urine. Daarnaast hebben de PTEC receptoren op hun celmembranen, die gefiltreerde stoffen uit de glomerulus kunnen binden en recyclen. Al deze transporteiwitten faciliteren ook de opname en afgifte van medicijnen in de nier, en spelen daarom een belangrijke rol bij de hoge gevoeligheid van PTEC voor geneesmiddeltoxiciteit.

Eén op de vijf gevallen van acuut nierfalen wordt veroorzaakt door medicijnen. De huidige wijze om bijwerkingen op de nieren in medicijnontwikkeling te onderzoeken moet dus worden verbeterd. **Hoofdstuk 1** beschrijft de beperkte waarde van dierproeven en de huidige PTEC-kweekmodellen om de klinische bijwerkingen te voorspellen. Voor de kweekmodellen geldt dat de activiteit van de transporteiwitten vaak is afgenomen of specifieke transporters zelfs afwezig zijn, waarmee de gevoeligheid van de cellen in kweek voor geneesmiddeltoxiciteit is verminderd. De aanwezigheid van fysiologisch relevante transporteiwitten in kweekmodellen is van cruciaal belang gebleken voor het bepalen van nierschade veroorzaakt door medicijnen. Het conditioneel-geïmmortaliseerde humane PTEC (ciPTEC) model heeft een reeks endogene transporteiwitten en receptoren die wel actief zijn. Echter, ciPTEC heeft net als veel andere humane niercellijnen een verminderde expressie van organisch-anion transporteiwitten (OAT). Daarom hebben we een ciPTEC ontwikkeld, die OAT1 (ciPTEC-OAT1) of OAT3 (ciPTEC-OAT3) tot expressie brengen, zoals beschreven in **Hoofdstuk 2**. Hiervoor hebben we gebruik gemaakt van een lentivirale transfectie met vectoren waarin elk van deze genen is gekoppeld aan de cytomegalovirus promotor. De succesvolle expressie van OAT1 en OAT3 kon worden bevestigd door middel van qPCR. Door opname van het fluorescerende OAT-modelsubstraat fluoresceïne, in combinatie met competitieve remming door de OAT-substraten para-aminohippuurzuur, estronsulfaat, probenecide en diclofenac konden we de functionele activiteit bepalen. Daarnaast kon een geneesmiddelinteractie met OAT1 en OAT3 worden aangetoond voor de antiretrovirale middelen adefovir, cidofovir, tenofovir en zidovudine. Voor de eerste drie geneesmiddelen hebben we

tevens laten zien dat de OAT-transportfunctie direct verantwoordelijk is voor de nierschade veroorzaakt door deze medicijnen.

Bij nierschade veroorzaakt door het chemotherapeuticum cisplatina speelt opname door het organisch-kationtransporteiwit 2 (OCT2) een grote rol. In **Hoofdstuk 3** laten we zien dat de aanwezigheid van OAT1 of OAT3 in ciPTEC resulteert in een verminderde gevoeligheid voor cisplatina, doordat het geneesmiddel minder stapelt in de cel. Dit effect kan deels worden verklaard door een verminderde aanwezigheid en transportcapaciteit van OCT2, zoals aangetoond door een verminderde stapeling van het fluorescerende OCT2-modelsubstraat ASP⁺ in ciPTEC-OAT1 en ciPTEC-OAT3. Ondanks een duidelijke verhoging in een van de effluxpompen, multidrug en toxine extrusietransporteiwit 1 (MATE1) in ciPTEC-OAT1 en ciPTEC-OAT3. Hieruit hebben we geconcludeerd dat MATE1 in ons humane model hoogstwaarschijnlijk geen effect heeft op cisplatina stapeling, in tegenstelling tot datgene wat in diermodellen is aangetoond. Bij elkaar laten deze resultaten zien dat expressie van OATs belangrijk is bij het onderzoek naar nierschade, zelfs voor medicijnen die worden uitgescheiden door organisch-kationtransporteiwitten. Het is daarom van belang dat celkweekmodellen die worden gebruikt voor het testen van bijwerkingen van medicijnen zowel organisch-anion- als organisch-kationtransporteiwitten hebben, zoals ciPTEC-OAT1.

De reabsorptie van nucleotiden, peptiden en eiwitten met laagmoleculaire massa uit het glomerulaire ultrafiltraat in PTEC vindt plaats door receptorgemedieerde endocytose. Dezelfde receptoren zijn echter ook verantwoordelijk voor de opname van nierschadelijke substraten, waaronder aminoglycoside antibiotica zoals gentamicine. Dit leidt uiteindelijk tot schade aan de PTEC en verlies van eiwitten, suikers en aminozuren via de urine. Antisense oligonucleotiden (AON) zijn in staat om de cellulaire eiwitexpressie te moduleren en hebben daarom een toepassing als geneesmiddel. In **Hoofdstuk 4** laten we zien dat de endocytose receptoren op de PTEC verantwoordelijk zijn voor opname van AON. Farmacologisch relevante concentraties van AON remmen de opname van α 1-microglobuline en albumine competitief in ciPTEC. Dit kan verklaren waarom (pre-) klinische behandeling met AON, die onder andere ontwikkeld worden voor de behandeling van de ziekte van Duchenne, tijdelijk eiwitverlies in de urine veroorzaakt. In ciPTEC kon de opname van AON worden aangetoond met stapeling in endosomen, intracellulaire blaasjes. Langdurige behandeling van AON had echter geen invloed op de viabiliteit en functionaliteit van de cellen, zoals aangetoond voor albumineopname in ons celmodel. Deze resultaten laten zien dat receptorgemedieerde endocytose verantwoordelijk is voor opname van AONs in PTEC en dat blootstelling aan deze geneesmiddelen de reabsorptie van andere eiwitten remt, zonder direct schadelijke effecten op de tubuluscellen.

Eén hypothese die kan verklaren waarom de activiteit van transporteiwitten in de huidige PTEC-kweekmodellen is afgenomen, is het gebrek aan natuurlijke omgevingsfactoren van de nier in reguliere 2D celkweek. Celkweeken van PTEC zouden daarom een verbeterde gevoeligheid voor geneesmiddeltoxiciteit kunnen verkrijgen door de microfysiologie van de niertubulus na te bootsen. Hiermee kunnen de cellen in kweek mogelijk hun differentiatie behouden of zelfs terugwinnen die verloren is in reguliere 2D celkweek. **Hoofdstuk 5** geeft een overzicht hoe 3-dimensionale (3D) reconstructies van PTEC gebruikt kunnen worden als model om nierschade door medicijnen te onderzoeken. Wanneer PTEC in een geperfuseerd buizensysteem met heel lage volumes (microliters) worden gekweekt, ontstaan zogenaamde nierchips, die door eigenschappen als de buisstructuur, de aanwezigheid van verschillende compartimenten en de blootstelling aan een vloeistofstroom de fysiologische gelijkenis van het *in vitro* model verhogen. Recente voorbeelden van nierchips laten zien dat het nabootsen van de microfysiologie op deze manier de transportfunctie van PTEC in kweek verhogen, en daarmee ook de gevoeligheid voor geneesmiddelen waarvan bekend is dat ze nierschade veroorzaken. In de toekomst kunnen nierchipmodellen toegepast worden bij de ontwikkeling van medicijnen of in fundamentele studies waar bijvoorbeeld de invloed van vloeistofstroom op het epitheliale karakter van PTEC of herstel na weefselschade kunnen worden onderzocht.

Alhoewel kweeksystemen met vloeistofstromen in de orde van microliters in staat zijn om de fysiologische gelijkenis van PTEC-kweekmodellen te verhogen, maken zij het systeem inherent complexer, wat automatisering door middel van pipeteerrobots en een verminderde studiec capaciteit tot gevolg heeft. Om dit probleem aan te pakken, beschrijven wij in **Hoofdstuk 6** de ontwikkeling van een nieuw nierchipmodel dat geschikt is voor *in vitro* onderzoek naar geneesmiddelinteracties. Het door ons ontwikkelde platvorm combineert het celmodel ciPTEC-OAT1 met het 3D microvloeistofsysteem OrganoPlate®. Dit systeem is gebaseerd op een reguliere celkweekplaat en maakt gebruik van zwaartekracht-gedreven perfusie van de kweekkanalen. Hierdoor kunnen 40 tot 96 nierchips in parallel worden gekweekt en geanalyseerd methogecapaciteit doorgebruikte maken van fluorescentiemicroscopie. Wanneer ciPTEC-OAT1 gekweekt wordt in de OrganoPlate® bleken de effluxpompen, P-glycoproteïne en multidrug-resistentieeiwitten 2 en 4 functioneel intact. Dit kon worden aangetoond door gebruik te maken van fluorescerende modelsubstraten en geautomatiseerde microscopieanalyse. Dit model toont aan dat de limiterende beperkingen van nierchips, hoofdzakelijk een gebrek aan automatisering en studiec capaciteit, overwonnen kunnen worden. Nierchips zijn dan ook op termijn geschikt voor toepassing op industriële schaal waardoor het gebruik van dierproeven voor studies naar geneesmiddeltoxiciteit mogelijk beperkt kan worden.

Tenslotte bevat **Hoofdstuk 7** een algemene discussie over de bevindingen in dit proefschrift en beschrijft het de rol van geavanceerde nierkweekmodellen in huidige en toekomstige studies naar geneesmiddeltoxiciteit en geneesmiddelinteracties. Geïnduceerde pluripotente stamcellen (iPSC) zijn gededifferentieerde cellen, potentieel afkomstig van vrijwel elk weefsel in het lichaam, die door middel van strikte kweekprotocollen naar een ander celtype kunnen differentiëren. In de toekomst zouden nierkweken die gegenereerd zijn vanuit iPSC de rol van geïmmortaliseerde cellijnen over kunnen nemen, aangezien deze bron onuitputtelijk is en de differentiatie van deze cellen is af te stellen, met mogelijk een verhoogde aanwezigheid van bijvoorbeeld transporteiwitten. Deze techniek maakt het mogelijk om celmodellen te gebruiken die afkomstig zijn van patiënten, waardoor geneesmiddeltoxiciteit ook voor deze risicogroepen beter voorspeld zou kunnen worden, resulterend in persoonlijk afgestelde therapie: *personalized medicine*. Om bevindingen in kweekmodellen goed te kunnen vertalen naar mensen speelt de ontwikkeling van klinisch-relevante biomarkers, stoffen in bloed of urine die aangeven of en wanneer nierschade optreedt, een belangrijke rol. Het belang van vloeistofstromen in complexe kweeksystemen, zoals nierchips, wordt in toenemende mate onderzocht. Nabootsen van de microfysiologische nier kenmerken kan bijdragen aan de voorspellende waarde van dergelijk systemen bij het testen van medicijnen. Het primaire cilium is een organel aanwezig op vrijwel alle epitheelcellen, waaronder PTEC, en detecteert de vloeistofstroom over de cellen met een intracellulaire reactie als gevolg. Om de rol van cilia op de nierfunctie te kunnen onderzoeken, wordt in dit hoofdstuk een ciPTEC model gepresenteerd waarbij het primaire cilium ontbreekt. Hiermee kan de bijdrage van vloeistofstroom en signaaltransductie door het primaire cilium op de functie en differentiatie van PTEC-kweekmodellen verder worden onderzocht.

De kweekmodellen en technieken die in dit proefschrift staan beschreven dragen bij aan het inzicht in de mechanismen waarop geneesmiddelen bijwerkingen veroorzaken op de niertubulus. Toekomstige toepassing van zulke geavanceerde modellen in een vroeg stadium van de ontwikkeling van nieuwe medicijnen zal de veiligheid van deze middelen in de preklinische ontwikkelingsfase kunnen verbeteren en mogelijk het aantal proefdieren dat nu voor geneesmiddelontwikkeling wordt gebruikt kunnen verminderen.



Dankwoord

Curriculum vitae

List of publications

PhD portfolio

Dankwoord

Wetenschap is mensenwerk en de voortgang van onze kennis en kunde is afhankelijk van gebundelde krachten, zowel van spieren als grijze massa. Nu het wetenschappelijk inhoudelijke gedeelte van dit proefschrift is afgesloten, wil ik de tijd en ruimte nemen om iedereen die op welke manier dan ook heeft bijgedragen aan mijn onderzoek, mijn proefschrift en mijn ontwikkeling, wetenschappelijk of niet, van harte te bedanken. Een aantal mensen wil ik in de komende alinea's in het bijzonder noemen.

Beste **Martijn**. Jouw aandeel in mijn ontwikkeling als onderzoeker is van onschatbare waarde. Als begeleider van mijn masterstage leerde je mij tal van labvaardigheden die ik nu nog bijna dagelijks toepas. Je enthousiasme voor en toewijding aan de wetenschap werkten aanstekelijk en samen ontdekten we de potentie om de door jou ontwikkelde ciPTEC te gebruiken voor toxiciteitsstudies. Toen je eind 2013 een subsidie verkreeg voor het NephroTube-project zat ik met één telefoontje weer tegenover je. Het vertrouwen dat je hierdoor in mij uitsprak is fenomenaal en stelde me in staat mijn PhD-traject te starten. Iets meer dan 6 maanden hadden we om de resultaten van vervolgstudies te laten zien. Met succes, zo bleek, en het project was verzekerd van de nodige liquide middelen. In de jaren die volgden verschoof je rol van dagelijkse begeleider naar projectleider en bleef je betrokkenheid bij mijn wetenschappelijke ontwikkeling onverminderd groot. Terwijl ik in allerlei details verzeild raakte, bleef jij altijd het grote plaatje van het project zien en legde ons soms deadlines voor waarvan ik nooit had gedacht ze te halen. Tijdens de vele discussies over onze onderzoeksplannen, methodes en resultaten kwam je kennis en ervaring van het onderzoeksveld altijd bovendrijven. Je directe stijl helpt om problemen te analyseren en hielp mij om mijn argumentatie te allen tijde op orde te hebben. Je stelde mij in staat om mijn werk op verschillende nationale en internationale congressen te presenteren waar ik telkens weer dankbaar gebruik maakte van jouw netwerk. Je bent een bedreven onderhandelaar en goed in organiseren en beide vaardigheden bleken uiterst nuttig tijdens de teleconferenties en vergaderingen met onze sponsors. Naast alle professionele kennis en vaardigheden, praat je heel makkelijk. Daardoor konden we open van gedachten wisselen over wat ons bezig hield, zowel wanneer het goed ging als wanneer het iets minder ging. Je bent een leider met oog voor mensen; dat had ik nodig en dat is unieker dan je misschien denkt. Dankzij jou heb ik het beste uit mezelf kunnen halen en daar kan ik je niet genoeg voor bedanken!

Beste **Roos**. Jouw deskundigheid was van cruciaal belang bij de totstandkoming van dit proefschrift. De manier waarop jij tijdens een vergadering kennis naar boven haalt voorzien van de juiste referentie en ook nog treffende schatting van het publicatiejaar is ongekend. Van deze kennis en kunde heb ik ontelbare malen gebruik gemaakt, bij situaties die uiteenlopen van de juiste experimentele condities tot strategische projectkeuzes. Je zeer ruime ervaring met het schrijven van wetenschappelijke teksten kwam veelvuldig van pas en was zeker nodig om mij op het juiste schrijfpad te houden. Dat liet je mij uiteraard weten op je eigen, humoristische manier door mijn eerste artikel volledig terecht ‘een hele bevalling’ te noemen. Ik heb heel veel respect voor de manier waarop jij succesvol je drukke gezinsleven combineert met een ontzettend veeleisende baan en toch altijd tijd kunt vinden voor die ene vraag in een mailtje laat op donderdagavond. Ongeveer halverwege mijn PhD werd jij welverdiend benoemd tot professor Experimentele Farmacologie bij de Universiteit Utrecht en daar ben je met hernieuwde energie begonnen. Om dat te vieren nodigde je ons na een rondleiding spontaan uit voor een etentje bij je thuis. Ondanks je fysieke verhuizing ben ik blij dat jij als professor betrokken bent gebleven bij het NephroTube-project en bij mijn ontwikkeling als wetenschapper. Daarbij dekken deze woorden van dank helaas nóg steeds de lading niet.

Beste **Frans**. Jouw kritische blik en onuitputtelijke farmacologische kennis hebben een belangrijke bijdrage geleverd aan de kwaliteit van mijn werk en mijn proefschrift. Ik waardeer je revisies van de vele manuscripten waar je onafhankelijk van het stadium, opmerkingen aanbracht die ik al lang over het hoofd was gaan zien. Ondanks je drukke schema vond je gelukkig vaak tijd om onze vergaderingen bij te wonen. Ik heb veel bewondering voor de bevlogenheid die jij als afdelingsleider dag in dag uit weet op te brengen om het onderzoek en onderwijs binnen de afdeling farmacologie en toxicologie naar een nog hoger niveau te tillen. Mijn dank dat je het NephroTube-project als onderdeel daarvan hebt gesteund.

De financiële zekerheid die het Nephrotube-project met zich meebracht, stelde de afdeling in staat om nóg een PhD-student aan te stellen. **Jelle**, al bij de eerste kennismaking toonde je aan over een vlotte stijl en een wetenschappelijk onderbouwde vragenmachine te beschikken. Met volle overgave stortte jij je op het project en dat is van cruciaal belang gebleken voor het uiteindelijke succes daarvan. Ik wil je bedanken voor ontelbare discussies, zowel tijdens vergaderingen als daarbuiten, je meningen over experimentele opzetten, het uitwisselen van gedachten over resultaten, alle suggesties voor artikelen die ik dankzij jou wél gelezen heb en alle andere zaken die ik me nu simpelweg niet meer herinner. Ik heb er heel veel van opgestoken. Ik heb bewondering voor de efficiënte manier waarop je werkt en de

eerlijke, directe manier waarop je mensen benadert. Dat maakt je niet alleen tot een fijne collega, maar ook buiten het lab konden we het goed vinden. Je enthousiaste verhalen over vliegreizen, Macbooks en hardlopen hebben een positieve impact gehad. Mijn inschrijving voor de halve marathon van Göteborg staat. Dankzij jouw Noord-Hollandse accent weet ik ook hoe een André Hazes-karaoke hoort te klinken; een stuk authentieker. Het afscheidsetentje bij jou thuis is memorabel en ik nodig je hierbij graag uit voor de return. Ik vind het geweldig dat je mijn paranimf wil zijn.

Janny, ik wil je eerst bedanken voor alle bergen werk die je voor mij hebt verzet. De nauwkeurigheid en grondige wijze waarmee jij niet alleen experimenteel werk, maar ook de meer administratieve taken vervult, zijn ongekend. Je stond altijd klaar om mij en anderen te voorzien van advies over zo'n beetje alles dat op het lab relevant is. Van gedetailleerde protocollen en trainingen tot organisatie van aankopen en zelfs IT. Door het netwerk dat je door de jaren heen bij het Radboud hebt opgebouwd, weet je precies bij wie je moet aankloppen om zaken te regelen en daar maakt iedereen op het lab dankbaar gebruik van. Jij bent voor mij de constante factor geweest die zoeken overbodig maakte en mij veel organisatie uit handen heeft genomen. Na werktijd bleven we regelmatig hangen op het lab om al dan niet werk-gerelateerde zaken te bespreken. Ik kwam erachter dat we beide een voorliefde hebben voor sport en iPhones en ik zal je hilarische verhalen over Nomi niet snel meer vergeten. Samenwerken met jou vond ik bijzonder aangenaam. Ik vind het super om je aan mijn zijde te hebben als paranimf.

Als PhD-student spendeer je heel wat uren op de afdeling en leer je je collega's goed kennen. Ik wil jullie allemaal hartelijk bedanken voor je interesse, enthousiasme en gezelligheid. **Jitske**, de efficiënte manier waarop jij bergen werk verzet is fenomenaal en daar heb ik veel respect voor. Bedankt dat je me als student wegwijs hebt gemaakt op het lab en me voortdurend liet zien wat je met ciPTEC kunt bereiken. Je eerlijkheid en openheid zorgde altijd wel voor hilariteit tijdens de pauzes. **Manoe**, het was fijn om met jou samen te werken en in die relatief korte tijd heb jij het AON-artikel naar een hoger niveau getild. Die publicatie komt er nu (hopelijk) echt aan. **Marieke** (H), dank voor al het kweekwerk dat je mij uit handen nam en voor de gezelligheid tijdens onze treintripjes terug naar het zuiden. **Milos**, thank you for being an oasis of calm in a world that does not seem to stop talking. I admire the choices you made to build your career and to do what you like best, science. **Michele**, thanks for all the coffee break talks and adding some Italian flair to the lab. The coffee you made is still the best. Period. **Pedro**, thanks for all the discussions we had about our work and on the fluorescence-based transporter assays in particular; I learned a lot from it. Thanks as well for joining me countless times to the local pub and giving me an inspiring peek into developing

one's career in an international world. As it turns out, even the global market is not all that big and I was quite surprised when you showed up as part of the evaluation panel during my job interview. I'm delighted to work with you again. **Tom (S)**, mijn dank voor je hulp met de BD Pathway en voor je motiverende kijk op onderzoek, al was het nog zo laat op de avond. Mijn dank is ook op zijn plaats voor al het werk dat je hebt gehad met inrichten van de IT-faciliteiten van de afdeling. Op het moment dat ik jouw taak overnam realiseerde ik me pas hoe complex dat systeem in elkaar zit. Dank aan **Laurens** voor het overnemen van diezelfde IT-taak van mij. **Sanne**, jij bent een harde werker en kunt echt doorzetten. Daar heb ik bewondering voor en dat heb ik ook aan den lijve ondervonden. Toen jij me vroeg of ik de Elfstedentocht wilde fietsen, realiseerde ik me niet hoe ver het eigenlijk was. Dankzij jouw haast professionele coaching waren onze trainingstochten die volgden een goede en vooral gezellige voorbereiding. Deze meer dan 230 kilometer lange tocht bleek een ware banden- en kuitensloper, maar we hielden vol en konden hem toevoegen aan onze palmaressen. Dank je wel voor deze prachtige ervaring. **Jan** en **Jeroen**, ik heb zeer veel bewondering voor de haast ultieme balans die jullie beiden gevonden lijken te hebben tussen werk en privé. Jullie zijn enthousiaste en bedreven collega's en ik dank jullie voor de vele verhelderende 'Maybe I missed it' vragen en ideeën voor vervolggelaxperimenten. **Carlijn**, dankzij jou weet ik nu meer van E-bikes dan ooit en was Limburg nooit verder weg dan één u'tje. Bedankt voor je gezelligheid. **Gaby**, als koorzanger was het fantastisch om een uitvoering van je theatergroep bij te wonen. Zoveel enthousiasme werkt altijd aanstekelijk. **Jolien**, als sportfanaat begreep jij gelukkig dat er ook gezonde verslavingen bestaan en daar geven we dan ook beiden graag aan toe. Gaby en jij zijn heel begaan met het placentaonderzoek en jullie hebben mijn fascinatie gewekt voor *ex vivo*-werk door de door jullie opgezette perfusie-opstelling eens live te demonstreren. Al kan ik nu nooit meer gewetenloos BBQ-en. Ik dank jullie voor alle suggesties en vragen die tijdens mijn presentaties naar boven kwamen, jullie interesse en gezelligheid. **Rick**, ik heb veel bewondering voor de manier waarop jij studenten bij je colleges en werkgroepen betreft, geholpen door je enorme kennis van de farmacologie. Ik dank je voor je kritische blik en voor het mede organiseren van het afdelingsuitje naar Den Bosch. Dat was een daverend succes. **Lindsey** en **Maarten**, bedankt voor alle discussies die we hebben gehad en voor de goede sfeer die jullie altijd meebrachten. **Saskia**, **Gerard**, **Daniëlle** en **Stan** wil ik graag bedanken voor hun klinische blik op mijn werk. Jullie herinnerden mij er op de juiste momenten aan dat mijn *in vitro*-werk uiteindelijk aan de patiënt ten goede komt. **Petra**, bedankt voor alle hulp en flexibiliteit bij het opzetten en meten van mijn metformine-experimenten. Petra, **Ab** en **Jeanne**, bedankt voor jullie gezelligheid bij de borrels. Tenslotte wil ik **Wendy**, **Lilibeth**, **Robert** en **Nicolai** bedanken voor alle organisatie en ondersteuning tijdens mijn jaren bij de afdeling.

Ik wil graag **Marieke** (W) en **Huib** bedanken voor het beschikbaar stellen van jullie microscopen, alle introducties en cursussen die jullie hebben gegeven en voor het beantwoorden van talloze vragen over microscopen en image-analyse.

Ger, mijn dank dat je af en toe tijd vrij maakte om samen een kop thee te drinken zodat ik de voortgang van mijn project kon delen met een kundig persoon buiten de farmacologie. Je blik als mentor werkte elke keer weer verhelderend.

Ik heb het geluk gehad om aan het NephroTube-project te mogen werken binnen een internationaal consortium samen met een groep betrokken en bekwame wetenschappers. Mijn dank gaat uit naar **Marianne, Henriëtte** en **Bas** van Mimetas voor alle discussies en het beantwoorden van talloze vragen over OrganoPlates. Dankzij jullie inzet konden we snel aan de slag en zijn jullie producten en protocollen door de jaren heen voortdurend geoptimaliseerd, wat een flink aandeel heeft gehad in het slagen van het project. **Paul** en **Jos** wil ik bedanken voor hun scherpe blik op het project vanuit een commercieel perspectief. **Laura**, despite your busy schedule as professor at the Fachhochschule Nordwest Schweiz you luckily managed to join many meetings and teleconferences. As toxicologist, your continuous contributions to the project turned out to be invaluable for its success. I would like to thank our collaborators at **Pfizer, Roche** and **GlaxoSmithKline** for their discussions and support. I thank the National Centre for the Replacement, Refinement and Reduction of animals in Research (**NC3Rs**) for financially supporting this project.

It's clear from the extended author lists on all experimental papers in this thesis that collaborations are important contributors to research and science. Therefore, I would like to thank **Niels** (S) for producing the OAT-constructs and **Rob** (W) for his FACS analyses that made the generation of the ciPTEC-OAT models possible. Many thanks in particular to **Constanze** (H) from AstraZeneca for her contributions and for supporting this project. Thanks as well to **Neslihan** (T) and **Thomas** (F) from the Technical University of Berlin for their help with setting up and measuring my cisplatin samples. Our work on antisense oligonucleotides was performed in collaboration with Biomarin Netherlands and I would like to thank **Cathaline** (B), **Tessa** (S) and **Melissa** (M) for their continuing discussions and help with analysis of samples.

De afdeling deelt de 7^{de} verdieping van het RIMLS-gebouw met de afdelingen Biochemie en Fysiologie. Ik wil alle huidige en oud-medewerkers bedanken voor het delen van apparatuur en voorraden en voor alle gezelligheid tijdens pauzes, spelletjesavonden en PhD-retreats. **Sander**, dankzij jouw inzet heeft het cisplatina-werk een enorme boost gekregen. Uiteindelijk heeft dat zelfs een artikel opgeleverd,

waar jouw bijdrage in zit verwerkt; mijn dank. **Lisanne**, ik wil je bedanken voor je gesprekjes over de voortgang van onze projecten en alle andere zaken die de revue passeerden tijdens pauzes en dinertjes. Wanneer ik weer in Nijmegen ben, kom ik graag nog eens langs. **Elianne**, je maakt er geen geheim van dat muziek maken een van je vele passies is en dat is er eentje die we delen. Ik vond het geweldig om een uitvoering van het studentenorkest bij te wonen en te zien met hoeveel enthousiasme jij je hobby beoefend. **Estel**, onze gezamenlijk interesse voor sport heeft ervoor gezorgd dat ik jou een echt sportmaatje mag noemen. Ik wil ik je bedanken voor alle gezellige uren die we samen hardgelopen hebben en op de spinningfiets hebben doorgebracht. Bovendien heeft je internationale kijk op de wereld mijn interesse gewekt. **Sanne** en **Anke**, dankzij jullie ben ik bekend geraakt met heerlijke glutenvrije biertjes en ook dat heeft bijgedragen aan mijn PhD. Dank voor jullie interesse, gezelligheid en de lach en een traan bij de cursus 'Management voor promovendi'.

Part of my development as a PhD student was to learn how to train, educate and supervise students from both the medical and science faculties. I would like to give many thanks to **Katja, Thom, Melanie, Ritchie, Milou, Dina, Daphne** and **Nina** for choosing my project for a Bachelor's or Master's traineeship. I appreciate your enthusiasm, commitment, tricky questions, refreshing views and hard work. The best way to check if you're into a subject is by explaining it to someone else and thanks to you I was able to do just that. I learned a great deal about teamwork and your feedback taught me how to become a (better) supervisor. Some of you have seen your work ending up in my thesis, but I realize that this does not apply to all of you, which is a real pity. I hope you find comfort in the fact that all the work you did contributed to our understanding of the models we worked with. By now, you know that adding knowledge usually takes a million small steps, not one giant leap. I have seen all of you grow tremendously in your practical skills and scientific attitude during the months in the lab. Some of you already have committed themselves to the next step on the scientific ladder and I'm proud to have played a part in that, if only a tiny bit. Thanks, I thoroughly enjoyed working with you. Although technically not supervised by me, I would also like to thank **Tom** (van H), **Tijmen** and **Renata** for all your help with my work, genuine interest and the thoughts and drinks we shared after work.

I realize I was extremely lucky to find a new job while my PhD project was still ongoing. As my Tour-de-Writing was, however, not yet finished, this meant that I had to double-job for a while. I would like to give many thanks to **Anna-Karin, Jorrit, Mikael**, and all other colleagues at the Department of Discovery Safety for the time

and space they allowed me to fulfil the tasks I was required to do. I'm looking forward to all the science and the years ahead!

Life is not only about work and I would like to thank all the members of the international Campus Choir 'Veelstemmig' for all the hours we indulged in our shared hobby. Singing in a choir is teamwork above else and I thoroughly enjoyed the official rehearsals and the unofficial ones. The fact that it required my undivided attention allowed me to completely immerse myself in a world of musical mindfulness for one evening a week. I liked the diversity and ever-changing dynamics of the group. I would like to give special thanks to **Willibrord** for his never-ending energy to drive the choir and to my fellow bases **Hendrik-Jan** and **Paul** for correcting all my mistakes and all the fun we had.

Marjolein, Samantha en Luc, als studievrienden hebben we samen vele uren college en ontelbare zelfstudieopdrachten en verslagen geproduceerd. Ik wil jullie bedanken voor jullie inzet; onze studie is immers de opmaat geweest voor dit proefschrift. Jullie zijn intelligente en gezellige mensen met een heel groot hart, waarbij ik me altijd thuis gevoeld heb. We zijn een heel eind gekomen; van ons eerste goede gesprek op de trap van (het oude) Doornroosje tijdens de introductieweek en een tuinfeest voor wat wel de halve opleiding leek, tot aan verhuizingen, promoties en zelfs een (aankomend) trouwfeest. Ook toen we later allemaal in een andere stad woonden, bleven jullie de moeite nemen om mij periodiek uit het verre oosten te plukken en tijd vrij te maken voor een dinertje, terrasje, potje midgetgolf of simpelweg een middagje aan zee. Ik waardeer jullie gesprekken, humor, enthousiasme en eerlijkheid. Ik heb veel van jullie geleerd, niet op zijn minst een aantal nodige sociale skills. Ondanks dat het voor mij allemaal iets meer logistieke planning vereist, hoop ik dat we die periodiek erin houden. Laten we samen nog heel wat hoogtepunten vieren!

Bart, een juiste mix van overeenkomsten en tegenstellingen bleken de basis van onze jarenlange vriendschap te zijn. Je bent als professional in de IT opgeleid in een heel ander vakgebied dan ik. Je interesse heeft mij aangezet tot nadenken over het grotere doel van het werk dat ik verricht en dat werkt op zijn beurt weer motiverend. Ik heb grote bewondering voor het ogenschijnlijke gemak waarmee je met mensen omgaat, je uitgebreide autodidactische kennis van de menselijke psychologie en voor je niet-te-stillen honger naar nieuwe ervaringen. Ik wil je graag bedanken voor alle ontspannen uren die we samen hebben zitten praten, lachen en gamen, alle drankjes die we gewijd hebben aan de toekomst en die ontelbare keren dat jij me de comfortabele zone uit hielp op weg naar een nieuwe ervaring. Onze filosofische overpeinzingen waarbij wereldproblemen keurig verpakt en opgelost worden in

het tijdsbestek van één avond, werken voor mij heel relativerend en ontzuenderend. Bedankt ook voor alle heerlijke zovakanties die mij in staat stelden om even bij te komen van alle beslommeringen en de batterij weer op te laden. Ik kijk alvast uit naar onze volgende reis en alle jaren die we van terrasjes mogen genieten!

Marco, wat ooit begon als huisgenoten die simpelweg geen zin hadden om (in hun eentje) te koken, groeide door onze gemeenschappelijke interesses al snel uit tot een hechte vriendschap. Je bent een echte denker, kunt helemaal opgaan in een ervaring of verhaal en voelt mensen goed aan; daar heb ik veel bewondering voor. Of het nu gaat om politiek, reizen, boeken, het klimaat of dopinggebruik in de sportwereld, ik dank je voor al die keren dat we samen ontspannen van gedachten wisselden en natuurlijk alles beter weten dan de échte experts. Onze gemeenschappelijke interesse in sport uit zich het beste in alle middagen die we doorgebracht hebben voor de tv, kijkend naar de Tour de France die we vervolgens van ons eigen hilarische commentaar voorzien. Als uitvoerend idealist voeg je de daad bij het woord en onze uitputtende, maar totaal ecologisch verantwoorde fietsvakanties en treinreizen naar alle uithoeken van respectievelijk Nederland en Europa, zijn daar het meest memorabele voorbeeld van. Het zijn geweldige ervaringen. Ik kan je ook niet genoeg bedanken voor alle keren die je mij hebt gemaand om het eens iets rustiger aan te doen. Mijn natuurlijke neiging om altijd alles uit alles te willen halen is niet altijd goed en jij begrijpt dat als geen ander. Ik kom snel nog eens langs in Utrecht voor een aangename avond in een versnellinkje lager!

Oma, ondanks dat de details van mijn werk meestal aan u voorbijgaan, blijft u toch altijd geïnteresseerd in waar ik mee bezig ben en daar wil ik u graag voor bedanken. Uw verhalen over opa, de enige andere bioloog binnen onze familie, zijn ontroerend en inspirerend en zullen mij altijd bijblijven. Mijn dank voor alle middagen die we samen thee hebben gedronken en ik hoop dat we dat nog een hele tijd kunnen blijven doen!

Mieke, de band die wij als broer en zus hebben opgebouwd is uniek. Jij kent me zo goed dat je vaak al weet wat ik ga zeggen, nog voordat ik het bedacht heb. Het maakte niet uit hoe lang ik van huis was geweest, dankzij jou kon ik altijd weer op een warm welkom rekenen en dat waardeer ik heel erg. En als het te lang duurde, dan reisde je mij samen met mam gewoon achterna. Dank je voor alle uren die we samen hebben zitten vertellen, lachen, lunchen, Netflixen en gamen en voor al die keren dat we samen broer-zusdag gevierd hebben. De Efteling heeft flink wat geld aan ons verdiend. Laten we snel nog maar eens een dagje uit plannen!

Pap en mam, jullie kan ik niet genoeg bedanken voor alle vrijheid en steun die ik de afgelopen jaren van jullie heb ontvangen. Jullie hebben mij altijd vrijgelaten om mijn eigen keuzes te maken, hoe ogenschijnlijk bizar mijn toekomstplannen ook werden. Van mijn aankondiging dat ik van plan was om in Nijmegen te gaan studeren tot aan mijn vertrek naar Zweden, jullie mening was altijd dat ik mijn hart diende te volgen waar dat ook toe zou leiden. Ik realiseer me dat ik door mijn drukke baan en volle reisschema het er de afgelopen jaren voor jullie niet altijd gemakkelijker op heb gemaakt om bereikbaar te zijn. Toch zijn jullie mij altijd blijven steunen door ervoor te zorgen dat ik écht thuiskwam wanneer ik er dan een keertje wél bij was. De weekendjes in Limburg voelen nog altijd alsof ik even op minivakantie ga, waardoor ik weer even energie kan tanken voor de weken die gaan komen. Ik hoop dat we samen nog van heel wat gezellige wandeltochten en familiedinertjes mogen genieten!

Tack så mycket mina vänner! Det var jätteroligt att jobba med er 😊

Vänliga hälsningar,

Tom

Curriculum vitae

Tom Theodurs Gerarda Nieskens werd geboren op 21 juni 1990 te Roermond. In 2008 behaalde hij daar cum laude zijn atheneumdiploma, profiel Natuur en Gezondheid, aan het Bisschoppelijk College Broekhin. Later dat jaar begon hij de bacheloropleiding Moleculaire Levenswetenschappen aan de Radboud Universiteit in Nijmegen. Hij deed hier kennis op van moleculaire celbiologie, biochemie, organische chemie en trainde hier zijn basislaboratoriumvaardigheden. Zijn bachelor werd vervolgd door de masteropleiding Molecular Life Sciences, tevens aan de Radboud Universiteit, waarbij hij twee onderzoeksstages doorliep. Zijn eerste masterstage volgde hij bij de afdeling Farmacologie-Toxicologie van het (toenmalig) Nijmegen Centre for Molecular Life Sciences, Nijmegen. Onder leiding van Dr. Martijn Wilmer, Prof. Dr. Roos Masereeuw en Prof. Dr. Frans Russel bestudeerde hij gedurende een periode van 8 maanden de mechanismen van nierschade veroorzaakt door cisplatina, alsmede mogelijke strategieën om deze effecten te voorkomen, gebruikmakend van een humaan kweekmodel van de proximale tubulus. Deze stage werd vervolgd door een onderzoeksproject van een maand, waarin de opname en mogelijk bijwerkingen van antisense-oligonucleotiden in de nieren met hetzelfde kweekmodel werden bestudeerd, in samenwerking met (het toenmalige) Prosensa in Leiden. Zijn tweede masterstage liep Tom bij de onderzoeksgroep van Prof. Jamie Davies aan de Universiteit van Edinburgh. Gedurende 7 maanden bestudeerde hij de mogelijkheden om Turingpatronen synthetisch te genereren, wat een bijdrage leverde aan het begrip van de autonome embryologische ontwikkeling van de nieren en het weefselherstel na acute nierschade. In 2013 studeerde hij cum laude af. Verder bouwend op zijn ervaring en kennis van de niertoxicologie, begon hij in januari 2014 aan zijn promotieonderzoek, met dit proefschrift als eindresultaat. Het doel was om met behulp van nierchips een model met een hoge screeningscapaciteit te ontwikkelen om hiermee nierschade veroorzaakt door medicijnen te kunnen onderzoeken, met een mogelijke industriële toepassing en beperking van dierproeven. Dit project is uitgevoerd in een internationaal consortium met verschillende partners van zowel de academie als het bedrijfsleven, waaronder MIMETAS in Leiden, de Fachhochschule Nordwest Schweiz (FHNW) in Basel en drie marktleidende farmaceutische bedrijven. Zijn onderzoek maakte deel uit van de Nephrotube CRACKIT Challenge, gefinancierd door het National Centre for Replacement, Reduction and Refinement of Animals in Research (NCR3s). Tom heeft meerdere bachelor- en masterstudenten begeleid en heeft zijn werk gepresenteerd op diverse nationale en internationale congressen. Hij zet zijn carrière voort als postdoctoraal onderzoeker binnen de niertoxicologie en is op dit moment werkzaam bij de Discovery Safety-Cardiovascular, Renal and Metabolic groep van de afdeling Drug Safety and Metabolism bij AstraZeneca in Gotenburg,

Zweden, onder leiding van Dr. Anna-Karin Sjögren en Dr. Mikael Persson. Zijn project heeft als doel om een geavanceerd kweekmodel van de proximale tubulus met een hoge fysiologische gelijkens te ontwikkelen, zodat de moleculaire en cellulaire bijwerkingen van medicijnen op de nier in detail kunnen worden onderzocht en veiligere geneesmiddelen kunnen worden ontwikkeld.

List of publications

- Vormann MK, Gijzen L, Hutter S, Boot L, Nicolas A, Van Den Heuvel A, Vriend J, Ng C, Nieskens TTG, De Wagenaar B, Masereeuw R, Suter-Dick L, Trietsch SJ, Wilmer MJ, Joore L, Vulto P, Lanz HL. **Nephrotoxicity and kidney transport assessment on 3D perfused proximal tubules**. *AAPS J*. 2018 Aug 14;20(5):90.
- Vriend J, Nieskens TTG, Vormann MK, van den Berge BT, van den Heuvel A, Russel FGM, Suter-Dick L, Lanz HL, Vulto P, Masereeuw R, Wilmer MJ. **Screening of Drug-Transporter Interactions in a 3D Microfluidic Renal Proximal Tubule on a Chip**. *AAPS J*. 2018 Jul 26;20(5):87.
- Nieskens TTG, Peters JGP, Dabaghie D, Korte D, Jansen K, Van Asbeck AH, Tavraz NN, Friedrich T, Russel FGM, Masereeuw R, Wilmer MJ. **Expression of Organic Anion Transporter 1 or 3 in Human Kidney Proximal Tubule Cells Reduces Cisplatin Sensitivity**. *Drug Metab Dispos*. 2018 May;46(5):592-599.
- Nieskens TTG, Wilmer MJ. **Kidney-on-a-chip technology for renal proximal tubule tissue reconstruction**. *Eur J Pharmacol*. 2016 Nov 5;790:46-56.
- Nieskens TTG, Peters JG, Schreurs MJ, Smits N, Woestenenk R, Jansen K, van der Made TK, Röring M, Hilgendorf C, Wilmer MJ, Masereeuw R. **A Human Renal Proximal Tubule Cell Line with Stable Organic Anion Transporter 1 and 3 Expression Predictive for Antiviral-Induced Toxicity**. *AAPS J*. 2016 Mar;18(2):465-75.

PhD PORTFOLIO

Institute for Molecular Life Sciences
Radboudumc

Name PhD student:	<i>Tom T. G. Nieskens</i>	PhD period:	<i>01-01-2014 until 31-12-2017</i>
Department:	<i>Pharmacology and Toxicology</i>	Promotors:	<i>Prof. Dr. R. Masereeuw</i>
Graduate school:	<i>Radboud Institute for Molecular Life Sciences</i>	Co-promotor:	<i>Dr. M. J. Wilmer</i>

TRAINING ACTIVITIES	Year(s)	ECTS
Courses & Workshops		
RIMLS Graduate Course	2014	1.75
Radboud Orientation Program for PhD Students	2014	0.2
Winterschool Dutch Kidney Foundation 2015	2015	1.75
Course: Management voor Promovendi	2015	1.75
Course: Fiji Microscopy Analysis	2015	1.0
Course: Scientific Integrity	2015	1.0
Course: Scientific Writing for PhD Candidates	2016	3.0
Workshop: InDesign, PhD Organization Nijmegen	2016	0.2
Seminars & Lectures		
Raymond Vanholder: An update on the Cinderella of protein bound uremic toxins	2014	0.1
Robert Walker: Mechanisms of Drug Nephrotoxicity	2014	0.1
Vishva Dixit: Role of Ubiquitin Modification in Cancer Pathogenesis	2014	0.1
Technical forum: Career Development	2014	0.1
Laurens van der Meer: CRISPR Cas 9 Genome editing	2014	0.1
Mike Murphy: Mitochondrial Reactive Oxygen Species in health and disease	2014	0.1
Dirk Schübeler: The genetics of epigenetics	2014	0.1
Kidney Theme Meeting (5x)	2015	0.5
Technical Forum: Statistics	2015	0.1
Technical Forum: Imaging	2015	0.1
Technical Forum: Nanoscience and Nanomedicine	2015	0.1
Technical Forum: From Bench to Bedside	2015	0.1
Technical Forum: Bioinformatics	2015	0.1
Technical Forum: Statistics	2016	0.1
Kidney Theme Meeting (8x)	2016	0.8
Technical Forum: Gene Expression/Repression Tools	2016	0.1
Technical Forum: Grant Writing	2016	0.1
Orson Moe: A Klotho-Centric View of Kidney Disease	2016	0.1
Organization of and presenting at Technical Forum: Organ-on-a-Chip ^b	2016	0.85
Kidney Theme Meeting (8x) ^b	2017	0.8

(Inter)national Symposia & Congresses		
RIMLS PhD Retreat 2014 ^a	2014	0.75
Symposium ESTIV 2014: Making sense of <i>in vitro</i> methods ^a	2014	1.5
Figon Dutch Medicines Days 2014 ^a	2014	0.75
Najaarsvergadering van de Nederlandse Federatie voor Nefrologie ^{a*}	2014	0.5
New Frontiers Symposium 2014: Regenerative Medicine	2014	0.5
Spring Meeting Dutch Society of Pharmacology ^a	2015	0.5
RIMLS PhD Retreat 2015 ^a	2015	0.75
Nephrotools Conference: The Kidney, Development, Disease and Regeneration ^a	2015	1.25
New Frontiers Symposium 2015: Cilia Medicine ^a	2015	0.75
Dutch Society for Toxicology, PhD Days 2016	2016	0.5
Figon Dutch Medicines Days 2016 ^b	2016	0.75
New Frontiers Symposium 2016: Cancer Research	2016	0.5
RIMLS PhD Retreat 2017 ^b	2017	0.75
Figon Dutch Medicines Days 2017	2017	0.5
Symposium: Transporttage 2017, Munster, Germany ^b	2017	1.0
Other		
Publieksavond 'Nier op maat' - Demo experimental setup	2014	0.2
World Kidney Day 2016	2016	0.2

TEACHING ACTIVITIES	Year(s)	ECTS
Lecturing		
Capita Selecta: De biologische kunstnier	2014	0.3
Capita Selecta: De biologische kunstnier	2014	0.4
Computer practical: Cellular, Organs and Systems Toxicology, Biomedical Sciences	2015	0.8
Other		
Supervision Katja Jansen, Bachelor internship	2014	1.0
Supervision Melanie Röring, Master internship	2015	2.0
Supervision Ritchie Timmermans, Bachelor internship	2015	1.0
Supervision Dina Dabaghie, Master internship	2016	2.0
Supervision Milou Smits, Bachelor internship	2016	1.0
Supervision student Biomedical Sciences 5AM08	2016	0.4
Supervision Daphne Korte, Master internship	2016	2.0
Supervision Nina Blaimschein, Master internship	2017	2.0
TOTAL		39.5

^a poster presentation, ^b oral presentation, * awarded

